DGK Deutsche Geodätische Kommission
der Bayerischen Akademie der Wissenschaften

Reihe C | Dissertationen | Heft Nr. 753

Daniel König

Determining a Terrestrial Geodetic Reference Frame Following the Integrated Approach of Space Geodesy

München 2015

Verlag der Bayerischen Akademie der Wissenschaften
in Kommission beim Verlag C. H. Beck

ISSN 0065-5325 ISBN 978-3-7696-5165-2

DGK Deutsche Geodätische Kommission
der Bayerischen Akademie der Wissenschaften

Reihe C Dissertationen Heft Nr. 753

Determining a Terrestrial Geodetic Reference Frame Following the Integrated Approach of Space Geodesy

Zur Erlangung des akademischen Grades eines
Doktor-Ingenieurs (Dr.-Ing.)
von der Fakultät für Bauingenieur-, Geo- und Umweltwissenschaften
des Karlsruher Instituts für Technologie (KIT)
genehmigte Dissertation
von

Dipl.-Ing. Daniel König

aus Bochum

München 2015

Verlag der Bayerischen Akademie der Wissenschaften
in Kommission beim Verlag C. H. Beck

ISSN 0065-5325 ISBN 978-3-7696-5168-3

Adresse der Deutschen Geodätischen Kommission:

Deutsche Geodätische Kommission

Alfons-Goppel-Straße 11 ● D – 80 539 München

Telefon +49 – 89 – 23 031 1113 ● Telefax +49 – 89 – 23 031 - 1283/ - 1100

e-mail hornik@dgfi.badw.de / rit@gfz-potsdam.de ● http://www.dgk.badw.de

Referent: Prof. Dr.-Ing. habil. Dr. h.c. Bernhard Heck, KIT

Korreferent: Prof. Dr. Markus Rothacher, ETH Zürich

Tag der mündlichen Prüfung: 10.01.2013

Diese Dissertation ist auf dem Server der Deutschen Geodätischen Kommission unter <http://dgk.badw.de/>
sowie auf dem Server des Karlsruher Instituts für Technologie unter
<http://digbib.ubka.uni-karlsruhe.de/volltexte/1000037169> elektronisch publiziert

ISSN 0065-5325 ISBN 978-3-7696-5165-2

Abstract

The goal followed within this work is to consistently and simultaneously determine the geometric as well as the dynamic part of a terrestrial reference frame (TRF) for geodetic-geophysical purposes. This is done by following the Integrated Approach of space geodesy as proposed by [Zhu 04] using a selection of GPS ground stations, the GPS satellite constellation, as well as the twin GRACE low Earth orbiters meaning the processing is done by combined precise orbit determination and parameter estimation using GPS measurements of the ground stations and the GRACE satellites, as well as K-band range-rate observations between the GRACE satellites based on state-of-the-art background and a priori models mainly following GRACE RL05 standards ([Dah 12]). Overall, the time span covered extends from 2004/02/04 to 2005/02/28 with satellite arcs of one day length delivering daily estimates of the TRF parameters. The integrated procedure followed here is opposed to the so-called Two-step Approach, where in a first step only the ground stations' GPS data are processed, and in a separate second step only the GRACE data are used with the orbits and clock parameters of the GPS satellites introduced as fixed.

Using the estimated degree-one and degree-two coefficients of the spherical harmonic expansion of the Earth gravity field the dynamic part of the TRF is established. The geometric part is derived from Helmert transformations between the a posteriori and the a priori ground station polyhedron. Representing a fundamental problem, determining and rectifying the datum defect inherent to the Integrated Approach is tackled by means of simulations. It finally turns out that beside a severe datum defect caused by the ground station network's z-translation and by its rotation about the z-axis, there is also a hidden datum deficiency in x- and y-translation. Counteracting the datum defect is done by imposing appropriate no-net conditions leading to a minimum constraints solution.

The time series of the estimated TRF parameters reveal a reasonable behaviour over time, i.e. stable with well-constrained scatter. For evaluating the external accuracy a comparison with independent sources is made for the determined GPS and GRACE satellite orbits as well as for the estimated gravity field coefficients. In terms of 3D position difference RMS the GPS orbits obtained from the integrated processing agree with the high-quality IGS final orbits at a level of about 6 cm, thereby not fully reaching the state-of-the-art of GPS orbit determination. Regarding the origin of the dynamic frame the three spatial components coincide with external time series at a level of 5mm and less in x and y and a level amounting up to about 15 mm in z. Results of a comparison w.r.t. the conventionally followed Two-step Approach confirm the expected outcome of the Integrated Approach delivering more accurate estimates of the unknown TRF parameters.

Additionally, several effects studied in detail reveal the influence of the relative weighting of the various observation types involved, the effect of different approaches to counteract the datum defect, and the interaction between the estimated gravity field coefficients and the GPS orbits. Considering the weighting of observations it can be shown that the origin of the dynamic frame is determined by the GPS data taken onboard the GRACE satellites whereas K-band range-rate data measured between both low Earth orbiters are responsible for accurately deriving the gravity field coefficients of degree two. Regarding rectifying the inherent datum defect it is shown that the no-net conditions are superior to the method of simply constraining all ground station coordinates to their a priori values. In this context it turns out that it is very helpful also to suppress the hidden datum defect in x- and y-translation in order to improve the position of the origin of the dynamic frame in x

and y. By constraining the GPS satellites' orbit force model, evidence is given for remaining high correlations between the translational x- and y-components of the gravity field's origin and those of Helmert transformations of the derived GPS constellation versus IGS final orbits. As revealed by using fixed high-quality IGS final orbits, high scatter in the time series of the estimated z-component of the dynamic origin as derived by the Integrated Approach is strongly caused by the quality of the GPS orbits.

Zusammenfassung

Die Bestimmung globaler Referenzrahmen für die Geometrie sowie das Schwerefeld der Erde sind seit jeher Hauptaufgaben der Geodäsie. Erste nennenswerte Versuche, geometrische Referenzrahmen zu bestimmen, stellen die Triangulationen mit dem Aufkommen der modernen Naturwissenschaften dar (z.B. Snellius, s. [Tor 01]). Die Einrichtung dynamischer Referenzrahmen begann im späten 19. Jahrhundert durch absolute und relative Schweremessungen. Waren diese Referenzrahmen lange Zeit von lediglich regionaler Ausdehnung, konnten sie mit der Verfügbarkeit von Satelltennavigationssystemen wie GPS mit ausreichender Genauigkeit global realisiert werden. Jedoch liegen bis heute geometrische und dynamische Referenzsysteme getrennt vor. Es war schliesslich das Ziel der "integrierten Geodäsie", z.B. in [Heck 95] dargestellt, diesen Nachteil dadurch zu beheben, indem Observablen ins geodätische Modell einfliessen, welche vom Schwerefeld abhängen, und indem der geometrische sowie der dynamische Referenzrahmen durch gleichzeitige Verarbeitung der Messdaten bestimmt werden. Das generelle Anliegen dieses Konzeptes besteht darin, Konsistenz in den verwendeten A-priori- und Hintergrundmodellen zu bewahren sowie Gleichzeitigkeit des Messzeitraumes, Berücksichtigung aller Korrelationen und Effizienz hinsichtlich der Durchführung zu erreichen. Die Begriffsbildung betreffend wird innerhalb eines integrierten Konzeptes ein terrestrischer Referenzrahmen bestimmt, welcher einen geometrischen Teil in Form eines Netzwerks von Bodenstationen sowie einen dynamischen Teil umfasst, der durch das Erdschwerefeld gegeben ist.

Die Zielsetzung der eingereichten Dissertation besteht aus den vorgenannten Gründen darin, auf konsistente Art und Weise sowohl den geometrischen als auch den dynamischen Teil eines terrestrischen Referenzrahmens zu geodätisch-geophysikalischen Anwendungen zu bestimmen. Hierzu wird der Weg des Integrierten Ansatzes der Weltraumgeodäsie, wie von [Zhu 04] vorgeschlagen, beschritten unter Verwendung einer Auswahl von GPS-Bodenstationen des IGS (International GNSS Service, [IGS 12a]), der GPS-Satellitenkonstellation sowie der beiden niedrigfliegenden Satelliten der GRACE-Mission ([Tap 04]). Die verwendete Konfiguration ist in Abb. 1.1 dargestellt.

Zunächst wird im zweiten Kapitel zum Verständnis der dem Integrierten Ansatz innewohnenden Prozessierung die Methodik der Bestimmung von Erdsystemparametern mit Hilfe von Satellitenmessdaten erläutert. Hierzu erfolgt ein Abriss der zur Schätzung der gesuchten Parameter notwendigen Schritte sowie der Satellitenbahnbestimmung.

Daraufhin wird in Kapitel drei sämtliche Hardware, Software als auch das Beobachtungsmaterial beschrieben, welches verwendet wird. Besonderes Augenmerk wird hierbei auf die GPS-Beobachtungen sowie auf die K-Band-Messungen zwischen den GRACE-Satelliten gelegt und diese hinsichtlich ihres Ursprungs sowie der zu erwartenden Genauigkeit beschrieben.

Im darauffolgenden Kapitel wird die Bestimmung des geometrischen und des dynamischen Teils eines terrestrischen geodätischen Referenzrahmens erläutert. Hierzu wird der Satz an Parametern mit Hilfe ihrer geophysikalischen Interpretation definiert, die zur vollen Bestimmung eines terrestrischen Referenzrahmens notwendig sind. Die Wahl der Parameter wird letztendlich derart getroffen, dass der dynamische Teil mit Hilfe der geschätzten Koeffizienten der Grade eins und zwei der sphärisch-harmonischen Entwicklung des Erdschwerefeldes aufgestellt wird. Hierbei stellen die Schwerefeldkoeffizienten vom Grade eins (C_{11}, S_{11}, C_{10}), welchen den Massenmittelpunkt der Erde in einem gewählten Koordinatensystem lokalisieren, den Ursprung des dynamischen Referenzrahmens dar. Die

Orientierung des dynamischen Referenzrahmens wird mit Hilfe von Koeffizienten vom Grade zwei (S_{21}, C_{21}, S_{22}) beschrieben. Der geometrische Teil besteht aus den geschätzten Positionskoordinaten der Bodenstationen sowie den Parametern von Helmert-Transformationen zwischen den geschätzten und den A-priori-Koordinaten. Mit Hilfe von Abb. 1.2 soll die grundlegende Idee verdeutlicht werden, sowohl den geometrischen als auch den dynamischen Teil des Referenzrahmens gleichzeitig mit Hilfe von Satelliten zu bestimmen. Nachfolgend werden die Beobachtungsgleichungen angegeben, über die der Zusammenhang zwischen den Messungen und eines Teils der Parameter gegeben ist. Abschliessend wird dargelegt, wie der dem Integrierten Ansatz innewohnende Datumsdefekt mit Hilfe von Simulationen bestimmt werden kann sowie die grundlegende Frage beantwortet, wie dieser durch "No-Net-Bedingungen" (s. [Alt 02b]) behoben wird. Die Ergebnisse zeigen, dass neben einem schwerwiegenden Datumsdefekt in z-Translation und Rotation um die z-Achse des Bodenstationsnetzes auch ein versteckter Defekt in x- und y-Translation besteht.

In Kapitel fünf wird ein Überblick über die durchgeführte Prozessierung im Integrierten Verfahren gegeben, vor allem hinsichtlich der Aufstellung der Prozessierungsumgebung sowie der ausgeführten Testberechnungen, welche als tagesweise kombinierte präzise Bahnbestimmung und Parameterschätzung über den Zeitraum 04.02.2004 bis 28.02.2005 durchgeführt wurde. Zudem werden die verwendeten Hintergrund- und A-priori-Modelle angegeben.

Im sechsten Kapitel werden die Ergebnisse der ausgeführten Prozessierungen zur Bestimmung des geometrischen sowie des dynamischen Teils eines terrestrischen Referenzrahmens dargestellt und diskutiert. Die gesuchten Parameter des terrestrischen Referenzrahmens werden in Form von Zeitreihen in ihrer zeitlichen Entwicklung gezeigt. Sie weisen sämtlich zu erwartendes Verhalten auf, d.h. über die Zeit stabil mit wohlbeschränkter Streuung. In Abb. 6.1 sind beispielhaft die Zeitreihen der x-, y- sowie z-Komponente (von oben nach unten) des Ursprungs des dynamischen Referenzrahmens dargestellt.

Zur Charakterisierung der erreichten internen Genauigkeit wird zudem ein Überblick der Beobachtungsresiduen gegeben. Demgegenüber werden zur Beurteilung der äusseren Genauigkeit Vergleiche mit unabhängigen Quellen durchgeführt. Dies betrifft die berechneten Bahnen der GPS- und der GRACE-Satelliten sowie die geschätzten Schwerefeldkoeffizienten. Im Sinne des quadratischen Mittels der 3D-Positionsdifferenzen der GPS-Bahnen im Vergleich mit hochqualitativen IGS-Bahnen ergibt sich eine Übereinstimmung auf einem Niveau von ungefähr 6 cm. Hinsichtlich des Ursprungs des dynamischen Referenzrahmens stimmen die drei räumlichen Komponenten mit entsprechenden externen Zeitreihen auf ca. 5 mm und weniger in X und Y überein und erreichen Spitzen in Z von ungefähr 15 mm. Ergebnisse eines Vergleichs mit einem konventionell beschrittenen Zweischritt-Verfahren bestätigen das erwartete Resultat, dass der Integrierte Ansatz genauere Schätzwerte der gesuchten Parameter liefert.

Verschiedene Detailuntersuchungen enthüllen den Einfluss der relativen Gewichtung der Beobachtungstypen, den Einfluss verschiedener Ansätze zur Behebung des Datumsdefektes sowie das Zusammenspiel der geschätzten Schwerefeldkoeffizienten mit den GPS-Bahnen. Im Falle der Beobachtungsgewichtung wird gezeigt, dass der Ursprung des dynamischen Rahmens durch die GPS-SST-Messungen der GRACE-Satelliten bestimmt wird, wohingegen die zwischen beiden Satelliten gemessenen K-Band-Beobachtungen für die genaue Bestimmung der Schwerefeldkoeffizienten vom Grade zwei unverzichtbar sind. Aus Abb. 6.10 ist z.B. ersichtlich, wie die K-Band-Messungen den Schwerefeldkoeffizienten C_{20} beeinflussen. Diese verursachen zum einen eine Verschiebung der Zeitreihe in Richtung der positiven Zeitachse, doch sind sie auf der anderen Seite unverzichtbar, C_{20} mit ausreichend kleinem Rauschen mit täglicher Auflösung zu bestimmen. Ähnlich verhält es sich mit den Schwerefeldkoeffizienten S_{21}, C_{21} und S_{22}, die erst durch Verwendung von K-Band-Beobachtungen mit täglicher Auflösung schätzbar werden, wie in Abb. 6.9 zu sehen ist. Hinsichtlich der Behebung des inhärenten Datumsdefektes wird nachgewiesen, dass No-Net-Bedingungen der Methode überlegen sind, in welcher sämtliche Stationskoordinaten an ihre A-priori-Werte gebunden werden. In diesem Zusammenhang stellt sich zudem heraus, dass es hilfreich ist, auch den versteckten Datumsdefekt in x- und y-Translation zu beheben, um den Ursprung des dynamischen Rahmens in X und Y zu verbessern. Durch Fesselung der Störkraftmodelle der GPS-Satelliten wird ein Beleg für verbleibende hohe Korrelationen zwischen den

x- und y-Translationen des Schwerefeldes und der GPS-Satellitenkonstellation gegeben. Ein möglicher Grund für die Schwäche der Bestimmung der z-Komponente des dynamischen Ursprungs wird durch die Einführung hochqualitativer IGS-Bahnen als fest vorgegeben aufgespürt. Hierdurch ergibt sich eine Zeitreihe der z-Komponente mit erheblich reduzierter Abweichung vom Erwartungswert sowie reduzierter Streuung.

Contents

Notations

Abbreviations

ACC	Accelerometer
APC	Antenna Phase Centre
ARP	Antenna Reference Point
A-S	Anti-spoofing
ATT	Attitude
CIS	Conventional Inertial System
CF	Centre of Figure
CM	Centre of Mass of the entire Earth system
CE	Centre of Mass of the solid Earth
CRF	Celestial Reference Frame
CTS	Conventional Terrestrial System
ca.	Circa
c.f.	Compare
DOWP	Dual One-way Phase
EPOS-OC	Earth Parameter and Orbit System - Orbit Computation
Eq.	Equation
ERP	Earth Rotation Parameter
e.g.	for example
GGOS	Global Geodetic Observing System
GFZ	German Research Centre for Geosciences (Deutsches GeoForschungsZentrum)
GMF-E	Global Mapping Function as implemented in EPOS-OC
GNSS	Global Navigation Satellite System
GPS	Global Positioning System
HT	Helmert Transform
IAG	International Association of Geodesy
ICRS	International Celestial Reference System
IGS	International GNSS Service
ILRS	International Laser Ranging Service
ITRF	International Terrestrial Reference Frame
ITRS	International Terrestrial Reference System
i.e.	That is
JPL	Jet Propulsion Laboratory
KBR	K-band Biased Range
KBRR	K-band Range Rate
LC	Linear Combination
LEO	Low Earth Orbiter
LRP	Laser Reference Point
LRR	Laser Retro-reflector

mas	Milli arcseconds
NEQ	Normal Equation
NP	Normal Point
ODS	Ordinary Differential Equation System
PCC	Phase Centre Correction
PCO	Phase Centre Offset
PCV	Phase Centre Variation
POD	Precise Orbit Determination
PSO	Precise Science Orbit
RMS	Root Mean Square
RSO	Rapid Science Orbit
SLR	Satellite Laser Ranging
SST	Satellite-to-satellite Tracking
STD	Standard Deviation
S/C	Spacecraft
TOF	Time of Flight
TRF	Terrestrial Reference Frame
VMF1	Vienna Mapping Function (updated)
w.r.t.	With respect to

Mathematical Symbols

$\underline{F}$	Force vector
$\underline{o}$	Observation vector
$\underline{O}_D$	Origin of the dynamic frame
$\underline{O}_G$	Origin of the geometric frame
$\underline{p}$	Parameter vector
$\underline{x}$	Position vector
$\underline{\dot{x}}$	Velocity vector
$\underline{\ddot{x}}$	Acceleration vector
$\underline{u}_1^2$	Unit vector pointing from point 1 to point 2
∇	Gradient operator
$< ., . >$	Scalar product operator
$\doteq$	Approximatively equal to
$:=$	Is defined as (from left to right)
$\sim$	Stochastically uncertain

Chapter 1

Introduction

Implementing and maintaining a geodetic terrestrial reference frame (TRF) of global extent for the geometry as well as for the gravity field of the Earth has always been one of the major tasks of geodesy. Thereby, a TRF represents the physical realisation of a terrestrial reference system which itself provides the underlying concept comprising the mathematical-physical theory, as well as the algorithms and constants used (see [Pet 10]). First noteworthy efforts in constructing a geometric TRF have been triangulations at the advent of modern natural sciences (e.g. Snellius around 1600 A.D., c.f. [Tor 01]). The furnishing of dynamic TRFs as gravimetric networks began in the late 19th century by absolute and relative gravity measurements. A limitation of all those reference frames has been their mere regional extent. Until the rise of global navigation satellite systems (GNSS) like the Global Positioning System (GPS) it has not been feasible to establish global geometric TRFs with satisfactory accuracy. Still geometric and dynamic TRFs have been separately put into practice. It has then been the aim of "integrated geodesy", as reviewed e.g. by [Heck 95], to overcome this drawback by incorporating observables depending on the gravity field into the geodetic model, and by simultaneously determining geometric as well as dynamic parameters. By following such an integrated concept a geodetic TRF is determined comprising its geometric part represented by a ground station network and its dynamic part given by the Earth gravity field. The general advantages of an approach like this are consistency in a priori and background models used, simultaneity in measurement time, consideration of all correlations, and efficiency in accomplishment. A recent activity within operational global geodesy is the Global Geodetic Observing System (GGOS, see [GGOS 12] and [Plag 05]) installed by the International Association of Geodesy (IAG, [IAG 12]). Its task is the monitoring of variations in the three fundamental fields of geodesy namely in Earth geometry, Earth gravity field, and Earth orientation ([Plag 05]). Thus, in order to achieve the goals of GGOS, there is need to provide a stable geodetic TRF in its geometric and its dynamic part along with its variations in time. To do so, it is necessary to integrate geometric as well as dynamic geodetic observation techniques as will be explained below.

The integrated determination of a geodetic TRF in its geometric and its dynamic part is the overall goal of the method presented here to derive those reference frames by following an approach that is space-geodetic, dynamic, and one-step. "Space-geodetic" means that the observations used to derive the reference frame parameters consist of tracking data to and between dedicated satellites orbiting the Earth. "Dynamic" denotes the method of determining the orbits of the satellites tracked, namely by integrating the underlying equations of motion based on a dynamic model for the acting forces. Finally, the approach is "one-step" as all observations are processed simultaneously and all desired parameters are estimated at the observation level. For this reason the procedure applied is also called the "Integrated Approach of Space of Geodesy" as proposed by [Zhu 04], or shortly and from now on "Integrated Approach".

As shown in Fig. 1.1, the Integrated Approach being space-geodetic makes use of Earth-orbiting satellites orbiting in two layers: the outer layer consists of a constellation of high-orbiting GNSS

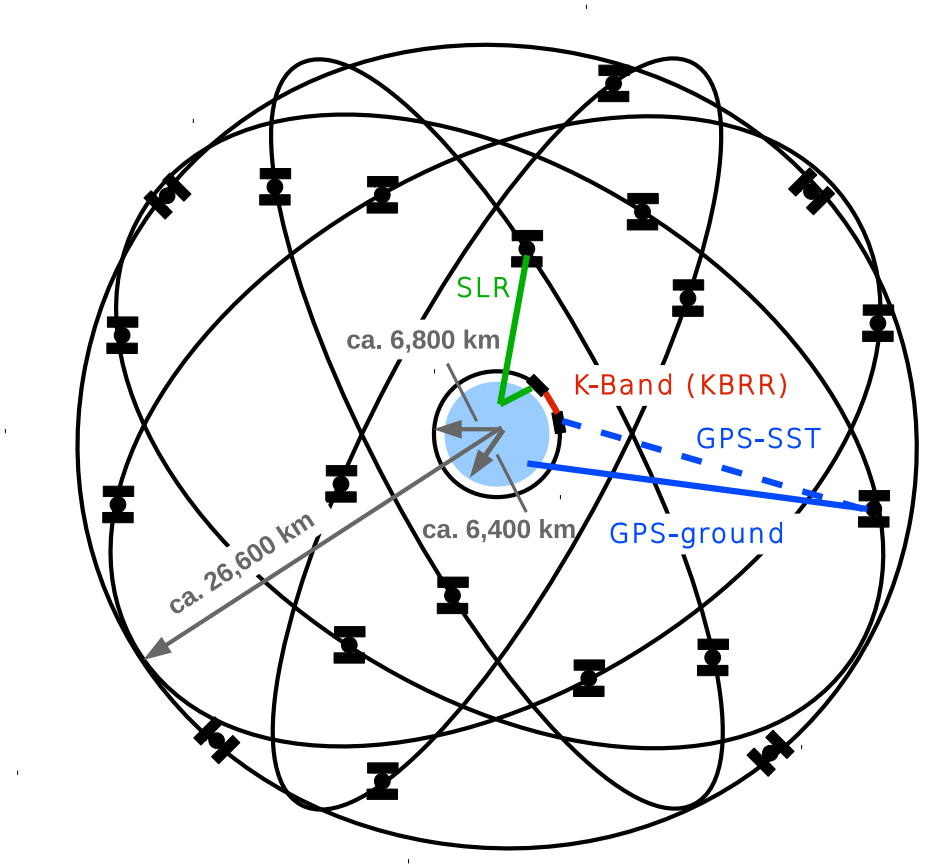

Figure 1.1: *The GPS-GRACE satellite constellation.*

satellites whereas low-orbiting LEOs are located in the inner layer. In the approach followed here the GNSS used is GPS, and the LEOs are the twin satellites of the GRACE mission, see [Tap 04]. The whole constellation is completed by a third level consisting of a network of GPS ground stations globally distributed over the Earth surface.

While the GNSS satellites provide an outer reference system almost not perturbed by anomalies of the Earth gravity field, the low orbit of the LEOs ensures high sensitivity to gravity feld variations and a dense scanning of them. By the choice of the aforementioned satellite systems the observations available for processing are GPS ground measurements as well as measurements taken by several instruments onboard the GRACE satellites. Those onboard measurements comprise GPS satellite-to-satellite tracking (SST) data between the GRACE LEOs and the GPS satellites also known as "high-low SST", range-rate observations (KBRR) coming from the inter-satellite K-band instrument also denoted as "low-low SST", as well as directly measured accelerations (ACC) and spacecraft attitude (ATT). Moreover, there are also Satellite Laser Ranging (SLR) data available to both GRACE LEOs as well as to the two GPS satellites PRN 5 and PRN 6. A visualisation of the observation types used in the present study is provided by Fig. 1.1.

Thanks to the GPS-SST and the KBRR observations a direct link between geometry and gravity parameters of the Earth is achieved at the observation level as sketched in Fig. 1.2. Throughout the processing this direct link remains uninterrupted due to the simultaneous processing of all satellites thus ensuring consistency in models and consideration of all correlations. Opposed to the Integrated Approach stands the conventionally applied two-step approach where in a first step the orbits and clocks of the GNSS satellites are determined which are then introduced as fixed into a second step which only the LEO observations are processed in. As a consequence, at the observation level, the direct

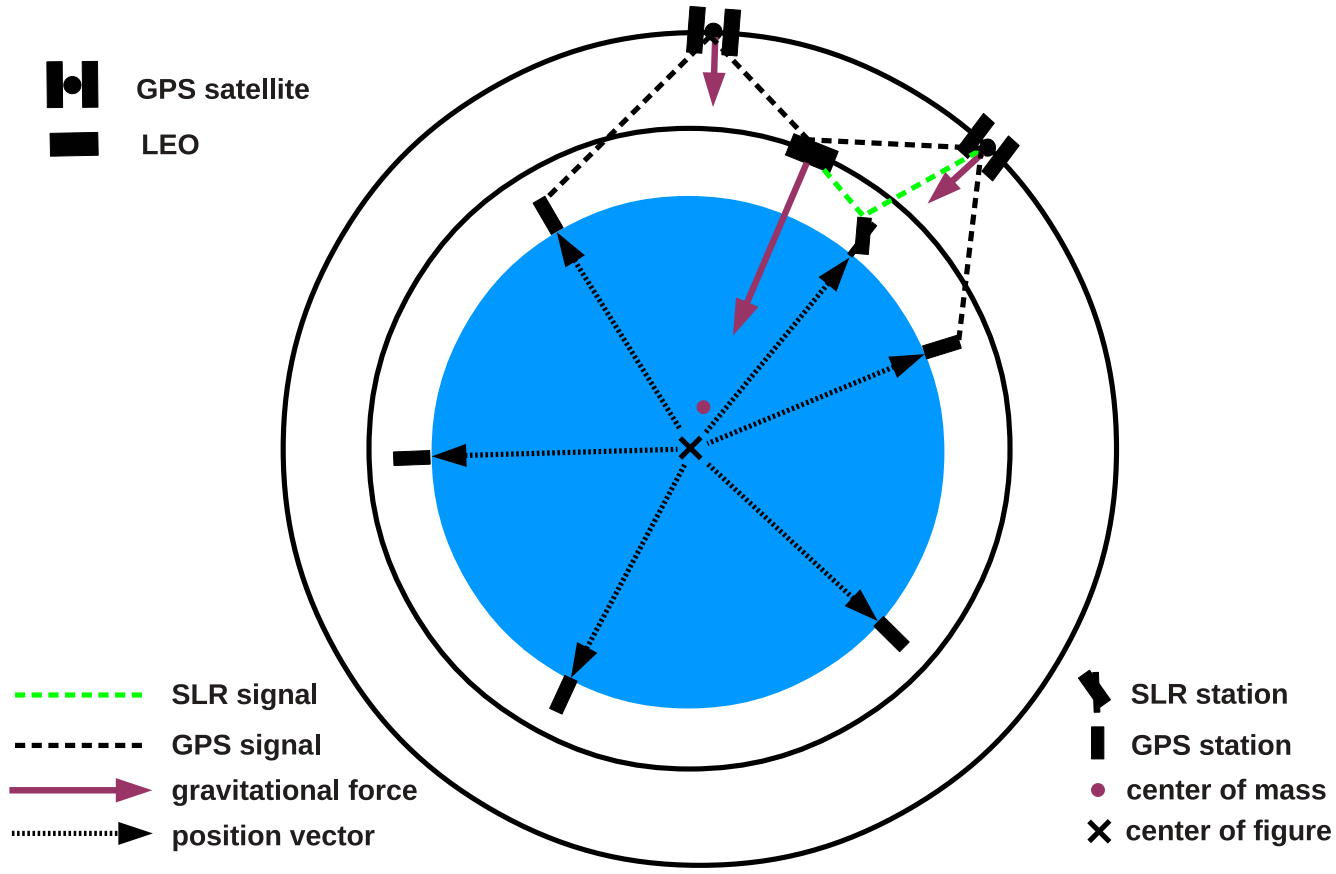

Figure 1.2: *The satellite link between the geometry and the gravity of the Earth. The centre of figure coincides with the origin of the coordinate system.*

link between the Earth's geometry and gravity parameters is interrupted meaning that considering all correlations as well as consistency in models is not automatically given.

As mentioned above, the global TRF to be determined consists of a geometric frame and a dynamic frame. While the geometric frame represents a coordinate system for geometric referencing, the dynamic frame is given by parts of the Earth's gravity field. Furthermore, establishing a global geodetic TRF means to determine an origin, a scale, and an orientation for each of the two parts by estimating appropriate Earth System Parameters. In case of the geometric frame origin, scale, and orientation can be derived from the estimated coordinates of the GNSS ground stations. On the other hand, the dynamic frame is defined by the estimated gravity field coefficients up to degree and order two. Estimating those parameters leads to a datum defect forcing to impose certain constraints on the set of unknown Earth System Parameters. Concerning geocentre motion, which is given by changes of the gravity field coefficients of degree one, the Integrated Approach as a dynamic space-geodetic method is measuring directly the integral effect. This is a great advantage against approaches where the geocentre motion is inferred from surface deformations provided by geophysical models or GNSS measurements. Considering the above given characterisation of the Integrated Approach, this procedure is suitable to contribute to the goals of GGOS by providing a stable as well as consistent geodetic TRF, comprising a geometric and a dynamic part, and by delivering estimates of variations

in each part. Up to the current date there have been no noteworthy efforts of other institutions to determine a global geodetic TRF based on GNSS observations following the Integrated Approach as described above.

The content is organised as follows. First of all, in Chapter 2 the methodology of the Integrated Approach is described. Thereby, the underlying procedures of satellite orbit determination and parameter estimation are outlined. Subsequently, the hardware, the software, as well as the space-geodetic observational data are introduced in Chapter 3. Especially the GPS data and the K-band inter-satellite observations between the GRACE satellites are described regarding data origin and expected accuracy.

In Chapter 4, the determination of a TRF in its geometric as well as dynamic part is explained. Thereby the set of parameters necessary to determine a TRF in its full range is defined and interpreted regarding its geophysical meaning. It is decided to put into practice the dynamic part using the estimated degree-one and degree-two coefficients of the spherical harmonic expansion of the Earth gravity field. The geometric part, on the one hand, is given by the estimated GNSS ground station positions while additional parameters, on the other hand, are derived from Helmert transformations between the ground stations' estimated and a priori set of positions. Furthermore, the auxiliary parameters needed to be estimated within the procedural model are explained. By presenting the observation equations the relation between the measurements and the parameters is clarified. The datum defect inherent to the Integrated Approach and the essential question how to rectify it by imposing no-net conditions are treated within the same chapter.

Chapter 5 is giving an overview concerning the data processing carried out following the Integrated Approach, especially the setup of the integrated processing environments, and the test computations performed. The various background and a priori models used are clarified, too. By day-by-day combined precise orbit determination and parameter estimation covering the time span extending from 2004/02/04 to 2005/02/28 the proper processing is done.

In Chapter 6 the results of the processings carried out for determining the geometric and the dynamic part of a TRF are presented and discussed. The time series of the TRF parameters obtained are shown in their time evolution. In order to give an idea of the internal precision achieved, an overview of the observational residuals is exhibited. On the contrary, for evaluating the external accuracy a comparison with independent sources is made for the GPS and GRACE satellite orbits as well as the estimated gravity field coefficients. A comparison with respect to the conventionally followed Two-step Approach is carried out, too, for evaluating which of both approaches delivers more accurate estimates of the unknown reference frame parameters. Additionally, several effects studied in detail reveal the influence of the relative weighting of the various observation types involved, the effect of different approaches to counteract the datum defect, and the interaction between the estimated gravity field coefficients and the GPS orbits.

Finally, some conclusions are drawn from the results obtained.

Chapter 2

Methodology

As this work is dedicated to investigate the potential of the Integrated Approach, as introduced by [Zhu 04], of determining simultaneously the geometric as well as the dynamic part of a global geodetic TRF, the underlying procedure for accomplishing this task is described in this chapter. After outlining the basic algorithm a description of the satellite orbit determination as well as of the parameter estimation procedure follows.

2.1 Integrated Approach

Basically, the procedure of the Integrated Approach consists of a POD of all satellites involved followed by a simultaneous estimation, using stochastic observational data, of all parameters needed to describe the physical system. Due to the parameter estimation in one step automatically consistency in models is ensured. Additionally, combining the POD with the parameter estimation, and carrying out the POD iteratively based on the updated parameters, allows for considering all correlations between the GNSS orbits, the LEO orbits, and the TRF parameters.

Basic Equations

The goal followed here is to determine the geometric as well as the dynamic part of a TRF by estimating appropriate parameters of a mathematical-physical model. In principal, it is most desirable to directly observe the parameters of interest. However, in the case of determining global parameters for a TRF this task would require a huge effort if done by terrestrial methods. For that reason the interesting parameters are indirectly determined via the observation of satellites orbiting the Earth as shown in Fig. 1.2.

In the present concept, high-orbiting GPS satellites are tracked by a polyhedron of ground GPS receiver stations as well as by LEO satellites orbiting the Earth at much lower altitude. That way the GPS satellites form an auxiliary reference system in space for determining a TRF. The idea is to parameterise a mathematical-physical model relating the set of TRF parameters, among others contained in a column vector $\underline{p}$, with the observations contained in $\underline{o}$ by making use of the satellite's motion along its trajectory $\underline{x}^S(t)$. In concise form the basic relations governing the model are

- the observation equations

$$\underline{o} = \underline{o}(\underline{p}) \tag{2-1}$$

- the equations of motion of the satellite's centre of mass following from Newton's second law related to an inertial frame

$$\ddot{\underline{x}}^S(t) = \frac{1}{m_S}\underline{F}\left(\underline{p}, t\right) \tag{2-2}$$

with

m_S *mass of the satellite*
$\underline{F}$ *total force acting on the satellite*
t $\in [t_0, t_1]$
t_0*: begin of the arc*
t_1*: end of the arc*

Thereby "arc" denotes a satellite's trajectory $\underline{x}^S(t)$ from the initial epoch t_0 to the final epoch t_1. The parameters in question in this context are the following:

$$\underline{p} = \left[(\underline{p}_D)^T, \ (\underline{p}_G)^T\right]^T \tag{2-3}$$

with $\underline{p}_D$ containing the dynamic parameters, and $\underline{p}_G$ the geometric parameters. The dynamic parameters are used for modelling orbit dynamics, i.e. in the equations of motion (2-6) they appear in the models used for calculating the forces acting on a satellite. On the other hand, the geometric parameters enter the observation equations to be presented in Section 4.2 in order to account for error sources affecting the observations. As a consequence, the satellites' state vectors $\underline{p}^S(t)$ are fully determined by $\underline{p}_D$ steering the equations of motion:

$$\begin{aligned} \underline{p}^S(t) &:= \left[(\underline{x}^S(t))^T, \ (\dot{\underline{x}}^S(t))^T\right] \\ &= \underline{p}^S(\underline{p}_D, t) \end{aligned} \tag{2-4}$$

$\underline{p}_D$ comprises the satellites' initial elements $\underline{p}^{S0} = \underline{p}^S(t_0)$, the gravity field coefficients, the parameters of the solar radiation force model for the GPS satellites, calibration parameters of the accelerometer measurements of the GRACE satellites, and empirical accelerations. Thus, in more details the two major sets of equations read as:

$$\underline{o} = \underline{o}\left(\underline{p}^S(\underline{p}_D), \underline{p}_G\right) \tag{2-5}$$

$$\ddot{\underline{x}}^S(t) = \frac{1}{m_S}\,\underline{F}\left(\underline{p}^S(\underline{p}_D, t), \underline{p}_D, t\right) \tag{2-6}$$

This system of equations establishes the mathematical-physical model needed to determine the parameters of a TRF by tracking satellites. It expresses the relationship between the observations $\underline{o}$, the satellite orbits $\underline{x}^S$, and the system parameters $\underline{p}$.

The free parameters inside $\underline{p}$ are going to be estimated applying a least-squares estimation procedure outlined in Section 2.3. This procedure requires the originally nonlinear observation equations to be linearised:

$$\begin{aligned} \underline{o} &\doteq \underline{o}\left(\underline{p}_0\right) + \left(\frac{\partial \underline{o}}{\partial \underline{p}}\right)_0 \underline{dp} \\ &=: \underline{o}_0 + \underline{\underline{A}}\,\underline{dp} \end{aligned} \tag{2-7}$$

with

$$\begin{aligned} \underline{dp} &= \underline{p} - \underline{p}_0 \\ \underline{\underline{A}} &= \left[\begin{array}{cc} \frac{\partial \underline{o}}{\partial \underline{p}_D} & \frac{\partial \underline{o}}{\partial \underline{p}_G} \end{array} \right]_0 \end{aligned} \tag{2-8}$$

$\underline{o}_0$ as well as $\underline{\underline{A}}$ are calculated using a priori values for the parameters contained in $\underline{p}_0$. In case of satellite positions $\underline{x}^S$ entering the partial derivatives the positions are provided by an initial satellite orbit determination based on a priori values for the parameters influencing it.

Partial Derivatives

Determining the partial derivatives is straightforward in case of the observations directly depending on the parameters. So, the partials

$$\frac{\partial \underline{o}}{\partial \underline{p}_G} \tag{2-9}$$

are obtained by direct differentiation of the observation equations with respect to $\underline{p}_G$, see Appendix E.

For the dynamic parameters having no direct relation to the observations the so-called variational equations have to be set up and solved. Determining these partials requires the application of the chain rule of differentiation:

$$\frac{\partial \underline{o}(\underline{p}^S(\underline{p}_D), \underline{p}_G)}{\partial \underline{p}_D} = \frac{\partial \underline{o}}{\partial \underline{x}^S}\frac{\partial \underline{x}^S}{\partial \underline{p}_D} + \frac{\partial \underline{o}}{\partial \dot{\underline{x}}^S}\frac{\partial \dot{\underline{x}}^S}{\partial \underline{p}_D} \tag{2-10}$$

$\partial \underline{o}/\partial \underline{x}^S$ and $\partial \underline{o}/\partial \dot{\underline{x}}^S$ are obtained by straightforward differentiation of the observation equations, c.f. Eqns. E-17, E-18, and E-19.

The procedure to determine $\partial \underline{x}^S/\partial \underline{p}_D$ and $\partial \dot{\underline{x}}^S/\partial \underline{p}_D$ makes use of the equations of motion (2-6) again by applying the chain rule:

$$\begin{aligned} \frac{\partial \ddot{\underline{x}}^S}{\partial \underline{p}_D} &= \frac{\partial}{\partial \underline{p}_D}\ddot{\underline{x}}^S(\underline{x}^S, \dot{\underline{x}}^S, \underline{p}_D, t) = \\ &= \frac{\partial \ddot{\underline{x}}^S}{\partial \underline{x}^S}\frac{\partial \underline{x}^S}{\partial \underline{p}_D} + \frac{\partial \ddot{\underline{x}}^S}{\partial \dot{\underline{x}}^S}\frac{\partial \dot{\underline{x}}^S}{\partial \underline{p}_D} + \left(\frac{\partial \ddot{\underline{x}}^S}{\partial \underline{p}_D}\right)_{explicitly} \end{aligned} \tag{2-11}$$

with $\left(\partial \ddot{\underline{x}}^S/\partial \underline{p}_D\right)_{explicitly}$ being non-zero in case there is a direct relation between $\ddot{\underline{x}}^S$ and the corresponding parameter p_i out of $\underline{p}_D$.

Let

$$\underline{Y}(t) = \frac{\partial \underline{x}^S}{\partial p_i}, \quad \dot{\underline{Y}}(t) = \frac{\partial \dot{\underline{x}}^S}{\partial p_i}, \quad \ddot{\underline{Y}}(t) = \frac{\partial \ddot{\underline{x}}^S}{\partial p_i} \tag{2-12}$$

$$\underline{A}_v(t) = \frac{\partial \ddot{\underline{x}}^S}{\partial \underline{x}^S}, \quad \underline{B}_v(t) = \frac{\partial \ddot{\underline{x}}^S}{\partial \dot{\underline{x}}^S}, \quad \underline{C}_v(t) = \left(\frac{\partial \ddot{\underline{x}}^S}{\partial p_i} \right)_{explicitly} \tag{2-13}$$

By linearly combining those terms the variational equations are set up, based on (2-11):

$$\ddot{\underline{Y}}(t) \;=\; \underline{A}_v(t)\underline{Y}(t) \;+\; \underline{B}_v(t)\dot{\underline{Y}}(t) \;+\; \underline{C}_v(t) \tag{2-14}$$

with the initial values (c.f. [Beu 05, I, 5.2])

$$\frac{\partial \underline{p}^S}{\partial p_i} \;=\; \begin{cases} \underline{e}_k, & p_i \;=\; k-th\ element\ of\ \underline{p}^S \\ \underline{0}, & else \end{cases} \tag{2-15}$$

$$\underline{e}_k \qquad k\text{-}th\ column\ of\ k \times k\ identity\ matrix \tag{2-16}$$

So, for determining $\partial \underline{x}^S / \partial p_i$ and $\partial \dot{\underline{x}}^S / \partial p_i$ these differential equations have to be solved, preferably by numerical integration. Finally, the obtained partial derivatives have to be interpolated to the observational epochs.

Differential Orbit Adjustment

Overall, the parameter determination process is carried out as so-called differential orbit adjustment. This process is iterative and consists of the following steps:

1. Preliminary orbit determination

   The orbits of the satellites involved are determined in a first step by numerical integration of the equations of motion (2-6) based on a priori parameters $\underline{p}_0$ initially given or estimated in the preceding iteration step. Part of them enters the models describing the forces acting on the satellites and thus determine the shape of the orbits. In general each of the single forces is described by a model containing certain unknown coefficients. Details of the orbit integration are presented in Section 2.2.

2. Parameter adjustment

   In this step the variational equations are solved and all free parameters are estimated as corrections $\hat{\underline{dp}}$. That way the a priori parameters $\underline{p}_0$ are improved to $\underline{p}_0 + \hat{\underline{dp}}$. Based on the improved parameters the observational residuals are calculated. For each residual its weighted square is compared to a chosen threshold, e.g. n-times the a posteriori standard deviation. If the residual surpasses the threshold it is marked as an outlier and eliminated from further processing.

3. Iteration

   The process is repeated until convergence is reached in the sense that the convergence criterion approaches asymptotically a limit. Thereby the improved parameters of one step are introduced as a priori parameters into the next step.

2.2 Satellite Orbit Determination

Numerical Integration

Determining the orbits of the satellites is done by means of numerical integration of the equations of motion (2-6) which represents an ordinary differential equation system (ODS) of second order. The algorithm for solving this ODS as implemented in EPOS-OC will not be reproduced here. It is similar to well-established procedures like those of Adams ([Dor 96]) or Cowell ([See 03, 3.3.2.2]). Common to those procedures is that the whole time interval $[t_0, t_N]$ is subdivided into subintervals $[t_i, t_{i+1}]$ with $i = 0, 1, 2, ..., N-1$. The proper numerical integration starts from the beginning of the arc (epoch t_0) using the initial elements

$$\left[\left(\underline{x}^{S0}\right)^T, \left(\underline{\dot{x}}^{S0}\right)^T\right]^T := \left[\left(\underline{x}^{S}(t_0)\right)^T, \left(\underline{\dot{x}}^{S}(t_0)\right)^T\right]^T \tag{2-17}$$

representing the satellite's position and velocity at time t_0 if given in cartesian coordinates. By advancing in time by $\Delta t_i = t_{i+1} - t_i$ the ODS is solved resulting in a state vector

$$\left[\left(\underline{x}^{S}(t_{i+1})\right)^T, \left(\underline{\dot{x}}^{S}(t_{i+1})\right)^T\right]^T \tag{2-18}$$

for the end of the current subinterval. After N-1 steps the final epoch is reached, and the satellite's orbit is given as a series of N state vectors. Within the processings carried out in the context of this work the step size Δt_i is fixed to 30 s for the GNNS and to 5 s for the LEO satellites. For those satellites moving in near-circular orbits a fixed step size is justified. As the equations of motion (2-6) are valid only in an inertial system the integration of the orbits is done in a Conventional Inertial System (CIS, see Appendix A), given by the International Celestial Reference System (ICRS, c.f. [McC 04] and [Pet 10]) in this context.

Orbit Forces Modelled

In the equations of motion (2-6) the total force $\underline{F}$ represents the sum of various partial forces acting on the satellite. Those partial forces can be classified into gravitational, surface, tidal, relativistic, and other forces, an overview of all of them except for the relativistic ones along with the range of accelerations they cause is given in Table 2.1. The magnitudes of the indicated ranges are quite consistent with those given in [Beu 05, II, 3.8]. As is obvious the gravitational forces caused by the various celestial bodies exert the largest accelerations on a satellite with the Earth gravitation naturally contributing the major part among them. In general, the accelerations due to the various surface and tidal forces are not negligible neither for the GPS nor for the GRACE satellites. Only in case of the GPS satellites $\underline{F}_d$ and $\underline{F}_{p,E}$ can be neglected due to the large orbital height. The relativistic orbit forces considered include the general relativistic effects of Schwarzschild, Lense-Thirring, and deSitter modelled according to [Pet 10, 10.3].

Formulas for selected forces are presented in Appendix B. Tables F.1 and F.2 give an overview of the force models used in the processing carried out in this context. However, in case of the GRACE LEOs there are currently no models at hand that would model the surface forces accurately enough. For this reason they are directly measured by the onboard accelerometers resulting in a combined "accelerometer" force:

$$\underline{F}_{acc} = \underline{F}_d + \underline{F}_{p,S} + \underline{F}_{p,E} \tag{2-19}$$

Since the integration of the equations of motion takes place in a CIS no apparent forces have to be considered. The purpose of introducing empirical forces $\underline{F}_{emp}$ is to account for unmodelled residual effects. Details of their modelling are given as well in Appendix B.

Table 2.1: *Overview of orbit forces and accelerations caused by them. The numerical values are calculated for one 24-h arc by EPOS-OC using implemented models.*

Source	Force	Acceleration $\underline{\ddot{x}}$ caused $[m/s^2]$	
Gravitation		GPS	GRACE
Earth gravitation	$\underline{F}_{g,E}$	0.56 ... 0.57	8.67 ... 8.73
Third Bodies gravitation			
- Moon	$\underline{F}_{g,M}$	2.10 ... 4.2E-06	5.53 ... 8.33E-07
- Sun, planets	$\underline{F}_{g,B}$	3.10 ... 6.0E-06	0.77 ... 1.24E-06
Solid Earth tides +	$\underline{F}_{set}$ +		
Solid Earth Pole tide	$\underline{F}_{spt}$	0.95 ... 1.66E-09	2.25 ... 2.81E-07
Ocean tides	$\underline{F}_{ot}$	0.49 ... 2.86E-10	0.24 ... 31.02E-08
Atmospheric tides	$\underline{F}_{at}$	0.92 ... 2.83E-11	0.52 ... 54.63E-09
Surface forces			
Atmospheric drag	$\underline{F}_{d}$	-	0.39 ... 0.53E-07
Solar radiation pressure	$\underline{F}_{p,S}$	8.80 ... 9.40E-08	0.28 ... 9.35E-08
Earth albedo pressure	$\underline{F}_{p,E}$	-	1.32 ... 1.41E-09
Others			
Empirical forces	$\underline{F}_{emp}$	0.51 ... 2.68E-09	0.51 ... 2.68E-09

2.3 Parameter Estimation

In Section 2.1 the basic goal of the Integrated Approach is already described as to determine a set of parameters $\underline{p}$ based on observations $\underline{o}$ and a priori parameters $\underline{p}_0$. Due to various reasons like rectifying a datum defect or ambiguity constraining, as discussed later, side constraints have to be added to the basic unconstrained model relating the parameters to the observations. For both the unconstrained as well as the constrained model the solution method is briefly outlined in the sequel, based on [Koch 99]. Details about the proper measurement models, including corrections and reductions to be applied to the observations and station positions as well as the a priori models used will be given in Sections 4.2 and 5.1.

Unconstrained Model

The unconstrained model for estimating parameters, as already stated in Eq. (2-7), is expressed as a system of linear equations reading as

$$\underline{do} = \underline{A}\underline{dp}$$

with

$$\begin{aligned} \underline{do} &= \underline{o} - \underline{o}_0 \\ \underline{A} &= \frac{\partial \underline{o}}{\partial \underline{p}}(\underline{p}_0) \end{aligned} \tag{2-20}$$

In general, this system of linear equations is inconsistent as there are more observations involved than parameters estimated. To obtain a consistent system of linear equations a vector $\underline{r}$ is added to the vector $\underline{o}$ resulting in the observation equations

$$\underline{do} + \underline{r} \;=\; \underline{A}\underline{dp} \tag{2-21}$$

As evoked by the relation

$$\underline{r} \;=\; (\underline{o}_0 + \underline{A}\underline{dp}) - \underline{o} \;=\; \underline{o}(\underline{p}) - \underline{o} \tag{2-22}$$

$\underline{r}$ is called *vector of observational residuals*. In order to consider the stochastic nature of the observations the vector $\underline{o}$ is assigned its covariance matrix $\underline{C}(\underline{o})$

$$\underline{C}(\underline{o}) \;=\; (\sigma_{ij}) \;=:\; \underline{W}^{-1} \tag{2-23}$$

with

$$\begin{array}{ll} i, j \;=\; 1, ..., N & \\ N & \textit{total number of observations} \\ \underline{W} & \textit{weight matrix} \\ \sigma_{ij} & \textit{covariance between observation } i \textit{ and } j \end{array}$$

In case there is no a priori information available about the covariances between different observations, $\underline{C}$ and thus $\underline{W} = (w_{ij})$ are assumed to be diagonal matrices. Consequently,

$$w_{ij} \;=\; \begin{cases} \sigma_i^{-2}, & i \;=\; j \\ 0, & i \;\neq\; j \end{cases} \tag{2-24}$$

meaning that only the diagonal elements (w_{ii}) of $\underline{W}$ take on nonzero values representing the weight of observation i determined by its assigned variance $\sigma_i^2 = \sigma_{ii}$. The whole system of observation equations (2-21) as well as the stochastic model (2-23) is also referred to as "Gaus-Markoff Model".

As this system of equations is overdetermined and since $\underline{do}$ is of stochastic nature $\underline{dp}$ cannot be solved by direct inversion. A solution $\underline{\hat{dp}}$ of $\underline{dp}$ is only possible if certain conditions are imposed on how the parameters have to fit to the observations. Here, the method to derive $\underline{\hat{dp}}$ is the well-known procedure of weighted least-squares which requires the weighted square sum $\underline{\hat{r}}^T \underline{W}^{-1} \underline{\hat{r}}$ with

$$\begin{aligned} \underline{\hat{r}} \;&=\; \underline{o}(\underline{\hat{p}}) - \underline{o} \\ \underline{\hat{p}} \;&=\; \underline{p}_0 + \underline{\hat{dp}} \end{aligned} \tag{2-25}$$

to become minimized. Omitting details, the solution $\underline{\hat{dp}}$ is obtained by inverting the normal equation (NEQ)

$$\left(\underline{A}^T \underline{W A}\right) \underline{\hat{dp}} \;=\; \underline{A}^T \underline{W}\; \underline{do} \tag{2-26}$$

with $\left(\underline{A}^T \underline{W A}\right)$ being the NEQ matrix. Applying linear error propagation the covariance matrix of the estimated parameters is obtained as

$$\underline{C}(\underline{\hat{p}}) \;=\; \underline{C}(\underline{\hat{dp}}) = \left(\underline{A}^T \underline{W A}\right)^{-1} \tag{2-27}$$

It becomes immediately clear that estimating $\underline{\hat{dp}}$ as well as $\underline{C}(\underline{\hat{p}})$ necessarily requires the Cayley inverse $\left(\underline{A}^T \underline{W A}\right)^{-1}$ to exist. This is only ensured if the whole set of parameters can be determined from the observations.

Constrained Model

Dependent on the specific application of the Gauss-Markoff model it may be necessary to impose side constraints on the parameters to be estimated. In the context of this work side constraints are set up as pseudo observations $\underline{o}_c$. Denoting the terms of the unconstrained model with subscript "u" and those of the constraining pseudo-observations with "c" the following enlarged system of observation equations results:

$$\begin{aligned} \underline{do}_u + \underline{r}_u &= \underline{A}_u \underline{dp} \\ \underline{do}_c + \underline{r}_c &= \underline{A}_c \underline{dp} \end{aligned} \tag{2-28}$$

Assuming no cross-correlations between $\underline{do}_u$ and $\underline{do}_c$ the covariance matrix $\underline{C}(\underline{o})$ and accordingly the weight matrix $\underline{W}$ for $\underline{o} := \left[\underline{o}_u^T,\ \underline{o}_c^T\right]^T$ are given by

$$\begin{aligned} \underline{C}(\underline{o}) &= \begin{pmatrix} \underline{C}(\underline{o}_u) & \underline{0} \\ \underline{0} & \underline{C}(\underline{o}_c) \end{pmatrix} \\ &= \begin{pmatrix} \underline{W}_u^{-1} & \underline{0} \\ \underline{0} & \underline{W}_c^{-1} \end{pmatrix} \qquad =: \underline{W}^{-1} \end{aligned} \tag{2-29}$$

By minimizing $\underline{\hat{r}}^T \underline{W}^{-1} \underline{\hat{r}}$ with $\underline{\hat{r}} = \left[\underline{\hat{r}}_u^T,\ \underline{\hat{r}}_c^T\right]^T$ the solution $\underline{\hat{dp}}$ in the least-squares sense results by inverting the NEQ

$$\left(\underline{A}_u^T \underline{W A}_u + \underline{A}_c^T \underline{W A}_c\right) \underline{\hat{dp}} \;=\; \underline{A}_u^T \underline{W}\; \underline{do}_u + \underline{A}_c^T \underline{W}\; \underline{do}_c \tag{2-30}$$

In this case the Cayley inverse $(\underline{A}_u^T \underline{W A}_u + \underline{A}_c^T \underline{W A}_c)^{-1}$ is required to exist in order to solve for $\underline{\hat{dp}}$. The general procedure using a generalized inverse, as covered by [Koch 99], is not of interest here and will therefore not be treated. Details about the specific selection of the stochastic model, i.e. $\underline{W}$, for the various observation groups, will be given in Section 5.1.

Chapter 3

Hardware, Software, and Data Used

For carrying out the task of deriving a global geodetic reference frame the use of dedicated hardware, software, and observational data is indispensable. As a basis for the following chapters these issues are addressed here. Concerning the hardware a subdivision is made into satellites and ground stations.

3.1 Satellites

The satellites used comprise the full constellation of the Global Positioning System (GPS) along with the twin GRACE Low Earth Orbiters (LEOs), GRACE-A and GRACE-B. As long as there is no danger of confusion, GRACE-A and GRACE-B are subsumed under "GRACE". In Fig. 1.1 the whole GPS-GRACE constellation is shown. All facts presented here about GPS satellites as well as basics about receivers are taken from [Hof 01] and from [Beu 98].

GPS

From 1973 on the Global Positioning System has been planned and established until reaching full operational service in 1994, now consisting of about 30 active satellites. It is a Global Navigation Satellite System (GNSS) mainly designed for navigation and time-transfer applications. Exploiting its full potential allows as well for high-precision geodetic applications. Overall, the whole system comprises a space, a control, and a user segment.

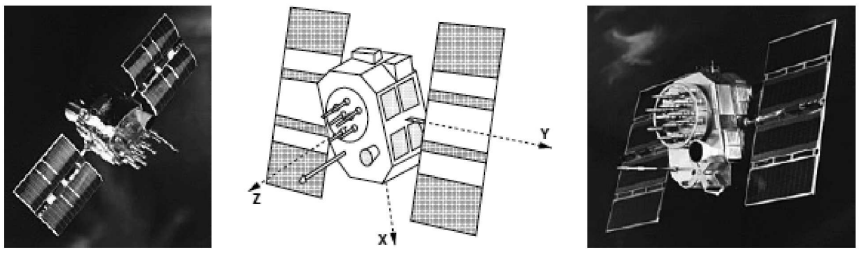

Figure 3.1: *Typical GPS satellites (from [Beu 98]).*

The space segment consists of the satellites that are distributed over six evenly spaced orbit planes. Each satellite is orbiting around the Earth at an altitude of about 20,000 km with an orbital period

very close to 12 sidereal hours, an eccentricity less than 0.006, and an inclination of approximately 55^o. In Fig. 3.1 typical examples of GPS satellites are shown. Their main components are a cube-like body, an antenna array for emitting navigation signals as well as a pair of solar panels producing electricity. The attitude of each satellite is maintained in such a way that the antenna array is always pointing towards Earth, and that the solar panel's axis is perpendicular to the plane defined by Earth, Sun, and the satellite itself.

GPS is a one-way navigation system meaning that the satellites are just broadcasting structured signals towards Earth. At a receiver station those signals are caught by an antenna and processed by appropriate electronic devices. The structured signals are modulated onto two carrier waves, L1 and L2, having the following structure:

$$\begin{aligned} L1(t) &= P(t)W(t)D(t)a_1\cos(f_1 t) + C_A(t)D(t)a_1\sin(f_1 t) \\ L2(t) &= P(t)W(t)D(t)a_2\cos(f_2 t) \end{aligned} \tag{3-1}$$

with

t	*time*
a_1	*amplitude of L1 carrier*
a_2	*amplitude of L2 carrier*
f_1	*frequency of L1 carrier (1.575 GHz)*
f_2	*frequency of L2 carrier (1.228 GHz)*
$C_A(t)$	*C/A-code (digital; chip length: 300 m)*
$P(t)$	*P-code (digital; chip length: 30 m)*
$W(t)$	*W-code*
$D(t)$	*navigation message*

Both carrier frequencies f_1, f_2 are derived by multiplying a fundamental frequency $f_0 = 10.23$ MHz by 154 and 120, respectively. By means of replica signals generated by the receiver it is possible to recover the C/A-code as well as the P-code, to determine their delay w.r.t. the replica signals, and to measure the instantaneous fractional phase $\varphi^S(t^S)$ of the carrier wave emitted by the satellite as well as the instantaneous fractional phase $\varphi_R(t_R)$ of the replica carrier signal generated in the receiver (t^S: epoch of signal emission, t_R: epoch of signal reception). While the measured delays of the codes deliver pseudoranges of m-precision, the instantaneous fractional phases are measured with mm-precision, and finally allow for precise geodetic applications. The classified W-code serves for encrypting the P-code for anti-spoofing (A-S) purposes. In case A-S is not switched on the P-code is also available for non-military users. State-of-the-art geodetic receivers deliver code and phase measurements on both signals L1 and L2 ("dual-frequency").

When processing GPS measurements several error sources have to be taken into account. They will be described in Section 4.2 in the context of the observational equations. Concerning the clocks of the GPS satellites as well as those of the receivers the exact offset to GPS time is unknown; it can be estimated using the measurements. In particular, it has to be noted that the GPS carrier phase observable represents only a fractional part of a full signal wavelength. Moreover, the actual emission of the signal as well as its reception takes place at the sender's and at the receiver's true antenna phase centres, respectively. For that reason the total displacement between the true antenna phase centre and the coordinate reference point has to be known, respectively for each sender satellite and each ground station. This displacement is made up of the ARP offset vector between the coordinate reference point and the antenna reference point (ARP) located at the bottom centre of the antenna, the constant Phase Centre Offset (PCO) vector between the ARP and the mean phase centre, as well

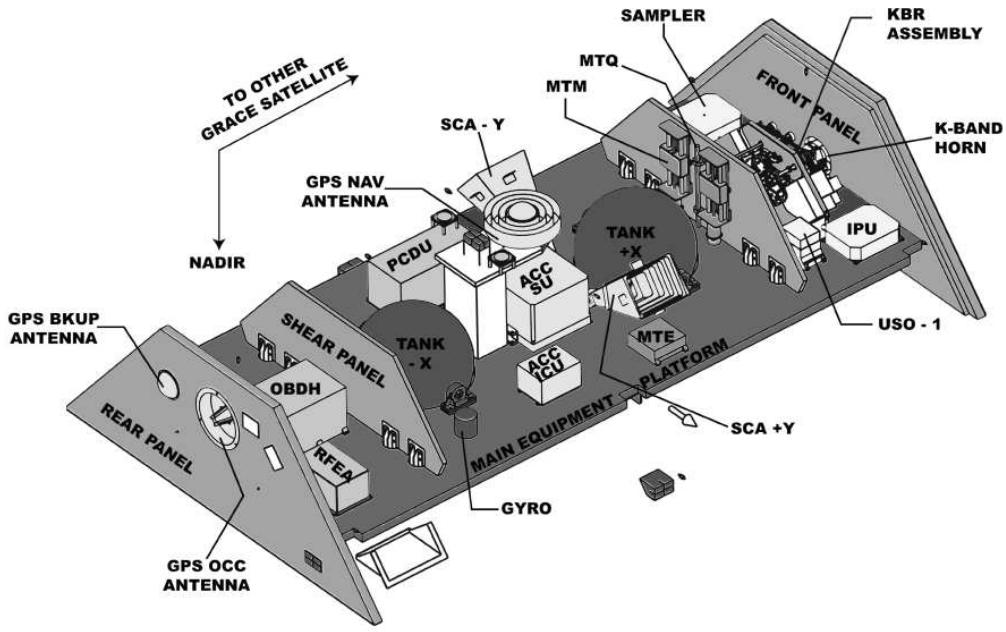

Figure 3.2: *GRACE internal structure (from [GRACE 12a]).*

as the Phase Centre Variation (PCV) between the mean and the true phase centre. Depending on the models applied the PCV corrections are elevation-dependent, and for some antenna types they are additionally provided azimuth-dependent. In case of the GPS sender satellites the ARP offset vector vanishes as the coordinate reference point being the satellite's centre of mass coincides with the ARP. The Global Positioning System's user segment as relevant in this context will be discussed in Section 3.2. A description of the control segment is omitted as it is of no interest here. Finally it should be noted that the two GPS satellites PRN05 and PRN06 are also equipped with laser retro-reflectors. This gives the possibility to track these two spacecrafts (S/C) by the satellite laser ranging technique.

GRACE

According to [Tap 04] GRACE (Gravity Recovery and Climate Experiment) is a satellite mission designed for mapping the global gravity field of the Earth and its temporal variations. GRACE was developed under NASA's Earth System Science Program, and launched on March 17, 2002. The mission consists of two nearly identical satellites orbiting the Earth in near-circular orbits of 89.5^o inclination at initially 500 km altitude. Both spacecrafts are separated by approximately 220 km. The low altitude makes it possible to recover the Earth's gravity field with a spatial resolution of 400 to 40,000 km. Such a spatial resolution can be obtained every 30 days because the satellites' short orbital period of about 90 min results in a dense ground track pattern. GRACE can be seen as the successor of the CHAMP mission ([Rei 99], in orbit 2000-2010) which has been the first GPS-tracked geopotential mission in history. From this precursor mission GRACE inherited much of the design, e.g. concerning the instrumentation.

In order to deliver scientifically useful data both GRACE S/Cs carry a payload of instruments dedicated to S/C operations on the one hand and instruments for carrying out scientific observations on the other hand. Fig. 3.2 shows the assembly of the satellites' instruments.

The following overview of the devices dedicated to S/C operations is taken from [Dun 03] and [Fro 06]. The so-called On-board Data Handling Computer (OBDH) serves as primary data managing system. Among other tasks it receives data to be transferred to the ground from the Instrument Processing Unit (IPU) and sends commands to it. The IPU and the Signal Processing Unit (SPU) are the central

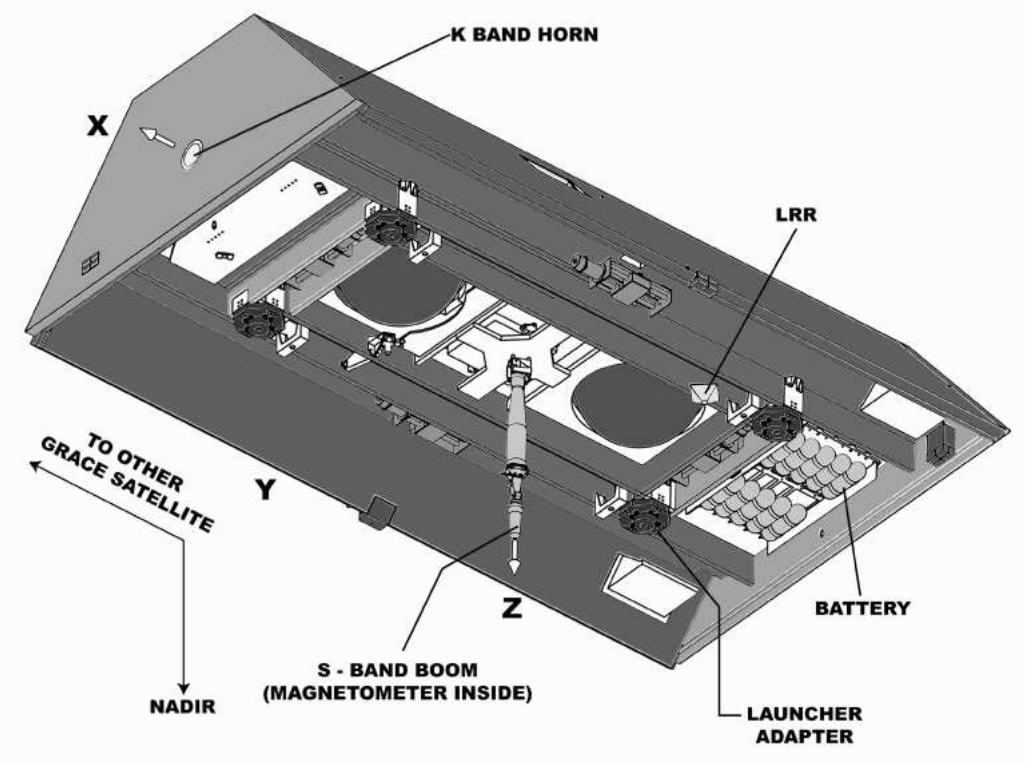

Figure 3.3: *GRACE bottom view (from [GRACE 12a]).*

devices of the science instruments. Representing a multi-purpose specialised computer the IPU hosts the signal processing hardware and the CPU for both the GPS receiver and the K-band interferometer (KBR), and it delivers signals for timing the Accelerometer (ACC) as well as the Attitude and Orbit Control System (AOCS). Passing through the SPU the signals received by the GPS antennas and those of the KBR antennas are down-converted and digitised. An Ultra-stable Oscillator (USO) serves for generating the onboard time scale, and for generating the signals of the KBR instrument. By means of a mass trim assembly (MTM, MTE) coincidence of the centre of the ACC with the satellite's centre of mass is accomplished. The attitude of each satellite is steered by magnetic torquers (MTQ) and cold gas thrusters. Telemetry, i.e. communication with ground antennas for downloading data and reception of new commands, is accomplished through an S-band antenna mounted at the bottom of the S/C, see Fig. 3.3.

Beside these operational devices the scientific payload aboard each satellite comprises the GPS equipment not hosted by the IPU, the ACC, a star camera assembly (SCA), the KBR, and a laser retro reflector (LRR). These instruments deliver the measurements essential for the space-geodetic purpose of the mission; in the following they will be shortly introduced.

- GPS: Antennas and Receiver

Each GRACE S/C is equipped with three antennas (NAV, OCC, BKUP) for collecting GPS signals. While the navigation (NAV) antenna serves Precise Orbit Determination (POD) the OCC antenna is used for atmospheric sounding by occultation measurements. The third antenna is meant for backup (BKUP). Interesting in the present context is solely the NAV antenna which is mounted on the top side of the satellite's casing, see Fig. 3.2.

The proper processing of the GPS signals takes place in the GPS receiver located inside the S/C's casing. Overall, the receiver is derived from the "BlackJack" receiver developped by JPL and used on CHAMP. It is a dual-frequency receiver capable of tracking up to 14 GPS satellites and of extracting

the code and carrier phase observables from the radio frequency (RF) link, c.f. [Dun 03]. According to [Tap 04] it is designed to measure carrier phases with 7-mm precision and pseudo-ranges with a precision of 20 cm. As a deviation from the classical GPS receiver concept, part of the signal processing is done within the multi-purpose IPU. Beside facilitating POD of the S/C the GPS receiver's measurements are as well used to time-tag all Level 1B data products with GPS time.

In contrast to the GPS satellites the coordinate reference point of each GRACE S/C, again being the centre of mass, does not coincide with the ARP of the NAV antenna leading to a nonzero ARP offset vector. Within this work the ARP offset vector is set to 0.0 m in x- and y-direction, and to -0.444 m along the z-axis in the satellite-fixed coordinate system as defined in Fig. 3.3. The PCO vector components, on the other hand, are set equal to zero.

- K-band Interferometer

The central science instrument run on GRACE is the KBR which is a dual one-way ranging system. This means that on each satellite the KBR assembly sends two own signals in K- and Ka-band (24.5 and 32.7 GHz, respectively) generated by the USO towards the other satellite and receives the corresponding two signals of the other S/C. At the same time the own signals serve as reference signals. As the frequencies are slightly shifted between both S/Cs the signals of each frequency band are generated with frequency f_1 on S/C 1 and with f_2 on S/C 2. A detailed description of the signal processing and modelling can be found in [Kim 00] of which the main facts are reproduced here.

For each frequency band the IPU of satellite i extracts the fractional phase of its reference signal ($\varphi_i(t)$) as well as of the signal received from satellite j ($\varphi^j(t)$). These phase measurements are downlinked to the ground processing facility where they are first of all time-tagged with GPS time and interpolated to common nominal epochs. Differencing the phase measurements results in single-frequency carrier phase measurements

$$\varphi_i^j(t) \quad = \quad \varphi_i(t) - \varphi^j(t) + \mathit{correction\ terms} \tag{3-2}$$

for each S/C with the correction terms comprising integer ambiguities, phase shifts due to ionosphere etc., and random measurement noise.

By forming the sum the dual one-way phase measurement (DOWP)

$$\theta(t) = \varphi_1^2(t) + \varphi_2^1(t) + \mathit{correction\ terms} \tag{3-3}$$

results for each frequency band with phase errors due to drift and frequency instability of the USO cancelled out. Based on the DOWP measurement the biased range

$$\begin{aligned} R(t) \quad &= \quad \frac{c}{f_1 + f_2}\theta(t) \\ &= \quad \rho(t) + \mathit{correction\ terms} \end{aligned} \tag{3-4}$$

with

c	*speed of light*
$\rho(t)$	*instantaneous range between both S/Cs*

is formed for K- and Ka-band observations respectively, with the correction terms accounting for, among others, the Time of Flight (TOF) difference of the signals due to satellite motion as well as for errors due to ionospheric refraction. Combining the biased ranges of both frequencies analogously to GPS L1 and L2 measurements as

$$\begin{aligned} R_{L3}(t) &= \frac{\overline{f}_K^2 R_K - \overline{f}_{Ka}^2 R_{Ka}}{\overline{f}_K^2 - \overline{f}_{Ka}^2} \\ &= \rho(t) + correction\ terms \end{aligned} \tag{3-5}$$

with

$$\begin{aligned} \overline{f}_K^2 &:= \sqrt{f_{K,1} f_{K,2}} \\ \overline{f}_{Ka}^2 &:= \sqrt{f_{Ka,1} f_{Ka,2}} \end{aligned}$$

gives an ionosphere-free (L3) biased range with the ionospheric errors cancelling out. This is the primary K-band observation. By digitally filtering the biased ranges K-band range-rate (KBRR) observations $\dot{\rho}(t)$ are derived. These KBRR data are finally used as observations in the proper POD and parameter estimation processing done with EPOS-OC (see below).

- Accelerometer

In order to determine high-quality Earth reference frames by POD it is crucial to account for the effects of non-gravitational forces exerted by air drag and radiation pressure. This can be done either by modelling or by measuring them. At the low altitude of the GRACE LEOs these forces have a significant influence on the orbits, and therefore they have to be measured accurately as there are no models available that are precise enough. For this purpose on each GRACE S/C the integral acceleration of the satellite's centre of mass due to non-gravitational forces is measured by an onboard accelerometer. This is done by a SuperSTAR accelerometer operated on either satellite. Developped by ONERA (France), this type of accelerometer evolved from CHAMP's STAR device ([Tou 98]). It is a six-axis, electrostatic accelerometer with a proof-mass enclosed in a cage. For keeping the proof-mass levitating electric forces are applied that are a measure of the non-gravitational forces acting on the satellite. By means of the measured electric forces of six axes, the linear as well as the angular accelerations can be derived. Due to the design there are two highly sensitive axes, and one less sensitive axis ([Tou 98]). The less sensitive axis is aligned with the satellite's cross-track direction the lowest non-gravitational perturbations are expected along.

- Star Camera Assembly

The absolute orientation of each satellite w.r.t. an inertial reference frame is permanently determined by a set of two star camera assemblies (SCAs). They have a field of view of 18^o by 16^o, and view the sky at a 45^o-angle with respect to the zenith, c.f. Fig. 3.2. The incoming light enters each assembly by a stray light baffle and goes through optical tools, and is finally detected by a CCD camera ([Dun 03]). The CCDs take images of the stars visible in the field of view, and compare them to star catalogues ([Fro 06]). After further processing the absolute orientation with respect to the "fixed" stars is determined represented by quaternions $q = (q_0, q_1, q_2, q_3)$, c.f. [Wu 06]. The SCA was developped by DTU (Danish Technical University), and is as well inherited from the CHAMP mission.

Knowing the exact orientation of each S/C is indispensable for correctly modelling the perturbation forces as well as for calculating certain partial derivatives needed in the process of differential orbit adjustment. Moreover, the nominal attitude w.r.t. the Earth and to the other satellite has to be maintained for telemetry and the KBR laser link to work properly.

Figure 3.4: *Typical IGS ground station (from [IGS 12a]).*

- Laser Retro-Reflector

On the bottom side of each satellite, see Fig. 3.3, there is a Laser Retro-Reflector (LRR) mounted consisting of four cube corner prisms arranged in a compact frame. Its purpose is to reflect laser pulses back to emitting ground Satellite Laser Ranging (SLR) stations. Originally developped by GFZ for the CHAMP mission and described in detail in [Neu 98] it is used as well aboard each GRACE S/C. The coordinate reference point of the respective satellite, i.e. its centre of mass, and the optical centre of its LRR are separated by the LRR offset vector. This offset vector is set to -0.6 m in x-, to -0.3275 m in y-, and to +0.2178 m in z-direction within the satellite-fixed coordinate system as defined in Fig. 3.3.

Tracking a satellite's orbit by SLR additionally to GPS is very useful as it allows for an independent validation of the orbit.

3.2 Ground Stations

Global Positioning System

In order to establish the link between the geometry and the gravity field of the Earth by tracking the GPS satellites, as shown in Fig. 1.2, a global network of GPS ground stations is necessary. The network used is that of the International GNSS Service (IGS, [IGS 12a]). According to [Dow 09] it consists of approximately 400 globally distributed tracking stations each made up of a monument carrying a GPS antenna, a GPS receiver, and an ultra-stable clock. A typical GPS site is shown in Fig. 3.4.

For ensuring a minimum level of quality the IGS set up guidelines ([IGS 12f]) containing the requirements each station has to meet. So, the receivers used have to be dual-frequency tracking both, code and phase even in the case of A-S. This means they have to observe the carrier phase on L1 and L2, as well as P-code on L2, and at least C/A- or P-code on L1. They have to track simultaneously at minimum eight satellites at a sampling rate of maximally 30 s with an elevation cutoff angle not exceeding 10^o. Each antenna used must have a well-defined phase pattern revealing a stability of the antenna phase centre of ± 2 mm horizontally, and ± 4 mm vertically. The phase centre variations (PCVs) have to be given in the official IGS PCV file (e.g. [IGS 12c]) based on calibrations. The antennas have to be rigidly attached to the monument allowing for not more than 0.1 mm motion. As the position of a GPS site is determined by the coordinates of the corresponding primary marker, i.e. its coordinate

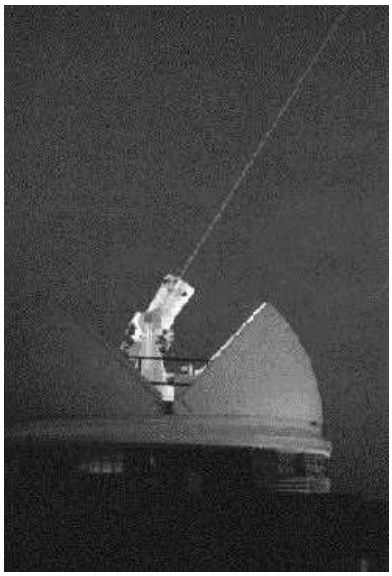

Figure 3.5: *Typical ILRS ground station (from [ILRS 12a]).*

reference point, and the proper measurement is made at the GPS antenna's position, the ARP offset vector has to be known with 1 mm or better. Local ties between GPS sites and the measurement devices of other space-geodetic techniques are not relevant here as the are only GPS ground station positions estimated in the context of this work.

Those requirements finally lead to a high quality of the IGS products as indicated in [Dow 09] or in [IGS 12e].

Satellite Laser Ranging

A valuable tool for an independent validation of satellite orbits determined by GPS are Satellite Laser Ranging (SLR) observations. SLR tracking data represent directly the distance between an SLR ground station and the satellite given by multiplying the measured two-way TOF of the laser signal with the speed of light. The SLR ground stations belong to the tracking network of the International Laser Ranging Service (ILRS, [Pea 02]), a typical site of it is shown in Fig. 3.5. Currently (2012), the network consists of about 48 operational stations each collocated by an IGS or IGS-standard GPS receiver. Being one of the space-geodetic services of the IAG the ILRS collects, evaluates, and distributes SLR observations to a multitude of Earth-orbiting satellites. Thereby the ground stations are run by various national institutions.

The SLR station network is not uniformly distributed around the globe with the great majority of stations located on the northern hemisphere with a strong concentration in Europe. As the SLR data are merely used for validation in the present context, the fact of the non-uniform spatial distribution of the network does not represent a significant drawback.

Derived from the full-rate tracking data so-called normal points (NPs) are distributed to the user community. Those NPs are caclulated following an algorithm accessible on the ILRS website [ILRS 12a]. For SLR data to be suitable for validation purposes it has to be of good quality. This is ensured by the ILRS through certain criteria each station has to meet, see [ILRS 12b]. Concerning the data quality the criteria are defined in such a way that within a period of three consecutive months a station has to submit at least 50 passes to selected geodetic satellites satisfying

- a NP RMS of 1cm,

- a short-term range bias stability of 4 cm,
- a NP acceptance rate of 80%.

As the distance measured refers to the ground stations's laser reference point (LRP), i.e. the optical centre of the laser instrument, the LRP offset vector between the ground station's marker and the LRP, also called eccentricity, has to be known with an accuracy on the level of a millimetre.

Error sources of the SLR technique include tropospheric and relativistic signal delay, as well as time delay inside the instrument, c.f. [See 03, 8.4.1]. The tropospheric and the relativistic effects are accounted for by models, c.f. Table F.3, whereas the time delay, caused by missing coincidence of the instrument's geometric reference point and its electronic zero point, is determined by calibration.

3.3 Software

Orbit Determination and Parameter Estimation

The software system used for carrying out Precise Orbit Determination (POD) and parameter estimation tasks is GFZ's EPOS-OC (Earth Parameter and Orbit System, see [Zhu 04]). It is a state-of-the-art software system capable of processing a multitude of different satellite observation types beside GPS and SLR. An essential property of EPOS-OC are its well-engineered algorithms that allow for a fast processing. Based on development work of approximately two decades it is possible to derive satellite orbits and Earth System Parameters by rigorous physical modeling of the forces acting on satellites thus minimising the number of artificial parameters like, e.g., empirical accelerations that have to be estimated. The modelling of observations and orbit forces as well as the background models used, as outlined in the subsequent sections, are implemented accordingly. EPOS-OC has been successfully applied at GFZ for many years for generating predictions for LEOs ([Sno 09]), for POD of GPS and LEO satellites resulting in so-called Rapid Science Orbits ([KoR 06]), as well as for deriving GFZ's EIGEN gravity fields ([För 07]). An overview of the process flow in EPOS-OC is given in Fig. 3.6.

Orbit Comparisons

For comparing satellite orbits GFZ's software tool EPOS-OA is used. Reading the orbits of the respective satellites from two different files, it calculates, after interpolation to common epochs, if necessary, on the one hand the direct position differences, and, on the other hand, it carries out seven-parameter Helmert transformations. The position differences are determined per epoch for each satellite separately for all three spatial components that can be chosen to be locally along-track, cross-track, and radial or globally X, Y, and Z. The Helmert transformations are performed per satellite as well as for the whole satellite constellation in each case resulting in three translations, a global scale, and three rotations. As part of each Helmert transformation the position differences in global X-, Y-, and Z-coordinates as well as the 3D differences are calculated before and after applying a spatial similarity transformation of the satellites' positions using the seven parameters estimated by the Helmert transformation.

Comparison of Ground Station Networks

In order to compare two networks of ground stations seven-parameter Helmert transformations between their coordinates are carried out using GFZ's SIMTRA software. This tool estimates three translations, a global scale, and three rotations of a spatial similarity transformation between both networks. Additionally, for each station separately the differences in the coordinates before and after ('misclosures') applying the spatial similarity transformation are calculated for the X-, Y-, and Z-component.

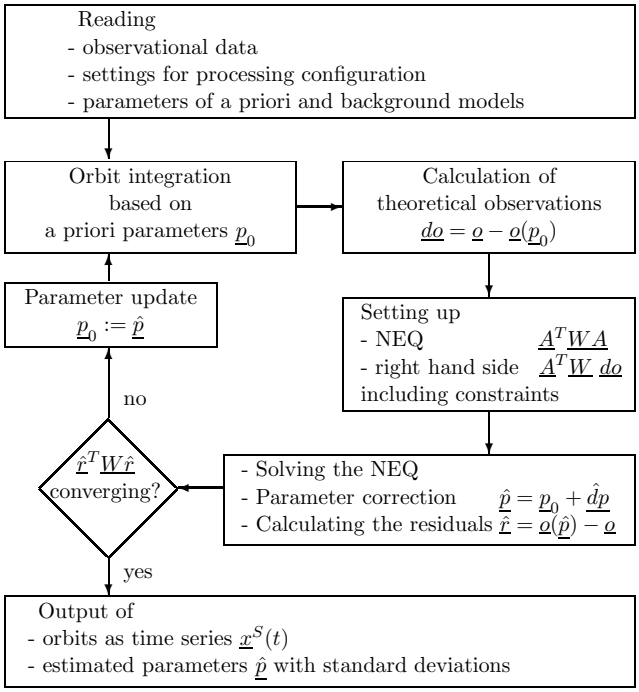

Figure 3.6: *Process flow in EPOS-OC. The "settings for processing configuration" comprise the begin and end epoch of the arc, the integration step size, the choice of time and coordinate systems etc.*

3.4 Data

The observational data used can be classified into ground data and satellite data each of them shortly characterised in the sequel. An overview of the data sets used is given in Table 3.1. The time span covered by the data sets used extends from 2004-02-04 to 2005-02-28 (391 days), due to missing K-band data the period 2004-01-01 to 2004-02-03 could not be processed. It should be noted that in case of GPS observations the measurements finally processed by EPOS-OC are zero-differenced L3 ionosphere-free linear combinations (LCs).

Ground Data

The ground data comprise GPS code and phase measurements (GPS-ground) collected by the GPS ground stations as well as laser ranging data (SLR) stemming from the SLR ground stations.

- GPS-ground

Originally the GPS data are retrieved as daily RINEX files from IGS. Before the GPS observations are introduced into the proper processing they are subject to a preprocessing.

This preprocessing consists first of all of some file reformatting, applying the P1-C1 biases, and cycle slip detection. Then, the satellites' initial elements are derived from IGS orbits and prepared accordingly for usage in EPOS-OC, and initial values of the satellites' clocks are generated from broadcast information. By a geometric optimisation about 70 uniformly distributed ground stations are selected. Within this optimisation the Earth surface is subdivided into 74 sectors of equal area, and one station per sector is selected if possible. In case several stations come into consideration for a sector priority is given to the site possessing the highest data volume. At maximum three maser

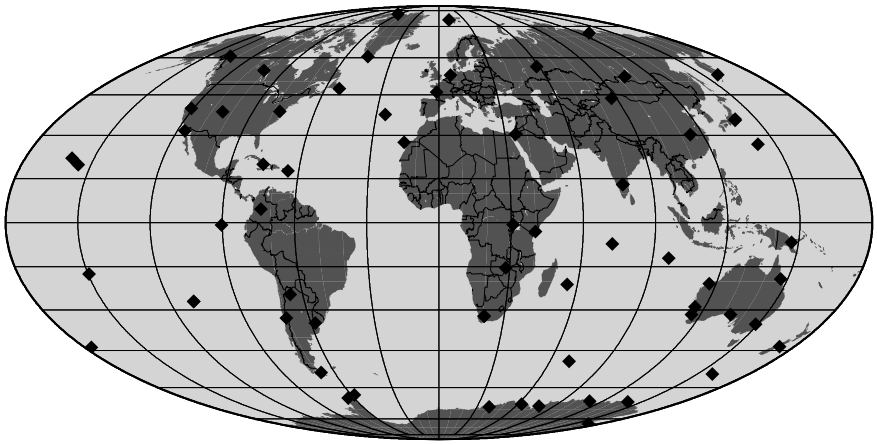

Figure 3.7: *Typical GPS ground station selection (2004/06/30).*

stations are selected in order to provide a highly accurate reference to GPS time. A sample ground station selection is shown in Fig. 3.7.

Subsequently, a preliminary calculation of the ground stations' clock offsets and rates as well as of phase ambiguities is carried out. Out of the three maser stations the clock revealing the lowest rate is selected as reference clock for the arc to be processed. The GPS-ground measurements are reduced to a temporal resolution of 30 s, to be used in EPOS-OC, for all ground stations thus coinciding with the integration step epochs of the GPS satellites. As revealed by post-fit residuals to be presented in Chapter 6, the phase measurements are on a level of precision of about 7 mm.

- SLR

The SLR data consist of Normal Points (NPs) provided by the ILRS in quick-look format. They are retrieved from the ILRS data centres and are merely reformatted at GFZ. As these observations are rather taken at opportunity than continuously they reveal a sparse coverage in time. On average, there are about 200 NPs per day for each GRACE satellite and roughly 10 NPs per day for each of the GPS satellites PRN05 and PRN06. The single-shot accuracy for CHAMP is in the range of 1 to 2 cm ([CHAMP 12]) and should be of comparable quality for GRACE and the GPS S/Cs PRN05 and PRN06. By applying the LRR offset vector of the satellite tracked the measurements are referred to the S/C's centre of mass.

Satellite Onboard Data

The group of satellite onboard data taken aboard the GRACE LEOs comprises the GPS satellite-to-satellite tracking data (GPS-SST), K-band observations (KBR), accelerations (ACC) and attitude (ATT). They are preprocessed by JPL from Level L0 to level L1B. Details about the preprocessing can be found in [Wu 06] and [Cas 02]. L0 denotes the level of the raw data as telemetred from the satellite to the ground. In a next step L1A data are generated by non-destructive processing, in detail by conversion from binary to ASCII, time-tagging to respective receiver clock time, editing, and adding

quality control flags. Finally, L1B data are gained by correct time-tagging to GPS time and filtering, thereby reducing the data sampling rate.

- GPS-SST

The GPS-SST measurements are collected by the onboard GPS receiver of each GRACE S/C. Due to its dual-frequency capability all code and carrier phases can be measured. According to [Cas 02] these are the C/A- and P-code on L1 as well as the P-code on L2, and in total three carrier phases of the two signals on L1 and the single signal on L2 as is obvious from Eq. (3-1) totalling six observations. Previous to be used in EPOS-OC for the purpose of this work, the GPS-SST data are subject to a further preprocessing at GFZ similar to the preprocessing of the GPS-ground data. Thereby the data volume is thinned out to 30-s intervals in order to fit the integration step size of the GPS satellites. By applying the ARP offset vector pointing from the satellite's centre of mass to the ARP and by applying the PCVs, the measurements are reduced to the S/C's centre of mass. Post-fit residuals to be reviewed in Chapter 6 show a level of precision of the L3 ionosphere-free phase observations of about 2 mm.

Table 3.1: *Data sets used; the temporal resolution of the data "as used" is chosen to match the integration step size of the corresponding satellites, see Section 2.2.*

Observation		Preprocessing	Temporal Resolution [s]		
Type	Source	Facility	of raw data	after preprocessing	as used
GPS-ground	IGS	GFZ	≤ 30	30	30
SLR NPs	ILRS	ILRS	-	-	-
GPS-SST	GRACE	JPL, GFZ	1	10	30
K-band	GRACE	JPL	0.1	5	5
ACC	GRACE	JPL	0.1	1	5
ATT	GRACE	JPL	1	5	5

- K-band

The raw measurements are instantaneous fractional phases of the received K-band signal as well as of the reference signal taken onboard each GRACE S/C at a frequency of 10 Hz. Finally, the phase data are converted to biased dual one-way range, range rate and range acceleration, and thereby filtered to 5-s data intervals matching the integration step size of the GRACE satellites. For the proper processing done with EPOS-OC only the K-band range-rate (KBRR) observations are used. Phase centre corrections determined within the L1B preprocessing are applied to the KBRR data during the POD and parameter estimation processing. Thus they are reduce to the satellites' centres of mass. The KBRR post-fit residuals as discussed in Chapter 6 indicate a level of precision around 0.2μm/s.

- ACC

The accelerations are measured by the on-board accelerometers. They comprise raw linear accelerations (3 components, 10 Hz data rate) and raw angular accelerations (3 components, 1Hz data rate). Within the L1B preprocessing they are filtered to 1-s time intervals. In order to fit the GRACE satellites' integration step size they are later reduced to a time interval of 5 s for use in EPOS-OC. Aboard each GRACE satellite, by means of a mass trim assembly as mentioned above coincidence of the centre of the accelerometer and the S/C's centre of mass is maintained. Analysing real data [Fro 06] revealed the precision achieved in terms of standard deviations to be $3 \cdot 10^{-10}$m/s^2, $2 \cdot 10^{-10}$m/s^2, and $7 \cdot 10^{-10}$m/s^2 for the along-track, the radial, and the cross-track axis, respectively.

- ATT

ATT denotes the attitude quaternions provided by the two star cameras on each GRACE S/C. Originally output by each star camera with a frequency of 1 Hz, the raw quaternion data from both cameras are combined within the preprocessing and filtered to a temporal resolution of 5 s for the same reason as for the K-band and ACC data. According to [Fro 10] the noise level of the quaternions, expressed in angular measure, is in the range of 9” to 11”.

Chapter 4

Reference Frame Determination

According to a widely accepted convention a reference frame is the physical realisation of a reference system. A reference system comprises conventions, constants, and algorithms whereas a reference frame is realised by a set of positions (and velocities) for physical points on the Earth surface. This work is dedicated to the determination of a Terrestrial Reference Frame (TRF) within well-established conventions, physical constants, as well as algorithms as listed in Table F.3 and mainly based on [Pet 10].

4.1 Components of a TRF

By identifying the components of a TRF a clear idea should be developped about the Earth system parameters searched for. A TRF in the geodetic sense consists of a geometric frame and a dynamic frame. Each frame requires an origin, an orientation, and a scale to be defined. This is done by convention as described in the following.

Geometric Frame

The geometric frame is determined by a set of ground station markers attached to the Earth's crust. In this it is the basis of a global Earth coordinate system for geolocation purposes. Its origin, orientation, and scale are indirectly defined by the triplet (x,y,z) of 3D spatial coordinates assigned to each marker.

Its origin $\underline{O}_G = (0,0,0)^T$, here also denoted as geometric geocentre, is arbitrarily defined by convention. In the end it is related to the coordinates assigned to the markers that define its location w.r.t. the Earth's crust. A natural definition would be to let $\underline{O}_G$ coincide with the Centre of Figure (CF) of the entire Earth surface S_E as applied in [Don 97], [Don 03], and [Ble 06a]:

$$\underline{O}_G := \frac{1}{S_E} \iint_{S_E} \underline{x} dS \qquad (CF) \tag{4-1}$$

with

$\underline{x}$	*position vector of an arbitrary point on the Earth's surface*
S_E	*total surface of the Earth*

In practice, however, S_E can only be approximated by a finite set of markers with geocentric position vectors $\underline{x}_{S,i}$. So, $\underline{O}_G$ would have to be defined as the Centre of Network (CN; [Wu 12]):

$$\underline{O}_G := \frac{1}{N}\sum_{i=1}^{N}\underline{x}_{S,i} \qquad (CN) \tag{4-2}$$

In this case $\underline{O}_G$ depends on the chosen set of ground stations. Of course, CN coincides the more with CF the more evenly and densely the markers are distributed on the Earth's crust.

The geometric orientation is defined by the direction of the three orthogonal base vectors $\underline{e}_x, \underline{e}_y, \underline{e}_z$ of the underlying coordinate system w.r.t. the Earth's crust. While the x-axis base vector $\underline{e}_x$ is given by the intersection of the Greenwich meridian plane with the equatorial plane, $\underline{e}_z$ points towards the North Pole. $\underline{e}_y$ completes the set of base vectors to a right-handed system $(\underline{e}_x, \underline{e}_y, \underline{e}_z)$. Finally, the scale is given by the speed of light.

Beside these fundamental definitions of origin, orientation, and scale all three items may as well be defined w.r.t. another geometric frame considered as a reference by means of a seven-parameter Helmert transformation between both frames. Then, the estimated translations T_x, T_y, T_z define the origin, the estimated rotations R_x, R_y, R_z the orientation, and the scale is defined as estimated by the scale parameter S. Such a procedure is only advisable if the geometric frame used as reference is of high quality, i.e. well adjusted and reflecting the mean evolution of the network's geometry over a long time span. This is e.g. the case for ITRF2008 ([Alt 11]).

Dynamic Frame

The dynamic frame is determined by the gravitational field of the Earth whose potential V at a point with geographical coordinates (r, φ, λ) can be represented by the well-known expansion into spherical harmonic base functions, c.f. [Tor 01, 3.3.2]:

$$V(r,\varphi,\lambda) = \frac{GM_E}{a_E}\left[\sum_{n=0}^{N}\left(\frac{a_E}{r}\right)^{n+1}\cdot \cdot \sum_{m=0}^{n} P_{nm}(\sin\varphi)\left(C_{nm}\cos(m\lambda) + S_{nm}\sin(m\lambda)\right)\right] \tag{4-3}$$

with

n, m	*degree, order*
GM_E	*geocentric gravitational constant, see* [Pet 10, 1.2]
a_E	*equatorial radius of the Earth, see* [Pet 10, 1.2]
P_{nm}	*associated Legendre functions*
C_{nm}, S_{nm}	*spherical harmonic coefficients*
r	*geocentric radial distance*
φ	*geocentric latitude*
λ	*geocentric longitude*

The dependence of V on the spherical coordinates r, φ, λ suggests the gravitational potential is defined w.r.t. the coordinate system of a geometric frame. Within such a coordinate system the gravity field coefficients C_{nm}, S_{nm} of low degree possess a geometric meaning([Tor 01, 3.3.4]):

- C_{00}

This coefficient is simply the ratio of the instantaneous mass of the central body and its nominal mass M_E:

$$C_{00} = \frac{1}{M_E}\iiint_B dm \qquad \approx 1 \tag{4-4}$$

That way it acts as the scale of the dynamic frame.

- C_{11}, S_{11}, C_{10}

As integrals over the Earth body B the degree-one terms are written as

$$\begin{aligned} C_{11} &= \frac{1}{a_E M_E}\iiint_B x dm \qquad &= \frac{1}{a_E} x_{CM} \\ S_{11} &= \frac{1}{a_E M_E}\iiint_B y dm \qquad &= \frac{1}{a_E} y_{CM} \\ C_{10} &= \frac{1}{a_E M_E}\iiint_B z dm \qquad &= \frac{1}{a_E} z_{CM} \end{aligned} \tag{4-5}$$

This means they are the rescaled x-, y, and z-components x_{CM}, y_{CM}, and z_{CM} of the Earth's CM in the above series defining the dynamic frame's origin. The CM is also denoted as dynamic geocentre in the context of this work. In case the CM coincides with the geometric geocentre these coefficients vanish.

- C_{20}

The integral representation of this gravity field coefficient reads as

$$C_{20} = \frac{1}{a_E^2 M_E}\iiint_B \left(z^2 - \frac{x^2+y^2}{2}\right) dm \tag{4-6}$$

expressing the negative polar flattening of the gravity field. For that reason it plays an important role in geophysics as variations in this coefficient reflect - among others - the response of the visco-elastic Earth to changes in surface loading caused by geophysical masses like ice or snow.

- $S_{21}, C_{21}, S_{22}, C_{22}$

Those gravity field coefficients of degree two have the following integral representations:

$$\begin{aligned} S_{21} &= \frac{1}{a_E^2 M_E}\iiint_B yz dm \\ C_{21} &= \frac{1}{a_E^2 M_E}\iiint_B xz dm \\ S_{22} &= \frac{1}{2a_E^2 M_E}\iiint_B xy dm \\ C_{22} &= \frac{1}{4a_E^2 M_E}\iiint_B (x^2 - y^2) dm \end{aligned} \tag{4-7}$$

Thus, S_{21}, C_{21}, and S_{22} are directly proportional to the moments of deviation (products of inertia) about the x-, y-, and z-axis as in the above order. This means they represent the deviation of the principal axes of inertia of the Earth body from the axes of the geometric frame. With the principal axes of inertia being the natural set of axes of the dynamic frame these coefficients are measures of the orientation of the dynamic frame w.r.t. the geometric frame. Caused by deformations of the Earth gravity field due to lunisolar global deformations of the Earth's body, daily variations are expected for S_{21} and C_{21}. It has to be noted that such variations simply reflect changes of the orientation of the Earth gravity field w.r.t. the geometric frame; variations of the coordinates of points on the Earth's surface, on the other hand, are unaffected by changes in S_{21} and C_{21}.

Finally, C_{22} is the difference of the moments of inertia about the y- and the x-axis, respectively. Thus, this parameter serves as a measure of the flattening of the gravity field either along the y- or the x-axis. It is estimated in this context, too, in order to prevent unmodelled changes to distort the other estimated spherical harmonic coefficients.

In the context of this work the dynamic frame is defined to be represented by all of the aforementioned gravity field parameters except C_{22} being regarded as a by-product for which reason it is not treated in the sequel.

4.2 Estimating a TRF

Parameter Space

In order to determine simultaneously a geometric frame as well as a dynamic frame constituting a TRF appropriate parameters have to be estimated based on the procedure described in Chapter 2 using the space-geodetic observations introduced in Chapter 3. The whole set of parameters to be estimated is subdivided into the two major groups of TRF parameters and auxiliary parameters. While the TRF parameters directly represent the geometric frame and the dynamic frame, the auxiliary parameters serve to adequately model orbit forces as well as the observations taken.

- TRF parameters

As visualised in Fig. 1.2 the configuration of the measurement system consists of ground tracking stations, of LEOs, and of GPS satellites. Within this assembly the dynamic and the geometric frame are linked through the tracking of the GPS satellites. Due to their rather low orbit altitude the GRACE LEOs are highly sensitive especially to the low-degree gravity field coefficients that are needed to establish the dynamic frame. For determining a TRF the parameters have to be identified that have to be estimated in a differential orbit adjustment (POD and parameter estimation processing). An overview of the estimated TRF parameters is given in Table 4.1.

Table 4.1: *Estimated TRF parameters and their sensitivity to observation types; 'xx' indicates the major contributor, 'x' indicates a supporting contributor.*

Observation type	GPS-ground	GPS-SST	KBRR
TRF Parameters			
$(C,S)_{nm}$ (n=1)	x	xx	
$(C,S)_{nm}$ (n=2)	x	x	xx
$\underline{x}_S$	xx	x	

In order to determine a geometric frame the geocentric coordinates $\underline{x}_S$ of the GPS ground station markers contained in the parameter vector $\underline{p}$ are estimated. Offline, i.e. after the differential orbit adjustment is finished, origin, scale, and orientation of the geometric frame are estimated by the

parameters T_x, T_y, T_z, S, R_x, R_y, R_z of a seven-parameter Helmert transformation between the estimated station coordinates $\underline{\hat{x}}_S$ and the a priori ones $\underline{x}_{S0}$. This means that the geometric frame to be determined is implicitly given by the estimated coordinates $\underline{\hat{x}}_S$, and that the parameters of the Helmert transformation simply represent the deviation of the geometric frame, as given by $\underline{\hat{x}}_S$, from the a priori model $\underline{x}_{S0}$ in terms of origin, scale, as well as orientation. $\underline{x}_{S0}$, thereby, is not completely arbitrary; it should already be quite close to the geometric frame $\underline{\hat{x}}_S$ in order to ensure the least-squares estimation model (2-28) to be linear. Moreover, applying this methodology it has to be ensured that the ground station network used is very dense and uniformly distributed over the Earth surface.

Exploiting the geometric meaning of the gravity field coefficients up to degree and order two, origin, scale, and orientation of the dynamic frame can be determined by estimating directly the corresponding gravity field coefficients within a differential orbit adjustment based on an a priori gravity field model. However, estimating a scale in form of C_{00} is problematic as it is highly correlated with the scale of the geometric frame through the satellites' radial position components. Also due to the direct proportionality of C_{00} to the total Earth mass it does not make sense to estimate this parameter as the total mass can be assumed constant over the short time spans considered here. Therefore the scale factor between the a priori and the estimated gravity field is fixed to 1.0.

For determining the dynamic geocentre, i.e. Earth's CM, various methods exist as summarised in [Wu 12]. On the one hand there are *geometric* methods, e.g. [Fri 10], used to derive geocentre motion from measured Earth surface deformations. Another method used is the *dynamic* method where the dynamic geocentre is determined as sensed by Earth-orbiting satellites within a fixed geometric frame. This method makes use of the fact that the satellites permanently orbit around Earth's CM defining the dynamic geocentre. Of course, the geometric frame used is not physically fixed as it is permanently deformed by the motion of the lithospheric plates, and in general the composition of stations used varies on a daily basis as not every station is available each day. However, *fixed* in the sense used here merely means that the station coordinates are not estimated. Basically, the Integrated Approach followed here is such a dynamic approach with the difference that the geometric frame is not treated as *fixed* but that it is also tried for estimating parts of it. As explained in Section 4.1 the dynamic geocentre components searched for are then given by the estimated gravity field coefficients of degree one (C_{11}, S_{11}, C_{10}). They finally represent an offset of the dynamic geocentre w.r.t. the CM of the a priori gravity field. Such a translation, also called geocentre motion, is caused by mass redistributions inside the Earth and, mainly, on the Earth's surface. By directly estimating the degree-one gravity field coefficients from the motion of LEOs this approach bears the advantage of directly measuring the integral effect of all mass redistributions taking place. Possible correlations with the geometric geocentre resulting in a datum defect are addressed in Section 4.3.

Determining the orientation of the dynamic frame is done by estimating S_{21}, C_{21}, S_{22}. The remaining gravity field coefficient of degree two, C_{22}, is estimated as a by-product.

- Auxiliary Parameters

In order to account for mismodelling some auxiliary parameters have to be estimated. These parameters are subdivided into dynamic and geometric parameters.

The dynamic auxiliary parameters are necessary for accurately modelling the satellite orbits. They comprise the satellite state vectors at the beginning of the arc $\underline{x}^{S0} = \underline{x}^S(t_0)$ (initial elements), coefficients for the GPS solar radiation force model, accelerometer calibration coefficients, and coefficients for modelling empirical accelerations. Though essential for a POD to be carried out and not used to account for mismodelling the initial elements are subsumed among the auxiliary parameters as they are no direct TRF parameters.

To account for error sources influencing the observations, a number of geometric auxiliary parameters are needed. These are GPS transmitter and receiver clock errors δt^S and δt_R, respectively, tropospheric signal delays for GPS-ground measurements, GPS phase ambiguities, as well as empirical parameters for KBRR observations.

Observation Equations

As already pointed out in Eq. (2-5) the observations used have to be expressed as functions of the parameters influencing them. These functional relations being the basis for the linear parameter estimation algorithm as outlined in Section 2.3 are presented in the sequel. In Appendix E the linearisation of the GPS-ground, GPS-SST, and KBRR observations is treated in detail. A general reference for setting up GPS observations and their linearisation is [Teu 98]. The GPS observation equations as presented here are tailored to the processing capabilities of EPOS-OC.

- GPS-ground

As mentioned in Section 3.4 the GPS measurements, taken at the phase centres of the GPS ground stations' as well as the LEOs' antennas, consist of code (C) and carrier phase (Φ) measurements on both the L1- and the L2-signal. Since the observations finally used are L3-LCs of corresponding L1- and L2-measurements ionospheric signal delays of first order cancel out, see Appendix E. For part of the processings done (RL05, see Table F.3) ionospheric signal delays $\delta_{iono,L3}$ of higher order are accounted for by ionosphere maps ([IGS 12d]). Several further corrections of the range ρ_G^S between the phase centres of the respective sender antenna as well as the receiver antenna have to be considered. These include relativistic signal delay, tropospheric signal delay, and corrections due to antenna PCOs as well as PCVs. Displacements of the ground station positions due to solid Earth tides loading as well as solid Earth pole tide loading are taken into account, too. In Table F.3 the models used for calculating the various corrections are listed.

The tropospheric signal delay is modelled per ground station as the product of an a priori delay T_0 and a scaling factor T_G that is estimated as a time series using the observational data. Thereby the a priori delay is obtained by mapping the sum of the dry and the wet zenith delay onto the respective elevation applying one of the mapping functions indicated in Table F.3. In order to refer the measurements to the respective coordinate reference points, $\underline{x}_S$ and $\underline{x}^S$, besides accounting for the PCOs and PCVs, as well the ARP offset vector has to be taken into account in case of ground stations, as explained in Section 3.1.

As the GPS carrier phase observable represents only a fractional part of a full wavelength the number of remaining wavelengths $N_{G,L3}^S$, also called "carrier phase ambiguity", for each pair of a GPS satellite and a receiving station has to be determined in order to fit the observational equation. This is done per satellite pass, and if necessary after cycle slips occurred. In case of raw L1- and L2-observations this carrier phase ambiguity is an integer number but for L3-linearly combined phase observations, as used here, it is a real number. Thus, see Section 5.1, for one processing part (RL04m) it is merely estimated as a real number whereas for the other part (RL05m) side constraints for double-differenced L3-ambiguities are computed and introduced into the NEQ of the least-squares parameter estimation (see Eq. (2-30)). The method applied for setting up those side constraints follows a procedure outlined in [Ble 89] and [Ge 08]. It is comparable to determine the L1- as well as the L2-ambiguities as integer numbers, and helps reduce significantly the part of the L3-carrier phase measurement noise that is due to the standard deviation of the ambiguity parameter.

For any GPS ground station 'G' with geocentric position vector $\underline{x}_G$ and GPS satellite 'S' the associated phase and code observations of type "GPS-ground", are the L3-LCs of the respective L1 and L2 code and carrier phase measurements, $C_{G,L3}^S$ and $\Phi_{G,L3}^S$, respectively. Their linearised observation equations read as

$$\begin{aligned} C_{G,L3}^S(t_G) &\doteq C_{G,L3}^S(t_G)|_0 + < \left(-\underline{u}_G^S\right)_0, \underline{\Delta x}_G > + \\ &\quad + c\Delta\delta t_G - c\Delta\delta t^S + T_0\Delta T_G \qquad (4\text{-}8) \\ \Phi_{G,L3}^S(t_G) &\doteq \Phi_{G,L3}^S(t_G)|_0 + < \left(-\underline{u}_G^S\right)_0, \underline{\Delta x}_G > + \\ &\quad + c\Delta\delta t_G - c\Delta\delta t^S + T_0\Delta T_G + \Delta N_{G,L3}^S \qquad (4\text{-}9) \end{aligned}$$

with

t_G	*epoch of signal reception at G*
$\underline{u}_G^S$	*unit vector pointing from G to S*
c	*speed of light ([Pet 10])*
T_0	*a priori tropospheric signal delay (model)*
$\underline{\Delta x}_G$	*correction to a priori coordinates of G ($\underline{x}_{G0}$)*
$\Delta\delta t_G$	*correction to a priori clock offset w.r.t. GPS time of G*
$\Delta\delta t^S$	*correction to a priori clock offset w.r.t. GPS time of S*
ΔT_G	*correction to a priori tropospheric scaling factor*
$\Delta N_{G,L3}^S$	*correction to a priori L3-ambiguity*

It should be noted that Eqs. (4-8) and (4-9) differ only by the phase ambiguity term $N_{G,L3}^S$. The parameters to be estimated comprise $\underline{\Delta x}_G$, $\Delta\delta t_G$, $\Delta\delta t^S$, ΔT_G, and $\Delta N_{G,L3}^S$. As the GPS ground stations are the only ones positions are estimated for the vector $\underline{x}_S$ constituting the geometric TRF contains only their position vectors $\underline{x}_G$. $C_{G,L3}^S(t_G)|_0$ as well as $\Phi_{G,L3}^S(t_G)|_0$ represent the calculated observations using a priori parameter values. They contain among others the correction terms $\delta_{iono,L3}$, $\delta\rho_{rel}$, $\delta\rho_{PCO,L3}$, $\delta\rho_{PCV,L3}$, $\underline{\Delta x}_{G,ARP}$, $\underline{\Delta x}_{G,ARP}$, and $\underline{\Delta x}_{G,load}$ present in the original non-linearised observation equations (E-5) and (E-6) as well as in the range equation (E-3).

- GPS-SST

Analogously to GPS-ground, the GPS observations of type "GPS-SST" are modelled similarly except for some peculiarities. In contrast to the GPS-ground case no tropospheric signal delays are accounted for due to the LEO's high altitude. Additionally, the range term ρ_L^S, Eq. (E-10), is not corrected for loading displacements, and the correction due to PCOs only contains the offsets of the GPS satellites' antennas. I.e., for the GRACE POD antennas no PCOs are considered but only PCVs. The ARP offset vector used in case of the LEOs is indicated in Section 3.4. Again, the models applied for calculating the various corrections are listed in Table F.3. Finally, with 'L' denoting a LEO receiver station the linearised GPS-SST observation equations read as

$$C_{L,L3}^S(t_L) \doteq C_{L,L3}^S(t_L)|_0 + c\Delta\delta t_L - c\Delta\delta t^S \tag{4-10}$$

$$\Phi_{L,L3}^S(t_L) \doteq \Phi_{L,L3}^S(t_L)|_0 + c\Delta\delta t_L - c\Delta\delta t^S + \Delta N_{L,L3}^S \tag{4-11}$$

with

t_L	*epoch of signal reception at L*
c	*speed of light ([Pet 10])*
$\Delta\delta t_L$	*correction to a priori clock offset w.r.t. GPS time of L*
$\Delta\delta t^S$	*correction to a priori clock offset w.r.t. GPS time of S*
$\Delta N_{L,L3}^S$	*correction to a priori L3-ambiguity*

As is obvious the observation equations for any GPS measurements directly contain only geometric parameters entering the vector $\underline{p}_G$ introduced in Section 2.1. Indirectly the GPS observations also depend on the dynamic parameters in $\underline{p}_D$ through the satellite positions $\underline{x}^S$ present in the range terms ρ_G^S and ρ_L^S.

- KBRR

As already mentioned in Section 3.1 the K-band observable used in this context is the unbiased K-band range-rate (KBRR) $\dot{\rho}_{KB}$ between GRACE-A and GRACE-B. It is derived from the nominal unbiased K-band range ρ_{KB} as its derivative w.r.t. time plus a polynomial P = P(P_1,P_2,C_0,S_0,$\dot{v}(t)$,$u(t)$,t), c.f. Appendix E. Based on the investigations of [Kim 00] such a polynomial reveals to be necessary in order to account for the influences of unmodelled residual perturbation forces on the KBRR measurement at frequencies of 0 Hz (constant) and one cycle per orbit revolution. The coefficients P_1, P_2, C_0, and S_0 are of empirical nature and therefore denoted as "K-band Empirical Parameters". Like the GPS case, this type of observation equation directly contains only geometric parameters, and is indirectly dependent on the dynamic parameters in $\underline{p}_D$ through $\underline{x}^S$ and $\dot{\underline{x}}^S$. The linearisation of the observation equation (E-11) w.r.t. all parameters is outlined in Appendix E. Since the differential position and velocity vectors between the satellites involved, $\underline{x}_{12}$ and $\dot{\underline{x}}_{12}$, are not treated as variables the linearisation is actually carried out only w.r.t. the parameters of the polynomial P resulting in

$$\begin{aligned} \dot{\rho}_{KB} &= \dot{\rho}_{KB}|_0 + \\ &\quad + \Delta P_1 + 2t\Delta P_2 + \dot{v}(t)\cos u(t)\Delta C_0 - \dot{v}(t)\sin u(t)\Delta S_0 \end{aligned} \tag{4-12}$$

where

t	*measurement epoch*
$\dot{v}(t)$	*mean anomaly rate*
$u(t)$	*argument of latitude*
ΔP_1	*correction to range-rate bias of polynomial model*
ΔP_2	*correction to range-acceleration bias of polynomial model*
ΔC_0	*correction to range bias cos amplitude of periodic model*
ΔS_0	*correction to range bias sin amplitude of periodic model*

The parameterisation actually chosen for KBRR measurements is indicated in Tables G.1 and G.4.

- SLR

The SLR observations used are one-way travel times $\tau^S_{GS,1}$ of the laser signal between the SLR ground station GS and the LRR mounted on the respective satellite S which are derived from the original NPs representing two-way signal travel times. For the same reason the ARP offset vector has to be considered in case of GPS-ground observations the LRP offset vector $\underline{\Delta x}_{GS,LRP}$, i.e. the spatial offset between the ground station marker (coordinate reference point) and the LRP, has to be accounted for. The same applies to the LRR offset vector $\underline{\Delta x}^S_{LRR}$ between the LRR and the satellite's centre of mass. In total, the SLR observation equation reads as (c.f. Appendix E)

$$\tau^S_{GS,1} = \frac{1}{c}\rho^S_{GS} + T_0 + \delta\rho_{rel} \tag{4-13}$$

with

$$\begin{aligned} \rho^S_{GS} &= |\underline{x}_{GS}(t_{LRR}) + \underline{\Delta x}_{GS,LRP} + \underline{\Delta x}_{GS,load} \\ &\quad -(\underline{x}^S(t_{LRR}) + \underline{\Delta x}^S_{LRR})| \end{aligned} \tag{4-14}$$

where

c	*speed of light ([Pet 10])*
T_0	*a priori tropospheric signal delay (model)*
$\delta\rho_{rel}$	*relativistic range correction (model)*
$\underline{x}_{GS}$	*geocentric coordinate vector of the marker of GS*
$\underline{x}^S$	*geocentric coordinate vector of the centre of mass of S*
$\underline{\Delta x}_{GS,load}$	*displacement of the marker of GS due to loading*
t_{LRR}	*epoch of signal reflection at the LRR of S*

However, in the context of this work SLR observations are only used for orbit validation. Therefore, the parameters appearing in Eq. (4-13) will not be estimated, and the observations are assigned a very low weight within the least-squares estimation (c.f. Section 2.3) in order not to influence the other parameters.

- ACC

The ACC data stem from the onboard accelerometers of the LEOs and represent the measured spatial acceleration $\underline{\ddot{x}}_m$ caused by all surface forces ($\underline{F}_{drag}$, $\underline{F}_{sol}$, $\underline{F}_{alb}$) acting on the satellite body, see Section 2.2. They are treated as errorless observations and are merely used in the equations of motion (2-6) for providing the sum of surface forces to the total sum of forces. For that reason they do not enter the vector $\underline{o}$ within the least-squares estimation procedure (c.f. Section 2.3), and consequently they do not influence the estimated parameters in Eq. 2-30. On the other hand, the measured accelerations need some calibration due to instrumental deficiencies. As proposed by [Schw 00] biases and scale factors for the measurement axes contained in vectors $\underline{b}$ and $\underline{k}$ respectively have to be estimated. By applying the biases and scale factors following

$$\underline{\ddot{x}}_c = \underline{b} + \underline{K}\,\underline{\ddot{x}}_m \tag{4-15}$$

with

$\underline{\ddot{x}}_m$	*3D vector of measured accelerations $\ddot{x}_{m,i}$ (i = 1, 2, 3)*
$\underline{\ddot{x}}_c$	*3D vector of calibrated accelerations $\ddot{x}_{c,i}$ (i = 1, 2, 3)*
$\underline{b}$	*3D vector of accelerometer biases b_i (i = 1, 2, 3)*
$\underline{K}$	*3x3 diagonal matrix of accelerometer scale factors*
i	*spatial component*

the measured accelerations $\underline{\ddot{x}}_m$ become calibrated observations $\underline{\ddot{x}}_c$. The biases and scale factors represent dynamic parameters entering the vector $\underline{p}_D$ introduced in Section 2.1. They are estimated based on the other observations appearing in $\underline{o}$ that contribute to the least-squares estimation procedure. By solving the variational equations (2-14) the necessary partial derivatives $\partial\underline{o}/\partial\underline{p}_D$ of those observations w.r.t. the accelerometer biases and scale factors are obtained.

In summary, the vector $\underline{o}$ of observations is filled as follows:

$$\underline{o} = \begin{pmatrix} \underline{C}_{ground} \\ \underline{\Phi}_{ground} \\ \underline{C}_{SST} \\ \underline{\Phi}_{SST} \\ \underline{\dot{\rho}}_{KB} \\ \underline{\tau}_{SLR} \end{pmatrix} \tag{4-16}$$

It should be emphasised that the SLR observations $\underline{\tau}_{SLR}$ are assigned a very low weight compared to the remaining observations in order not to influence the parameter estimation.

Expected Sensitivities

In order to successfully estimate the unknown parameters it has to be ensured that the observations used are sensitive to them. Table 4.1 presents a qualitative overview of the expected contribution of each observation type to the different Earth system parameters.

Thereby, GPS-ground measurements are the major contributor to estimating ground station positions $\underline{x}_S$, and thus to deriving the scale S as well as the orientation parameters R_x, R_y, R_z of the geometric TRF. Due to the high altitude of the GPS satellites GPS-ground contributes only very weakly to the estimation of gravity field coefficients.

The GPS-SST observations represent the link between the GRACE satellites that are highly sensitive to changes in the gravity field and the GPS satellites that act as an outer reference frame much less influenced by gravitational disturbances. For that reason GPS-SST measurements are indispensable for determining the gravity field coefficients of degree one. Moreover, they are expected to enhance the quality of the estimated ground station coordinates by stabilising the GPS orbit constellation.

In contrast, KBRR observations contribute significantly only to the determination of the gravity field coefficients of degree two as they deliver only the rate of change of the distance between both GRACE satellites but no absolute displacements of their orbits. Concerning the gravity field coefficients of degree two, however, their contribution is very strong due to their extremely high measurement precision.

Principally, SLR observations are suited for determining gravity field coefficients, ERP, and ground station coordinates. In particular, they would be very helpful for defining the geometric scale as they represent directly measured distances between ground stations and satellites without the necessity of estimating an ambiguity term as in case of GPS measurements. However, as mentioned above, they are only used for validation purposes in the context of this work.

4.3 The Inherent Datum Defect

Prior to making efforts to estimate parameters for defining a dynamic frame and a geometric frame it has to be clear whether the parameters are solvable and whether they can be separated from each other. This question is investigated in the following applying an empirical strategy based on simulated observations. First some basic simulations are carried out in order to identify a possible severe datum defect that would prevent any processing. Secondly, supplementary simulations should reveal a hidden datum defect that is not severe but might deteriorate some parameters. In both cases ground and space-borne GPS data are simulated based on up-to-date a priori models acting as reference. By systematically changing these a priori models and introducing them into a recovery process of POD and parameter estimation the deviations of the estimated parameters of the dynamic frame and of the geometric frame from the reference can be analysed. This procedure finally leads to the qualification

of the intrinsic datum defect of the chosen solution as well. The basic simulations presented here can also be found in [KoD 12].

Basic Simulations

For the basic simulations a satellite constellation is chosen consisting of all GPS satellites available and a single CHAMP-type LEO ([Rei 99]). The ground station network is synthetic consisting of 60 regularly distributed stations on a 30^ox30^o mesh not including the poles. Using such an ideal ground station network is advantegeous in order to exclude disturbing effects coming from a non-uniform distribution of the stations. Investigating such disturbing effects would be worthwile but is not pursued here. The a priori and background models used are mainly those of RL04 as indicated in Table F.1. The orbit perturbations due to non-conservative forces are modelled according to accelerations resulting from CHAMP POD based on real data. Fixing all a priori models, GPS observations are simulated as L3-LCs with a temporal spacing of 30 s, a measurement standard deviation (STD) of 0.5 m (ground stations) and 0.3 m (LEOs) for code observations as well as 5.0 mm (ground stations) and 3.0 mm (LEOs) for phase observations. By choosing these STDs for the phase observations which might seem to be rather high it should be ensured that the results obtained are not on an artificially high level of accuracy but rather realistic. For the GRACE-type satellite pair also K-band range rate (KBRR) observations are simulated as an inter-satellite link with a temporal spacing of 5 s and a measurement STD of 0.3 μm/s. The observational data is simulated for any distinct satellite constellation. Each test covers the same period of 28 days consisting of daily solutions of 24 h length. For both the simulations as well as the subsequent POD and parameter estimation the software used is GFZ's EPOS-OC as described in Section 3.3. The recoveries are carried out as combined POD and parameter estimation processes following the Integrated Approach outlined in Chapter 2 using the simulated data and modified a priori models. As specified in Section 4.2 the parameters solved for comprise, on the one hand, TRF parameters being the gravity field coefficients $(\mathrm{C,S})_{nm}$ up to degree and order two as well as the ground station coordinates $\underline{x}_S$, and, on the other hand, auxiliary parameters given by the initial elements $\underline{x}^{S0}$ as well as dynamic and geometric parameters for modeling orbit perturbations and measurement errors, respectively. Earth Rotation Parameters (ERPs; polar motion, UT1-UTC) are not estimated as this simulation study should examine the possibility to separately estimate the TRF parameters as specified in Section 4.2. Thus, this simulation study is consistent with the parameter space of the real-data processing done within this work. Moreover, not solving for ERPs ensures a clear interpretation of the results obtained, especially concerning the rotation about the Earth's z-axis. The a priori model changes are applied to C_{10}, C_{11}, S_{11} and to all station coordinates by adding 6 cm to each parameter of these parameter groups. I.e., the gravity field as a whole and the complete set of ground station positions are translated in x, y, and z by this amount. 6 cm in all three spatial directions corresponds to roughly 10 cm in 3D. Such a model change does not harm the linearity of the least-squares estimation but causes a clear effect.

Assessment of the results is done by comparing the estimated parameters to the unbiased model values. In case of the gravity field coefficients this is simply done by calculating the difference between the corresponding parameters. The estimated ground station coordinates are compared to the reference coordinates by 7-parameter Helmert transformations using the SIMTRA software, c.f. Section 3.3, per daily solution delivering global translations in T_x, T_y, T_z, a global scale S, and global rotations R_x, R_y, R_z. Analogously, the orbits are compared to the reference orbits by 7-parameter Helmert transformations using EPOS-OA (Section 3.3). Those reference orbits are the orbits from the simulation process that is based on the unchanged a priori models. In the following, for the sake of intuitive comparison, all non-metric parameters are rescaled to metric distances on the Earth surface.

The test cases presented here are arranged in four groups, the results are presented in Table 4.2. All parameters not considered here are resolved very well in all test cases. Concerning the Helmert transformations between the orbits, results of the transformations only between the GPS orbits are discussed since the results of the transformations between the LEOs' orbits do not differ significantly

from the GPS results. In Table 4.2 the values given are the mean values together with the STDs of the respective 28-day time series. It should be noted that a STD refers to the mean of a series of values, i.e. it indicates the series' remaining deviation after removing the mean. As a reference for all test cases serves an initial test called "standard case" hereafter, i.e. an integrated solution of the CHAMP-GPS constellation without imposing any a priori constraints on any estimated parameter.

First of all it should be stated that for all test cases the resolved values in the x- as well as in the y-component are very stable and accurate: their STDs do not exceed 0.3 mm, the mean values are between -0.1 and +0.1 mm. This means that both components are extremely well solvable simultaneously. Therefore the following discussion is focusing on the z-component.

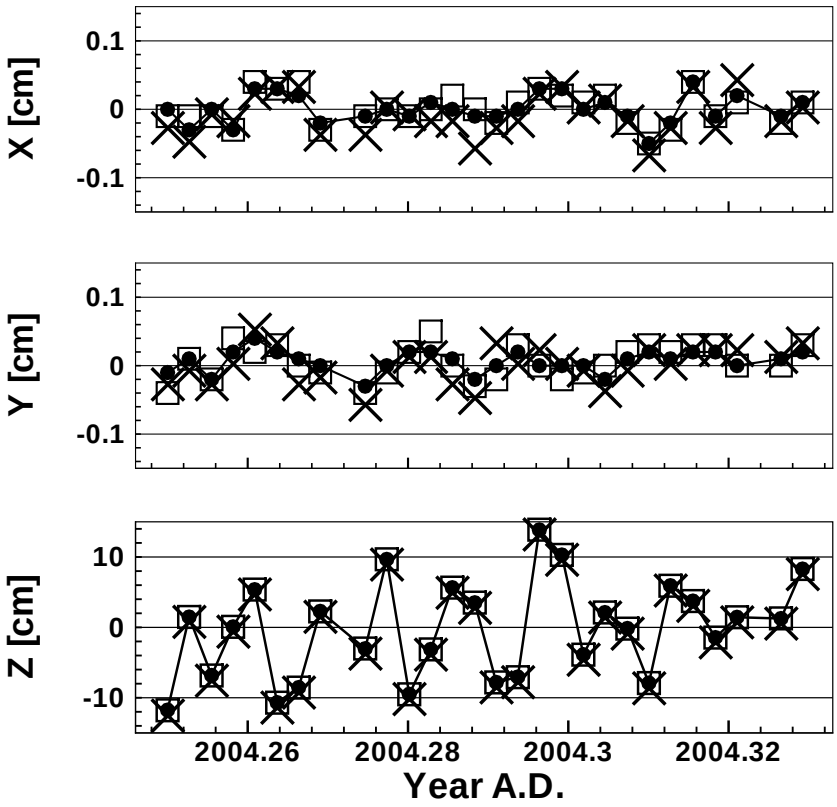

Figure 4.1: *Basic simulations: time series of the deviation from the reference of dynamic geocentre (circles), geometric geocentre (squares), and translations of GPS orbits (crosses) for the standard case (no constraints).*

In order to give an idea of the characteristics of the solutions, the time series of the translational parameters of the dynamic geocentre, the geometric geocentre as well as of the GPS orbits are shown for the standard case in Fig. 4.1. The maximum difference between the time series is 0.4 mm in the x-, 0.6 mm in the y-, and 0.7 mm in the z-component. From this it can be concluded that the translational parameters are highly correlated in each spatial component; considering that the time series of both geocentres and of the translations of the GPS orbits reveal the same sign it is clear that they represent the same physical effect.

The first test case derived from the standard case, called "Constrained initial elements" in Table 4.2, is a solution where the initial elements of all satellite orbits are constrained with a STD of 1.0 mm to their a priori values. Regarding the z-component of the translational parameters the standard case cannot resolve them as seen by the STDs between 68.5 and 68.7 mm corresponding to the modelled changes of 6 cm. The case with perfect orbits, on the other hand, delivers a stable day by day recovery of these parameters with STDs of 0.2 mm. In contrast, for the standard case, the mean values of the

Table 4.2: *Basic simulations: mean values and standard deviations of time series resulting from different test cases; the characteristics of each test case indicate the discrepancy w.r.t. the standard case.*

Test Case	Characteristics	Deviations from Reference				
		mean standard deviation				
		Geocentre	Station Coord.		GPS orbits	
		C_{10}	TZ	RZ	TZ	RZ
		[mm]	-[mm]-		-[mm]-	
Standard	LEO used: CHAMP	-2.4	-2.4	+28.1	-2.5	-28.1
	No constraints	±68.5	±68.6	±205.7	±68.7	±205.7
Constrained initial elements	Standard deviations of	0.0	0.0	0.0	0.0	0.0
	initial elements: 1 mm	±0.2	±0.2	±0.0	±0.2	±0.1
Constrained station coordinates	Standard deviations of	+57.8	+57.9	+0.4	+57.8	-0.4
	station coordinates: 10 cm	±2.4	±2.4	±1.8	±2.5	±1.7
Multi-LEO constellation	LEOs used:					
	GRACE (no KBRR)	-3.2	-3.2	-77.8	-3.3	+77.8
		±101.0	±101.2	±296.2	±101.2	±296.2
	CHAMP+GRACE (no KBRR)	-5.0	-5.0	+24.3	-5.0	-24.3
		±47.8	±47.9	±122.9	±47.9	±122.9
	CHAMP+GRACE (+ KBRR)	-8.5	-8.5	-9.5	-7.7	+9.5
		±23.3	±23.4	±152.1	±23.4	±152.1
Additional GPS orbit plane	Orbital elements: a = 26600 km,	-11.2	-11.3	+21.8	-11.3	-21.7
of 5 satellites	e = 0.005, i = 89^o, $\Omega = 85^o$	±55.7	±55.8	±169.9	±55.8	±169.9

z-translations deviate from the reference by -2.5 to -2.4 mm only. So, by sampling over a certain time period an unbiased solution can be gained. The whole constellation of ground stations and satellite orbits is rotationally unstable about the z-axis as can be seen by considering the RZs in the standard case with STDs of 205.7 mm and mean biases of +28.1 and -28.1 mm.

Again with perfect orbits the RZs could be resolved day by day with STDs of 0.1 mm maximum and no biases. Summarizing, an integrated CHAMP-GPS constellation solution delivers highly accurate daily x- and y-components of the geometric and dynamic origin simultaneously, however the z-translations need long-term sampling to become free of systematics. With perfect orbits, however out of reality, daily resolution of the z-translations would be possible and the rotational defect would disappear. The obvious asymmetry between the x- and y-components on the one hand and the z-component on the other hand will be investigated by means of supplementary simulations to be presented in the next subsection.

In the second test case ("Constrained station coordinates" in Table 4.2) 10-cm stochastic constraints are imposed on the station coordinates. Such constraints have been in use for operational GPS processing for a long time at GFZ for producing GPS RSOs for preventing any impact of unexpected antenna changes on the overall solution. As revealed by the STDs of 2.4 to 2.5 mm, c.f. Table 4.2, this case leads to much more stable time series of the z-translations than the standard case with STDs of 68.5 and 68.7 mm. On the other hand, in case of constrained station coordinates the biases of these time series, +57.8 to +57.9 mm, are at the level of the artificial shift of 6 cm. This is certainly due to the constraints of 10 cm that are relatively strong compared to the changes of 6 cm. Regarding the RZ estimates, as opposed to the standard case, the case of constrained station coordinates causes the solutions to become rotationally stable about the z-axis as revealed by STDs of 1.7 and 1.8 mm and biases of +0.4 and -0.4 mm. So, in summary putting 10-cm a priori constraints on the station coordinates allows to efficiently care for the rotational stability of the solution. If such a solution is used for resolving the geocentre motion with expected amplitudes in the millimeters, c.f. [Don 97], the 10-cm a priori constraints would allow the recovery of daily translations with a few mm accuracy, however with a severely biased z-component.

The third group of tests, named "Multi-LEO constellation" in Table 4.2, aims at clarifying the effect of making use of additional LEOs or of KBRR observations. Using a GRACE satellite pair without KBRR data leads to increased STDs of 101.0 to 101.2 mm in the z-translations in comparison to the standard CHAMP case, c.f. Table 4.2. The reason may be that correlations of environmental perturbations between both satellites are not taken into account here, and that the GRACE satellites are less sensitive than the CHAMP S/C due to their higher altitude. In case of combining CHAMP and GRACE the STDs reduce to 47.8 to 47.9 mm being also smaller than in the standard case. By using KBRR data the STDs improve further down to 23.3 to 23.4 mm. This can be expected as combining CHAMP and GRACE means to increase the number of observations, and using KBRR data means to introduce high-quality relative measurements. Compared to the standard case the biases increase up to approximately -8 mm, however staying well below the STDs. Concerning the z-rotations the STDs behave similar as above for all cases with the only difference that they increase in case KBRR observations are introduced. But then they still remain below the level of the standard case. The biases of the z-rotations remain non-significant. In summary, combining CHAMP and GRACE as well as adding KBRR data helps to improve the rotational stability around the z-axis.

In the fourth and last test group, "Additional GPS orbit plane" in Table 4.2 the benefit of an additional near-polar GPS orbit plane of five equally distributed satellites is investigated whose Keplerian elements are a = 26600 km, e = 0.005, i = 89^o, $\Omega = 85^o$. Compared to the standard case the STDs of the translational parameters in Z reduce slightly. Also the STDs of the z-rotations are reduced. The biases in the z-translations and -rotations are not significant. Overall, an additional near-polar GPS orbit plane would make the z-translations and -rotations more stable but would not allow an accurate solution in the end.

The results of the basic simulations finally allow the conclusion that applying the Integrated Approach of space geodesy it is possible to determine simultaneously all gravity field coefficients except for C_{10} as

well as all components of a geometric reference frame except for its z- translation and its rotation about the z-axis. Even in the absence of any a priori constraints it is possible to resolve simultaneously the geometric and the dynamic x- and y-components with daily resolution. On the other hand, it follows that C_{10} as well as the z-translations and z-rotations of the ground station network and the GPS orbit constellation cannot be separated. This means there is a datum defect imminent to the chosen configuration of two comprising its z-translation and its rotation about the z-axis. An explanation might be that it is possible to shift the whole configuration in z-direction and to rotate it about its z-axis without changing the observations.

Furthermore, the following additional conclusions may be drawn. Averaging over a longer period leads to nearly unbiased z-coordinates of the origins. Also a perfect estimation of all the components of the origins apparently seems to be possible in case the orbits would become a factor of 10 more accurate than in current practice. Constraining the ground station coordinates removes the rotational freedom about the z-axis but leaves the z-translations unresolved. Extending the basic constellation by a GRACE-type satellite pair leads to improved stabilities of the z-translations and the z-rotations. This improvement is largely pronounced for the z-translations if KBRR data are used. An additional near-polar GPS orbit plane would not lead to a thorough elimination of the deficiencies in the z-translations and -rotations.

Supplementary Simulations

Within a similar processing environment supplementary simulations are carried out for a 30-day time span (June 2004) for investigating the stability of the estimated x- and y-translations. The procedure of evaluating the recoveries is the same as in the case of the basic simulations. In this case none of the a priori models used for simulating the GPS data is changed for the subsequent recoveries. The idea is to study the potential of recovering especially the translational parameters depending on the Earth rotation rate. For that reason GPS data are simulated for various Earth rotation rates starting at 1.0 revolutions per sidereal day and going down to 1/128 revolutions by bisecting each value. Data are simulated for a completely non-rotating Earth, too.

The recovered translational components of the dynamic geocentre, the geometric geocentre, and the GPS orbits origin are shown in Fig. C.2 for the case of a nominally rotating Earth (1.0 revolutions per sidereal day) and in Fig. C.3 for the case of a non-rotating Earth. For a nominally rotating Earth the result is comparable to the standard case of the basic simulations: the x- and y-translations are very well resolved with less than a millimetre deviation but the z-translation is very unreliable with amplitudes in the range of up to 10 cm. In case of a non-rotating Earth, however, also the x- and y-translations become not resolvable. As neither the a priori gravity field nor the a priori ground station coordinates were subject to dedicated changes this is a strong evidence that such dedicated changes, e.g. 6 cm in the case of the basic simulations, cannot be resolved.

In order to investigate the influence of the Earth rotation rate on the recovery of the translations further recoveries for various Earth rotation rates as mentioned above are performed. The mean values and STDs of the resulting time series are plotted in Figs. C.4 and 4.2, respectively. It can be recognised that for Earth rotation rates of less than 1/8 revolutions per sidereal day the time series of the resolved translations reveal significant biases and STDs of a few centimetres. This means that none of the three translational components can be resolved for such low Earth rotation rates. But for rotation rates of 1/8 revolutions and upward biases and STDs reduce to the mm-level in case of the x- and y-translations. In case of the z-translations, on the other hand, indeed the biases of the time series reduce down to zero but the STDs converge to around 5 cm meaning that the resolved z-component of the different origins remains not reliable per day.

Based on these supplementary simulations the conclusion may be drawn that beside the severe datum defect in the z-component of both translations and rotations there is as well a hidden datum defect in the x- and y-translation attenuated by Earth rotation. This means that T_x and T_y, the x- and

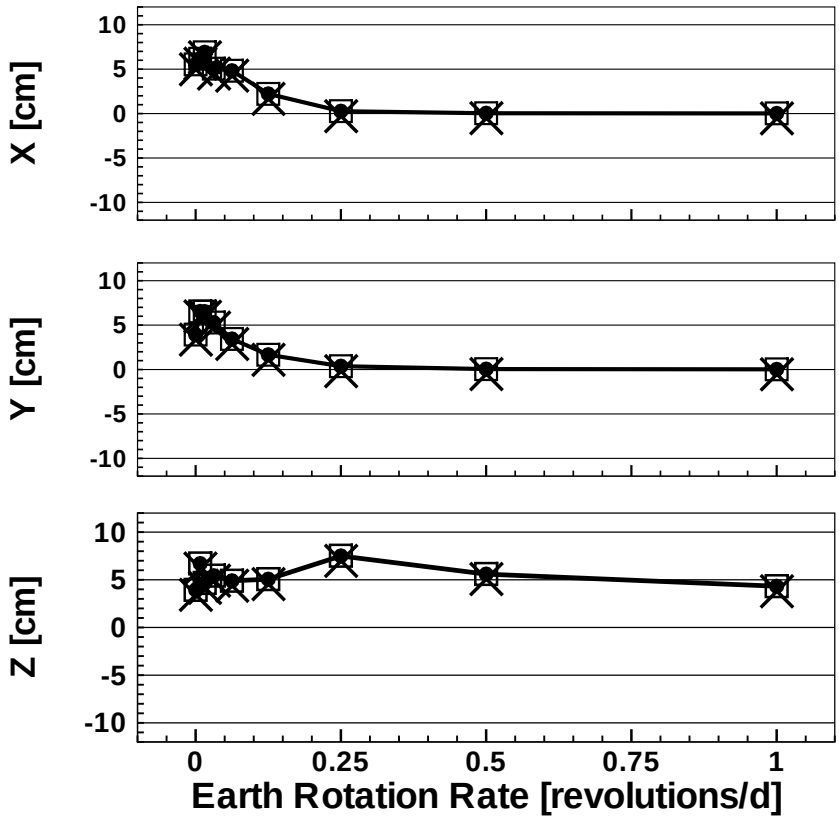

Figure 4.2: *Supplementary simulations: standard deviations of time series of dynamic geocentre (circles), geometric geocentre (squares), and translations of GPS orbits (crosses) vs Earth rotation rate.*

y-translation of the geometric frame, can be separated from C_{11} and S_{11} only because the Earth is rotating. As will be shown in Chapter 6 C_{11} and S_{11} can be improved at the expense of constraining T_x and T_y. Regarding the remaining parameters, e.g. R_x, R_y, S_{21}, and C_{21}, no difficulties in resolving them are detected here. Thus, they are assumed to be independently estimable in the context of this work. The deeper reason of this possibility is certainly given by the fact that any rotational defect is avoided as the ERPs are not estimated here.

Rectifying the Datum Defect

In order to carry out a TRF estimation following the Integrated Approach as described in Section 4.2 it is indispensable to rectify at least the severe datum defect of the translation in z-direction and the rotation about the z-axis revealed by the basic simulations. Moreover, it may be useful also to remove the two hidden defects of the x- and the y-translation. According to [Alt 02c] rectifying the geometric datum defect in the context of space-geodetic TRF determination can be achieved by constraining ground station coordinates (CC) or by imposing so-called "No-Net Conditions" (NN) on the normal equation.

- Constrained Coordinates (CC)

This method consists of introducing pseudo-observations into the NEQ system that set the estimated station coordinates $\underline{\hat{x}}_S$ equal to their a priori values at the level of a chosen STD. As already mentioned in conjunction with the basic simulations this method has been used in operational GPS-RSO processing at GFZ for many years in order to prevent a few stations with large estimated corrections

to their a priori coordinates to degrade the overall TRF solution. Such could happen e.g. in case of antenna switches or changes in the multipath regime at specific ground stations. In view of the quality of the TRF solution the drawback of constraining all coordinates of each station is that the solution obtained is overconstrained because there are $3N$ pseudo-observations introduced (if N is the number of ground stations involved) opposed to the maximum datum defect of four caused by the coordinate transformation parameters T_x, T_y, T_z, and R_z. On the other hand, constraining only a subset of ground stations lets considerable freedom to the estimated coordinates of the remaining stations that could finally distort the whole network.

- No-net Conditions (NN)

In order not to overconstrain the overall TRF solution there is a need of getting rid of exactly the inherent degree of freedom comprising three translations (T_x, T_y, T_z) and one rotation (R_z). This can be achieved by preventing the ground station network as a whole from shifting in x-, y, and z-direction as well as from rotating about the z-axis. In other words this means to force the frame to perform a no-net translation in the chosen direction and a no-net rotation about the specified axis. Such constraints can be imposed applying the NN method as outlined in Appendix D based on [Alt 02c]. The idea is to impose for each geometric datum defect a single suitable condition on the NEQ $\underline{N} = \underline{A}^T \underline{WA}$ in Eq. (2-30). For that reason the obtained TRF solution is called "minimum-constraints" ([Sil 01]) as only the minimum amount of constraints is introduced.

Technically, the necessary conditions are derived from an implicit similarity transformation between the coordinates $\underline{\hat{x}}_S$ of the TRF stations that are to be estimated and the coordinates $\underline{x}_r$ of a set of reference stations. Thereby the similarity transformation comprises only those transformation parameters needed to account for the datum defect. According to Appendix D the similarity transformation is then set up as

$$\underline{x}_r = [T_x\ T_y\ T_z]^T + \underline{R}_3(R_z)\underline{\hat{x}}_S \tag{4-17}$$

where

$\underline{x}_r$	*coordinates of a reference station network*
$\underline{\hat{x}}_S$	*coordinates of the TRF station network to be estimated*
$\underline{R}_3$	*matrix of rotation about the z-axis*
T_x, T_y, T_z	*translation in x-, y-, z-direction, respectively*
R_z	*angle of rotation about z-axis*

The resulting normal equation system of the NN-conditions is given by

$$\underline{B}^T \underline{W}_t \underline{B}\,(\underline{\hat{x}}_S - \underline{x}_0) = \underline{B}^T \underline{W}_t \underline{B}\,(\underline{x}_r - \underline{x}_0) \tag{4-18}$$

with

$$\underline{B} = \left(\underline{A}_t^T \underline{A}_t\right)^{-1} \underline{A}_t^T \tag{4-19}$$

$\underline{x}_0$	*a priori coordinates of the TRF station network*
$\underline{W}_t$	*weight matrix of T_x, T_y, T_z, R_z*

The a priori station coordinates $\underline{x}_0$ change from iteration to iteration within the iterative POD and parameter estimation procedure: they are given in the first iteration by the TRF station network read in by the program (EPOS-OC), and are then in the further iterations taken to be the estimated

coordinates of the respective preceding iteration. For each ground station contributing to the NN-conditions $\underline{A}_t$ contains the following three lines

$$\underline{A}_t = \begin{pmatrix} \vdots & \vdots & \vdots & \vdots \\ 1 & 0 & 0 & -y_{i,0} \\ 0 & 1 & 0 & x_{i,0} \\ 0 & 0 & 1 & 0 \\ \vdots & \vdots & \vdots & \vdots \end{pmatrix} \tag{4-20}$$

where

i	*number of the contributing station*
$x_{i,0}, y_{i,0}$	*a priori coordinates of i-th contributing station*

In Fig. 4.3 the principles of both the CC and the NN method of rectifying a geometric datum defect are visualised. As shown, CC conditions keep the estimated station coordinates bounded to their a prioris but let the frame translate, rotate, and change its scale. In contrast, NN-conditions prevent the network as a whole to move as specified by the chosen conditions but let the single stations some freedom to move.

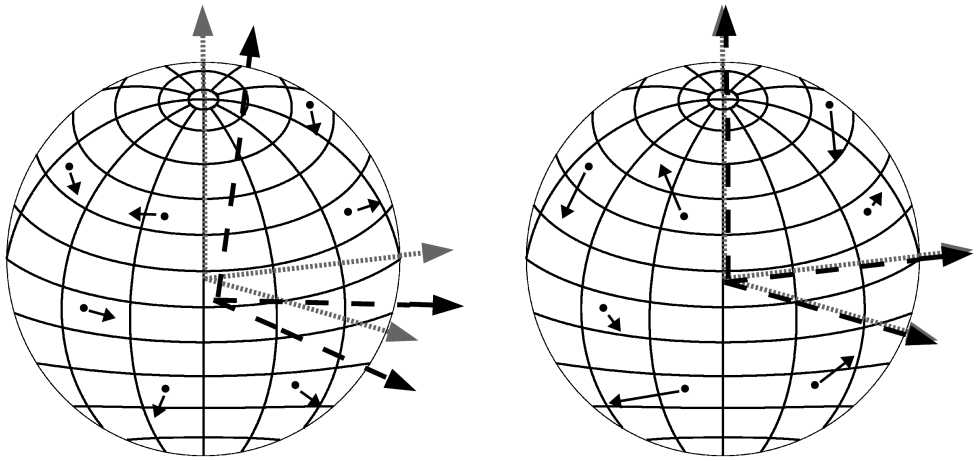

Figure 4.3: *Methods for rectifying a geometric datum defect: in case of constrained coordinates (left) each ground station can only variate within the chosen a priori sigma; in case of no-net conditions (right) the network as a whole is prevented to move, but not the individual stations.*

Chapter 5

Data Processing

Based on the prerequisites described in the preceding chapters data processings following the Integrated Approach are carried out. This processing is mainly subdivided into a data screening part resulting in an initial setup of integrated processing environments and a part comprising a test programme of different integrated runs. In order to obtain TRF parameters of daily resolution the length of the satellite orbits covers exactly one day. This time interval is also called "arc length" or shortly "arc". The whole time span processed extends from 2004/02/04 00:00:00 (JD2000 1494.5) to 2005/02/28 24:00:00 (JD2000 1885.5) resulting in nominally 391 days or arcs. Because of processing failures due to singular normal equation matrices, CPU failures, or other reasons this nominal amount of days can be reduced. Hereafter, "run" is used as an abbreviated form of a processing consisting of per-day POD and parameter estimation applying a specific set of models and a specific parameterisation, and covering the whole time span indicated above. The computational effort in processing such a long time span is quite considerable as the normal equation of each arc contains between 5000 and 6000 parameters to be estimated, and the amount of observations is on the level of 1,000,000 per day. Moreover, in case of applying L3-ambiguity constraining each run has to be carried out more than once as explained below. In sum, it takes approximately three hours on a PC for a single arc to be performed.

After setting up an initial environment a test programme of various integrated runs is carried out in order to study certain effects and eventually to improve the time series of the estimated TRF parameters. For the purpose of efficient referencing, each run is assigned a number of the format rr-nn-t, with "rr" denoting the release (4 or 5), "nn" the test number, and "t" the type (0: integrated; 1: two-step (GPS); 2: two-step (LEO)). Thereby, in case of a two-step processing, "t" indicates the step: "1" denotes the GPS-only part whereas "2" stands for the LEO-only part.

5.1 Models Used and Parameterisation

Due to several model upgrades and permanent developments of EPOS-OC the whole chain of data screening and integrated test runs are carried out based on upgraded GRACE RL04 standards (RL04++, [Fle 10a]), and are repeated based on GRACE RL05 standards ([Dah 12]). These standards apply for the models used whereas the chosen parameterisation differs slightly from the official GRACE releases. The parameterisations applied are summarised in Tables G.1 and G.4. They are denoted "RL04m" and "RL05m" representing *modified* versions of the official GRACE releases. A significant difference between RL05m and RL04m not mentioned in the tables is the fact that in the RL05m processing a method for handling the GPS ground stations L3-ambiguities as appearing in Eq. (4-9) is applied that is equivalent to fixing L1- and L2-ambiguities to integers. Precisely, this means that for double-differenced L3-ambiguities side conditions, as mentioned in Section 2.3, are computed and introduced into the NEQ system for least-squares parameter estimation (see Eq. (2-30)). The method applied mainly follows a procedure outlined in [Ble 89] and [Ge 08]. As this procedure is implemented

outside EPOS-OC each run with L3-ambiguity constraining has to be carried out twice. After a first run the side constraints for the double-differenced L3-ambiguities are set up outside EPOS-OC. The run is then repeated, with the constraints applied from that iteration onwards that was reached by the first run. This procedure is inevitable due to EPOS-OC-internal parameter numbering.

Models Used

The models used for the RL04m and RL05m processing are listed in Table F.3. In case of RL05m they are identical with the GRACE RL05 standards ([Dah 12]). Specifically, concerning the modelling of orbit forces an overview of the models used is given in Tables F.1 and F.2.

The models are state-of-the-art with those of GRACE RL05 being currently the most recent ones. An exception might be the use of the old ROCK4 solar radiation pressure model for GPS satellites that is currently the only one implemented in EPOS-OC. Specifically, concerning the a priori TRF used it should be noted that both ITRF2008 as well as IGS08 contain plate tectonic movements of the ground stations, and thus they ensure a very close a priori approximation of the station positions to physical reality.

Parameterisation

In Tables G.1 and G.4 the parameterisation chosen for the initial setup is specified that is basically determined by the RL04 and RL05 standards. The temporal resolution of once per day for TRF parameters is due to the goal of this work to derive variations of the dynamic frame and the geometric frame per day. Concerning the auxiliary parameters a compromise is chosen between a good adaptation of the parameterised models to physical reality on the one hand and computational burden on the other. The difference between the RL04m and RL05m parameterisations for the initial setup is the temporal resolution of the empirical accelerations for the GRACE satellites. With 16 parameters per day they are set up much denser compared to RL04m processing with only five in 24 h. To account for tropospheric signal delays of the GPS-ground measurements a quite dense parameterisation of 10 scaling factors per station is chosen resulting in a temporal resolution of 2.4 h. As well a rather dense series of 17 polynomial parameters and nine periodic parameters are chosen for modelling the empirical KBRR coefficients. These deviations from the RL04m and RL05m standards from RL04 and RL05, respectively, were found by extensive testing.

For establishing the weight model (2-24) per observation type a weight w is assigned to each measurement according to

$$w \;=\; w_{ii} \;:=\; f\sigma^{-2} \tag{5-1}$$

with

f : *real-valued factor per observation type*
σ : *a priori STD of the observation type*

Thereby the unit-less factor f serves for additionally weighting each observation type without changing σ. This weight w is entering the weight matrix $\underline{W}$ in Eq. (2-30) which is defined as a diagonal matrix.

Concerning the test programme of RL04m integrated runs the differences in parameterisation are listed in Tables G.2 and G.3. They differ regarding the ITRF used, the absolute phase centre corrections (PCCs) for GPS transmitter and ground receiver antennas, the handling of the gravity field coefficients as well as of the ground station coordinates, and the resolution of the empirical accelerations. For the weight model (5-1) the real-valued factor and the a priori measurement STD are indicated. Concerning handling the ground stations coordinates, "CC" stands for "Constrained Coordinates" and "NN" for

"No-net"-conditions as introduced earlier. Within the RL05m integrated processing the runs differ in gravity field coefficients, ground station coordinates, in the weight model, and in applying NN-conditions, c.f. Tables G.5 and G.6.

5.2 Initial Setup

Creating an initial setup, i.e., a basic processing environment for performing integrated runs, is preceded by a screening of the GPS-ground data as well as of the LEO onboard observations (GPS-SST, KBRR) for outliers. Thereby improved initial values of the various estimated parameters are obtained, too.

Data Screening: GPS-ground

As a first step the GPS-ground data is cleaned from outliers by eliminating each observation whose residual is larger than three times the STD of all residuals of this data type. In order to prevent these observations to influence the LEOs' data or parameters this is performed as GPS-only processing, i.e. merely by processing the GPS ground stations plus the GPS satellites. Beside cleaned data a consistent set of GPS satellite orbits and estimated clock parameters result.

Data Screening: GPS-SST, KBRR

Introducing the GPS orbits and clock parameters resulting from the preceding step as fixed, LEO-only processings using the GRACE onboard data are carried out. This data screening is done in two steps with the GPS-SST data cleaned first by setting an elimination limit of three times the residuals' STD as done in the GPS-ground case. Subsequently, using the cleaned GPS-SST data the KBRR observations are screened with a threshold of eight times the residuals' STD. Thereby, the factor eight was determined empirically during the development of the RL05 standards. Choosing the elimination limits as indicated is based on experience aiming at retaining as much observations as possible but eliminating gross outliers that are likely to distort some parameters.

Initial Integrated Run

The initial processing environment is finally obtained by merging the cleaned GPS-ground, GPS-SST, and KBRR data as well as the various a priori and background model files into a common environment. In view of the satellite constellation the twin GRACE LEOs are added to the GPS satellites. For RL04m processing the initial setup is given by run 4-00-0, see Table G.2, and run 5-00-0 is the initial run for RL05m processing, c.f. Table G.5. The parameterisation of these runs is the nominal one summarised correspondingly in Tables G.1 and G.4.

5.3 Computations

Integrated Processings

After the initial setup of the integrated processing being completed various test scenarios are carried out. By changing only a few items, preferably only one, at the same time it is tried to study certain effects and thereby improving the obtained time series of TRF parameters. Correspondingly for the RL04m as well as for the RL05m processing the specifications of the computations are summarised in Tables G.2, G.3, and in Tables G.5, G.6. They also contain the two-step processing and the SLR validation described below.

Two-step Processing

As already mentioned the commonly followed procedure for estimating TRF parameters based on LEO satellite-to-satellite tracking data is the Two-step Approach. There, in a first step only GPS-ground observations are processed resulting in GPS satellite orbits and clock parameters, as well as ground station coordinates. The GPS satellite orbits and clock parameters are subsequently introduced into a second step where only the GPS-SST and the KBRR data are used for estimating gravity field coefficients.

For the purpose of comparing the Integrated to the Two-step Approach also two-step processing is carried out. This is done by splitting an integrated run environment into its GPS and into its LEO part. As described above the GPS orbits and clock parameters of the GPS-only run are subsequently introduced as fixed into the LEO-run with GPS ground stations excluded. Within the RL04m processing such a two-step approach is given by run 4-04-1 representing the GPS-only part and by 4-04-2 as the LEO run. In case of the RL05m processing the corresponding runs are 5-02-1 and 5-02-2.

SLR Validation

Introducing SLR observations to the GRACE LEOs as well as to the GPS satellites PRN05 and PRN06 is an excellent means of validating the resulting orbits by an independent measurement technique. If added to the vector of observations (4-16) they have to be given a very low weight (5-1) in order to prevent them from influencing the POD and parameter estimation. As is done for the other observation types within such a run also for the SLR measurements the observational residuals are calculated. Assuming the modern SLR technique to deliver reliable range observations with a precision of a few mm those residuals are well suited to indicate the orbits' accuracy at the few mm-level.

Chapter 6

Discussion

In the following the results are presented stemming from the integrated runs carried out as outlined in the preceding chapter. Correspondingly, for the RL04m and the RL05m processing, runs 4-04-0 as well as 5-02-0 serve as reference for all others as they represent unconstrained integrated solutions with only the inherent datum defect rectified. Each of these runs is also performed as an equivalent two-step approach denoted by -1 and -2 instead of the trailing -0, c.f. Tables G.3 and G.5.

First of all, the time series of the estimated TRF parameters are shown for run 5-02-0 as well as the time series of the resulting observational residuals. Subsequently, results of the validation w.r.t. external sources are presented followed by the outcome of the two-step processing 5-02-1 and 5-02-2. Finally, some effects due to changing the parameterisation are discussed. The time series displayed in the sequel as well as the statistical measures given refer to the parameters themselves as obtained according to (2-25) by updating the a priori parameters $\underline{p}_0$ by the estimated corrections $\underline{\hat{dp}}$.

The measures used to assess the quality of the resulting time series are either the mean, the standard deviation (STD), or the root mean square (RMS) as appropriate to the parameter in question. In case the expectation of a parameter is zero a relatively small mean indicates that over the time span studied the parameter is estimated without systematic errors. On the other hand, a small STD of a time series reveals that the parameter is estimated reliably day by day.

For a perfect comparison of the processing results the number of arcs processed should be the same. Unfortunately, due to various reasons like CPU or input/output errors or singular normal equation matrices a few runs failed. For that reason, considering the full time span of 391 arcs for run 4-04-0 and run 5-02-0, there are 359 and 382 arcs successfully finished, respectively. Concerning the other runs within the corresponding processing group, RL04m or RL05m, the number of arcs might again differ from these reference values. Of course, it is desirable to have all results perfectly comparable, but in the end it is a minor issue in the context of the experimental studies carried out and presented here. The results to be presented below should anyway give clear evidence. It should be noted that the time series of the reference frame parameters presented are cleaned from only a few, i.e. not more than five and in most cases none, *large* outliers in order not to distort the derived statistical measures. Such procedure is certainly allowed in the context of this work which does not strive for developping an operational system but that is rather devoted to examine basic characteristics of the Intergrated Approach. There is a wide range of reasons for those outliers comprising undetected outliers among the observational data as well as ill-modelled perturbation forces leading to erroneous satellite orbits. Moreover, for the sake of not overcrowding the plots, the daily estimates constituting the time series are drawn without error bars. Instead, the maximum value of the STDs of the daily values is given where appropriate. If indicated in a corresponding metric unit, non-metric measures like gravity field coefficients, scale parameters or angles are rescaled to metric distance on the Earth surface by multiplication with the mean Earth radius. All figures displayed below within the text are reproduced in Appendix H.

6.1 TRF Parameters

For run 5-02-0 the estimated TRF parameters for both the geometric frame and the dynamic frame are treated in the following.

Geometric Geocentre

Though tightly constrained to zero by NN-conditions imposed on T_x, T_y, and T_z, each with a sigma of 0.1 mm, the components of the geometric geocentre are plotted in Fig. H.2 for the purpose of completeness. Their means and STDs of +0.23 ±0.33 mm, -0.12 ±0.38 mm, and +0.15 ±0.33 mm, respectively (Table I.1), indicate that the a priori ground station network follows well these constraints evenly in each component.

Dynamic Geocentre

The time series of the dynamic geocentre components are displayed in Fig. 6.1 with the corresponding statistical values listed in Table I.3.

Overall, the time series of C_{11} and S_{11} are of quite good quality with corresponding means of +1.20 mm, +3.64 mm and STDs of 3.87 mm, 4.21 mm. In contrast, C_{10} is worse determined with a mean of +5.88 and a STD of 6.03 mm. Not shown in Fig. 6.1, the maximum formal errors of the daily estimates are 0.95, 0.96, and 1.00 mm for C_{11}, S_{11}, and C_{10}, respectively, indicating stochastic significance.

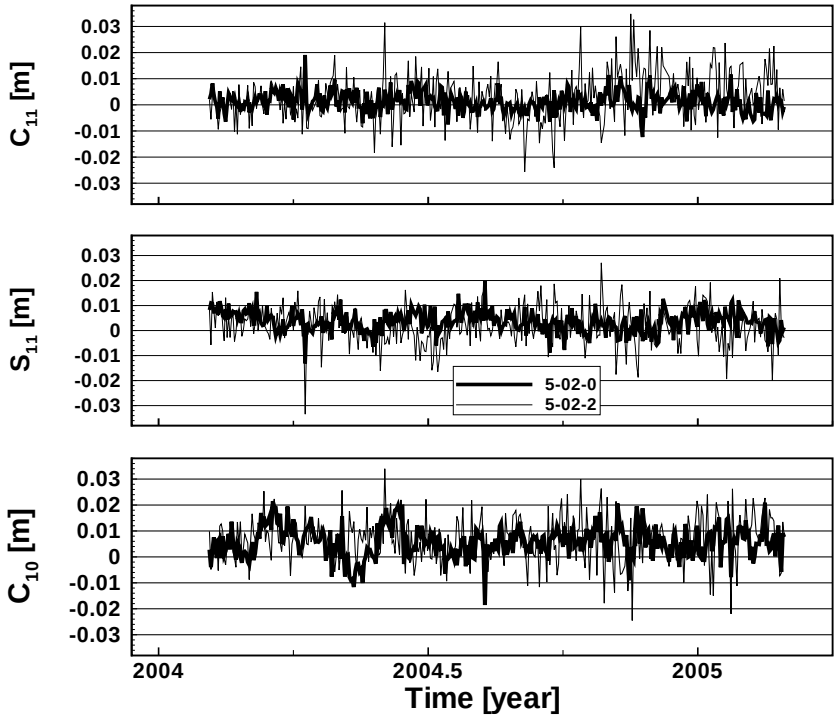

Figure 6.1: *Dynamic Geocentre x-, y-, z-component per day.*

The amplitudes of C_{11} and S_{11}, mostly staying within a band of ±1 cm, are consistent with the statement of [Don 97] that the integral geocentre variations due to surface mass loads is within a level of 1 cm. None of the components exhibits a clearly visible trend that would be unreasonable as in the course of a year's time span mass displacements on the Earth surface are expected to be balanced. An interpretation of the clear bias in C_{10} is not tried as it certainly coheres with the NN-condition

imposed on T_z and the underlying a priori ITRF as well as with the quality of the orbit modelling implemented in EPOS-OC.

As obvious from Table 6.1 the correlation coefficients between dynamic geocentre components and the geometric geocentre translational components of run 5-02-0 reach values up to 0.304 meaning that there is a weak stochastic dependence between the dynamic and the geometric geocentre. This is consistent with the results of the simulations presented in Section 4.3 revealing that it is not possible to separate the dynamic and the geometric geocentre. However, imposing NN-conditions on all three translational components of the geometric geocentre in run 5-02-0 obviously mitigates the dependence between both geocentres.

Scale of the Geometric Frame

In Fig. H.4 the time series of the geometric frame's differential scale $S - 1.0$ is shown. It reveals a mean of +1.23 mm and a STD at 1.88 mm (Table I.1). Considering also the amplitudes ranging between +5 and -5 mm the daily solutions can be regarded as very reliable. This high quality gives evidence that the geometric scale can be determined by a GPS-based processing method as stated in [Col 11]. As the estimated scale is strongly dependent on the absolute PCCs of the GPS antennas used, the solution presented here indicates a good agreement of the adopted a priori TRF and the absolute PCCs introduced, c.f. Table F.3. The slight oscillation exhibited by the series is not further investigated.

Flattening of the Earth Gravity Field

For the flattening of the Earth's gravity field (C_{20}) the series of daily values is displayed in Fig. H.3. It shows a resonable scatter for solutions of daily resolution as well as roughly a semi-annual oscillation. The mean is indicated in Table I.5 and the maximum formal error of the daily estimates is $0.92{\cdot}10^{-11}$. A correlation coefficient of -0.210 w.r.t. the geometric scale S, c.f. Table 6.1, reveals a slight negative dependency between these two parameters. Remembering that C_{20} represents the negative polar flattening of the Earth gravity field, c.f. Section 4.1, a lower value of C_{20} means an increased expansion of the Earth body parallel to the equatorial plane that may be equivalent to some extent to an increase in geometric scale. This relationship between C_{20} and the geometric scale S is consistent with a negative correlation coefficient. On the other hand, subject to further investigations, these two parameters seem to be quite independently estimated.

Table 6.1: *Correlation coefficients between time series of dynamic frame and geometric frame parameters (run 5-02-0).*

	T_x	T_y	T_z	S	R_x	R_y	R_z
C_{11}	-0.061	-0.092	-0.001	+0.031	+0.052	+0.009	+0.016
S_{11}	-0.060	-0.304	+0.092	+0.107	+0.137	-0.028	+0.069
C_{10}	+0.026	+0.076	-0.276	+0.001	-0.063	+0.008	-0.017
C_{20}	+0.041	+0.267	-0.058	-0.210	+0.017	+0.057	-0.069
S_{21}	-0.048	-0.050	+0.097	-0.006	+0.088	+0.068	-0.067
C_{21}	-0.008	+0.068	+0.060	-0.100	+0.000	+0.007	-0.037
S_{22}	-0.058	-0.113	+0.041	-0.053	+0.033	-0.030	+0.076

Orientation of the Geometric Frame

In Fig. 6.2 the geometric frame's orientation parameters are plotted. The series are characterised by means and STDs of +0.63 ±5.47 mm for R_x, +1.75 ±3.97 mm for R_y, and -0.12 ±0.33 mm in case of

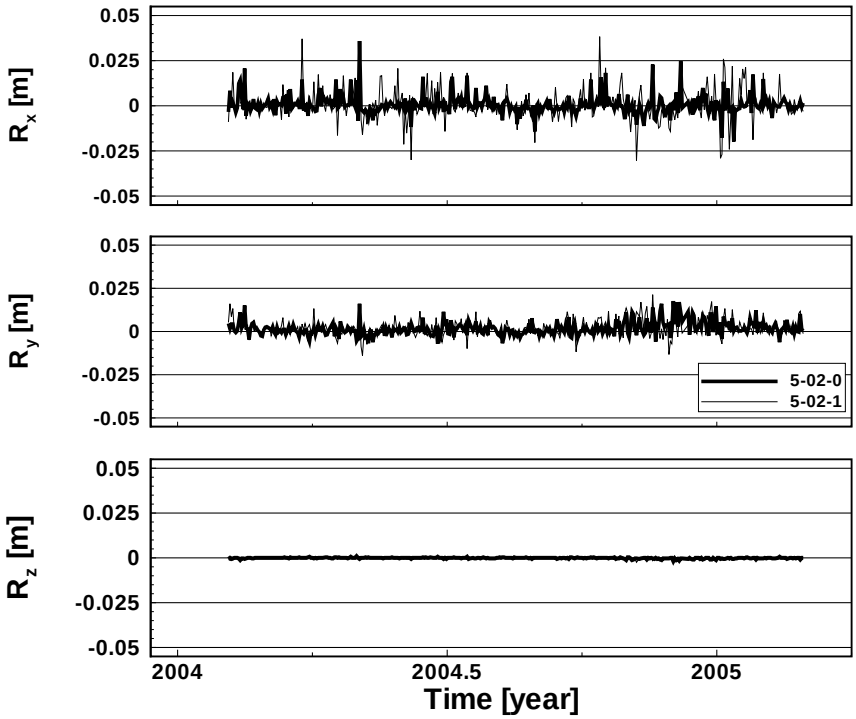

Figure 6.2: *Geometric Frame orientation x-, y-, z-component per day (rescaled to metric distance on Earth surface).*

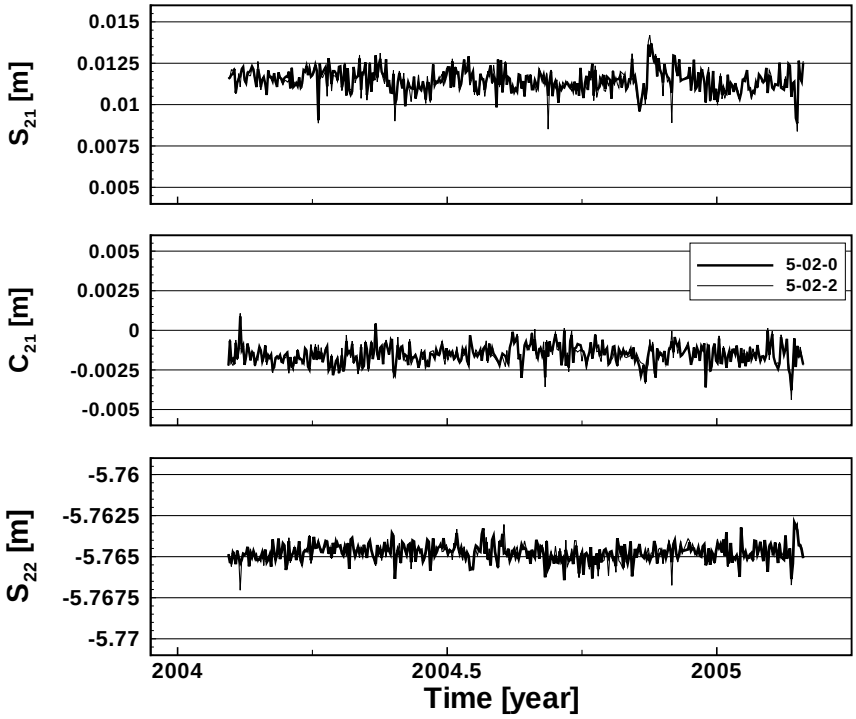

Figure 6.3: *Dynamic Frame orientation x-, y-, z-component per day (rescaled to metric distance on Earth surface).*

R_z (Table I.2). None of the series exhibits a clear trend or a clear periodic signal. For R_z, following well the NN-condition imposed, this is natural. In case of R_x and R_y this means that the geometric frame is rotationally stable around the x- and the y-axis. Compared to S_{21} and C_{21} (see below), R_x and R_y are much noisier. While for the dynamic frame's orientation the low scatter can be regarded as physical truth as detected by the highly accurate KBRR observations in case of the geometric frame's orientation the scatter rather reveals a comparatively higher day-by-day fluctuation of the estimated GPS ground station network w.r.t. the a priori one.

Orientation of the Dynamic Frame

The time series of the components of the dynamic frame's orientation, given by S_{21}, C_{21}, and S_{22}, can be seen in Fig. 6.3. For the parameters indicated in the above order the series' means and STDs are +11.47 ±0.69 mm, -1.53 ±0.61 mm, and -5764.76 ±0.54 mm (Table I.4). Each parameter is estimated with stochastic significance as the maximum daily formal errors are 0.06, 0.06, and 0.04 mm, respectively. Additionally, the absolute values of correlation coefficients w.r.t. the geometric frame orientation components are below 0.088, see Table 6.1, indicating a low correlation.

The sizes of S_{21}, C_{21}, and S_{22} indicate how strong the axes of the dynamic frame deviate from those of the geometric frame. Thereby, S_{22} has the largest absolute value among those three spherical harmonic coefficients. According to Eq. (4-7) S_{22} is influenced by inhomogeneities of the Earth's mass distribution in the planes perpendicular to the z-axis. For that reason the large absolute value of S_{22} indicates a non-uniform mass distribution perpendicular to the z-axis that is much more pronounced than the inhomogeneous mass distributions perpendicular to the x- and y-axis reflected by S_{21} as well as C_{21}, respectively. Concerning S_{21} and C_{21} it can be stated that the much larger absolute value of S_{21} indicates larger inhomogeneities in mass distribution perpendicular to the x-axis than perpendicular to the y-axis.

As already mentioned in Section 4.1 C_{22} is estimated as well but is not regarded to be part of the dynamic frame. Therefore, this parameter is not treated here.

6.2 Observational Residuals

Though only indicating the internal accuracy the observational residuals as defined in Section 2.3 are nonetheless important indicators of a solution's quality. For the various observation types used the number of observations as well as the global RMS values are listed in Table 6.2.

GPS-ground

The daily RMS of code and phase residuals as well as the number of observations in case of GPS-ground data are shown in Fig. H.7. As is expected from geodetic GPS receivers the residuals' RMS per day is at the level of 50 cm in the case of code and in the range of 5 to 7.5 mm for phase observations. With roughly 900,000 to 1,000,000 measurements per day for both, code and carrier phase, on the one hand the dominance of the GPS ground data w.r.t. the other observation types becomes clear as well as the high computational burden of carrying out a processing following the Integrated Approach. The larger RMS values for both code and phase observations of GPS-ground compared to the corresponding RMS values of GPS-SST are most probably due to remaining errors in the GPS orbits, to residual mismodelling of ionospheric and tropospheric signal delays, and to less accurate receivers than those operated onboard GRACE producing GPS-SST observations.

GPS-SST

In case of GPS-SST the time series are shown in Fig. H.8 incorporating both GRACE-A and -B. Compared to the GPS-ground case the daily code RMS is only slightly reduced to ca. 40 cm whereas the phase residuals' RMS goes down to 2 mm and less revealing the high internal quality delivered by the POD GPS receivers aboard the GRACE satellites. The amount of data per day in sum for GRACE-A and -B reaches 40,000 at maximum.

Table 6.2: *Statistics of GPS-ground, GPS-SST, and KBRR residuals.*

Run	GPS-ground			GPS-SST			KBRR	
	number of obs. (code, phase)	global RMS code	global RMS phase	number of obs. (code, phase)	global RMS code	global RMS phase	number of obs.	global RMS
	[/]	[cm]	[cm]	[/]	[cm]	[cm]	[/]	[μm/s]
4-04-0	345350253	66.14	0.72	13756589	43.86	0.18	6080582	0.25
5-02-0	359983114	46.29	0.61	14218306	36.51	0.17	6295760	0.19
5-02-1	366762779	46.08	0.67	-	-	-	-	-
5-02-2	-	-	-	14249234	37.53	0.54	6276459	0.19

KBRR

The series of the RMS of KBRR residuals is displayed in Fig. H.9. Being in most cases at the level of 0.2 μm/s it exhibits a time-dependent behaviour as well as a few peaks that are not investigated here. With maximally 17,280 measurements per day the amount of data might be reduced due to phase breaks or other disturbances inside the GRACE satellites.

6.3 Validation

While the observational residuals indicate a solution's internal accuracy it is indispensable to compare the obtained results to external sources. This is done for run 5-02-0 with the satellite orbits and the gravity field coefficients. The satellite orbits are validated by SLR residuals, too.

Satellite Orbits

Orbits of the GPS satellites of high quality are the IGS final orbits ([IGS 12e]). For that reason the GPS orbits derived by run 5-02-0 are compared to them. In detail this is done by calculating for every satellite at each epoch the difference in coordinates for all three spatial components. Additionally a global seven-parameter Helmert transformation is performed resulting in the same parameters of a similarity transformation as in the case of Helmert transformations between ground station networks.

For those global Helmert transformations carried out per arc the time series of the parameters in the CTS are displayed in Figs. H.10, H.11, and H.12. Concerning T_x and T_y the time series show a stable behaviour with low biases and amplitudes much below 2 cm for most arcs. T_z, too, is stable viewed over the whole time span but has a significant mean and a higher STD than the other two components. Moreover, c.f. Table I.7, T_x and T_y are strongly correlated with the corresponding dynamic geocentre components C_{11} and S_{11} as revealed by correlation coefficients of +0.760 and +0.816, respectively. This suggests that a more fair comparison can be achieved by applying the dynamic geocentre's

components to the translational components T_x, T_y, and T_z of the global Helmert transformations. The corresponding RMS values of the translational parameters for both cases, i.e. without and with the dynamic geocentre's components applied, are displayed in Table I.9. As expected the RMS values significantly reduce to 3.81, 3.41, and 9.71 mm with the components of the dynamic geocentre applied.

The scale parameter can also be regarded as stable with amplitudes in a range of roughly 0.5 ppb corresponding to 3.2 mm on the Earth surface. However, it exhibits a small but significant bias of ca. -0.25 ppb (-1.6 mm arc). Such a bias in scale can appear for several reasons including different gravity fields used for orbit determination, the antenna PCOs and PCVs used, as well as the clock parameters and carrier phase ambiguities estimated in the underlying solution that are highly correlated with the scale.

Regarding the rotational parameters R_x, R_y, and R_z no systematic discrepancies w.r.t. IGS final orbits are detected. They are all very stable with amplitudes well below 0.0002" (6.2 mm arc) and do not show any significant correlation with the dynamic frame's orientation parameters, c.f. Table I.8.

Quite helpful, too, is the RMS of the 3D coordinate differences of all GPS satellites at all epochs *previous* to the similarity transformation carried out using the transformation parameters estimated by the Helmert transformation. The time series of arc-wise RMS is shown in Fig. H.13. A level of about 6 cm indicates a quite high quality of the GPS orbits derived by run 5-02-0.

Validating the twin GRACE satellites is done by comparison to JPL GNV1b orbits. In this case the arc-wise RMS of the coordinate differences in the local RTN-system (see Appendix A) is determined. The time series for the three components are shown in Fig. H.14. As indicated in Table I.10 the RMS of the transversal and of the normal component is at a level of 2 to 3 cm, and in case of the radial component the RMS ranges at about 6 cm. A possible reason for the comparatively higher RMS of the radial component might be the use of a different radial offset for the GPS-POD antennas' reference point when deriving the JPL orbits.

Gravity Field Coefficients

The validation of the gravity field coefficients is accomplished by comparison with corresponding time series stemming from external institutions.

In case of the dynamic geocentre components the corresponding time series originate from the JIGOG project (weekly resolution; [Rie 11]) and from CSR (Center for Space Research, Austin, Texas; monthly resolution; [Che 10]).

Within the JIGOG project the processed data are weekly normal equations of global GPS solutions, weekly normal equations of GRACE global gravity field solutions, as well as modelled Ocean Bottom Pressure. Thereby the global GPS solutions serve for covering the Earth's surface, and the modelled Ocean Bottom Pressure is used to cover the oceans. While the GRACE global gravity solutions cover both land and sea they carry information only about the Earth gravity's spherical harmonic coefficients of degree two and higher. Considering the GPS orbits being negligibly sensitive to variations of the Earth's centre of mass this means that none of the three input data sets contain direct and precise measurements of geocentre motion. Overall, spherical harmonic coefficients of surface loading up to degree and order 30 are estimated with weekly resolution by a joint inversion of the above-mentioned three data sets. The geocentre motion vector is finally derived as the offset between the centre of mass of the entire Earth system and the centre of mass of the solid Earth ("CE"; assumed to coincide with the centre of figure at a level of about 3%) from the estimated surface loading coefficients of degree one. Its time series is denoted as "JIGOG (CE)" in Fig. 6.4.

In contrast to JIGOG the approach followed by CSR is at the observation level making use of SLR observations to five geodetic satellites processed by dynamic POD and parameter estimation. Introducing the station coordinates as fixed the estimated parameters comprise an explicitly modelled 3D geocentre motion vector along with gravity spherical harmonic coefficients from degree 2 to 5, and

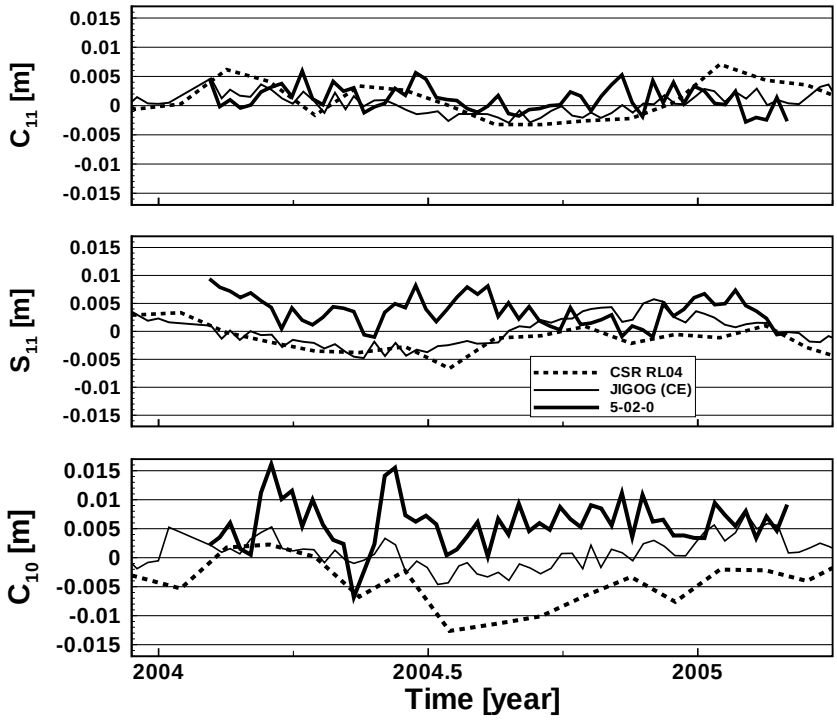

Figure 6.4: *Validation of Dynamic Geocentre components with external time series (5-02-0: weekly averaged; CSR: monthly solution; JIGOG (CE): weekly solution). In case of CSR and JIGOG the parameters are not directly estimated gravity spherical harmonic coefficients but indirect geocentre motion components.*

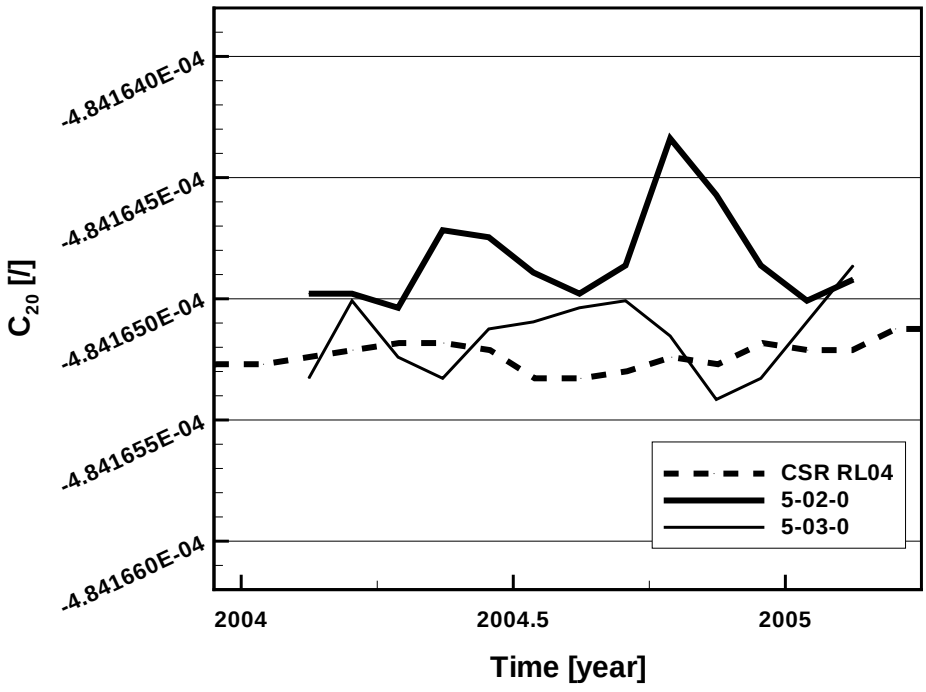

Figure 6.5: *Validation of C_{20} with external time series (CSR: monthly solution) using KBRR (5-02-0: monthly averaged) and without KBRR (5-03-0: monthly averaged).*

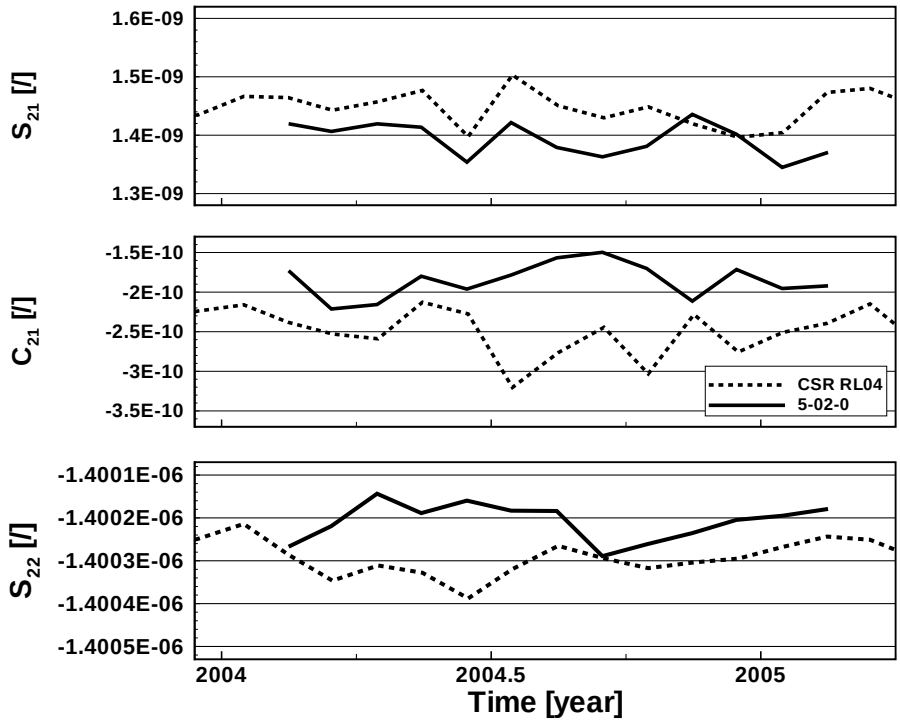

Figure 6.6: *Validation of S_{21}, C_{21}, and S_{22} with external time series (5-02-0: monthly averaged; CSR: monthly solution).*

parameters usually used in dynamic POD for the orbit perturbation force models as well as for the SLR observation model. The resulting time series of the geocentre motion's components are denoted as "CSR RL04" in Fig. 6.4 as most of the background models used in the processing are consistent with GRACE RL04 ([Fle 10a]).

In Fig. 6.4 the JIGOG as well as the CSR time series are plotted together with the values of run 5-02-0 as averaged per GPS week. While C_{11} fits very well to the other solutions, S_{11} reveals some discrepancies at the level of +5 mm in the first half of the time span covered. C_{10}, too, shows fairly good agreement in the second half irrespective of a bias of the order of about +5 mm w.r.t. the JIGOG solution whereas the agreement is not so obvious in the first half. An explanation might be the high correlation of the z-components of the dynamic geocentre as well as of the global Helmert transformations of the GPS orbits w.r.t. IGS final orbits.

The degree-two gravity field coefficients are compared to the monthly SLR solutions of CSR ([Che 11]). For the purpose of a fair comparison the estimates of run 5-02-0 are averaged per month. Fig. 6.5 displays the comparison in case of C_{20}, and the comparison of S_{21}, C_{21}, and S_{22} is shown in Fig. 6.6.

In case of C_{20} a clear bias is visible that is most probably due to an unknown K-band effect as will also be shown in Section 6.5. Beside this bias the time series of run 5-02-0 reveals a much higher noise level compared to the CSR time series as well as w.r.t. run 5-03-0 where KBRR data is not used. Both the bias as well as the higher noise level are caused by a shift and by a higher amplitude, respectively, of the original time series with daily resolution of run 5-02-0 compared to the corresponding time series of run 5-03-0, as displayed in Fig. 6.10. Concerning S_{21}, C_{21}, and S_{22} the time series have approximately the same amplitude while revealing tiny biases. The S_{21} series are quite similar whereas the other two parameters partly reveal different time-variable behavior: C_{21} from roughly 2004.5 to 2005.0, S_{21} between 2004.35 and 2004.6.

SLR Residuals

Another measure suitable for validating orbits are the residuals of SLR observations that are introduced with very low weight into the differential orbit adjustment. In this they do not influence the solution and act as an independent quality measure assuming the SLR ground station network not being distorted. As it may happen that there are some gross outliers within the SLR observations provided by the ILRS the obtained residuals are cleaned afterwards by applying a threshold of 20 cm. The global RMS values of the SLR residuals for GRACE-A, -B, PRN05, PRN06 thus derived are listed in Table I.11. For the run 5-02-0 considered here they reveal a quite high orbit accuracy for the GRACE LEOs with global RMS values of 3.71 and 3.34 cm. For the two GPS satellites PRN05 as well as PRN06 the orbit accuracy is worse with 7.94 and 7.42 cm global RMS but still well below the 10-cm level.

6.4 Comparison with the Two-step Approach

As outlined by [Zhu 04] it is expected that a comparable two-step approach delivers worse orbits and parameter time series compared to an integrated processing. In order to illustrate this effect the results of the two-step processing mentioned in the preceding chapter are discussed below. These are mainly the results of runs 5-02-1 and 5-02-2. For the runs 4-04-1 and 4-04-2 results concerning SLR residuals are used.

GPS Part

First of all it can be seen that the internal accuracy for the GPS part 5-02-1 degrades slightly as revealed by the global RMS of phase residuals increasing from 0.61 to 0.67 cm as listed in Table 6.2 and visible in Fig. H.7.

Evaluating the GPS orbits' external accuracy is done by Helmert transformations w.r.t. IGS final orbits. As expected there is higher scatter for the two-step part 5-02-1 in terms of the time series STD for T_z, S, R_x, R_y, and R_z as indicated in Table 6.3. This result is slightly disturbed by smaller scatter for T_x and T_y. On the other hand, the results for T_x, T_y, and T_z are not quite expressive because of the NN-conditions imposed on these parameters during the runs (see Table G.5). The corresponding time series are displayed in Figs. H.10, H.11, and H.12. On the other hand, the RMS values of 3D differences, c.f. Fig. H.13, increase significantly to a level of seven to eight cm exhibiting a degraded orbit accuracy, too.

Table 6.3: *STDs of parameters of global Helmert transformations between GPS orbits (Integrated ('Run') vs IGS final).*

Run	T_x [mm]	T_y [mm]	T_z [mm]	S [mm]	R_x [mm]	R_y [mm]	R_z [mm]
5-02-0	4.79	5.43	7.60	0.46	1.67	2.16	1.45
5-02-1	4.27	5.20	9.56	0.47	1.86	2.60	2.01

The effect of degraded orbit accuracy in terms of GPS SLR residuals, as revealed by Table I.11, is only visible for run 4-04-1 with the global RMS values increasing from 5.54 and 5.52 cm to 6.02 and 5.83 cm for PRN05 and PRN06, respectively. In contrast, the two-step approach astonishingly leads to slightly reduced global RMS values for PRN05 and PRN06 in case of run 5-02-1. A potential reason for these smaller RMS values is the quite large difference in the number of SLR observations used between release 04 and release 05 processing as well as the different models used for absolute PCCs of the GPS ground station antennas (see Table F.3).

A decline in quality is also visible for the geometric frame's parameters as plotted in Figs. H.2, H.4, and 6.2. The visible increase in time series scatter is underlined by the statistical measures given in Tables I.1 and I.2 indicating, as expected, significantly higher STDs for the two-step approach.

LEO Part

Concerning the GPS-SST phase residuals a strong increase in the level of arc-wise RMS is detected, see Fig. H.8, that is underlined by the global RMS growing from 0.17 to 0.54 cm (Table 6.2). For the KBRR residuals no significant change occurs meaning that the relative orbit accuracy in the GRACE satellites' transversal direction is at the same level as in the case of the integrated processing. A clear degradation comes out regarding the SLR residuals. Their global RMS rises from 3.71 to 3.98 cm and from 3.34 to 3.72 cm for GRACE-A and -B, respectively.

The effects on the gravity field coefficients are visible in Figs. 6.1, H.3, and 6.3. From Tables I.3, I.4, and I.5 the changes in the time series' STDs are obvious. In terms of increased STD there is a quite pronounced degradation in case of the dynamic geocentre's components and a rather tiny one for the dynamic frame's orientation parameters. However, C_{20} represents an exception revealing a STD improving from 0.242E-09 to 0.213E-09.

6.5 Effects Studied

After having presented a reference solution following the Integrated Approach some alternative solutions are discussed in this section. In that way the reasons for choosing the parameterisation of run 5-02-0 as well as some deficiencies should be clarified.

Sensitivity to Observation Types

In order to evaluate the influence of the different observation types on the estimated TRF parameters various weighting schemes for GPS and KBRR observations have been tried. An alternative approach to find an optimal weighting scheme is the method of variance component estimation that is not applied here. Below, only those schemes are presented that turned out to be most promising.

First of all, the idea is to adapt the a priori sigmas used in the weighting scheme of the initial setup to the RMS of a posteriori residuals. Second, by means of the factor f, see Eq. (5-1), the relative weighting between the observation types is steered additionally. For that reason a priori STDs as well as factors f are chosen as indicated in Tables G.2 and G.5 for runs 4-02-0 and 5-01-0, respectively. Each GPS-SST observation, especially for phases, is thus given double weight compared to GPS-ground data. This is justified because GPS-SST measurements are less influenced by residual ionospheric errors, because the POD receivers onboard the GRACE LEOs are of very high quality, and because the LEOs' orbits are highly sensitive to the gravity field coefficients of low degree.

It should be emphasised that only the cumulative effect of the modified weighting model can be evaluated as the weighting is changed here for all three observation types simultaneously. Doing so for both RL04m as well as for RL05m processing there are clear effects seen in the dynamic geocentre components. For RL04m processing, i.e. runs 4-01-0 and 4-02-0, the STDs slightly increase for the x- and y-component but become significantly reduced from 12.54 to 8.48 mm for the z-component, c.f. Table I.3 and Fig. H.18 for visual inspection. As will become clearer below, this positive effect on C_{10} is due to the higher relative weighting of the GPS-SST measurements. In case of RL05m processing (runs 5-00-0, 5-01-0) there is not only a similar improvement in C_{10} from 9.87 to 6.00 mm, see Table I.3; the STDs of C_{11} and S_{11} are significantly reduced, too, as is obvious from Fig. 6.7.

In order to fully exploit the potential of its high precision the KBRR data is assigned a factor of 50 found empirically to yield best time series for C_{20}. With run 4-03-0 a RL04m processing is given that

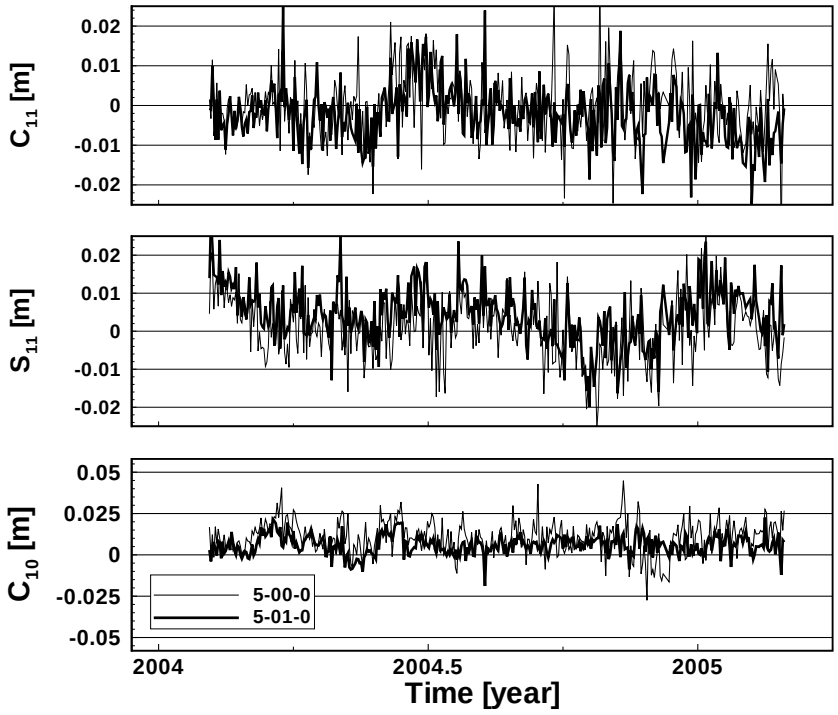

Figure 6.7: *Effect of observational weighting: modified weight model for GPS-ground, GPS-SST, KBRR; Dynamic Geocentre x-, y-, z-component per day.*

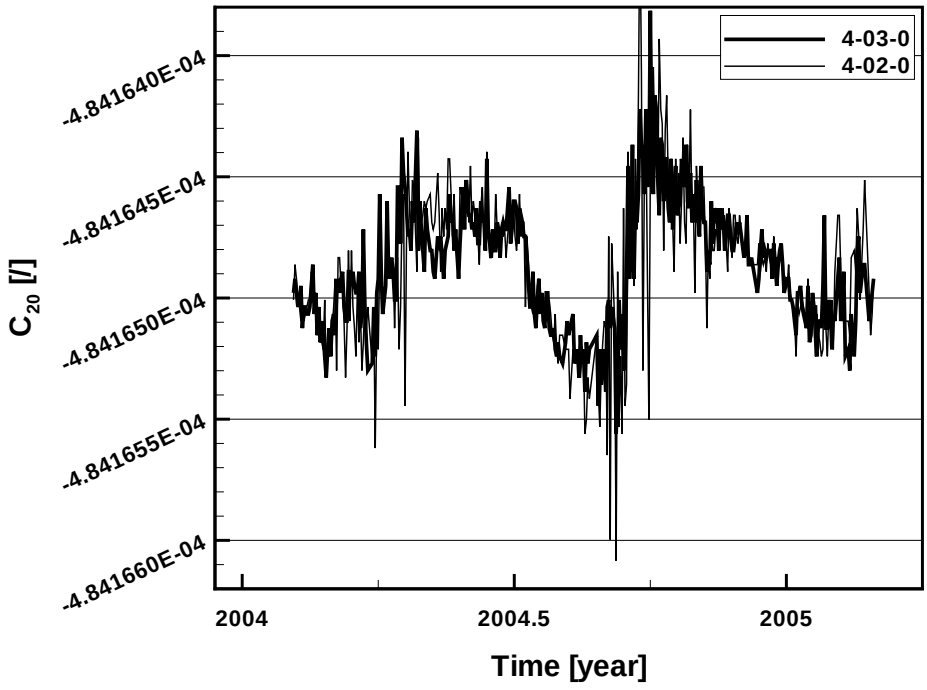

Figure 6.8: *Effect of observational weighting: modified weight model for GPS-ground, GPS-SST, KBRR.*

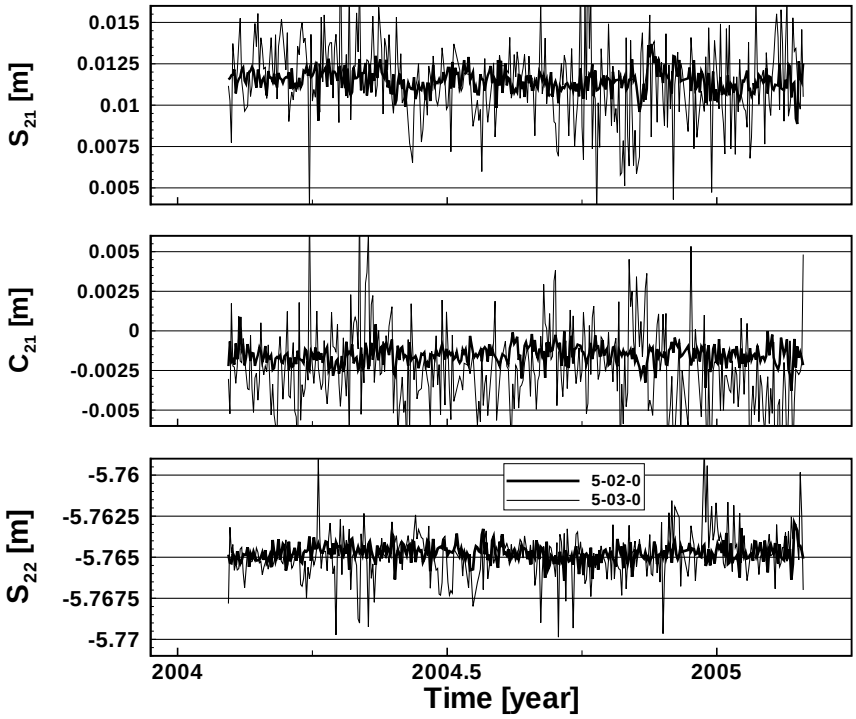

Figure 6.9: *Effect of excluding KBRR observations (5-03-0) on S_{21}, C_{21}, S_{22}.*

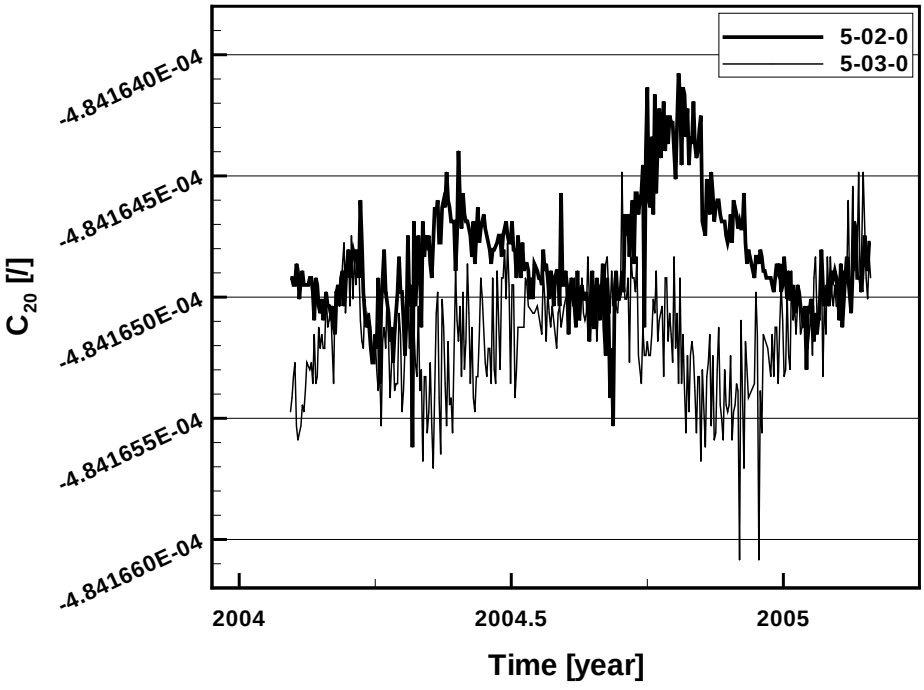

Figure 6.10: *Effect of excluding KBRR observations (5-03-0) on C_{20}.*

is assigned a five times higher weight factor f for KBRR compared to run 4-02-0. These two runs also differ in the model applied for GPS absolute phase centre corrections. As the phase centre corrections mainly affect the geometric scale it is the difference in KBRR weighting that influences the dynamic geocentre and C_{20}. The positive effect on C_{20} is seen in Fig. 6.8 revealing a clearly reduced scatter of the time series for 4-03-0. However, the higher weight for KBRR leads to slightly increased STDs of the dynamic geocentre components, c.f. Table I.3.

In case of RL05m run 5-03-0 differs from run 5-02-0 only by completely excluding KBRR observations being equivalent to assigning them zero weight. Concerning the dynamic geocentre there is clear improvement in the time series' STDs in all components as obvious from Table I.3 with the drawback of an increased bias of +8.93 mm in C_{10}. This means that KBRR does not contribute to determining the dynamic geocentre. As visible from Fig. 6.9 and from Table I.4 the components of the dynamic frame's orientation parameters strongly degrade revealed by increased STDs.

The resulting time series of C_{20}, however, is contradictory. On the one hand, as displayed in Fig. 6.10, the day-to-day scatter clearly increases revealing the importance of KBRR observations for accurately deriving gravity field coefficients of degree two and higher. On the other hand, appearing as a positive effect, the mean of the time series reduces so far that the bias w.r.t. the CSR SLR solution diminishes as shown by Fig. 6.5. For that reason it can be concluded that the bias visible in case of high-weighted KBRR is an effect of the K-band instrument. Finally, by comparing the outcome of runs 5-03-0 and 5-04-0 the effect of excluding KBRR as well as not estimating degree-two gravity field coefficients on the dynamic geocentre can be studied. The statistical measures listed in Table I.3 indicate that there is no significant change neither in the means nor regarding the STDs. The value used for C_{20} in run 5-04-0 is -4.841652E-04 which is taken as a priori in the runs where degree-two gravity field coefficients are estimated.

In summary, it can be stated that precisely estimating the dynamic geocentre components is achieved by GPS-SST observations, and precisely estimating the degree-two gravity field coefficients is accomplished by KBRR data.

Constraints on Ground Station Coordinates

As outlined in Section 4.3 inherent to the Integrated Approach there is a severe as well as an attenuated datum defect, and there exist the CC as well as the NN methods to rectify them.

By assessing runs 4-00-0 and 4-01-0 the CC-method and the NN-method can be compared. In case of run 4-00-0 the CC-method is set up as to constrain each ground station coordinate to its a priori value with a STD of 10.0 cm. Contrarily, for run 4-01-0 NN-conditions with a sigma of 0.1 mm are imposed on the geometric frame's parameters T_z and R_z. Clearly revealed by Fig. 6.11 the NN-conditions help to drastically improve the C_{10} time series. This is also underlined by the statistical measures listed in Table I.3. While there is negligible change in mean and STD in the C_{11} and S_{11} series the mean for the z-component reduces from +43.82 to +14.78 mm and the STD from 59.31 to 12.54 mm.

Next, the effect of additionally rectifying the hidden datum defect in T_x and T_y is investigated. This is done in case of RL04m processing by runs 4-03-0 and 4-04-0, and by runs 5-01-0 and 5-02-0 for the RL05m case. In both cases, as perceptible from Figs. H.24 and 6.12, there is lower scatter for C_{11} and S_{11} being very pronounced for 5-02-0. Considering the mean values in case of 4-04-0 S_{11} improves down to a negligible bias of +0.05 mm while C_{11} becomes worse with +3.59 mm. In case of 5-02-0 there is improvement in the means for both C_{11} and S_{11}. Concerning C_{10} there is no significant change in either case as the two added NN-constraints are expected to influence only the x- and the y-component.

As a result of these tests it can be concluded that, in contrast to the CC-method, NN-conditions on T_z and R_z help to improve C_{10}, and that further improvement is achieved for C_{11} as well as S_{11} by additionally imposing NN-conditions on T_x and Ty.

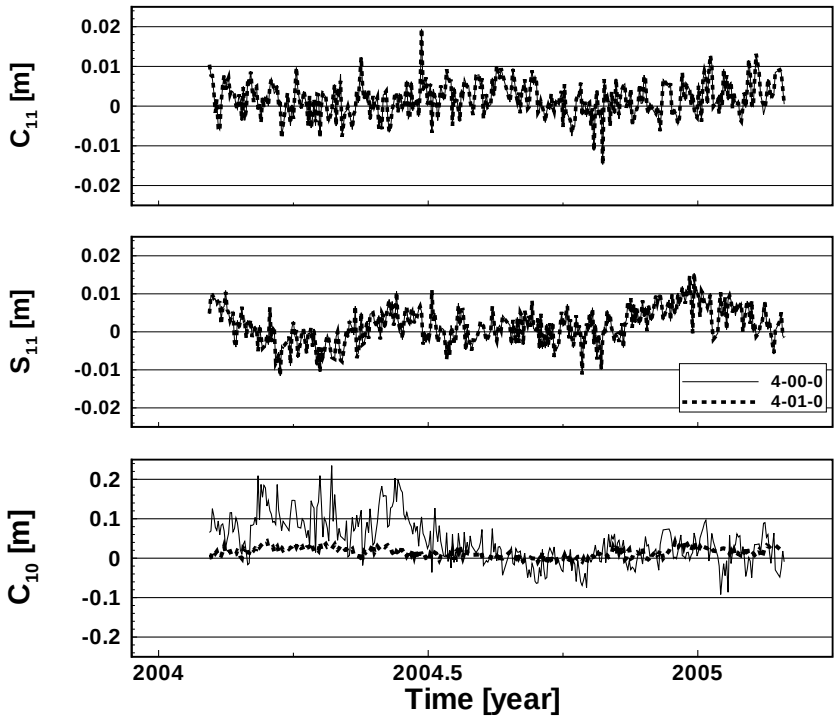

Figure 6.11: *Effect of constraints on ground station coordinates: CC (4-00-0) vs NN(T_z,R_z) (4-01-0); Dynamic Geocentre x-, y-, z-component per day.*

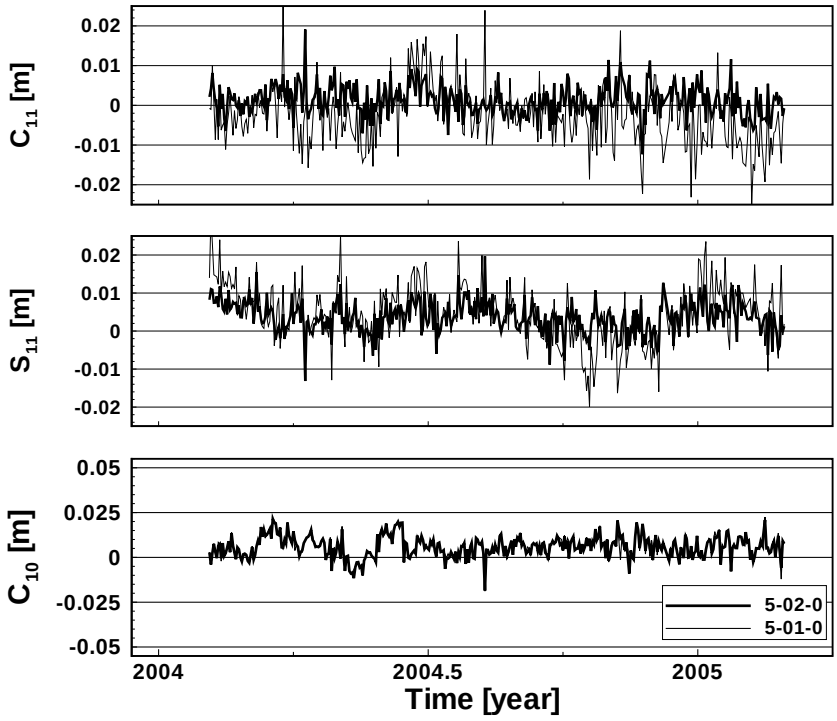

Figure 6.12: *Effect of constraints on ground station coordinates: NN(T_z,R_z) (5-01-0) vs NN(T_x,$T_y$$T_z$,$R_z$) (5-02-0); Dynamic Geocentre x-, y-, z-component per day.*

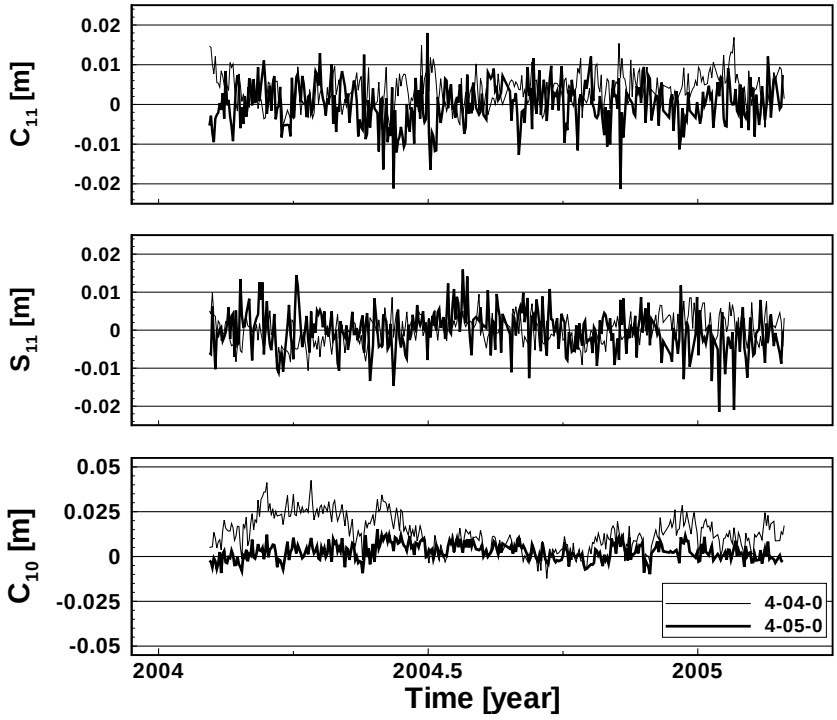

Figure 6.13: *Effect of constrained GPS orbits: totally unconstrained (4-04-0) vs fixed IGS final orbits (4-05-0); Dynamic Geocentre x-, y-, z-component per day.*

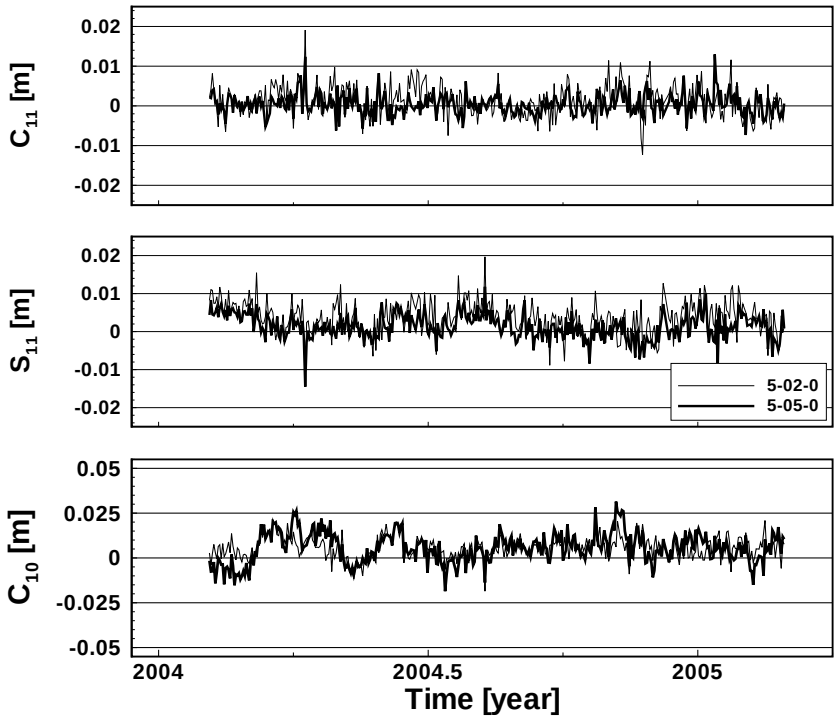

Figure 6.14: *Effect of constrained GPS orbits: totally unconstrained (5-02-0) vs constrained (5-05-0); Dynamic Geocentre x-, y-, z-component per day.*

Constrained GPS Orbits

Finally, the special role of the GPS orbits within the Integrated Approach is studied. This is accomplished by constraining them as done in the two runs 4-05-0 as well as 5-05-0.

In case of run 4-05-0 no GPS orbits are adjusted but IGS final orbits are introduced as fixed being equivalent to constraining them with infinitely high weight. Here, beside constraining the GPS orbits the aspect of orbit quality has an effect as the IGS final orbits are currently the most accurate available. The GPS-related parameters that are estimated here are receiver and transmitter clock corrections as well as ambiguities and tropospheric scaling factors. A remarkable improvement in C_{10} results with the bias reducing from +12.84 to +2.59 mm and the STD from 9.73 to 4.75 mm whereas C_{11} and S_{11} become degraded (Table I.3 and Fig. 6.13).

In run 5-05-0 the GPS orbits are adjusted but their orbit force models are kept constrained to the a priori parameters according to Table G.6. This approach is similar to introducing IGS final orbits as fixed since the GPS orbits derived by integrated processing (run 5-02-0) are in quite good agreement with IGS ones concerning the RMS of 3D differences (Fig. H.13). By evaluating run 5-05-0 considerable effects on the dynamic geocentre components appear as is obvious from Fig. 6.14. In contrast to the case of fixed IGS final orbits there is significant degradation in C_{10} underlined by an increased STD from 6.03 to 8.47 mm (Table I.3). On the other hand the time series of C_{11} and S_{11} significantly improve evidenced by reduced mean values and clearly smaller STDs. The validation w.r.t. JIGOG and CSR shown in Fig. 6.15, too, shows better agreement in the x- and y-component than in case of run 5-02-0 (Fig. 6.4). These results are consistent with the considerable correlations detected between C_{11} and S_{11} and correspondingly the translational x- and y-component of the Helmert transformations w.r.t. IGS final orbits (Table I.7). I.e., C_{11} and S_{11} become more independently estimated and less affected by a residual global translation of the constrained GPS constellation.

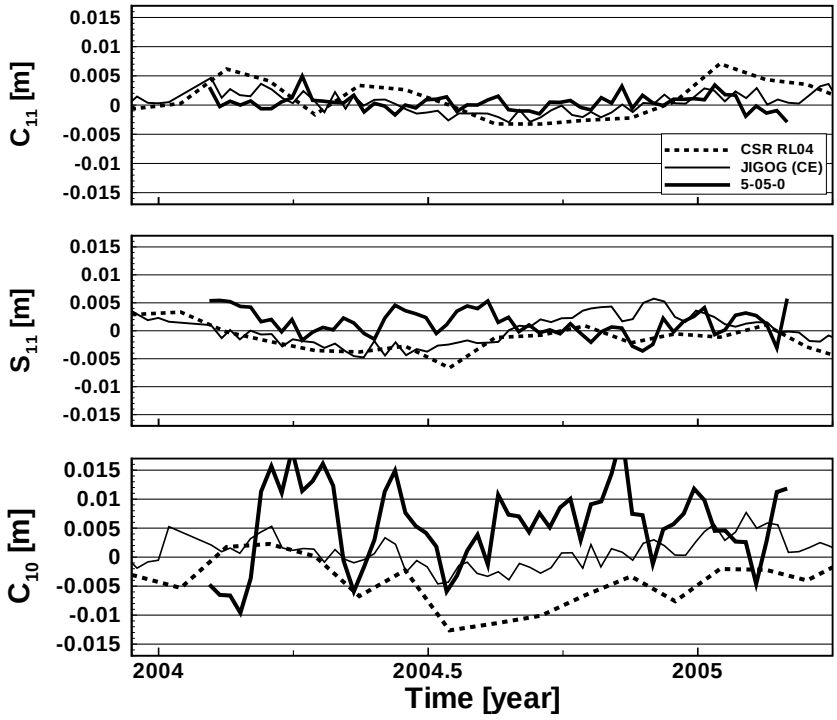

Figure 6.15: *Effect of constrained GPS orbits (constrained parameters; 5-05-0 weekly averaged): validation of Dynamic Geocentre components with external time series.*

In summary, these two tests highlight unfavourable correlations between the dynamic geocentre and the satellite constellation of the GNSS used. On the one hand, introducing high-quality IGS final

orbits as fixed leads to an exceedingly improved time series of the geocentre's z-component. This gives clear evidence of poor modelling of the orbit dynamics, in particular of the solar radiation force, of the GPS satellites in case of the Integrated Approach due to deficient capabilities of EPOS-OC, the POD and parameter estimation software applied. On the other hand, completely fixing the orbits causes degraded geocentre components in X and Y. Contrarily, by not constraining too tightly the GNSS orbit force model in the adjustment process reveals that the geocentre's x- and y-component become improved because of mitigated correlations with the residual translations of the GNSS constellation.

Chapter 7

Conclusions

Within this work parameters constituting a geodetic TRF with daily resolution are determined applying the Integrated Approach of space geodesy as proposed by [Zhu 04] covering the time span extending from 2004/02/04 to 2005/02/28. Thereby use is made of the combined constellation of GPS satellites as well as the GRACE LEOs and a set of GPS ground stations selected from the IGS network. The space-geodetic observations used comprise GPS-ground measurements as well as GPS-SST and KBRR measurements taken onboard the GRACE satellites. In order to determine the dynamic as well as the geometric part of the TRF gravity harmonic coefficients up to degree and order two, positions of GPS ground stations, and several auxiliary parameters are estimated.

The datum defect inherent to the Integrated Approach is clarified by means of simulations to consist of undefined translations of both the geometric and the dynamic geocentre, and of an undefined rotation of the ground station network about the z-axis. By imposing no-net translation conditions on all translational parameters of the ground station network as well as a no-net rotation condition on its rotation about the z-axis this datum defect is rectified. Concerning the parameters constituting the dynamic frame all of them are estimated, and for the geometric part all those not constrained by the no-net conditions. In particular, for the dynamic frame all parameters of its origin and its orientation as well as the flattening of the Earth gravity field are estimated stochastically significantly and only weakly correlated with the free parameters of the geometric frame. With the datum defect rectified the free parameters of the geometric frame left are its scale as well as its x- and y-rotation.

Evaluating the parameter time series obtained from the Integrated Approach with appropriate no-net translation and no-net rotation conditions imposed it turns out that the results are more accurate than a corresponding two-step approach except for C_{20}. In terms of standard deviation of the time series this effect is clearly seen for all three spatial components of the dynamic geocentre. There is reduced scatter, too, for the orientation parameters of both the dynamic as well as the geometric TRF. A subsequent validation of the derived GPS orbits reveals 3D orbit difference RMS values per day on the level of 6 cm. Comparing the derived gravity field coefficients with external sources shows quite good agreement, e.g. on the level of roughly 5 mm and less for the dynamic frame's origin components, but not perfect coincidence. This, on the other hand, cannot be expected due to the totally different approaches in determining the parameters of the dynamic frame. Concerning the geometric frame it can be concluded that the no-net conditions work as expected yielding very stable x- and y-rotations as well as a reliable and precise scale at the level of a few mm.

Additionally, several effects studied in detail exhibit the influence of the relative weighting of the various observation types involved, the effect of different approaches to rectify the datum defect, and the interaction of estimated gravity field coefficients and the GPS orbits. In case of the weighting of observations it is clearly shown that the origin of the dynamic frame is determined by the GPS-SST data taken onboard the GRACE satellites whereas K-band range-rate data measured between both low Earth orbiters is responsible for accurately deriving the gravity field coefficients of degree two. Concerning the different methods in fixing the datum defect the superiority of the no-net conditions

over simply constraining all ground station coordinates to their a priori values is evidenced. Especially it turns out that it is very helpful also to suppress the hidden datum defect in x- and y-translation in order to improve the x- and y-component of the dynamic frame's origin. Constraining the GPS satellites' orbit force models reveals further strong correlations between the translational x- and y-components of the gravity field and those of the GPS constellation. Introducing high-quality IGS final orbits as fixed detects a deficiency in estimating the z-component of the dynamic origin possibly due to non-optimal modelling of the GPS satellites' orbit forces inside the orbit determination software EPOS-OC.

Overall, at the current stage the Integrated Approach of [Zhu 04] is too optimistic as revealed by the validation w.r.t. parameter time series of external sources exhibiting significant offsets or larger amplitudes of the time series produced by integrated processing. This drawback, on the other hand, sketches a path for further investigations aiming at improving the Integrated Approach of space geodesy. First of all, remaining correlations should be investigated that appear to exist between the geometric TRF, the dynamic TRF, the satellite orbits, and the models used to describe orbit perturbation forces as well as measurement errors. Above all, an improved modelling of the GPS orbit forces is certainly quite promising for improving the accuracy of the TRF's parameters, in particular of the dynamic geocentre's z-component by improving the model of the solar radiation force. Extending the Integrated Approach by a combination with SLR-tracked satellites is certainly helpful for improving the reliability of the dynamic geocentre, of C_{20}, and the geometric scale. Finally, additionally estimating ERPs would certainly help to mitigate remaining short-term errors of the background ERP series used, and in this to improve the orientation parameters of both the geometric as well as the dynamic TRF.

Acknowledgements

This thesis is made possible through funding of the projects GGOS-D (BMBF, grant 03F0425A) and TOBACO-CHAMP/GRACE (BMBF, grant 03G0728A).

Data has been provided by the IAG services IGS and ILRS as well as by GFZ and JPL.

Some graphs are created using the Generic Mapping Tools ([We 91]).

Appendix A

Coordinate Systems

The main coordinate systems used throughout this work are:

- CIS

This is the Conventional Inertial System, see [Pet 10], which the equations of motion (2-6) are valid in.

- CTS

This is the Conventional Terrestrial System which moves and rotates with the Earth and which the ground station coordinates are referred to.

The transformation between the CIS and the CTS is accomplished as follows ([See 03, 2.1.2.3]):

$$\begin{aligned} \underline{x}_{CTS} &= \underline{SNP}\underline{x}_{CIS} \\ \underline{x}_{CIS} &= (\underline{SNP})^T \underline{x}_{CTS} \end{aligned} \tag{A-1}$$

with $\underline{SNP}$ being a product of three orthogonal matrices performing the following rotations:

$\underline{S}$	polar motion, Earth rotation
$\underline{N}$	nutation
$\underline{P}$	precession

- RTN

This is the moving local triad attached to the satellite as visualised by Fig. A.1. Using the satellite's position and velocity vectors $\underline{x}^S$ and $\dot{\underline{x}}^S$, respectively, its axes are defined as follows:

$$\begin{aligned} \underline{e}_R &= \frac{\underline{x}^S}{|\underline{x}^S|} \\ \underline{e}_N &= \frac{\underline{x}^S \times \dot{\underline{x}}^S}{|\underline{x}^S \times \dot{\underline{x}}^S|} \\ \underline{e}_T &= \underline{e}_N \times \underline{e}_R \end{aligned} \tag{A-2}$$

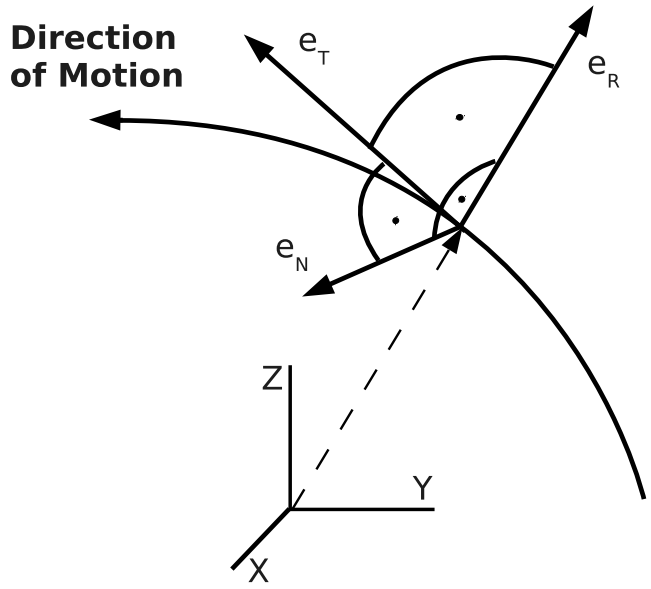

Figure A.1: *The moving local triad RTN.*

This means that $\underline{e}_R$ ("radial") points radially into the direction averted from the central body, $\underline{e}_N$ ("normal") is perpendicular to the plane erected by the satellite's position vector $\underline{x}^S$ and its velocity vector $\dot{\underline{x}}^S$, and $\underline{e}_T$ ("transversal") completes a right-handed coordinate system. In general $\underline{e}_T$ is only approximately tangential w.r.t. the trajectory because $\underline{x}^S$ is not necessarily perpendicular to the orbit's tangent.

Appendix B

Orbit Forces

Indicated are the respective accelerations $\underline{\ddot{x}}^S$ of the satellite. The corresponding force is obtained by the well-known relationship $\underline{F}^S = m_S\, \underline{\ddot{x}}^S$ with m_S being the satellite's mass.

- Gravitational attraction of the Earth

$$\begin{aligned}
\underline{\ddot{x}}^S_{g,E}|_{CIS} &= (\underline{SNP})^T\ \underline{\ddot{x}}^S_{g,E}|_{CTS} \\
&= (\underline{SNP})^T\ \nabla V_{g,E}(r,\phi,\lambda)|_{CTS} \\
&= (\underline{SNP})^T\ \nabla \left[\frac{GM_E}{a_E} \sum_{n=0}^{N} \left(\frac{a_E}{r} \right)^{n+1} \cdot \right. \\
&\quad \left. \cdot \sum_{m=0}^{n} P_{nm}(\sin\varphi)\,(C_{nm}\cos(m\lambda) + S_{nm}\sin(m\lambda)) \right]
\end{aligned} \tag{B-1}$$

c.f. [Tor 01], with

$\underline{S}$	*polar motion, Earth rotation*
$\underline{N}$	*nutation*
$\underline{P}$	*precession*
$\underline{\ddot{x}}^S_{g,E}\|_B$	*acceleration of satellite S due to Earth gravitation expressed in the TRS B*
$V_{g,E}$	*gravitational potential of the Earth*
n, m	*degree, order*
GM_E	*geocentric gravitational constant, see* [Pet 10, 1.2]
a_E	*equatorial radius of the Earth, see* [Pet 10, 1.2]
P_{nm}	*associated Legendre functions*
C_{nm}, S_{nm}	*spherical harmonic coefficients*
r	*geocentric radial distance of satellite S*
φ	*geocentric latitude of satellite S*
λ	*geocentric longitude of satellite S*

- Gravitational attraction $\ddot{\underline{x}}^S_{g,M}$ of the Moon

This perturbation force is modelled according to [Fer 77] the same way as the Earth's gravitational attraction by treating the Moon as an expanded body. The force is thereby computed in the system of selenographic coordinates and then transformed into the CIS.

- Gravitational attraction of Third Bodies

The gravitational attraction is considered for the Sun as well as the planets Venus, Mercury, Mars, Jupiter, Saturn, Uranus, and Neptune. Modelling these celestial bodies as point masses the gravitational attraction $\ddot{\underline{x}}^S_{g,B}$ caused by body B reads as

$$\ddot{\underline{x}}^S_{g,B} = GM_B \left(\frac{\underline{x}_B - \underline{x}^S}{|\underline{x}_B - \underline{x}^S|^3} - \frac{\underline{x}^B}{|\underline{x}_B|^3} \right) \tag{B-2}$$

with

$\underline{x}^S$	*geocentric position vector of the satellite*
$\underline{x}_B$	*geocentric position vector of the disturbing body*
M_B	*mass of the disturbing body*

- Atmospheric drag

The perturbation force due to atmospheric drag is neglected in case of GPS satellites, in case of the GRACE satellites it is directly measured.

- Solar radiation pressure

The formulas for the perturbation force caused by solar radiation pressure acting on GPS satellites are given in [Fli 92] and [Fli 96]. Corresponding perturbation forces acting on the GRACE satellites are not modelled but measured directly.

- Atmospheric tides (attraction plus loading)

This perturbation force is considered according to [Bia 06] as

$$\ddot{\underline{x}}^S_{at} = \nabla \left(4\pi G a_E \sum_l \frac{1+k'_l}{2l+1} \left(\frac{a_E}{r} \right)^{l+1} \sum_m q_{lm}(\varphi, \lambda, t) \right) \tag{B-3}$$

with

$q_{lm}(\varphi, \lambda, t)$	=	$\frac{1}{g} \left[\Delta C_{lm}(t) \cos m\lambda \; + \; \Delta S_{lm}(t) \sin m\lambda \right] P_{lm}(\sin \varphi)$
$\Delta C_{lm}, \Delta S_{lm}$		*harmonic coefficients of the atmospheric surface pressure (temporal variations)*
$P_{lm}(\sin \varphi)$		*associated Legendre functions*
G		*gravitational constant*
a_E		*semi-major axis of the Earth gravity field model*
l, m		*degree, order*
k'_l		*load Love number*
(r, φ, λ)		*spherical coordinates of a point outside the Earth's surface*
t		*mean sidereal time*
g		*mean acceleration of gravity*

- Ocean and solid Earth tides, Ocean pole and solid Earth pole tide

The formulas for these perturbation forces are given in [McC 04] and [Pet 10].

- Empirical accelerations

$$\ddot{x}^S_{emp,j} = S^S_{emp,j}\sin(nu) + C^S_{emp,j}\cos(nu) \tag{B-4}$$

with

$S^S_{emp,j}, C^S_{emp,j}$	*sine, cosine amplitude*
j	*spatial component in the RTN-system (Appendix A)*
	corresponding to j = 1, 2, 3
u	$\omega + v$
ω	*argument of perigee*
v	*mean anomaly*

- General Relativity

The formulas for these perturbation forces are given in [Pet 10, 10.3]. They comprise the effects of Schwarzschild, Lense-Thirring, and deSitter.

Appendix C

Results of Simulations

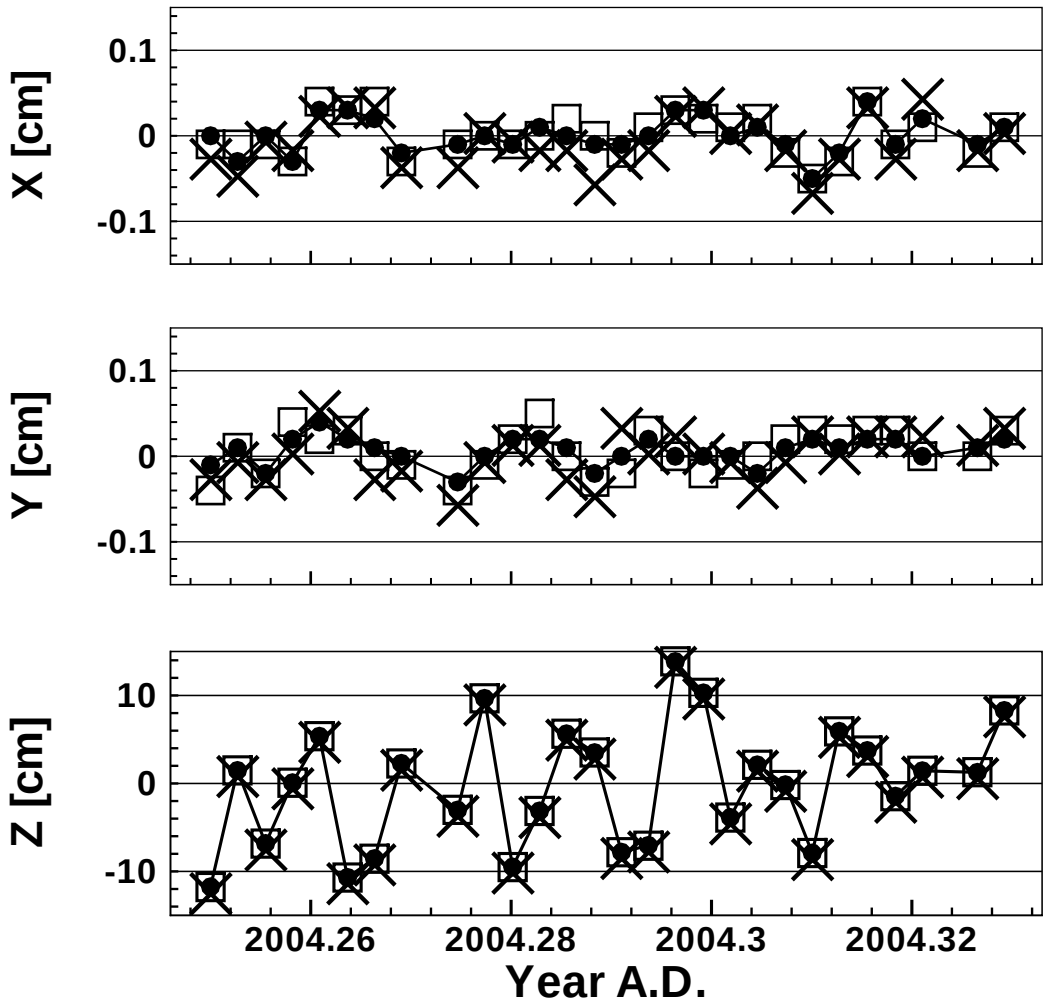

Figure C.1: *Basic simulations: time series of dynamic geocentre (circles), geometric geocentre (squares), and translations of GPS orbits (crosses) for the standard case (no constraints).*

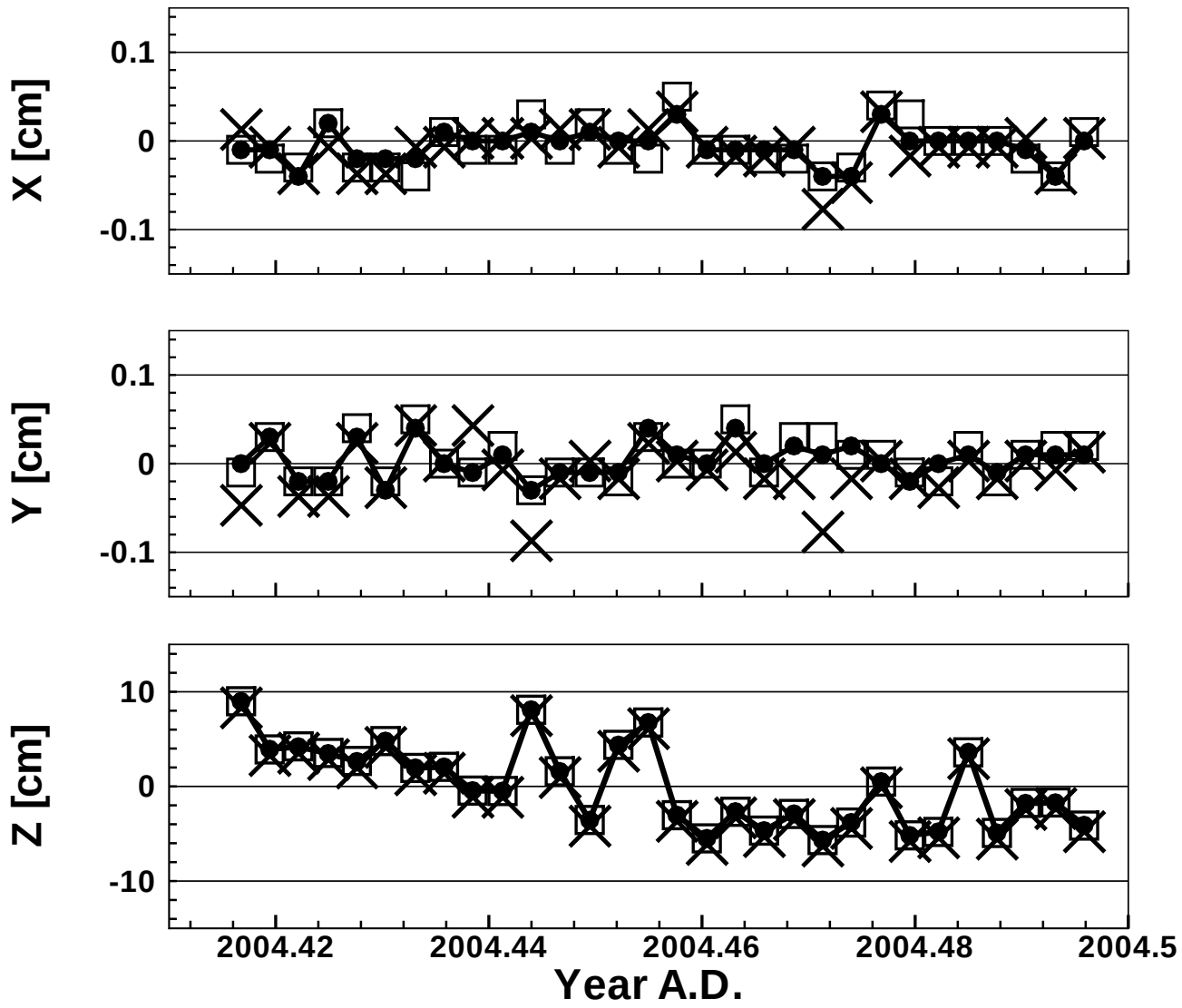

Figure C.2: *Supplementary simulations: time series of dynamic geocentre (circles), geometric geocentre (squares), and translations of GPS orbits (crosses); Earth rotation rate: 1 revolution/sidereal day.*

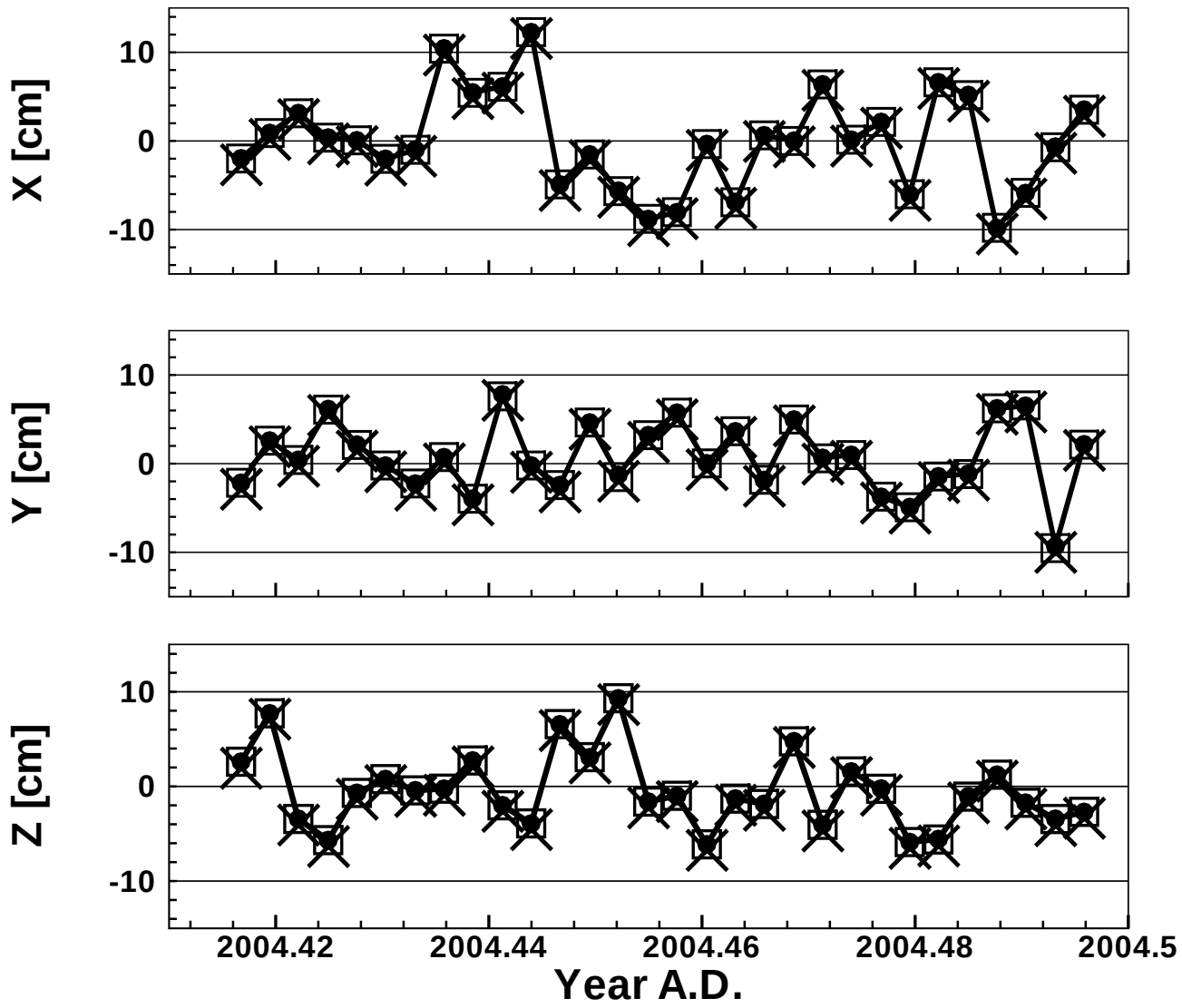

Figure C.3: *Supplementary simulations: time series of dynamic geocentre (circles), geometric geocentre (squares), and translations of GPS orbits (crosses); Earth rotation rate: 0 revolutions/sidereal day.*

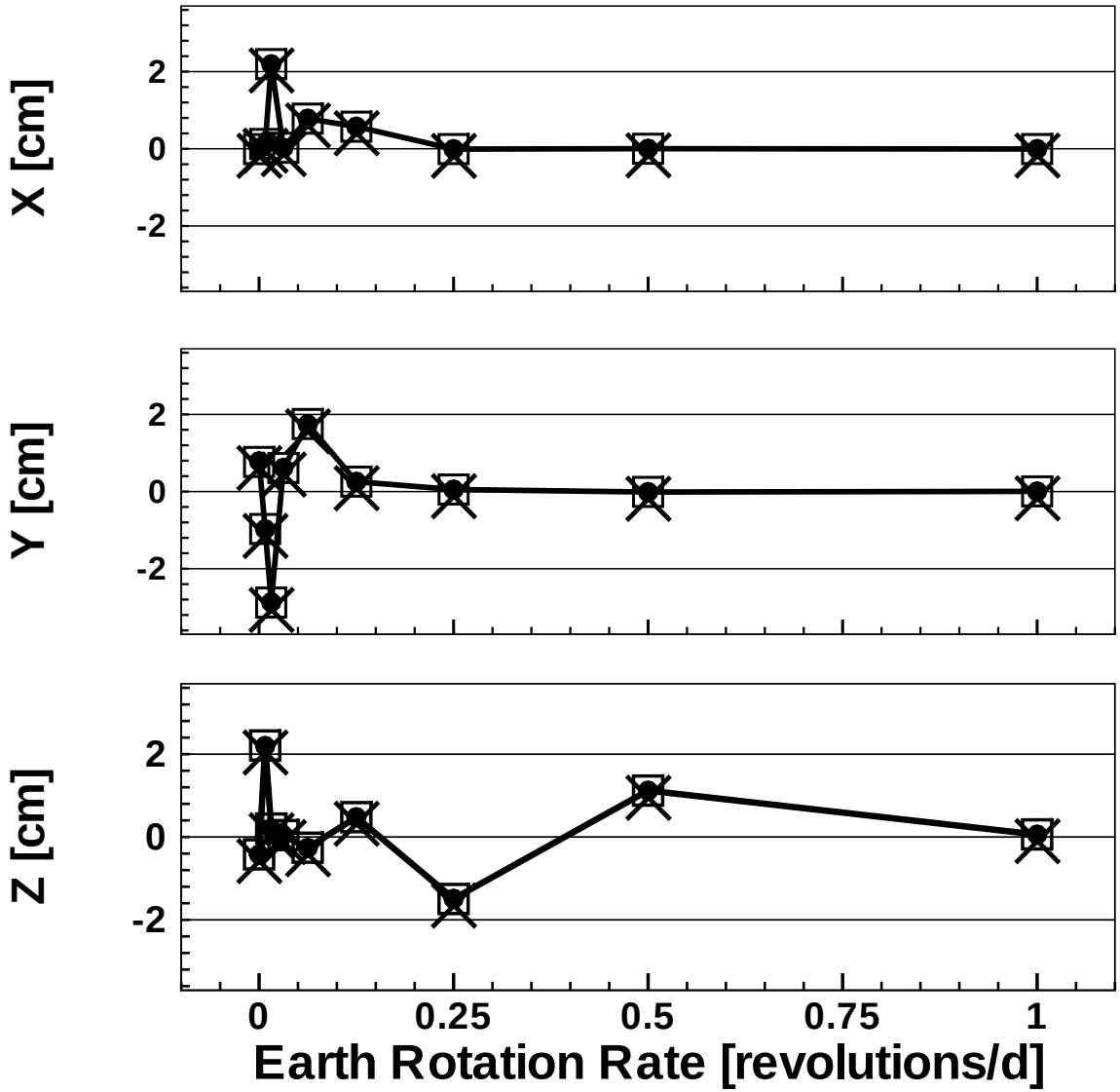

Figure C.4: *Supplementary simulations: mean values of time series of dynamic geocentre (circles), geometric geocentre (squares), and translations of GPS orbits (crosses) vs Earth rotation rate.*

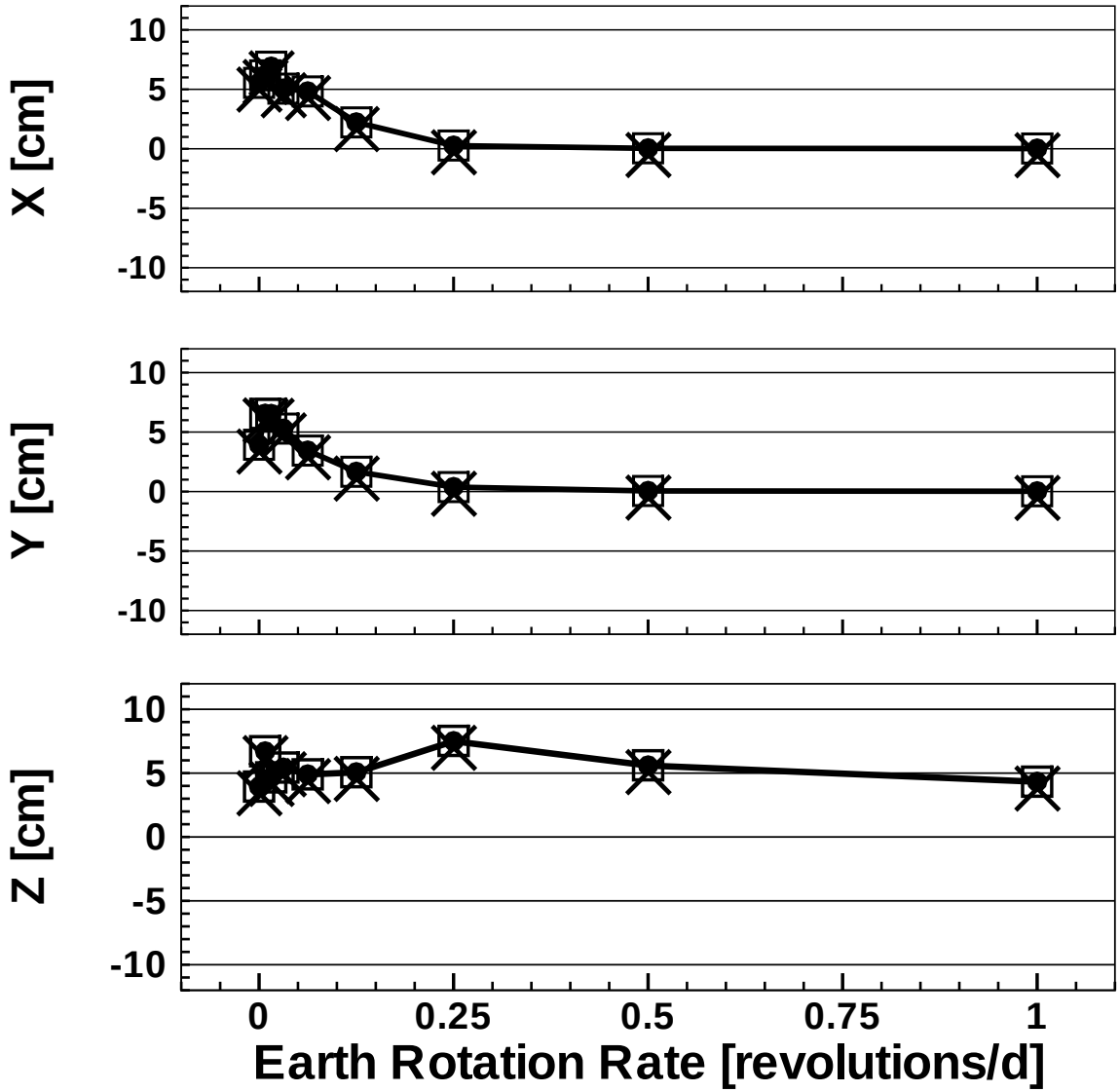

Figure C.5: *Supplementary simulations: standard deviations of time series of dynamic geocentre (circles), geometric geocentre (squares), and translations of GPS orbits (crosses) vs Earth rotation rate.*

Appendix D

No-net Translation/Scale/Rotation Conditions

The basis for NN-conditions is a similarity transformation between a set of position coordinates $\underline{x}_r$ of N stations of a reference TRF and a set $\underline{x}$ of position coordinates to be estimated, c.f. [Alt 02b] and [Alt 02c]. Considering the general case of arranging all seven transformation parameters, the coordinate transformation looks like

$$\begin{aligned} \underline{x}_r &= S\left([T_x\ T_y\ T_z]^T + \underline{R}_3(R_z)\underline{R}_2(R_y)\underline{R}_1(R_x)\underline{x}\right) \\ &=: \underline{F}(\underline{x},\underline{t}) \end{aligned} \tag{D-1}$$

with

$$\underline{t} = [T_x\ T_y\ T_z\ S\ R_x\ R_y\ R_z]^T$$

and $\underline{R}_k(\alpha)$ being an elementary rotation matrix describing the rotation about the k-axis given as

$$\begin{aligned} \underline{R}_1(\alpha) &= \begin{pmatrix} 1 & 0 & 0 \\ 0 & \cos\alpha & \sin\alpha \\ 0 & -\sin\alpha & \cos\alpha \end{pmatrix} \\ \underline{R}_2(\alpha) &= \begin{pmatrix} \cos\alpha & 0 & -\sin\alpha \\ 0 & 1 & 0 \\ \sin\alpha & 0 & \cos\alpha \end{pmatrix} \\ \underline{R}_3(\alpha) &= \begin{pmatrix} \cos\alpha & \sin\alpha & 0 \\ -\sin\alpha & \cos\alpha & 0 \\ 0 & 0 & 1 \end{pmatrix} \end{aligned} \tag{D-2}$$

Assuming small rotation angles R_x, R_y, R_z the linearisation w.r.t. the transformation parameters results in

$$\begin{aligned} \underline{x}_r &= \underline{F}(\underline{x},\underline{t}) \\ &\doteq \underline{x} + \underline{A}_t\underline{dt} \end{aligned} \tag{D-3}$$

with

$$\begin{aligned} \underline{t} &= \underline{t}_0 + \underline{dt} \\ &= [0\ 0\ 0\ 1\ 0\ 0\ 0]^T + [dT_x\ dT_y\ dT_z\ dS\ dR_x\ dR_y\ dR_z]^T \end{aligned} \tag{D-4}$$

$$\underline{A}_t = \begin{pmatrix} \vdots & \vdots & \vdots & \vdots & \vdots & \vdots & \vdots \\ 1 & 0 & 0 & x_{i,a} & 0 & z_{i,a} & -y_{i,a} \\ 0 & 1 & 0 & y_{i,a} & -z_{i,a} & 0 & x_{i,a} \\ 0 & 0 & 1 & z_{i,a} & y_{i,a} & -x_{i,a} & 0 \\ \vdots & \vdots & \vdots & \vdots & \vdots & \vdots & \vdots \end{pmatrix} \tag{D-5}$$

$x_{i,a}, y_{i,a}, z_{i,a}$: approximate coordinates of i-th station

In $\underline{A}_t$ the columns refer to the individual transformation parameters and the lines refer to a station's x-, y-, and z-coordinates as appearing in the order shown above.

In order to achieve a no-net change between $\underline{x}$ and $\underline{x}_r$, i.e. no-net translation (NNT), no-net scale (NNS), and no-net rotation (NNR), the transformation parameters are forced to vanish at the level of a chosen standard deviation σ_k (no-net conditions):

$$\underline{t} = \underline{0} \qquad \sim (\sigma_k) \tag{D-6}$$

with

k : k-th parameter in $\underline{t}$ (k = 1,...,7)

This is accomplished by solving for $\underline{t}$ by means of an unweighted least-squares procedure based on the linearised system (D-3):

$$\begin{array}{rcl} \underline{t} & = & \left(\underline{A}_t^T \underline{A}_t\right)^{-1} \underline{A}_t^T \, (\underline{x}_r - \underline{x}) \\ & =: & \underline{B} \;\; (\underline{x}_r - \underline{x}) \end{array}$$

The condition (D-6) is then added to an unconstrained least-squares problem (with only station coordinates $\underline{x}$ estimated for convenience) reading as

$$\begin{array}{ll} \underline{A}\,(\underline{x} - \underline{x}_0) = \underline{do} & \sim \underline{C} \;\; =: \sigma^2 \underline{W}^{-1} \; (see\, Eq.\,(2-23)) \\ \underline{B}\,(\underline{x}_r - \underline{x}) = \underline{0} & \sim \underline{C}_t =: \underline{W}_t^{-1} \end{array}$$

where

$\underline{x}_0$: vector of a priori coordinates

$$\underline{W}_t = \begin{pmatrix} \sigma_1^{-2} & & 0 \\ & \ddots & \\ 0 & & \sigma_7^{-2} \end{pmatrix}$$

In matrix form this results in

$$\begin{pmatrix} \underline{A} \\ \underline{B} \end{pmatrix} (\underline{x} - \underline{x}_0) = \begin{pmatrix} \underline{do} \\ \underline{B}(\underline{x}_r - \underline{x}_0) \end{pmatrix} \qquad \sim \begin{pmatrix} \underline{W} & \underline{0} \\ \underline{0} & \underline{W}_t \end{pmatrix} \tag{D-7}$$

or in short form:

$$\underline{A}_c \, \underline{dx} = \underline{do}_c \qquad \sim \underline{W}_c \tag{D-8}$$

From the combined system of observation equations the associated normal equation system

$$\begin{aligned}\left(\underline{A}^T\underline{W}\underline{A}+\underline{B}^T\underline{W}_t\underline{B}\right)(\underline{x}-\underline{x}_0) &= \underline{A}^T\underline{W}\underline{do}+\\ &\quad +\underline{B}^T\underline{W}_t\underline{B}\,(\underline{x}_r-\underline{x}_0)\end{aligned} \tag{D-9}$$

follows by simply adding the normal equations as well as the right-hand sides of both the original system and the system of no-net conditions.

Appendix E

Observation Equations and Partials

Observation Equations

- GPS-ground

For a specific pair of a transmitting satellite 'S' and a ground station receiver 'G' the original L1/L2 observations in metric unit [m] as preprocessed read as:

$$\begin{aligned} C^S_{G,Li}(t_G) &= \rho^S_G(t_G, t_G-\tau) + c\delta t_G - c\delta t^S + T_G T_0 + I_{Li} + \\ &\quad +\delta_{iono,Li} + \delta\rho_{rel} + \delta\rho_{PCO,Li} + \delta\rho_{PCV,Li} \qquad \text{(E-1)} \\ \Phi^S_{G,Li}(t_G) &= \rho^S_G(t_G, t_G-\tau) + c\delta t_G - c\delta t^S + T_G T_0 - I_{Li} + \\ &\quad -\delta_{iono,Li} + \delta\rho_{rel} + \delta\rho_{PCO,Li} + \delta\rho_{PCV,Li} + \lambda_{Li} N^S_{G,Li} \qquad \text{(E-2)} \end{aligned}$$

with

$$\rho^S_G = |\underline{x}_G(t_G) + \underline{\Delta x}_{G,ARP} + \underline{\Delta x}_{G,load} - \underline{x}^S(t_G-\tau)| \qquad \text{(E-3)}$$

and

C	*code delay observation*
Φ	*fractional carrier phase observation*
S	*GPS satellite (transmitter)*
G	*GPS ground station (receiver)*
Li	*GPS signal (i = 1,2)*
c	*speed of light ([Pet 10])*
δt_G	*clock offset w.r.t. GPS time of G*
δt^S	*clock offset w.r.t. GPS time of S*
t_G	*epoch of signal reception at the ground station*
T_0	*a priori tropospheric signal delay (model)*
T_G	*scaling factor of tropospheric signal delay at G*
I_{Li}	*ionospheric signal delay of first order of signal Li*
$\delta_{iono,Li}$	*ionospheric signal delay of second and higher order of signal Li*
$\delta\rho_{rel}$	*relativistic signal delay*
$\delta\rho_{PCO,Li}$	*PCO range correction of signal Li (sum of G and S)*

$\delta\rho_{PCV,Li}$	*PCV range correction of signal Li (sum of G and S)*
λ_{Li}	*wavelength of signal Li*
$N^S_{G,Li}$	*integer phase ambiguity for signal Li*
$\underline{x}_G$	*geocentric coordinate vector of the marker of G*
$\underline{x}^S$	*geocentric coordinate vector of the centre of mass of S*
τ	*one-way signal travel time*
$\underline{\Delta x}_{G,ARP}$	*ARP offset vector of G*
$\underline{\Delta x}_{G,load}$	*displacement of the marker of G due to loading*

Using the first-order relation (c.f. [Teu 98])

$$I_{L2} = \frac{f^2_{L1}}{f^2_{L2}} I_{L1}$$

with

f_{Li} *frequency of signal Li (i = 1,2)*

and introducing

$$C_{L3,1} := \frac{f^2_{L1}}{f^2_{L1} - f^2_{L2}} \qquad C_{L3,2} := \frac{f^2_{L2}}{f^2_{L1} - f^2_{L2}}$$

the L3 ionosphere-free LC is formed as

$$\begin{aligned}
\Phi^S_{G,L3}(t_G) &:= C_{L3,1}\Phi^S_{G,L1}(t_G) - C_{L3,2}\Phi^S_{G,L2}(t_G) \\
&= \left(\frac{f^2_{L1} - f^2_{L2}}{f^2_{L1} - f^2_{L2}}\right)\left(\rho^S_G + c\delta t_G - c\delta t^S + T_G T_0 + \delta\rho_{rel}\right) + \\
&+ \left(-C_{L3,1} I_{L1} + C_{L3,2}\frac{f^2_{L1}}{f^2_{L2}} I_{L1}\right) + \\
&+ C_{L3,1}\left(\delta\rho_{PCO,L1} + \delta\rho_{PCV,L1} - \delta_{iono,L1} + \lambda_{L1} N^S_{G,L1}\right) \\
&- C_{L3,2}\left(\delta\rho_{PCO,L2} + \delta\rho_{PCV,L2} - \delta_{iono,L2} + \lambda_{L2} N^S_{G,L2}\right) \\
&= \rho^S_G + c\delta t_G - c\delta t^S + T_G T_0 - \delta_{iono,L3} + \delta\rho_{rel} + \\
&\quad + \delta\rho_{PCO,L3} + \delta\rho_{PCV,L3} + N^S_{G,L3}
\end{aligned} \tag{E-4}$$

using

$$\begin{aligned}
\delta\rho_{PCO,L3} &:= C_{L3,1}\delta\rho_{PCO,L1} - C_{L3,2}\delta\rho_{PCO,L2} \\
\delta\rho_{PCV,L3} &:= C_{L3,1}\delta\rho_{PCV,L1} - C_{L3,2}\delta\rho_{PCV,L2} \\
\delta_{iono,L3} &:= C_{L3,1}\delta_{iono,L1} - C_{L3,2}\delta_{iono,L2} \\
N^S_{G,L3} &:= C_{L3,1}\lambda_{L1} N^S_{G,L1} - C_{L3,2}\lambda_{L2} N^S_{G,L2}
\end{aligned}$$

It has to be noted that $N^S_{G,L3}$ is of metric unit, and it is no longer an integer value. The L3 ionosphere-free LC is formed analogously for code observations. The relations finally read as:

$$\begin{aligned}
C^S_{G,L3}(t_R) &= \rho^S_G + c\delta t_G - c\delta t^S + T_G T_0 + \delta_{iono,L3} + \delta\rho_{rel} + \\
&\quad + \delta\rho_{PCO,L3} + \delta\rho_{PCV,L3}
\end{aligned} \tag{E-5}$$

$$\begin{aligned}
\Phi^S_{G,L3}(t_R) &= \rho^S_G + c\delta t_G - c\delta t^S + T_G T_0 - \delta_{iono,L3} + \delta\rho_{rel} + \\
&\quad + \delta\rho_{PCO,L3} + \delta\rho_{PCV,L3} + N^S_{G,L3}
\end{aligned} \tag{E-6}$$

The linearisation of the observation equations w.r.t. the unknown parameters is done as follows:

$$\begin{aligned}\Phi^S_{G,L3}(t_G) &\doteq \Phi^S_{G,L3}(t_G)|_0 + < \left(\frac{\partial \rho^S_G}{\partial \underline{x}_G}\right)_0, \underline{\Delta x}_G > + \\ &+ \left(\frac{\partial \Phi^S_{G,L3}}{\partial \delta t_G}\right)_0 \Delta\delta t_G + \left(\frac{\partial \Phi^S_{G,L3}}{\partial \delta t^S}\right)_0 \Delta\delta t^S + \\ &+ \left(\frac{\partial \Phi^S_{G,L3}}{\partial T_G}\right)_0 \Delta T_G + \left(\frac{\partial \Phi^S_{G,L3}}{\partial N^S_{G,L3}}\right)_0 \Delta N^S_{G,L3} \end{aligned} \tag{E-7}$$

where

$\underline{\Delta x}_G$	*correction to a priori coordinates of G*
$\Delta\delta t_G$	*correction to a priori value of* δt_G
$\Delta\delta t^S$	*correction to a priori value of* δt^S
ΔT_G	*correction to a priori value of* T_G
$\Delta N^S_{G,L3}$	*correction to a priori value of* $N^S_{G,L3}$

The partial derivatives are obtained by straightforward differentiation:

$$\left(\frac{\partial \rho^S_G}{\partial \underline{x}_G}\right)_0 = \left(-\underline{u}^S_G\right)_0$$

$$\left(\frac{\partial \Phi^S_{G,L3}}{\partial \delta t_G}\right)_0 = c \qquad \left(\frac{\partial \Phi^S_{G,L3}}{\partial \delta t^S}\right)_0 = -c$$

$$\left(\frac{\partial \Phi^S_{G,L3}}{\partial T_G}\right)_0 = T_0 \qquad \left(\frac{\partial \Phi^S_{G,L3}}{\partial N^S_{G,L3}}\right)_0 = 1$$

with

$\underline{u}^S_G$	*unit vector pointing from G to S*

It should be noted that the partial derivatives $\partial\Phi^S_{G,L3}/\partial\delta t_G$ as well as $\partial\Phi^S_{G,L3}/\partial\delta t^S$ as stated above possess merely formal meaning. They should not be used for numerical computations because they are approximately 10^8 times larger than the other partial derivatives as their magnitude is that of c.

The linearisation is done analogously for code observations.

- GPS-SST

Without the need to account for tropospheric signal delays the L3 observations respectively for code and phase observations between S and the LEO 'L' are obtained analogously to the GPS-ground case with all terms bearing the corresponding meaning:

$$C^S_{L,L3}(t_R) = \rho^S_L + c\delta t_L - c\delta t^S + \delta\rho_{rel} + \delta\rho_{PCO} + \delta\rho_{PCV} \tag{E-8}$$

$$\begin{aligned}\Phi^S_{L,L3}(t_R) &= \rho^S_L + c\delta t_L - c\delta t^S + \delta\rho_{rel} + \delta\rho_{PCO} + \delta\rho_{PCV} \\ &\quad + N^S_{L,L3}\end{aligned} \tag{E-9}$$

where

$$\rho^S_L = |\underline{x}_L(t_L) + \underline{\Delta x}_{L,ARP} - \underline{x}^S(t_L - \tau)| \tag{E-10}$$

The linearisation is done the same way as for GPS-ground measurements and is not repeated here.

- KBRR

The KBRR observation $\dot{\rho}_{KB}$ is derived from the nominal unbiased K-band range observation ρ_{KB} between both satellites, defined as (c.f. [Kim 00])

$$\rho_{KB}(t) \;=\; \sqrt{<\underline{x}_{12}(t), \underline{x}_{12}(t)>}$$

with

t		*measurement epoch*
$\underline{x}_{12}(t)$	$=$	$\underline{x}_{L2}(t) - \underline{x}_{L1}(t)$
$\underline{x}_{Li}(t)$		*geocentric position vector of LEO i (i = 1, 2)*

by derivation w.r.t. time and adding a polynomial P according to [Kim 00] to account for several biases:

$$\begin{aligned}\dot{\rho}_{KB}(t) \;&:=\; \frac{d}{dt}\left(\rho_{KB}(t)\right) \;+\; P\left(P_1, P_2, C_0, S_0, \dot{v}(t), u(t), t\right) \\ &:=\; \frac{1}{\rho_{KB}} <\dot{\underline{x}}_{12}(t), \underline{x}_{12}(t)> \;+ \\ &\quad + P_1 \;+\; 2P_2 t \;+\; C_0 \dot{v}(t)\cos u(t) \;-\; S_0 \dot{v}(t)\sin u(t)\end{aligned} \tag{E-11}$$

with

t	*measurement epoch*
$\dot{v}(t)$	*mean anomaly rate*
$u(t)$	*argument of latitude*
P_1	*polynomial model: range-rate bias*
P_2	*polynomial model: range-acceleration bias*
C_0	*periodic model: range bias cos amplitude*
S_0	*periodic model: range bias sin amplitude*

The linearisation is accomplished by the usual expansion into a Taylor series as

$$\begin{aligned}\dot{\rho}_{KB} \;\doteq\; \dot{\rho}_{KB}|_0 &+ \frac{\partial \dot{\rho}_{KB}}{\partial P_1}|_0 \Delta P_1 + \frac{\partial \dot{\rho}_{KB}}{\partial P_2}|_0 \Delta P_2 + \\ &+ \frac{\partial \dot{\rho}_{KB}}{\partial C_0}|_0 \Delta C_0 + \frac{\partial \dot{\rho}_{KB}}{\partial S_0}|_0 \Delta S_0\end{aligned} \tag{E-12}$$

with the partial derivatives derived by straightforward differentiation, c.f. [Kim 00]:

$$\begin{aligned}\frac{\partial \dot{\rho}_{KB}}{\partial P_1} &= 1 & \frac{\partial \dot{\rho}_{KB}}{\partial P_2} &= 2t \\ \frac{\partial \dot{\rho}_{KB}}{\partial C_0} &= \dot{v}(t)\cos u(t) & \frac{\partial \dot{\rho}_{KB}}{\partial S_0} &= -\dot{v}(t)\sin u(t)\end{aligned} \tag{E-13}$$

- SLR

In the context of this work the SLR observations are only used for validating the satellite orbits derived by the Integrated Approach, and thus they do not enter the parameter estimation. For this reason their observation equations merely comprise the distance ρ^S_{GS} between a SLR ground station and a retro-reflecting satellite as well as a few non-estimated corrections. The proper observations used are one-way travel times $\tau^S_{GS,1}$ of the laser signal between the SLR ground station 'GS' and the LRR mounted on the respective satellite 'S'. They are derived from the originally measured two-way travel times $\tau^S_{GS,2}$ according to

$$\tau^S_{GS,1} = \tfrac{1}{2}\tau^S_{GS,2} \tag{E-14}$$

The observation equations then read as

$$\tau^S_{GS,1} = \frac{1}{c}\rho^S_{GS} + T_0 + \delta\rho_{rel} \tag{E-15}$$

with

$$\begin{aligned} \rho^S_{GS} \;=\; & |\underline{x}_{GS}(t_{LRR}) + \underline{\Delta x}_{GS,LRP} + \underline{\Delta x}_{GS,load} \\ & -(\underline{x}^S(t_{LRR}) + \underline{\Delta x}^S_{LRR})| \end{aligned} \tag{E-16}$$

and

GS	*SLR ground station*
S	*LRR-equipped satellite*
c	*speed of light ([Pet 10])*
T_0	*a priori tropospheric signal delay (model)*
$\delta\rho_{rel}$	*relativistic range correction (model)*
$\underline{x}_{GS}$	*geocentric coordinate vector of the marker of GS*
$\underline{x}^S$	*geocentric coordinate vector of the centre of mass of S*
$\underline{\Delta x}_{GS,LRP}$	*LRP offset vector*
$\underline{\Delta x}^S_{LRR}$	*LRR offset vector*
$\underline{\Delta x}_{GS,load}$	*displacement of the marker of GS due to loading*
t_{LRR}	*epoch of signal reflection at the LRR of S*

As the parameters appearing in the above observation equation will not be estimated, a linearisation is obsolete.

Partial Derivatives of $\underline{o}$ w.r.t. satellite position and velocity

The partial derivatives of the observations contained in $\underline{o}$ w.r.t. a satellite's position and velocity, i.e. $\partial\underline{o}/\partial\underline{x}^S$ and $\partial\underline{o}/\partial\dot{\underline{x}}^S$, are necessary for determining the partial derivatives $\partial\underline{o}/\partial\underline{p}_D$ in Eq. (2-10). For the various observation types they read as follows using the same notations as for the observation equations:

- GPS-ground

$$\begin{aligned}
\frac{\partial \Phi^S_{G,L3}}{\partial \underline{x}^S} &= \frac{\partial C^S_{G,L3}}{\partial \underline{x}^S} = \frac{\partial \rho^S_G}{\partial \underline{x}^S} = \underline{u}^S_G \\
\frac{\partial \Phi^S_{G,L3}}{\partial \underline{\dot{x}}^S} &= \frac{\partial C^S_{G,L3}}{\partial \underline{\dot{x}}^S} = \frac{\partial \rho^S_G}{\partial \underline{\dot{x}}^S} = 0
\end{aligned} \tag{E-17}$$

- GPS-SST

$$\begin{aligned}
\frac{\partial \Phi^S_{L,L3}}{\partial \underline{x}^S} &= \frac{\partial C^S_{L,L3}}{\partial \underline{x}^S} = \frac{\partial \rho^S_L}{\partial \underline{x}^S} = \underline{u}^S_L \\
\frac{\partial \Phi^S_{L,L3}}{\partial \underline{\dot{x}}^S} &= \frac{\partial C^S_{L,L3}}{\partial \underline{\dot{x}}^S} = \frac{\partial \rho^S_L}{\partial \underline{\dot{x}}^S} = 0
\end{aligned} \tag{E-18}$$

- KBRR

$$\begin{aligned}
\frac{\partial \dot{\rho}_{KB}}{\partial \underline{x}_{L1}} &= \frac{1}{\rho_{KB}}\left(\underline{\dot{x}}_{12} - \frac{\dot{\rho}_{KB}}{\rho_{KB}}\underline{x}_{12}\right) & \frac{\partial \dot{\rho}_{KB}}{\partial \underline{x}_{L2}} &= -\frac{\partial \dot{\rho}_{KB}}{\partial \underline{x}_{L1}} \\
\frac{\partial \dot{\rho}_{KB}}{\partial \underline{\dot{x}}_{L1}} &= \frac{1}{\rho_{KB}}\underline{x}_{12} & \frac{\partial \dot{\rho}_{KB}}{\partial \underline{\dot{x}}_{L2}} &= -\frac{\partial \dot{\rho}_{KB}}{\partial \underline{\dot{x}}_{L1}}
\end{aligned} \tag{E-19}$$

Appendix F

Models

Table F.1: *Models used for orbit forces (RL04++).*

	GPS		GRACE	
Force	*Model*	*Reference*	*Model*	*Reference*
Gravitation				
Earth gravity	EIGEN-GL04S1 ($n \leq 120$)	[För 07]	EIGEN-GL04S1 ($n \leq 120$)	[För 07]
Lunar gravity	Ferrari 77 ($n \leq 4$)	[Fer 77]	Ferrari 77 ($n \leq 4$)	[Fer 77]
Third bodies	*Planetary and lunar ephemeris:*		*Planetary and lunar ephemeris:*	
	JPL DE405	[JPL 12a]	JPL DE405	[JPL 12a]
Atmospheric tides	Biancale&Bode	[Bia 06]	Biancale&Bode	[Bia 06]
Ocean tides	FES2004	[Lya 04]	FES2004	[Lya 04]
Ocean Pole tide	IERS2003	[McC 04]	IERS2003	[McC 04]
Solid Earth tides	IERS2003	[McC 04]	IERS2003	[McC 04]
Solid Earth Pole tide	IERS2003	[McC 04]	IERS2003	[McC 04]
Short-term non-tidal atmospheric and oceanic mass variations	AOD1B (GRACE RL04)	[Fle 07]	AOD1B (GRACE RL04)	[Fle 07]
Surface forces				
Air drag	neglected	-	measured	-
Solar radiation pressure	ROCK4	[Fli 92], [Fli 96]	measured	-
Earth albedo	neglected	-	measured	-
Others				
Empirical forces	amplitudes for cos, sin	-	amplitudes for cos, sin	-
General relativistic effects	IERS2010	[Pet 10, 10.3]	IERS2010	[Pet 10, 10.3]

Table F.2: *Models used for orbit forces (RL05).*

	GPS		GRACE	
Force	*Model*	*Reference*	*Model*	*Reference*
Gravitation				
Earth gravity	EIGEN-6C ($n \leq 200$)	[För 11]	EIGEN-6C ($n \leq 200$)	[För 11]
Lunar gravity	Ferrari 77 ($n \leq 4$)	[Fer 77]	Ferrari 77 ($n \leq 4$)	[Fer 77]
Third bodies	*Planetary and lunar ephemeris:*		*Planetary and lunar ephemeris:*	
	JPL DE421	[JPL 12b]	JPL DE421	[JPL 12b]
Atmospheric tides	Biancale&Bode	[Bia 06]	Biancale&Bode	[Bia 06]
Ocean tides	EOT11a	[Sav 12]	EOT11a	[Sav 12]
Ocean Pole tide	IERS2010	[Pet 10]	IERS2010	[Pet 10]
Solid Earth tides	IERS2010	[Pet 10]	IERS2010	[Pet 10]
Solid Earth Pole tide	IERS2010	[Pet 10]	IERS2010	[Pet 10]
Short-term non-tidal atmospheric and oceanic mass variations	AOD1B (GRACE RL05)	-	AOD1B (GRACE RL05)	-
Surface forces				
Air drag	neglected	-	measured	-
Solar radiation pressure	ROCK4	[Fli 92], [Fli 96]	measured	-
Earth albedo	neglected	-	measured	-
Others				
Empirical forces	amplitudes for cos, sin	-	amplitudes for cos, sin	-
General relativistic effects	IERS2010	[Pet 10, 10.3]	IERS2010	[Pet 10, 10.3]

Table F.3: *A priori and background models used.*

	RL04++		RL05	
Application	*Model*	*Reference*	*Model*	*Reference*
A Priori Models				
Earth gravity	EIGEN-GL04S1	[För 07]	EIGEN-6C	[För 11]
Station coordinates	ITRF2008	[Alt 11]	IGS08	[IGS 12b]
GPS initial elements	igs rapid	[IGS 12a]	igs final	[IGS 12a]
GPS tropospheric signal delay	GMF-E (c.f. description past table)	[Boe 06a]	VMF1 (c.f. description past table)	[Boe 06b]
Background Models				
GPS ground stations ARP offset vectors	-	[IGS 12g]	-	[IGS 12g]
GPS absolute phase centre corrections - ground antennas - GRACE POD antennas resolution: azim.[^{o}] x elev.[^{o}]	 igs08_1604_woGLO_final custom PCV masks derived from GPS-SST residuals $5^o \times 2^o$	 [IGS 12c] -	 igs05_1473 custom PCV masks derived from GPS-SST residuals $1^o \times 1^o$	 [Schm 07] -
Earth Orientation Parameters	IERS2003	[McC 04]	IERS2010	[Pet 10]
Planetary and lunar ephemeris	JPL DE 405	[JPL 12a]	JPL DE 421	[JPL 12b]
SLR tropospheric signal delay	Mendes&Pavlis	[Men 04]	Mendes&Pavlis	[Men 04]
GPS ionospheric signal delay	-	-	IGS ionospheric maps	[IGS 12d]
GPS and SLR relativistic signal delay	 IERS2010	 [Pet 10, 11.2]	 IERS2010	 [Pet 10, 11.2]
Solid Earth tides loading	IERS2003	[McC 04]	IERS2010	[Pet 10]
Solid Earth pole tide loading	IERS2003	[McC 04]	IERS2010	[Pet 10]

A priori models for GPS tropospheric delays

The computation of the a priori tropospheric delay T_0 of GPS signals according to GMF-E and VMF1 is done in detail as follows. In the context of this work "GMF-E" as well as "VMF1" not only imply merely a mapping function but also the computation of the dry and the wet zenith delays. Both GMF-E and VMF1 have in common formula (F-1) for computing the total tropospheric delay T_0 as well as formula (F-2) of the mapping function f_m:

$$T_0 = (f_m(a_d, b_d, c_d, e) + \Delta h_d)\ T_d^z + f_m(a_w, b_w, c_w, e)\ T_w^z \tag{F-1}$$

with

$$f_m(a, b, c, e) = \frac{1 + \frac{a}{1+\frac{b}{1+c}}}{sine + \frac{a}{sine+\frac{b}{sine+c}}} \tag{F-2}$$

$$\Delta h_d = \frac{h}{1000}\left(\frac{1}{\sin(e)} - f_m(a_t, b_t, c_t, e)\right) \tag{F-3}$$

and

$$\begin{aligned} T_d^z &: \textit{dry zenith delay} \\ T_w^z &: \textit{wet zenith delay} \\ e &: \textit{elevation of signal direction} \\ \Delta h_d &: \textit{height correction ([Nie 96])} \\ a_t &= 2.53 \cdot 10^{-5} \\ b_t &= 5.49 \cdot 10^{-3} \\ c_t &= 1.14 \cdot 10^{-3} \end{aligned}$$

The two sets of coefficients (a_d, b_d, c_d) as well as (a_w, b_w, c_w) determining the mapping of the dry and the wet zenith delay, respectively, are explained further below.

- Dry zenith delay

For both GMF-E and VMF1 the dry zenith delay is determined according to [Saa 73] as

$$T_d^z = \frac{0.0022768\ p}{1 - 0.00266\ \cos(2\varphi) - 0.28 \cdot 10^{-6}\ h} \tag{F-4}$$

where

$$\begin{aligned} \varphi &: \textit{geodetic latitude} \\ h &: \textit{geodetic height above sea level in metres} \\ p &: \textit{total atmospheric pressure in hPa} \end{aligned}$$

- Wet zenith delay

In case of GMF-E the wet zenith delay is computed following [Dav 84] as

$$T_w^z = \frac{0.0022768\ p_{wv}}{0.99734 + 0.00532\sin^2\varphi - 0.28 \cdot 10^{-6}\ h}\left(0.053 + \frac{1277}{T}\right) \tag{F-5}$$

with

$$\begin{aligned} T &: \textit{temperature in Kelvin} \\ p_{wv} &: \textit{partial pressure of water vapour in hPa} \end{aligned}$$

For VMF1 the wet zenith delay at height h of the station is calculated as

$$T_w^z = T_w^z(h_{oro}) e^{\frac{h_{oro}-h}{2000}} \tag{F-6}$$

with

$$h_{oro} : \textit{orography height}$$

and $T_w^z(h_{oro})$ interpolated from a grid provided at [IGG 12a].

- Mapping function coefficients

The a-coefficients a_h and a_w are computed differently for GMF-E and VMF1. In case of GMF-E they are respectively determined as

$$a = a_0 + A\cos\left(2\pi\frac{doy-28}{365.25}\right) \tag{F-7}$$

with

$$\begin{aligned} a_0 &= \sum_{n=0}^{9}\sum_{m=0}^{n} P_{nm}(\sin\varphi)[A_{nm}\cos(m\lambda) + B_{nm}\sin(m\lambda)] \\ A &= \sum_{n=0}^{9}\sum_{m=0}^{n} P_{nm}(\sin\varphi)[A'_{nm}\cos(m\lambda) + B'_{nm}\sin(m\lambda)] \\ doy &: \textit{day of year} \\ P_{nm} &: \textit{associated Legendre functions} \end{aligned}$$

The coefficients A_{nm}, B_{nm}, A'_{nm}, B'_{nm} are given in the sample source code [IGG 12b]. In case of VMF1 a_h and a_w are interpolated from a grid provided through [IGG 12a]. The b- as well as the c-coefficients b_h, b_w, c_h, c_w are the same applying either GMF-E or VMF1:

$$\begin{aligned} b_h &= 0.0029 \\ b_w &= 0.00146 \\ c_h &= c_0\left\{\left[\cos\left(2\pi\frac{doy-28}{365.25}+\psi\right)+1\right]\frac{c_{11}}{2}+c_{10}\right\}(1-\cos\varphi) \\ c_w &= 0.04391 \end{aligned} \tag{F-8}$$

where

$$\begin{aligned} c_0 &= 0.062 \\ (\psi, c_{10}, c_{11}) &= \begin{cases} (0, 0.001, 0.005) & \textit{on northern hemisphere} \\ (\pi, 0.002, 0.007) & \textit{on southern hemisphere} \end{cases} \end{aligned}$$

Appendix G

Processing Configurations

Table G.1: *Overview of nominal parameterisation (RL04m).*

Parameter type	Items estimated	Spatial components	Temporal resolution
TRF			
Earth gravity field coefficients	$(C/S)_{nm}$	-	$1/day$
Station coordinates	$\underline{x}_S$	X, Y, Z (CTS)	$1/day$
auxiliary dynamic			
initial elements	$\underline{x}^{S0}$	X, Y, Z (CTS)	$1/day$
GPS solar radiation pressure	*correction of a priori model*		
	bias	global	$1/day$
	scale	global	$1/day$
Empirical accelerations			
- GPS	*periodic model*		-
	- cosine amplitude	T, N	$1/day$
	- sine amplitude	T, N	$1/day$
- GRACE	*periodic model*		-
	- cosine amplitude	T, N	$5/day$
	- sine amplitude	T, N	$5/day$
Accelerometer calibration	bias	R, T, N	$5/day$
	scale	R, T, N	$5/day$
auxiliary geometric			
GPS clock corrections	$\delta t_R, \delta t^S$	-	per epoch
GPS ambiguities	N_R^S	-	per session
GPS tropospheric scaling factors	T_R	-	$10/day$
empirical KBRR coefficients	*polynomial model*		
	- bias (P_1)	-	$17/day$
	- acceleration (P_2)	-	$17/day$
	periodic model		
	- bias cosine amplitude (C_0)	-	$9/day$
	- bias sine amplitude (S_0)	-	$9/day$

Table G.2: *Characteristics of integrated processings carried out (RL04m; 'CC': constrained coordinates, 'NN': No-net conditions).*

Run 4-nn-t	ITRF	GPS abs. PCCs	$(C/S)_{nm}$		$\underline{x}_S$	Empirical accelerations		Weight model for observations weight = f/σ^2		
nn: test no. t: type			n = 0	n = 1, 2				f, σ		
0 (integrated) 1 (2-step, GPS) 2 (2-step, LEO)	model used	model used	a priori sigma		a priori sigma	resolution		GPS-ground C: code, P: phase	GPS-SST	KBRR
			$[cm]$	$[cm]$	$[cm]$	GPS	GRACE	$[/]$, $[cm]$	$[/]$, $[cm]$	$[/]$, $[\mu m/s]$
					CC					
4-00-0	RL04++	RL05	10	10	10	1/d	5/d	C: 1, 100.0 P: 1, 1.0	C: 1.0, 70.0 P: 1.0, 0.7	1.0, 0.3
					NN: T_z,R_z					
4-01-0	RL04++	RL05	0	∞	0.01	1/d	5/d	C: 1, 100.0 P: 1, 1.0	C: 1, 70.0 P: 1, 0.7	1, 0.3
4-02-0	RL04++	RL05	0	∞	0.01	1/d	5/d	C: 1, 70.0 P: 1, 0.7	C: 20, 45.0 P: 2, 0.14	10, 0.3

Table G.3: *Characteristics of integrated processings carried out (RL04m; continued; 'NN': No-net conditions).*

Run 4-nn-t	ITRF	GPS abs. PCCs	$(C/S)_{nm}$		$\underline{x}_S$	Empirical accelerations		Weight model for observations weight = f/σ^2		
nn: test no. t: type			n = 0	n = 1, 2				f, σ		
0 (integrated) 1 (2-step, GPS) 2 (2-step, LEO)	model used	model used	a priori sigma		a priori sigma	resolution		GPS-ground C: code, P: phase	GPS-SST	KBRR
			[cm]	[cm]	[cm]	GPS	GRACE	[/], [cm]	[/], [cm]	[/], [$\mu m/s$]
					NN: T_z,R_z					
4-03-0	RL04++	RL04++	0	∞	0.01	1/d	16/d	C: 1, 70.0 P: 1, 0.7	C: 20, 45.0 P: 2, 0.14	50, 0.3
					NN: T_x,T_y,T_z,R_z					
4-04-0	RL04++	RL04++	0	∞	0.01	1/d	16/d	C: 1, 70.0 P: 1, 0.7	C: 20, 45.0 P: 2, 0.14	50, 0.3
4-04-1	RL04++	RL04++	0	0	0.01	1/d	-	C: 1, 70.0 P: 1, 0.7	- -	- -
4-04-2	RL04++	RL04++	0	∞	-	-	16/d	- -	C: 20, 45.0 P: 2, 0.14	50, 0.3
fixed IGS final orbits										
					NN: T_z,SC,R_z					
4-05-0	RL04++	RL04++	0	∞	0.001	-	16/d	C: 1, 70.0 P: 1, 0.7	C: 20, 45.0 P: 2, 0.14	50, 0.3

Table G.4: *Overview of nominal parameterisation (RL05m).*

Parameter type	Items estimated	Spatial components	Temporal resolution
TRF			
Earth gravity field coefficients	$(C/S)_{nm}$	-	$1/day$
Station coordinates	$\underline{x}_S$	X, Y, Z (CTS)	$1/day$
auxiliary dynamic			
initial elements	$\underline{x}^{S0}$	X, Y, Z (CTS)	$1/day$
GPS solar radiation pressure	*correction of a priori model*		
	bias	global	$1/day$
	scale	global	$1/day$
Empirical accelerations			
- GPS	*periodic model*		-
	- cosine amplitude	T, N	$1/day$
	- sine amplitude	T, N	$1/day$
- GRACE	*periodic model*		-
	- cosine amplitude	T, N	$16/day$
	- sine amplitude	T, N	$16/day$
Accelerometer calibration	bias	R, T, N	$5/day$
	scale	R, T, N	$5/day$
auxiliary geometric			
GPS clock corrections	$\delta t_R, \delta t^S$	-	per epoch
GPS ambiguities	N_R^S	-	per session
GPS tropospheric scaling factors	T_R	-	$10/day$
empirical KBRR coefficients	*polynomial model*		
	- bias (P_1)	-	$17/day$
	- acceleration (P_2)	-	$17/day$
	periodic model		
	- bias cosine amplitude (C_0)	-	$9/day$
	- bias sine amplitude (S_0)	-	$9/day$

Table G.5: *Characteristics of integrated processings carried out (RL05m; 'NN': No-net conditions).*

Run 5-nn-t	$(C/S)_{nm}$		$\underline{x}_S$	Weight model for observations weight = f/σ^2		
nn: test no. t: type 0 (integrated) 1 (2-step, GPS) 2 (2-step, LEO)	n = 1 a priori sigma	n = 2	a priori sigma $[cm]$	f, σ GPS-ground C: code, P: phase [/], $[cm]$	GPS-SST [/], $[cm]$	KBRR [/], $[\mu m/s]$
			NN: T_z,R_z			
5-00-0	∞	∞	0.01	C: 1, 100.0 P: 1, 1.0	C: 1, 70.0 P: 1, 0.7	1, 0.3
5-01-0	∞	∞	0.01	C: 1, 70.0 P: 1, 0.7	C: 20, 45.0 P: 2, 0.14	50, 0.2
			NN: T_x,T_y,T_z,R_z			
5-02-0	∞	∞	0.01	C: 1, 70.0 P: 1, 0.7	C: 20, 45.0 P: 2, 0.14	50, 0.2
5-02-1	0	0	0.01	C: 1, 70.0 P: 1, 0.7	- -	-
5-02-2	∞	∞	-	- -	C: 20, 45.0 P: 2, 0.14	50, 0.2
5-03-0	∞	∞	0.01	C: 1, 70.0 P: 1, 0.7	C: 20, 45.0 P: 2, 0.14	-
5-04-0	∞	0	0.01	C: 1, 70.0 P: 1, 0.7	C: 20, 45.0 P: 2, 0.14	-

Table G.6: *Characteristics of integrated processings carried out (RL05m; continued; 'NN': No-net conditions).*

Run 5-nn-t	$(C/S)_{nm}$		$\underline{x}_S$	Weight model for observations weight = f/σ^2		
nn: test no. t: type 0 (integrated) 1 (2-step, GPS) 2 (2-step, LEO)	n = 1	n = 2		f, σ		
	a priori sigma		a priori sigma	GPS-ground	GPS-SST	KBRR
				C: code, P: phase		
			$[cm]$	[/], $[cm]$	[/], $[cm]$	[/], $[\mu m/s]$
constrained GPS orbits:			*initial elements*		$\underline{X}^0 \sim 1[cm]$	
			solar radiation pressure		*scale* $\sim 10^{-3}[/]$	
					bias $\sim 10^{-11}[m/s^2]$	
			empirical accelerations		$T, N \sim 10^{-10}[m/s^2]$	
			NN: T_x,T_y,T_z,R_z			
5-05-0	∞	∞	0.01	C: 1, 70.0 P: 1, 0.7	C: 20, 45.0 P: 2, 0.14	50, 0.2

Appendix H

Results: Plots

H.1 TRF parameters

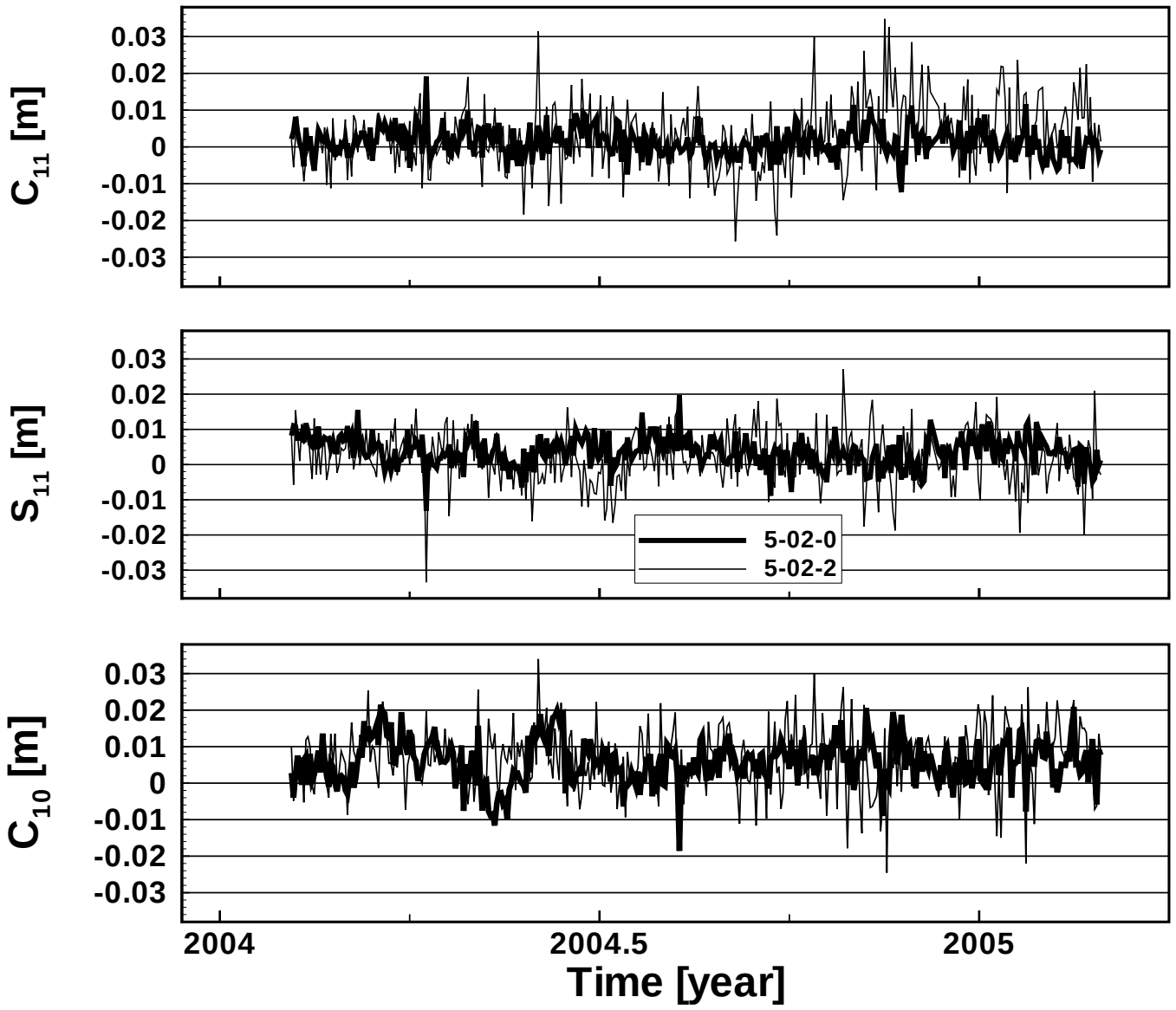

Figure H.1: *Dynamic Geocentre x-, y-, z-component per day.*

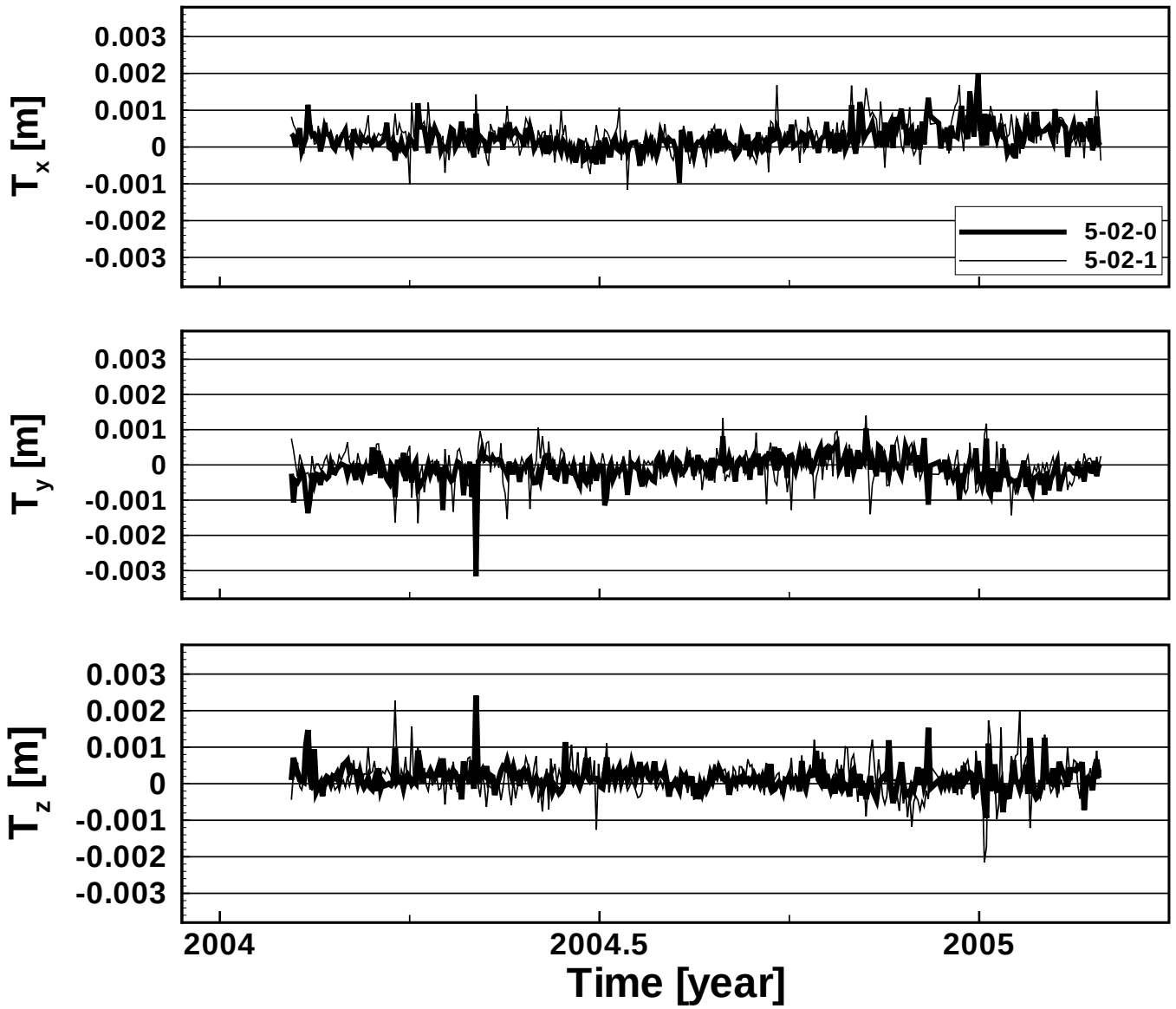

Figure H.2: *Geometric Geocentre x-, y-, z-component per day.*

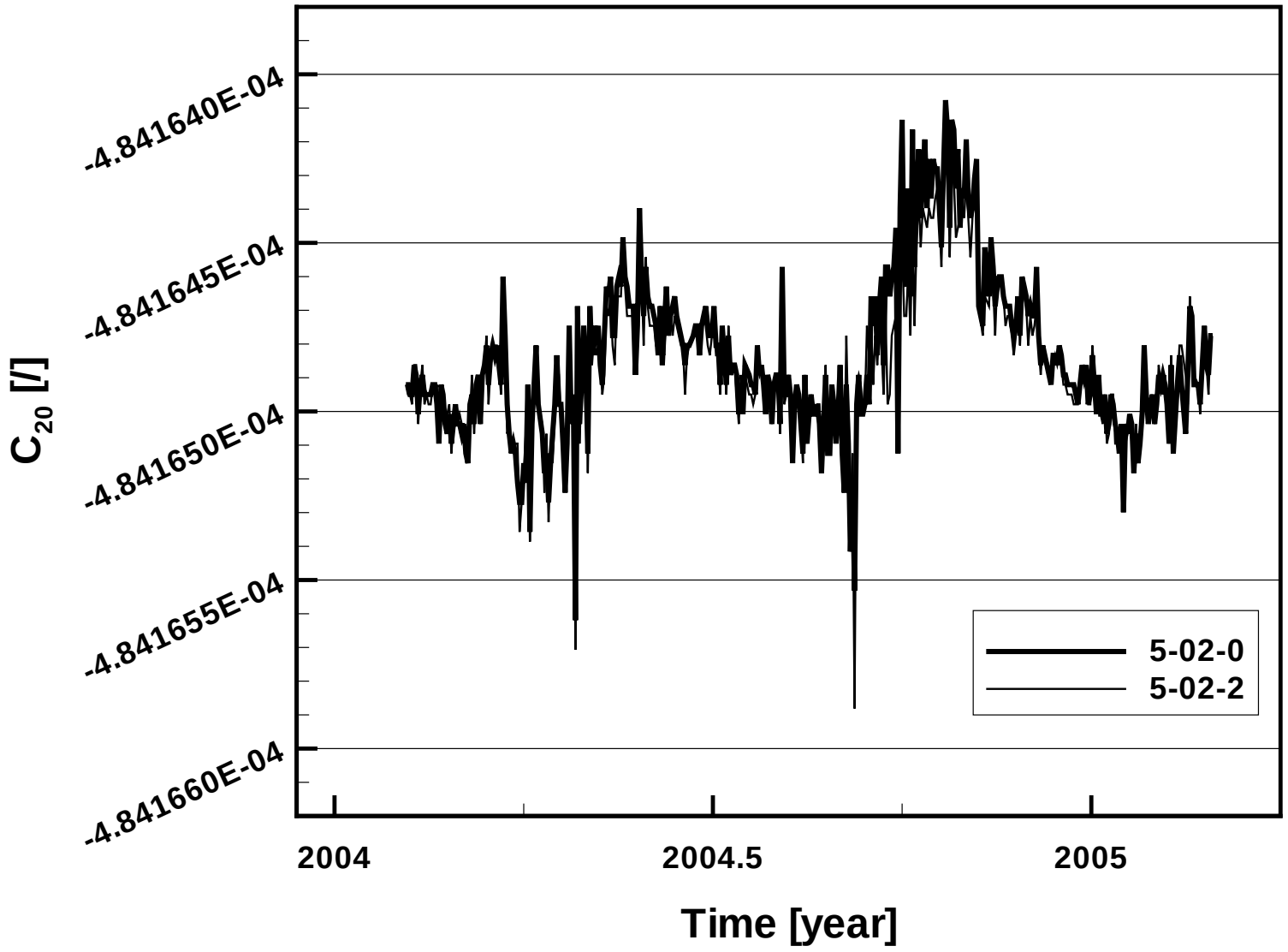

Figure H.3: *Flattening of Earth gravity field per day.*

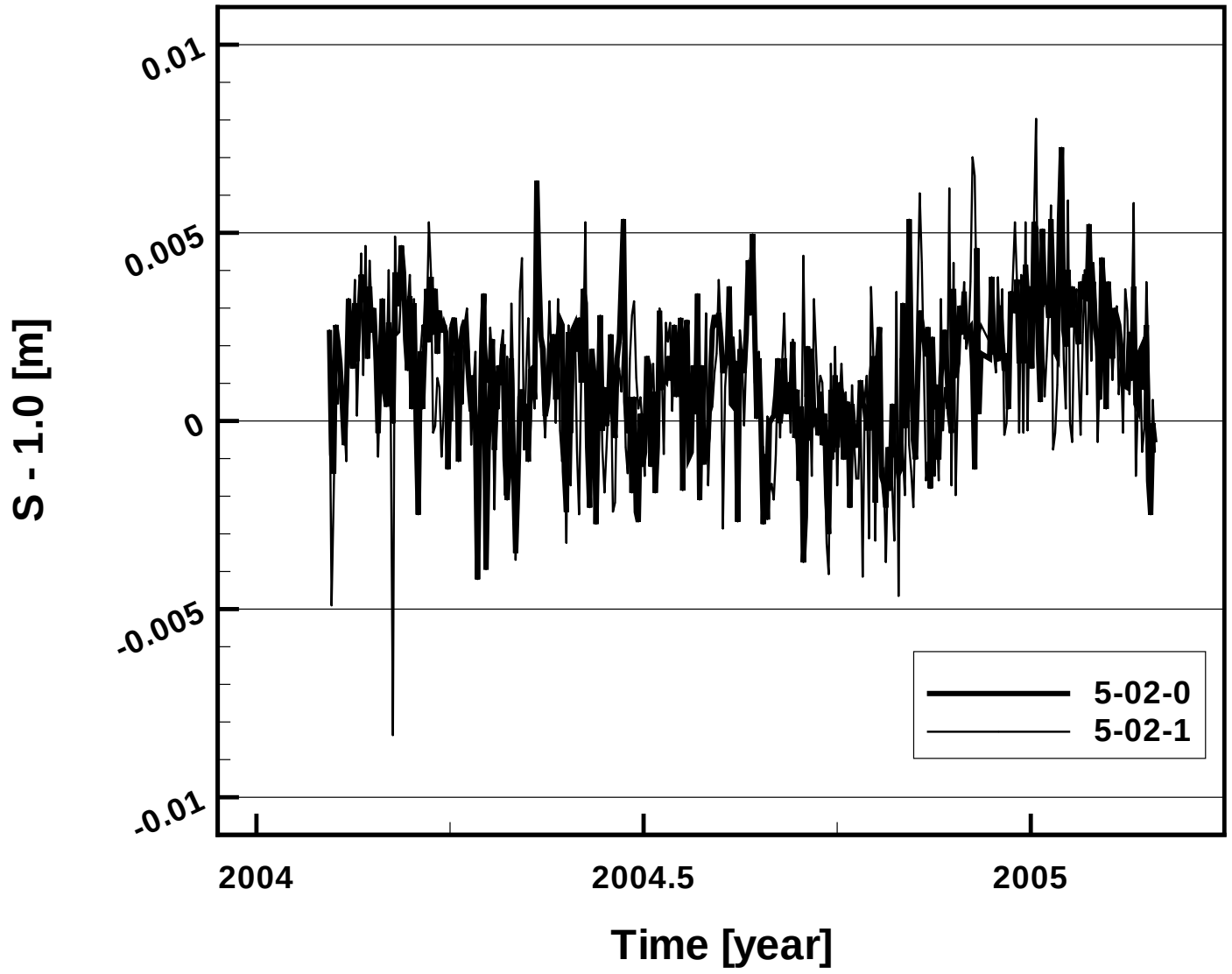

Figure H.4: *Geometric Frame differential scale per day.*

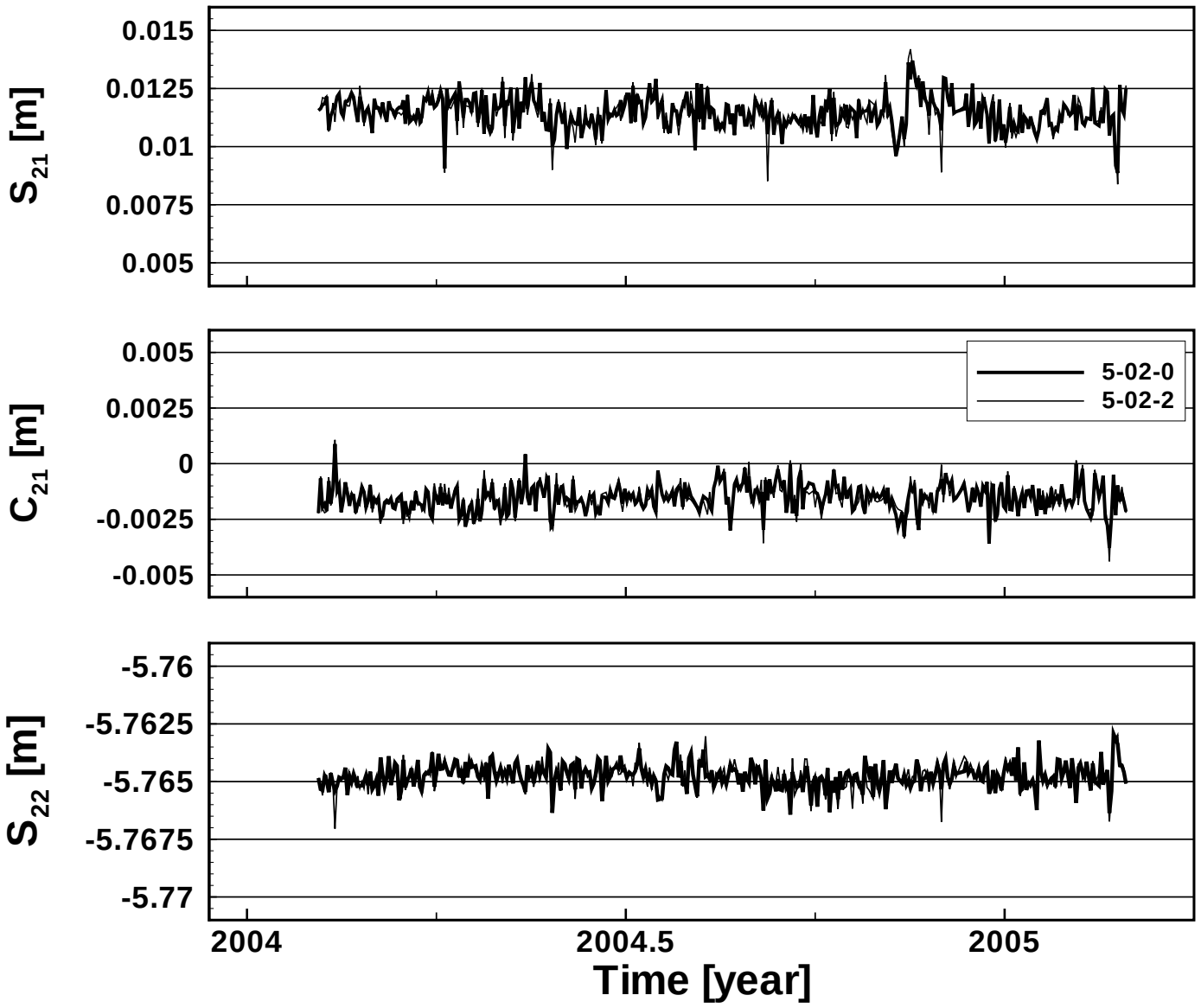

Figure H.5: *Dynamic Frame orientation x-, y-, z-component per day.*

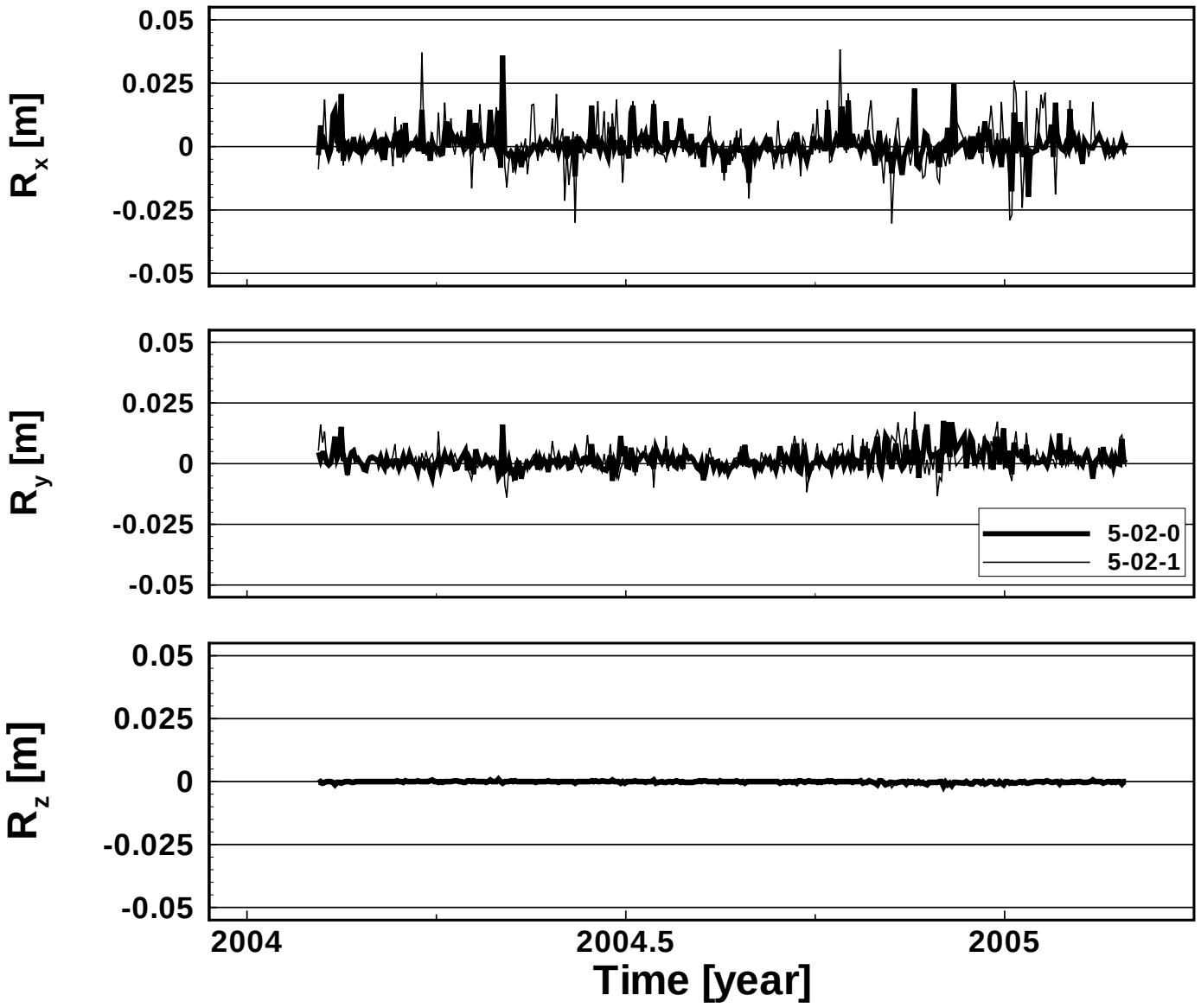

Figure H.6: *Geometric Frame orientation x-, y-, z-component per day.*

H.2 Observational Residuals

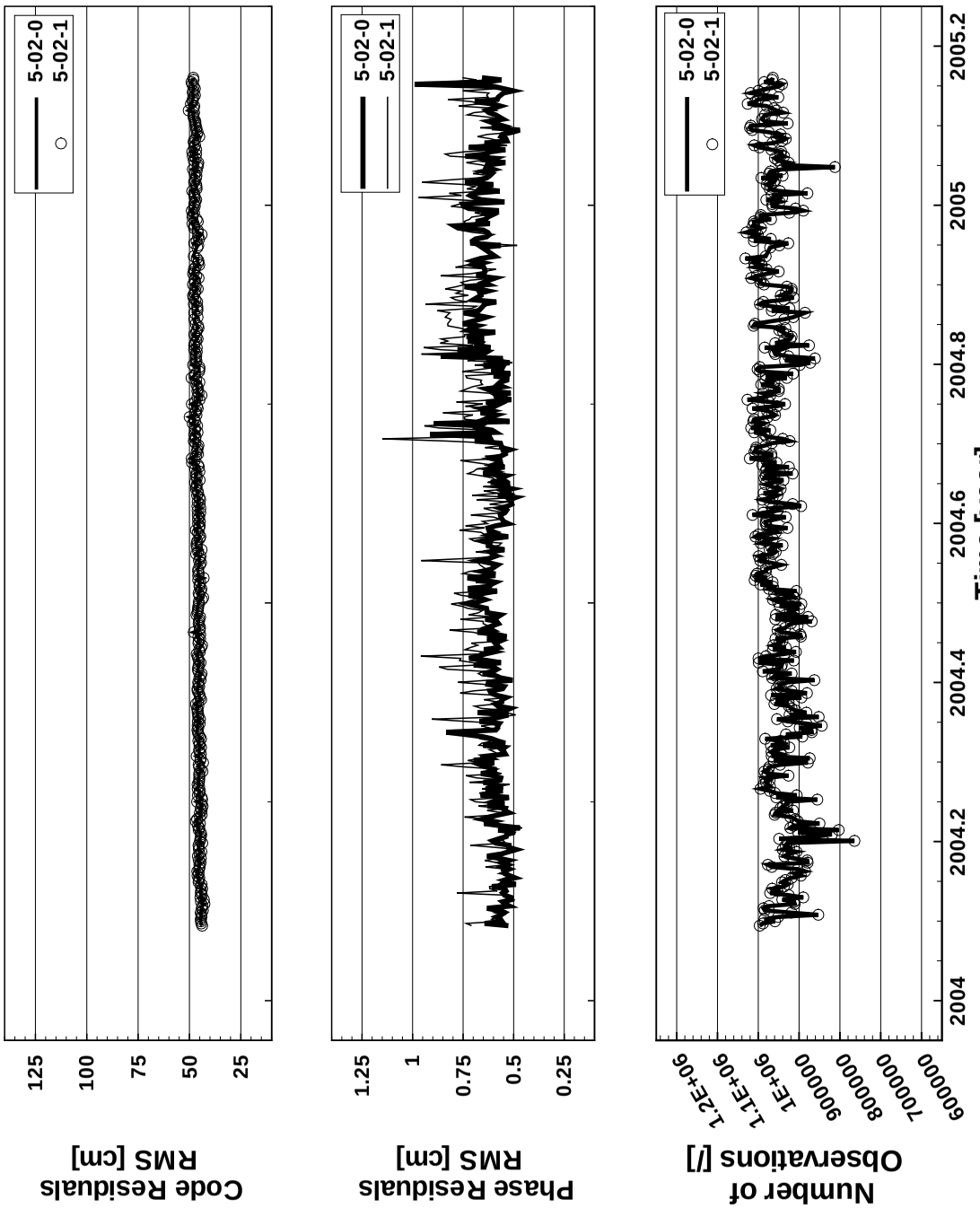

Figure H.7: *Statistics of GPS-ground observations per day.*

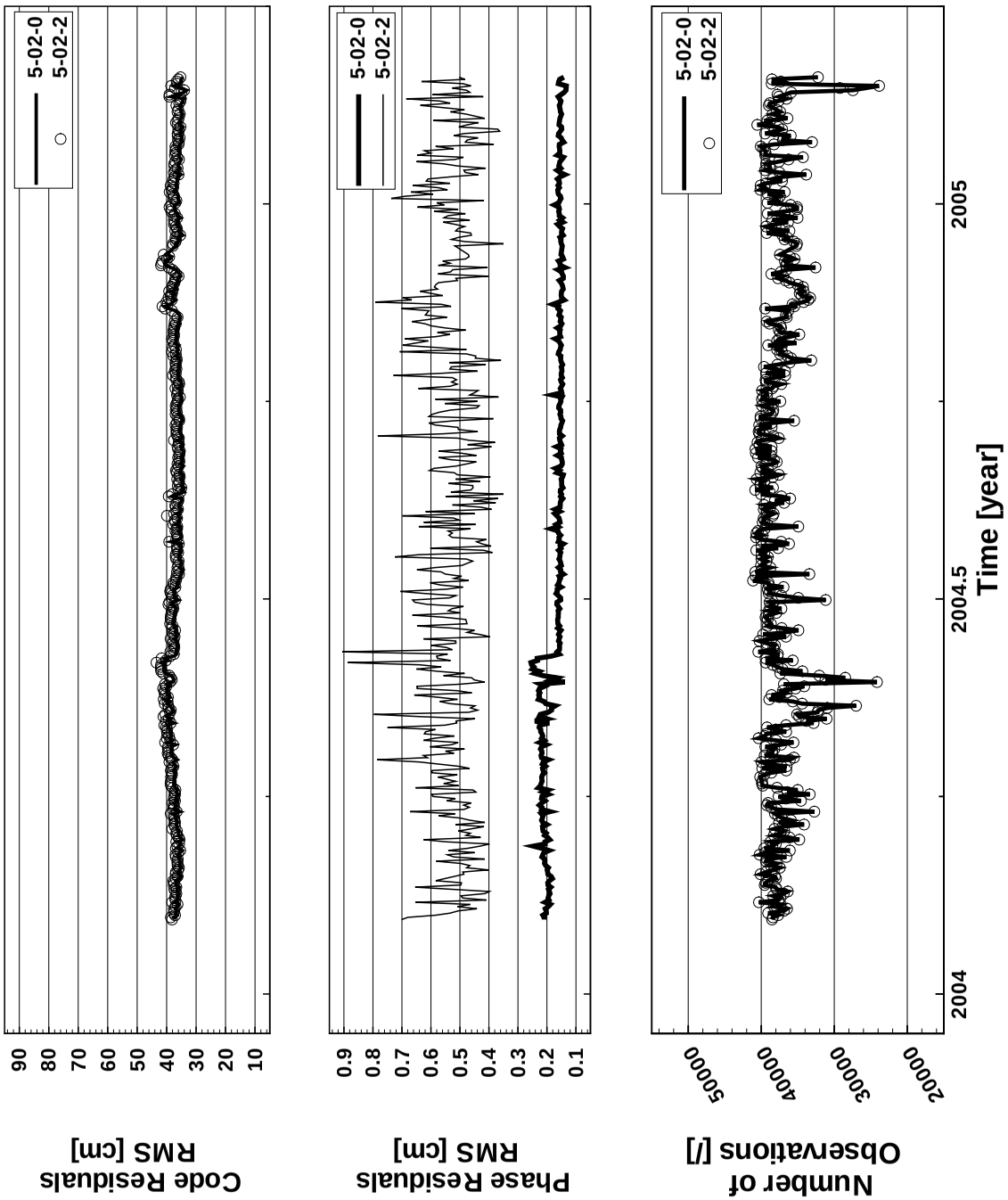

Figure H.8: *Statistics of GPS-SST observations per day.*

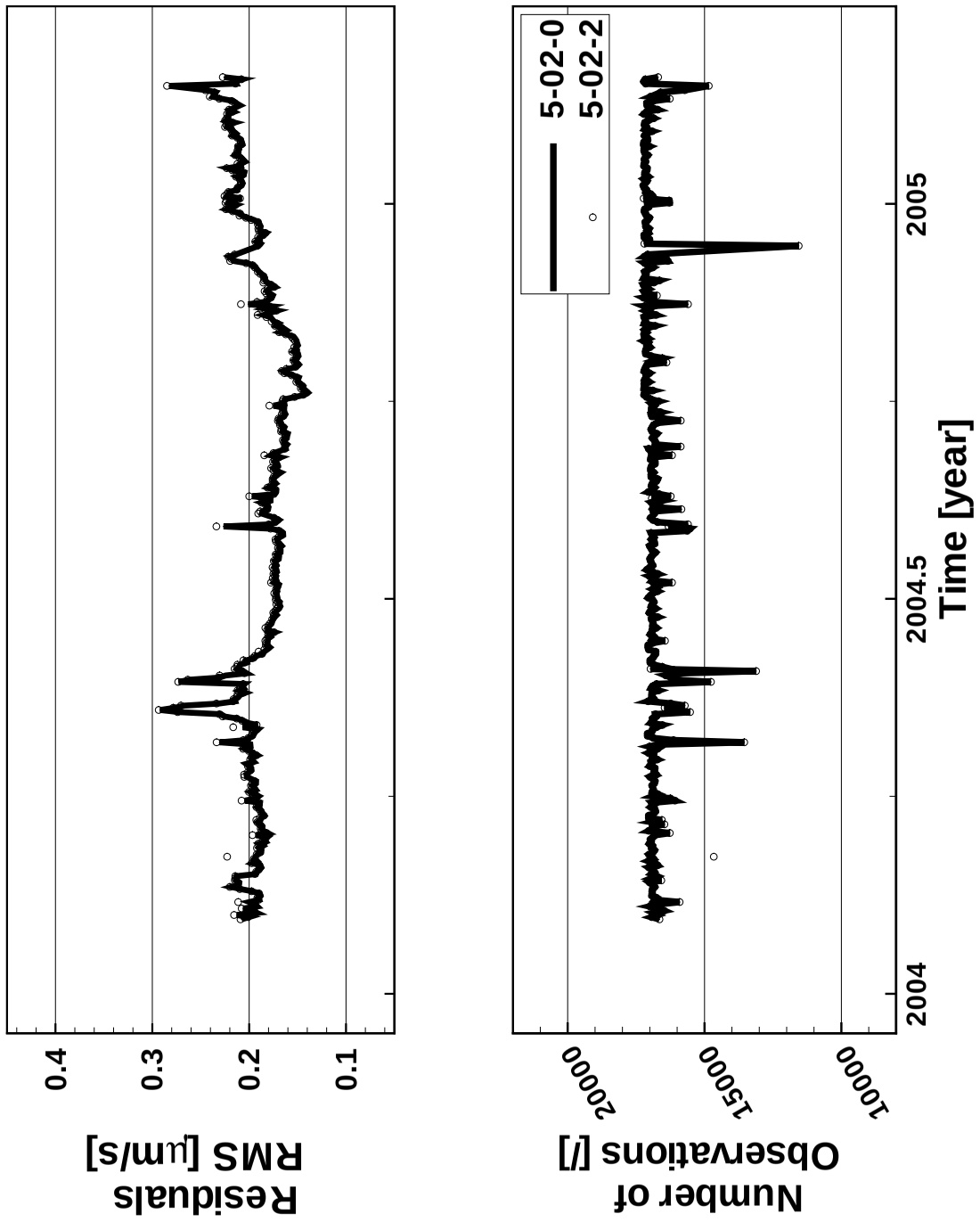

Figure H.9: *Statistics of KBRR observations per day.*

H.3 Orbit Comparisons

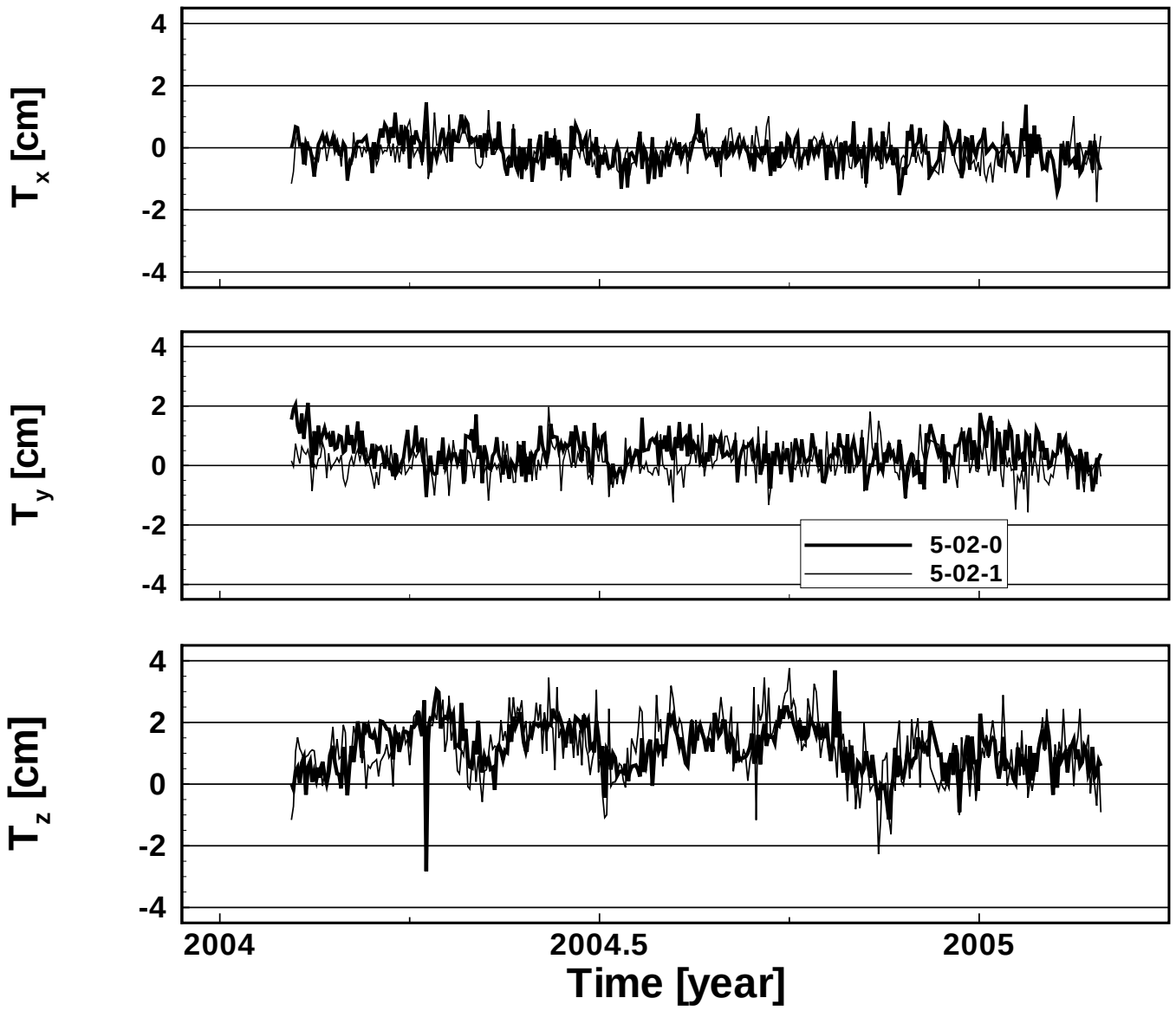

Figure H.10: *Comparisons of GPS orbits to IGS final orbits per day: translational parameters of global HT.*

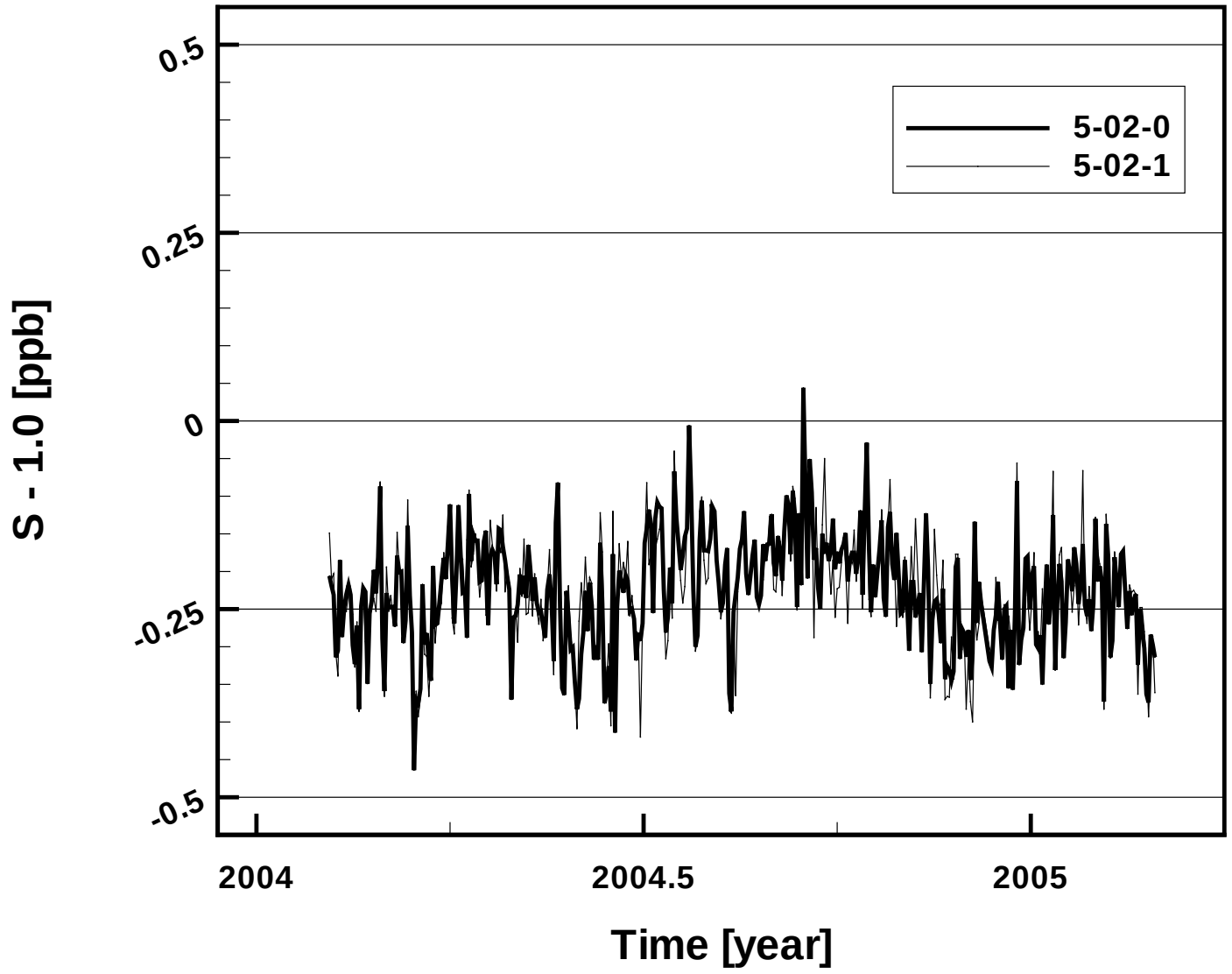

Figure H.11: *Comparisons of GPS orbits to IGS final orbits per day: differential scale parameter of global HT.*

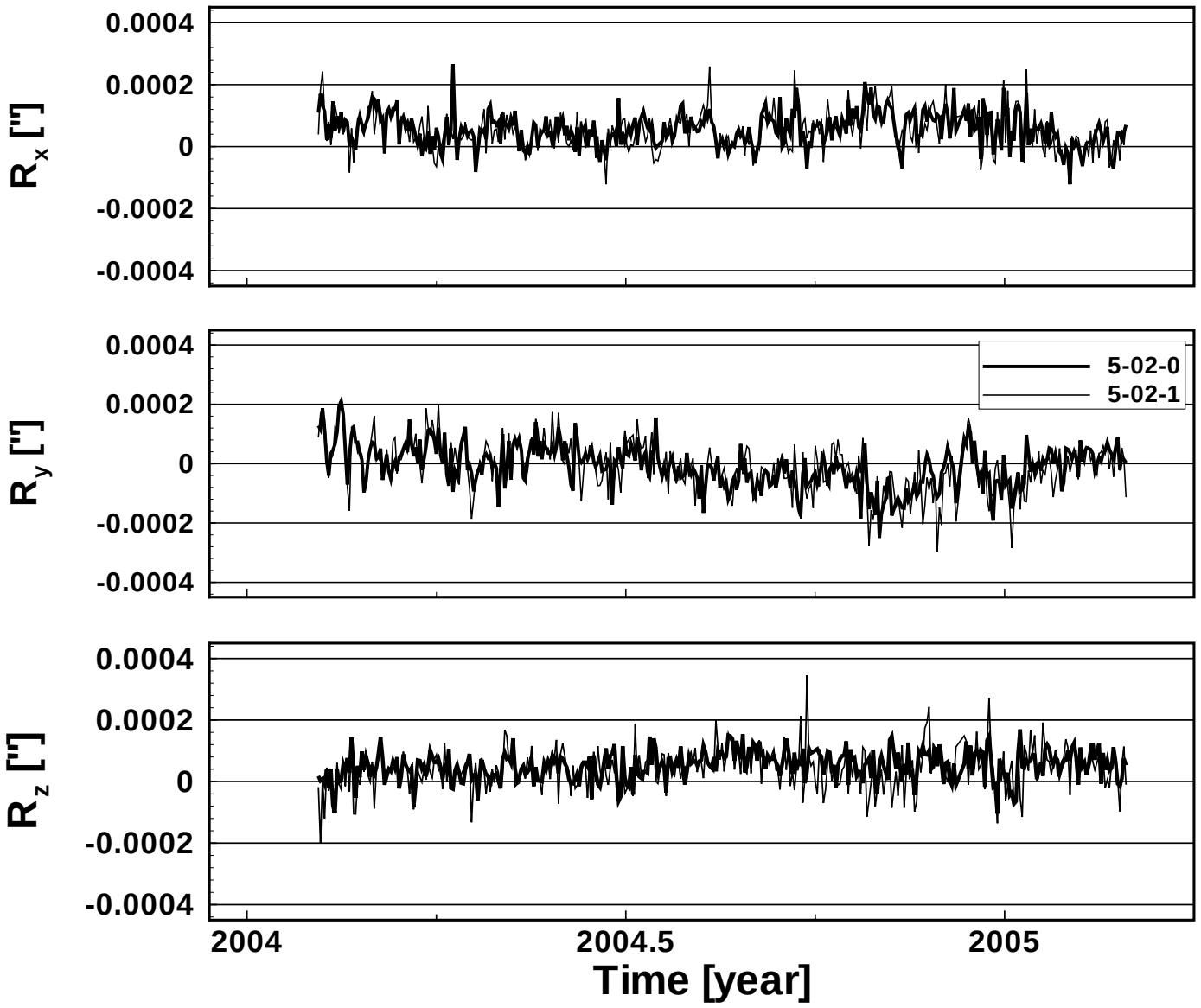

Figure H.12: *Comparisons of GPS orbits to IGS final orbits per day: rotational parameters of global HT.*

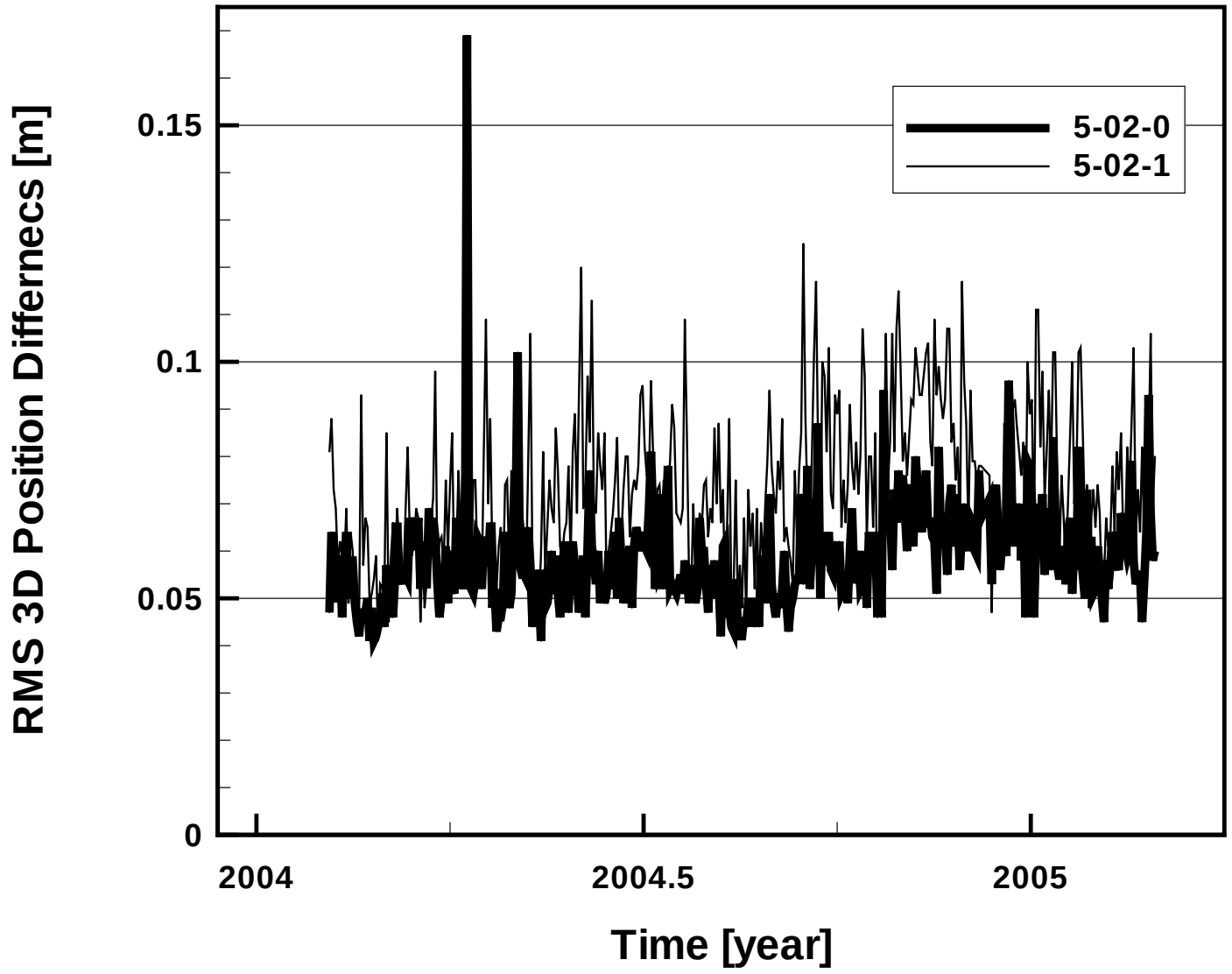

Figure H.13: *Comparisons of GPS orbits to IGS final orbits per day: RMS of 3D position differences previous to transformation.*

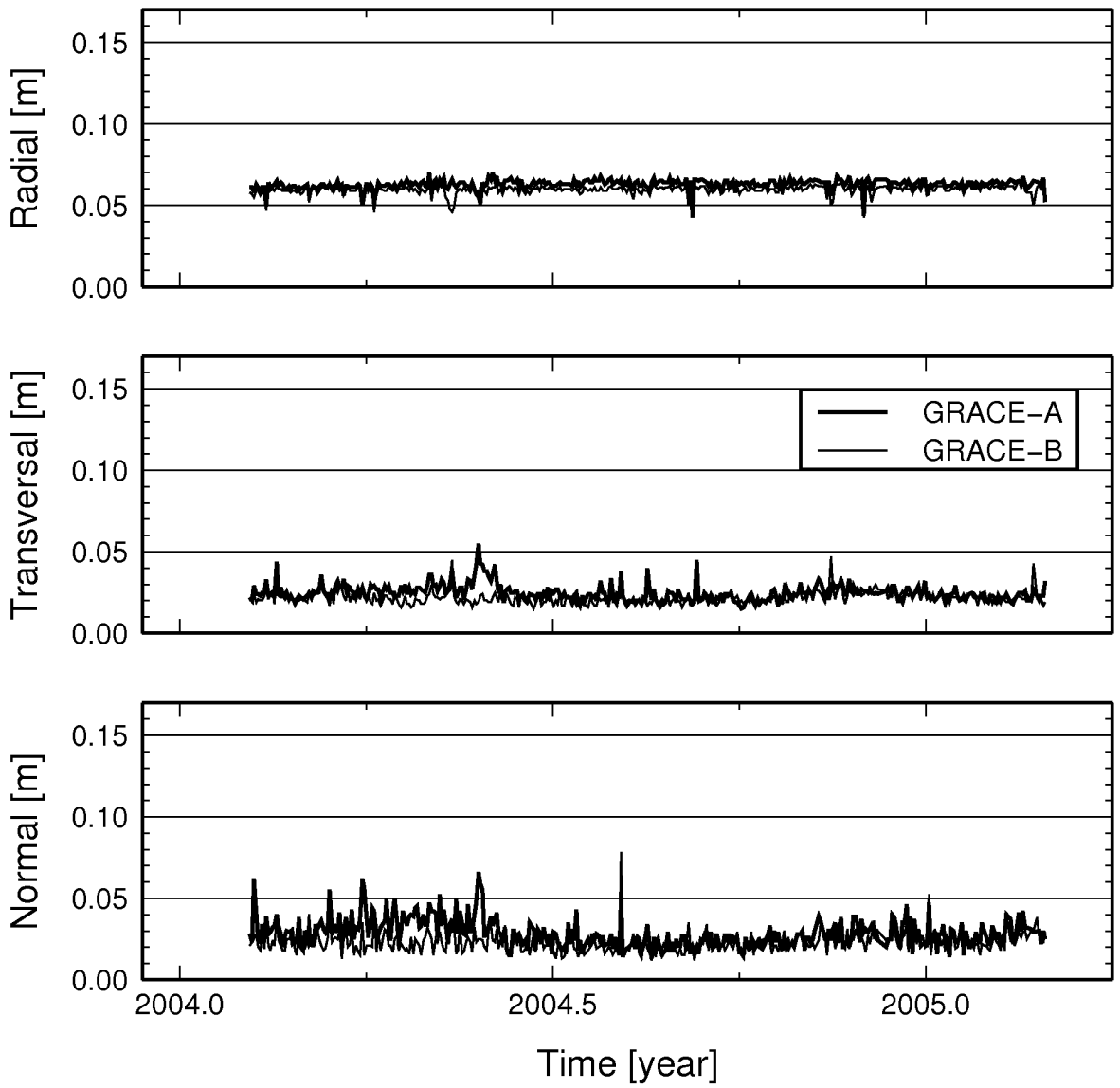

Figure H.14: *Comparisons of GRACE orbits to JPL GNV1B orbits per day: RMS of position differences in R-, T-, N-direction (from above; run 5-02-0).*

H.4 Validation

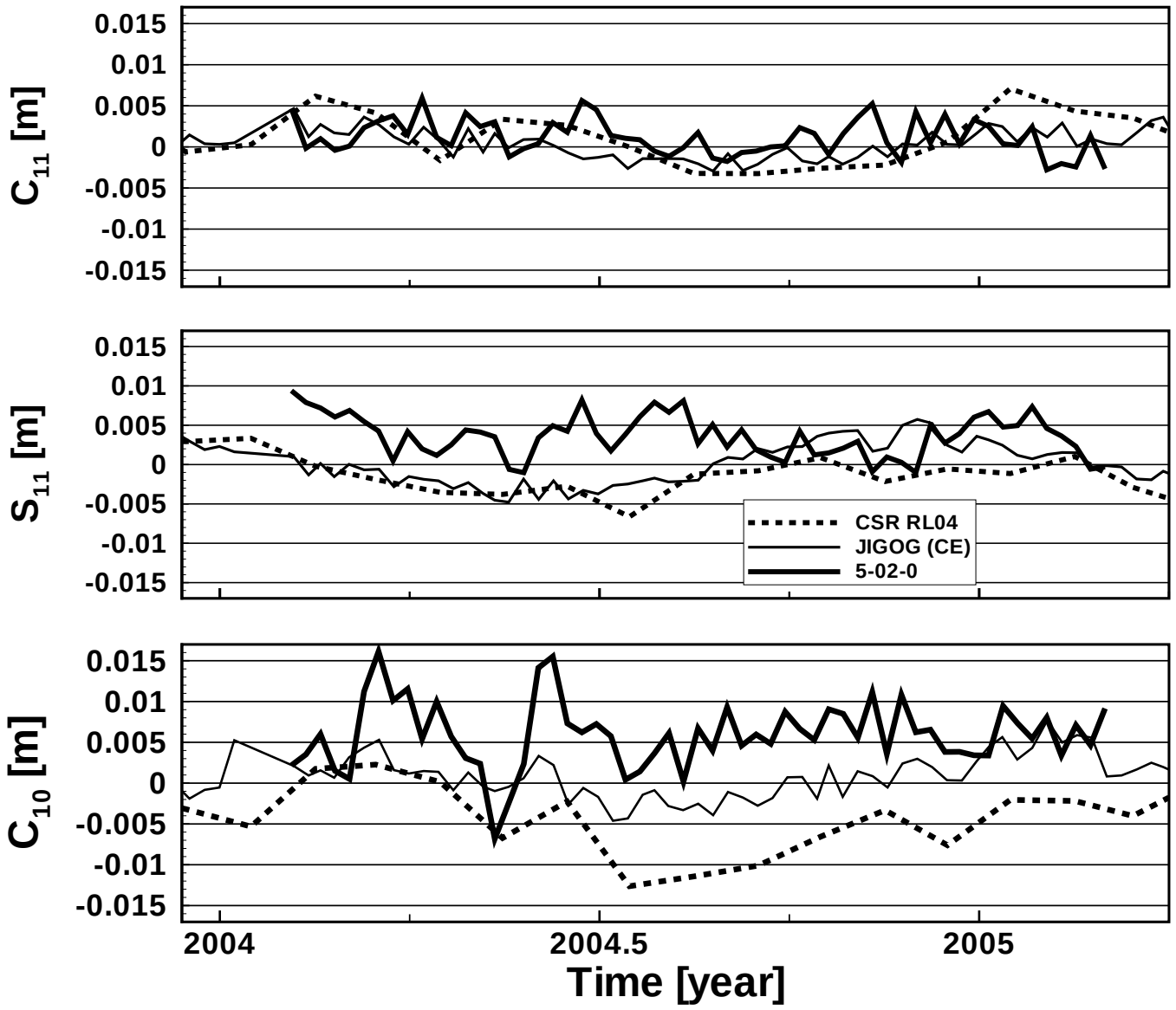

Figure H.15: *Validation of Dynamic Geocentre components with external time series (5-02-0: weekly averaged; CSR: monthly solution; JIGOG (CE): weekly solution.*

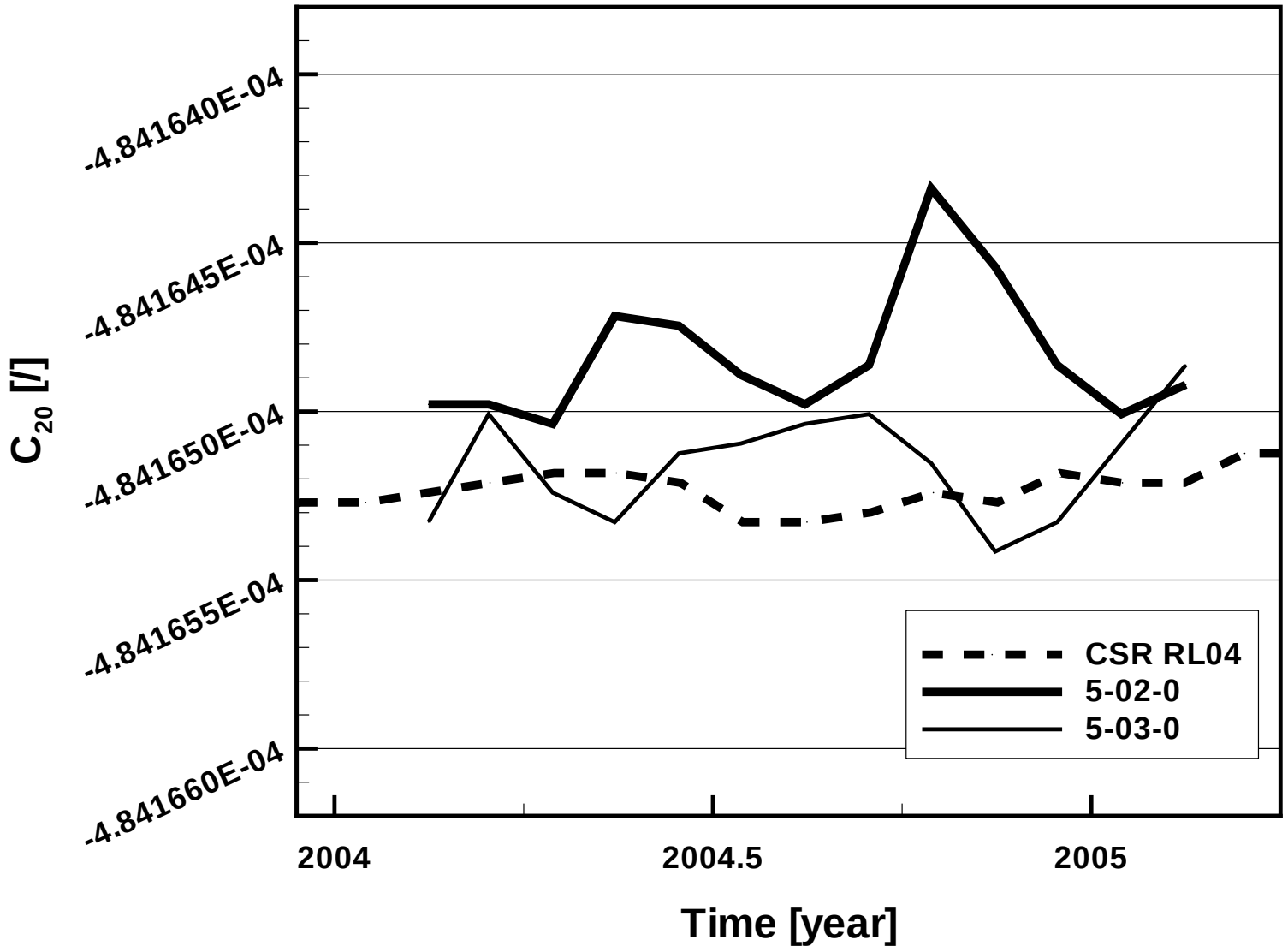

Figure H.16: *Validation of C_{20} with external time series (5-02-0: monthly averaged; CSR: monthly solution).*

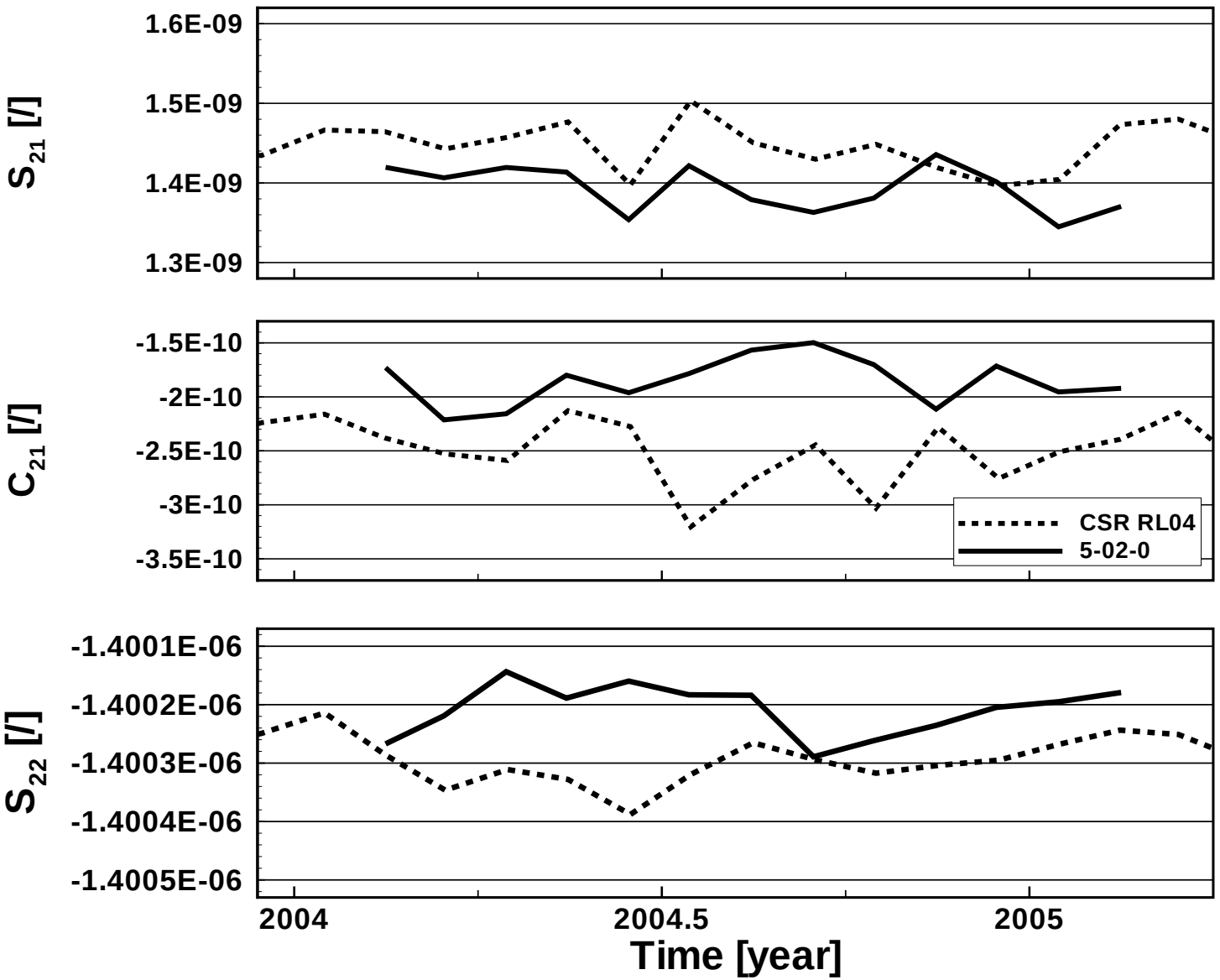

Figure H.17: *Validation of S_{21}, C_{21}, and S_{22} with external time series (5-02-0: monthly averaged; CSR: monthly solution).*

H.5 Effects Studied

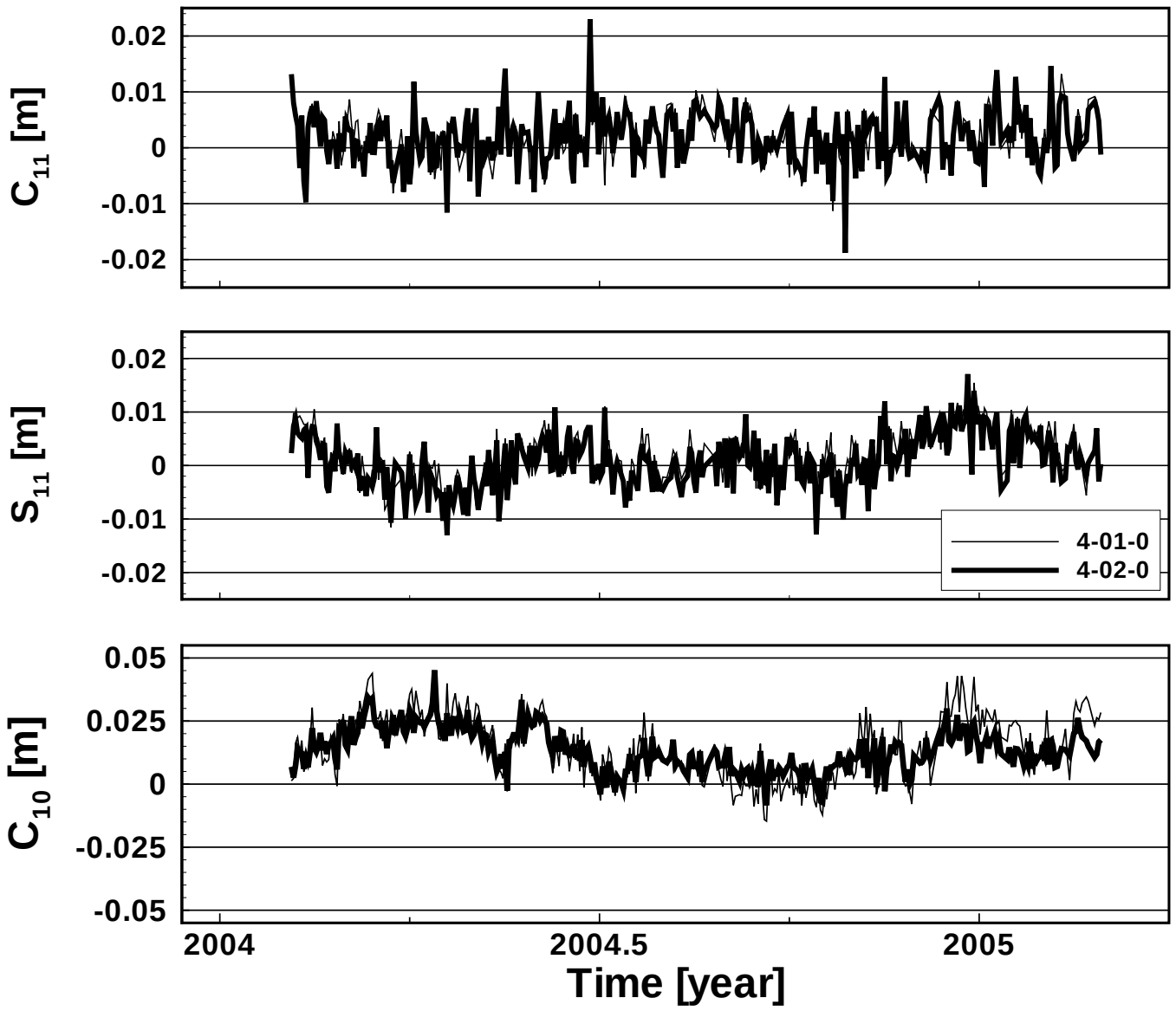

Figure H.18: *Effect of observational weighting: modified weight model for GPS-ground, GPS-SST, KBRR; Dynamic Geocentre x-, y-, z-component per day.*

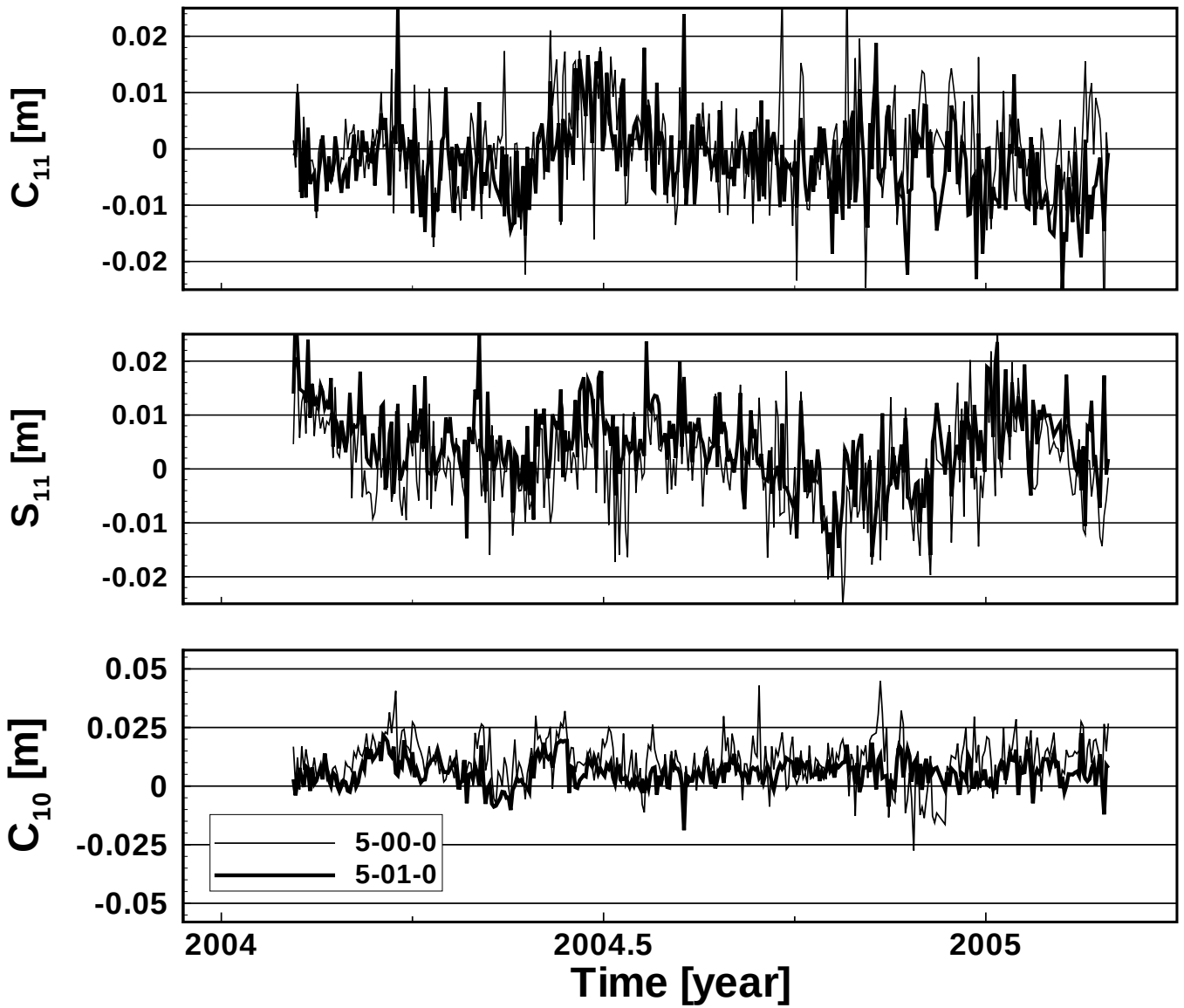

Figure H.19: *Effect of observational weighting: modified weight model for GPS-ground, GPS-SST, KBRR; Dynamic Geocentre x-, y-, z-component per day.*

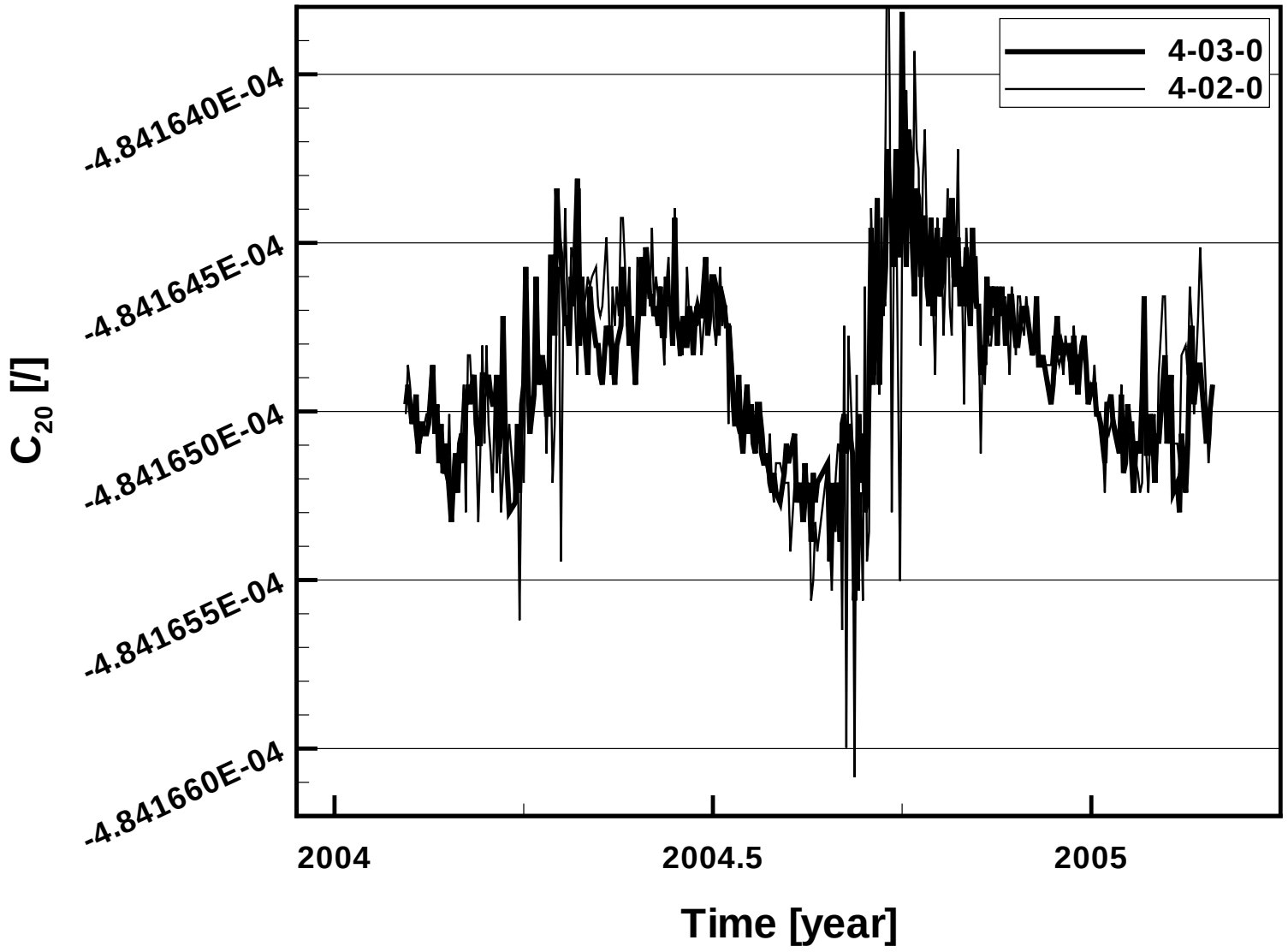

Figure H.20: *Effect of observational weighting: modified weight model for GPS-ground, GPS-SST, KBRR.*

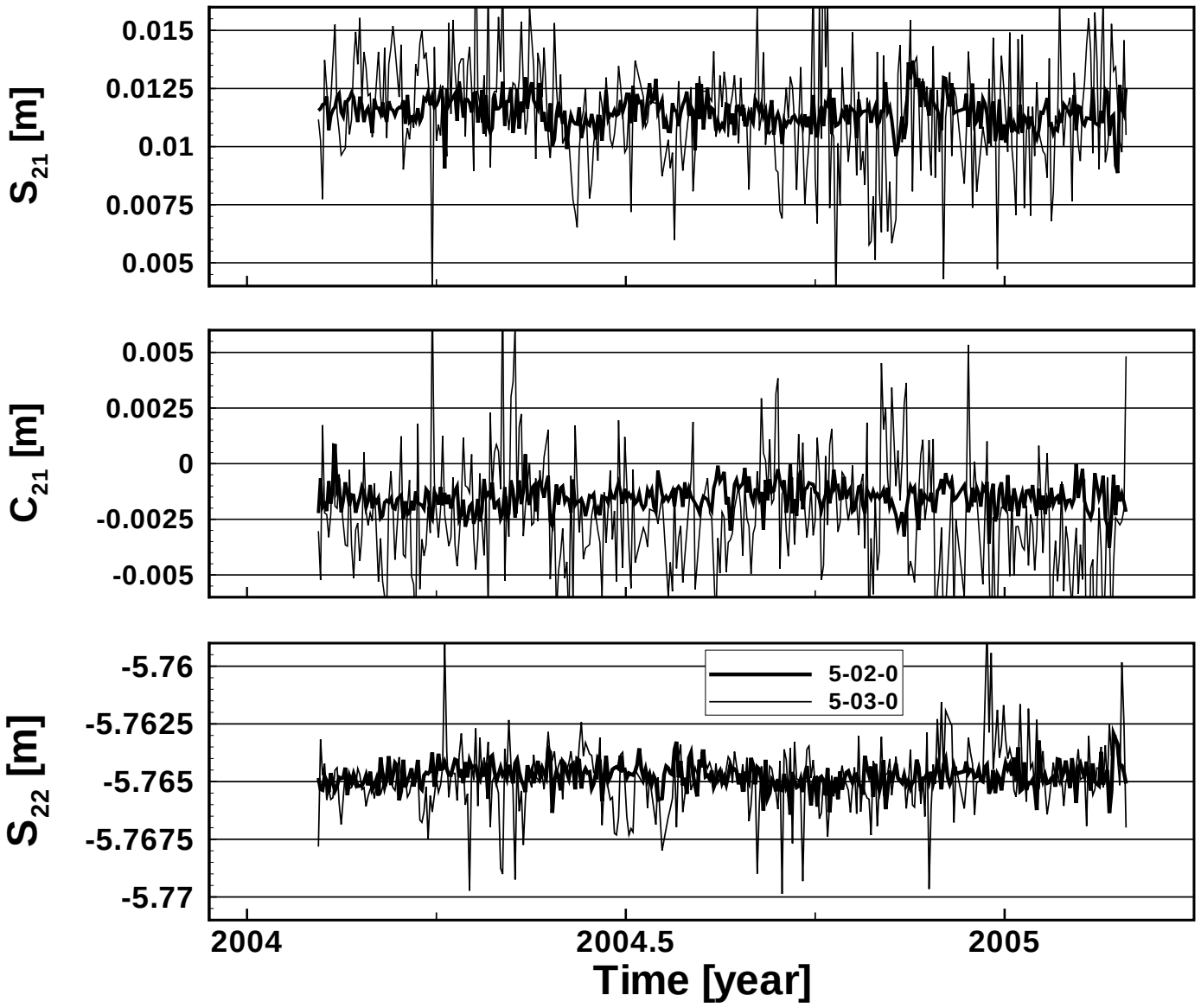

Figure H.21: *Effect of excluding KBRR observations (5-03-0).*

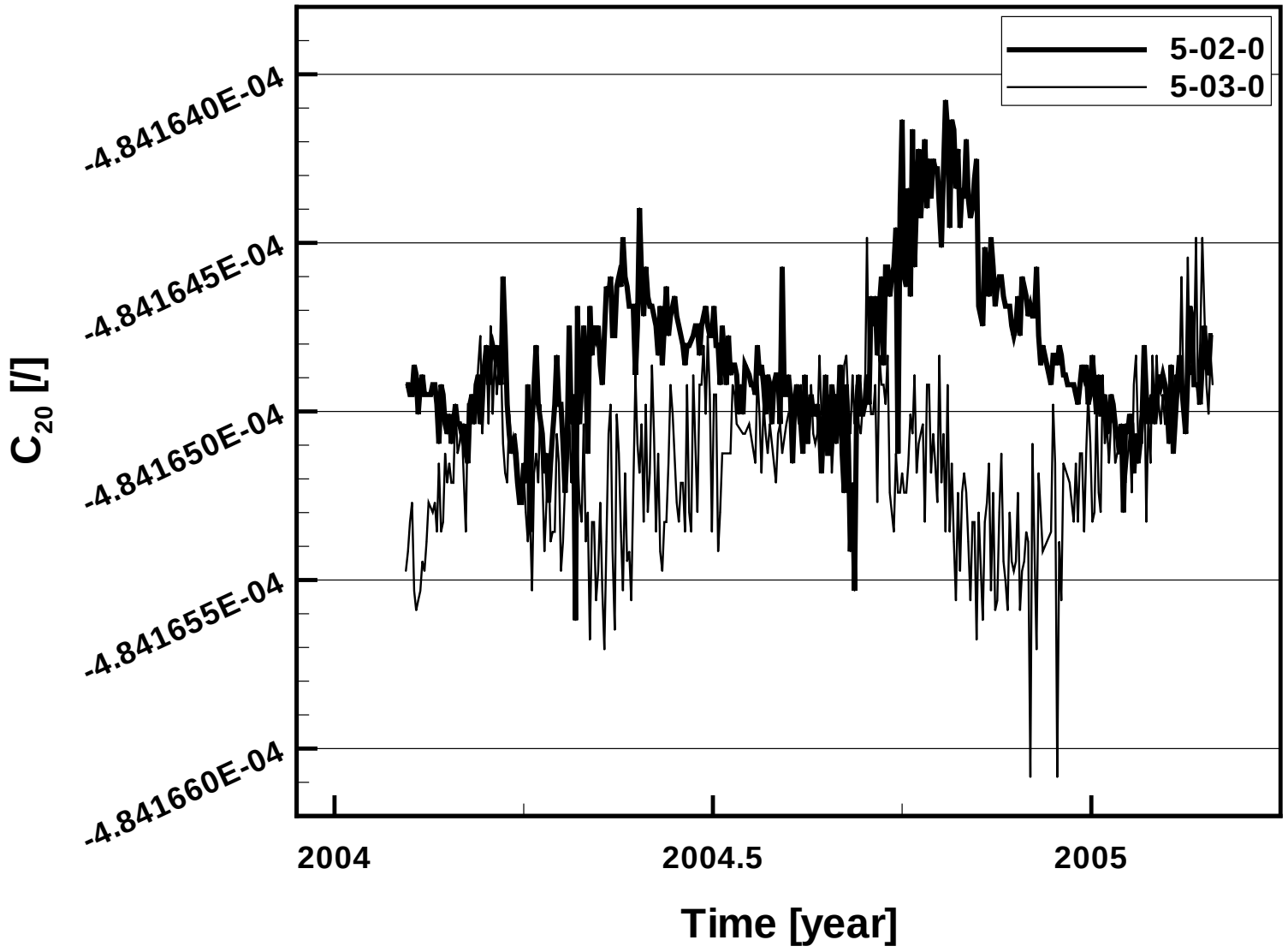

Figure H.22: *Effect of excluding KBRR observations (5-03-0).*

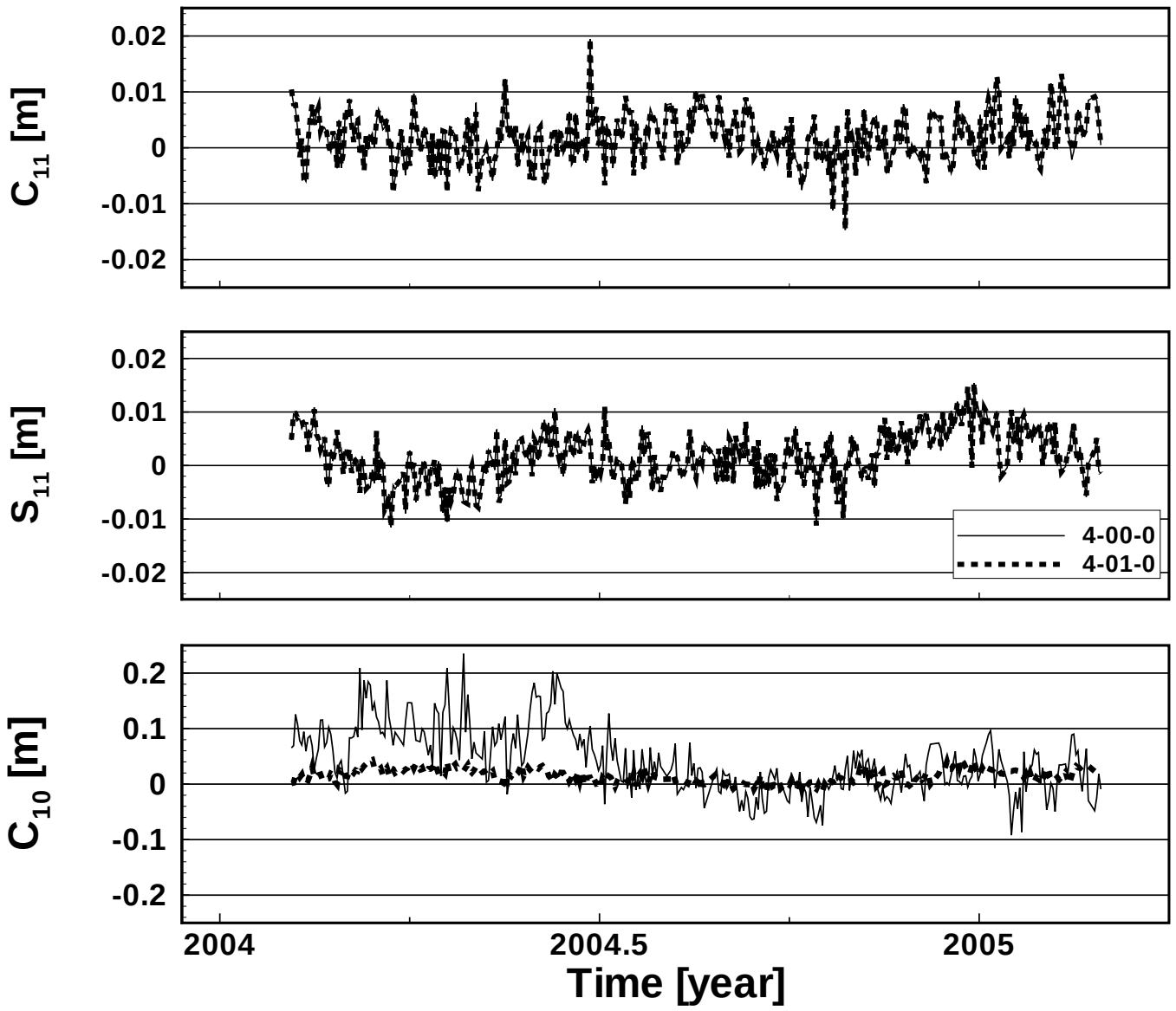

Figure H.23: *Effect of constraints on ground station coordinates: CC (4-00-0) vs NN(T_z,R_z) (4-01-0); Dynamic Geocentre x-, y-, z-component per day.*

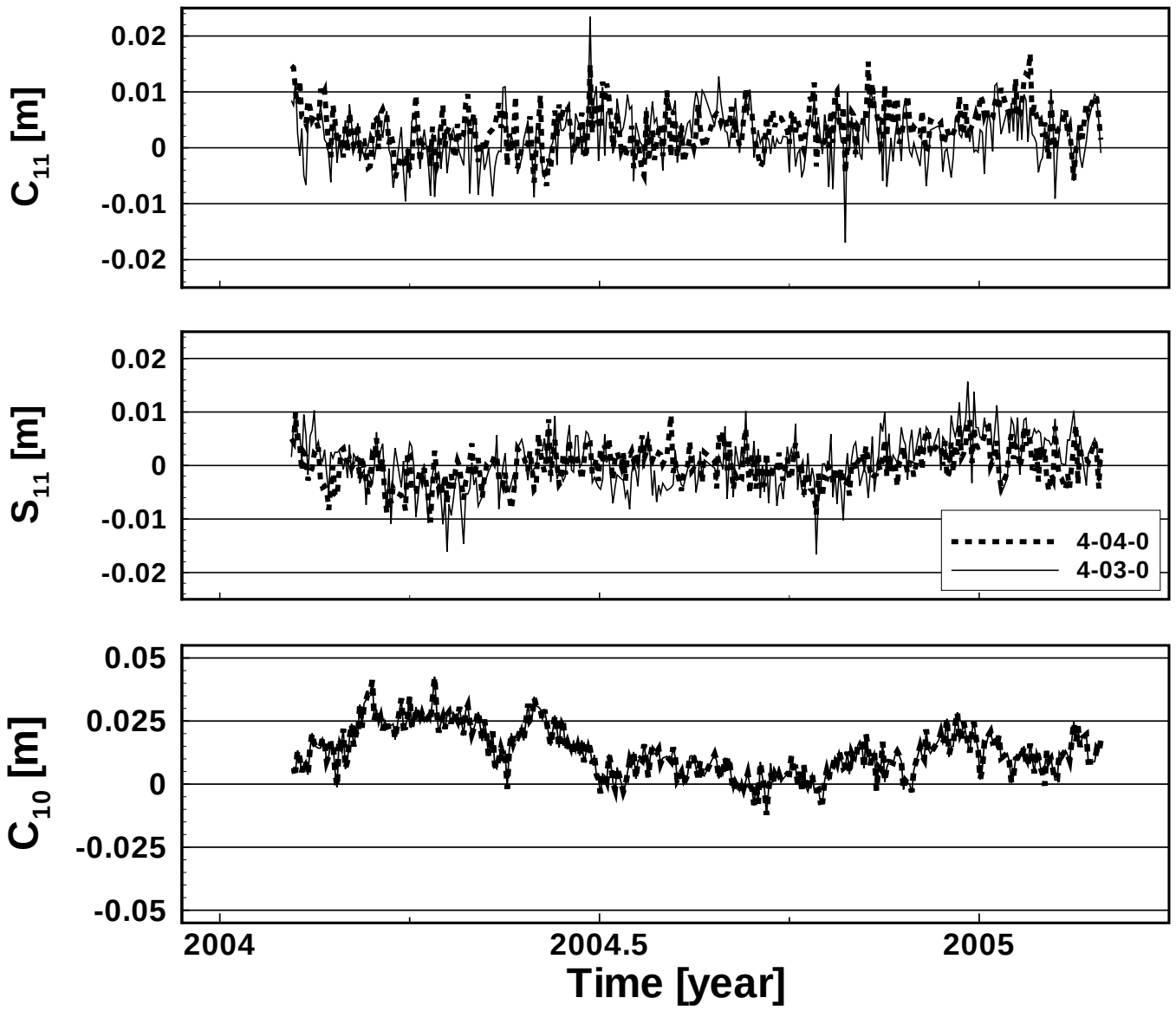

Figure H.24: *Effect of constraints on ground station coordinates: NN(T_z,R_z) (4-03-0) vs NN(T_x,$T_y$$T_z$,$R_z$) (4-04-0); Dynamic Geocentre x-, y-, z-component per day.*

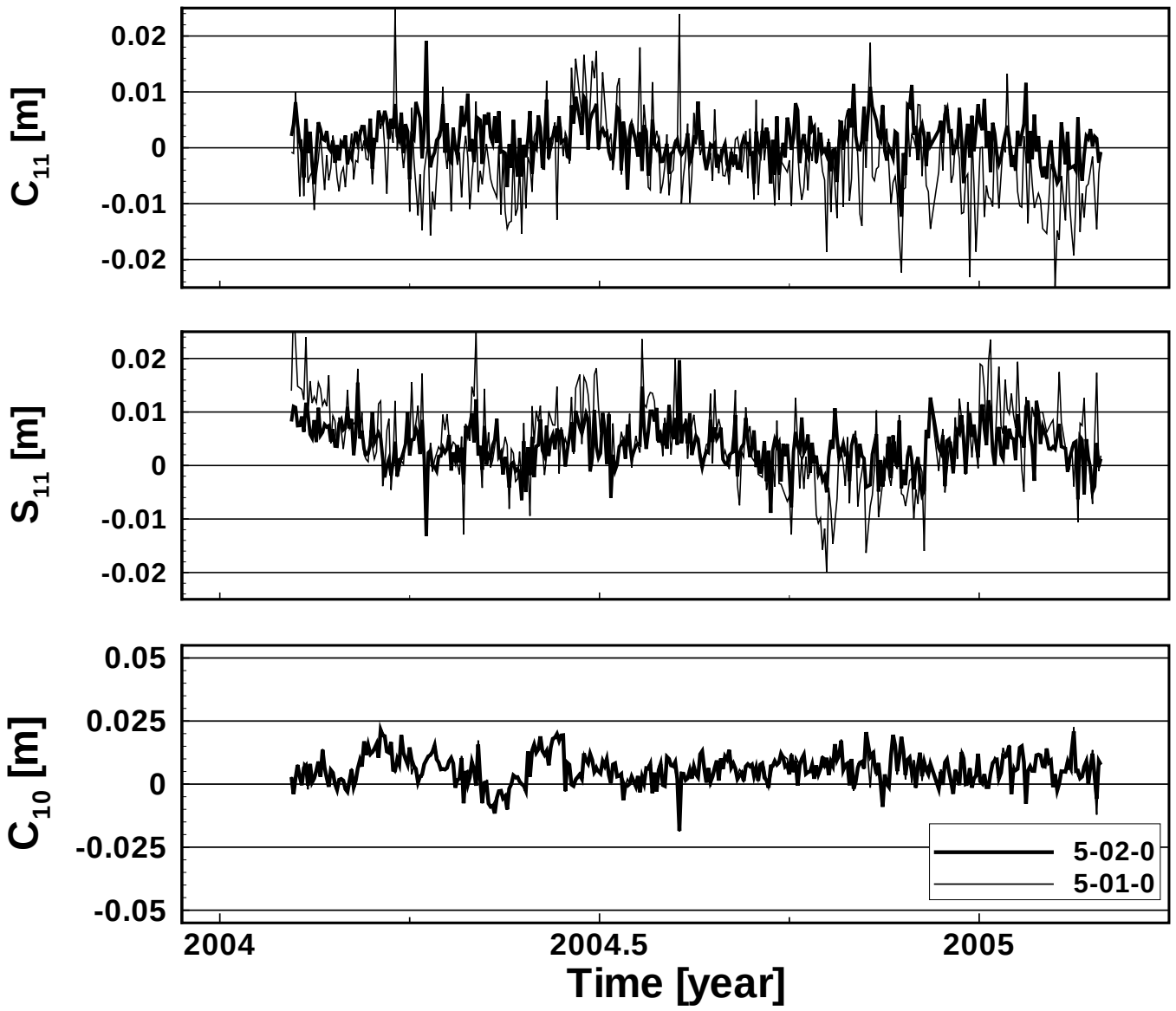

Figure H.25: *Effect of constraints on ground station coordinates: NN(T_z,R_z) (5-01-0) vs NN(T_x,$T_y$$T_z$,$R_z$) (5-02-0); Dynamic Geocentre x-, y-, z-component per day.*

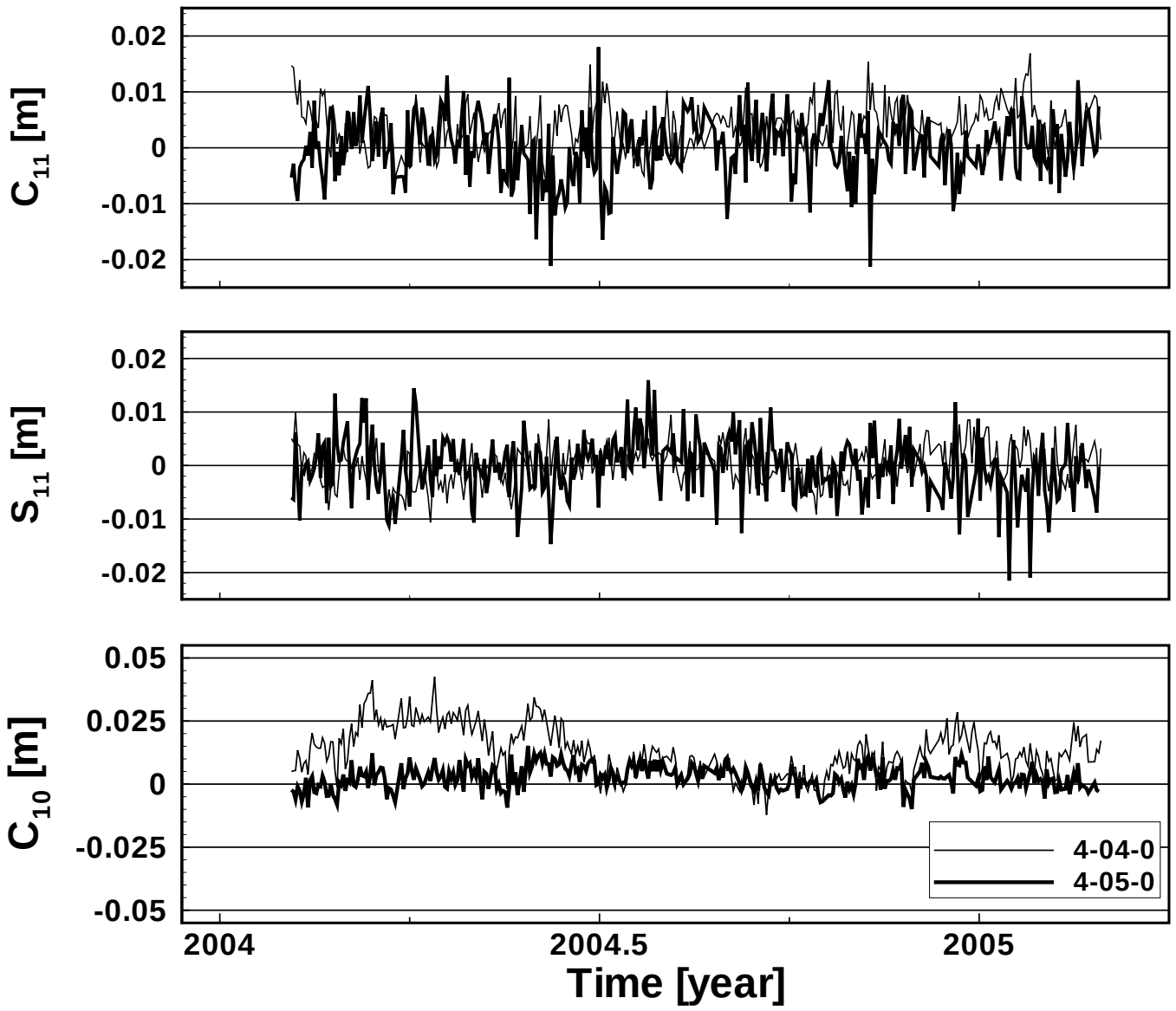

Figure H.26: *Effect of constrained GPS orbits: totally unconstrained (4-04-0) vs fixed IGS final orbits (4-05-0); Dynamic Geocentre x-, y-, z-component per day.*

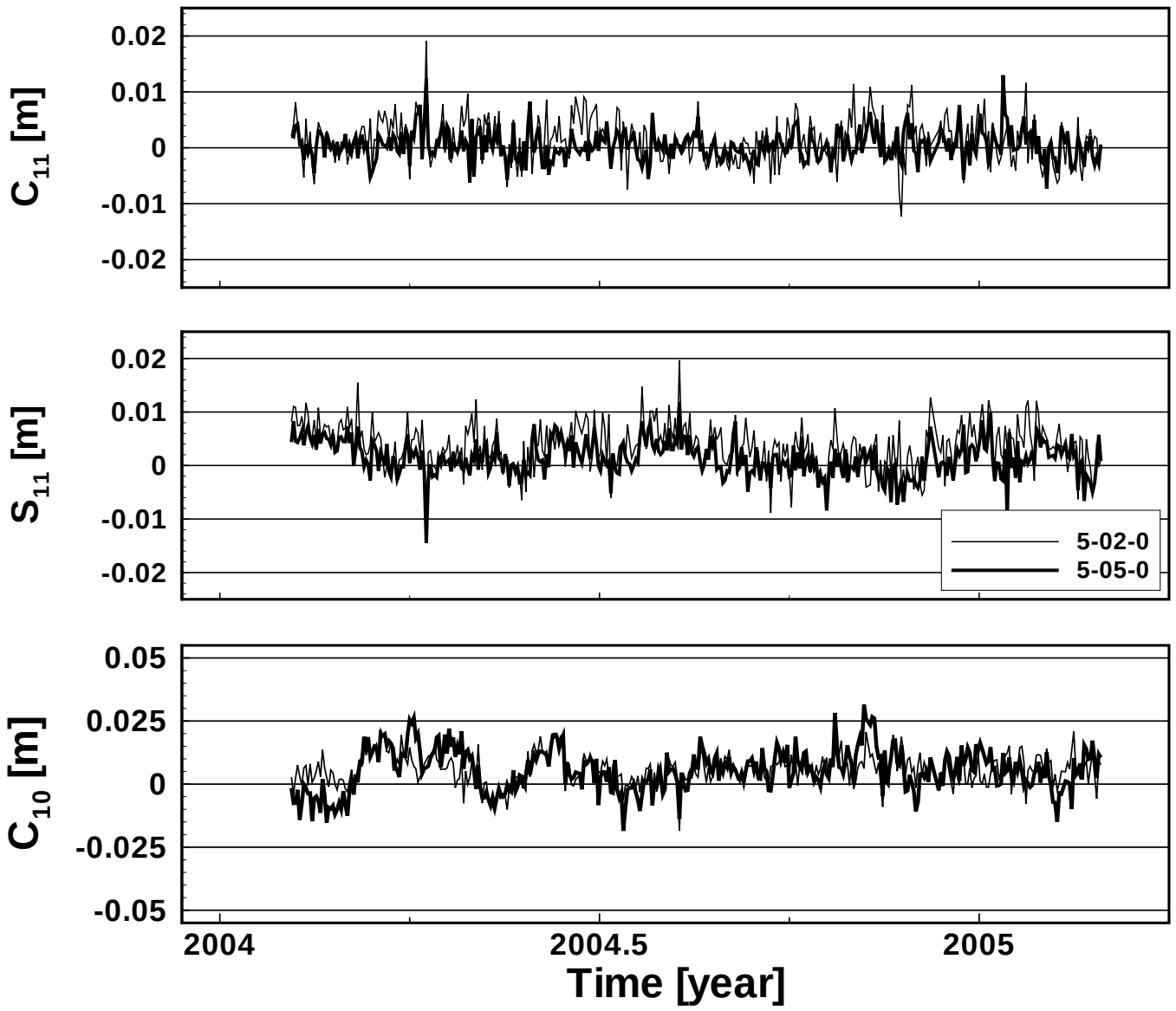

Figure H.27: *Effect of constrained GPS orbits: totally unconstrained (5-02-0) vs constrained (5-05-0); Dynamic Geocentre x-, y-, z-component per day.*

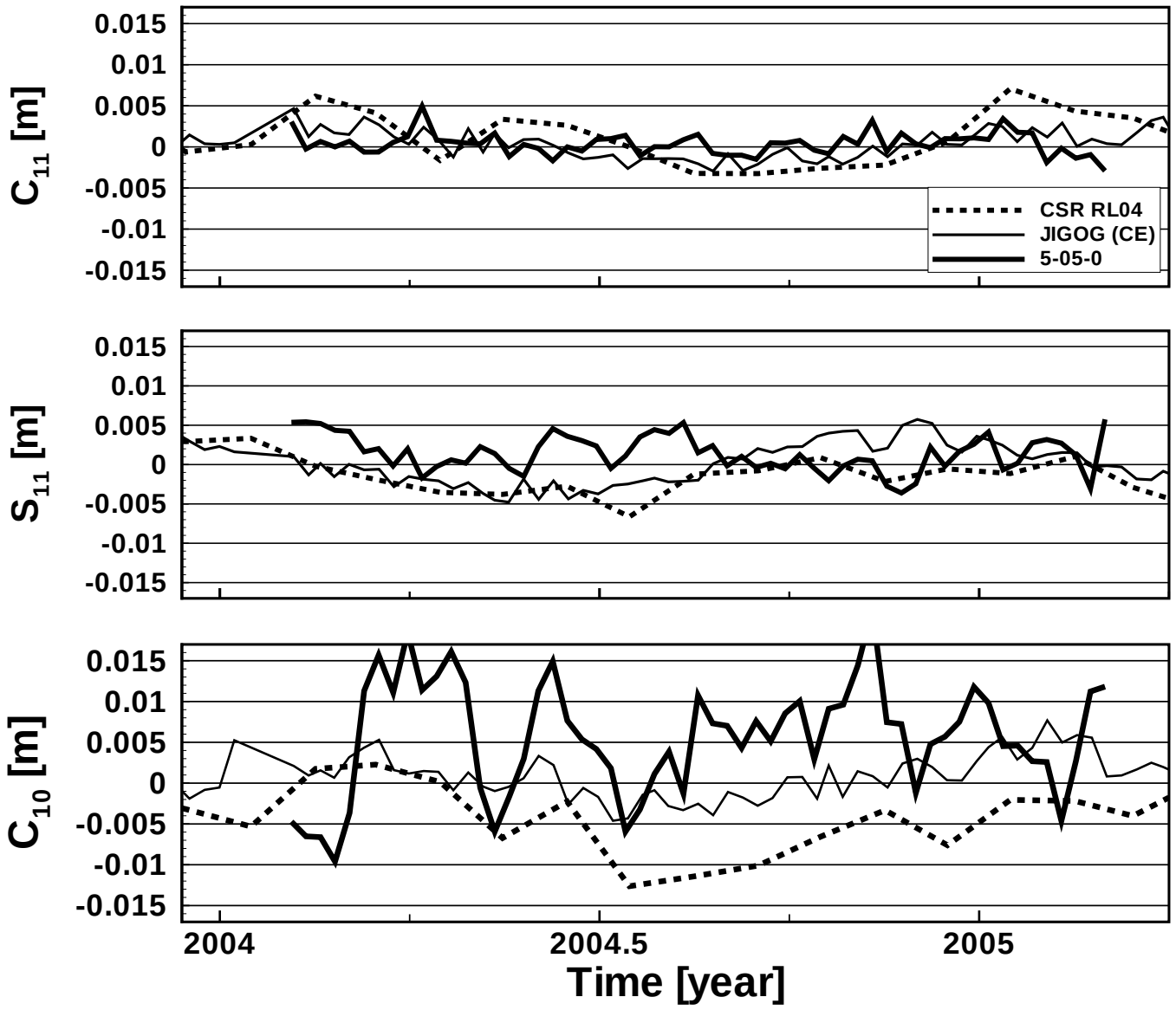

Figure H.28: *Effect of constrained GPS orbits (constrained parameters; 5-05-0 weekly averaged): validation of Dynamic Geocentre components with external time series.*

Appendix I

Results: Statistics

The referencing of the runs is done by assigning a number of the format "rr-nn-t" with

rr : *release no. (4 or 5)*
nn : *test no.*
t : *type (0: integrated; 1: two-step (GPS); 2: two-step (LEO))*

I.1 TRF Parameters

Table I.1: *Statistics of Geometric Frame's components time series: translations and differential scale.*

Run	T_x		T_y		T_z		$S - 1.0$	
	Mean [mm]	STD [mm]	Mean [mm]	STD [mm]	Mean [mm]	STD [mm]	Mean [mm]	STD [mm]
4-04-0	+0.12	0.20	-0.03	0.21	-0.10	0.19	+1.34	1.79
5-02-0	+0.23	0.33	-0.12	0.38	+0.15	0.33	+1.23	1.88
5-02-1	+0.30	0.42	-0.06	0.44	+0.14	0.48	+1.09	2.15

Table I.2: *Statistics of Geometric Frame's components time series: rotations.*

Run	R_x		R_y		R_z	
	Mean [mm]	STD [mm]	Mean [mm]	STD [mm]	Mean [mm]	STD [mm]
4-04-0	+0.37	2.73	+2.32	2.87	-0.17	0.26
5-02-0	+0.63	5.47	+1.75	3.97	-0.12	0.33
5-02-1	+0.90	8.32	+2.07	4.71	-0.15	0.40

Table I.3: *Statistics of Dynamic Geocentre's components time series.*

Run	C_{11}		S_{11}		C_{10}	
	Mean [mm]	STD [mm]	Mean [mm]	STD [mm]	Mean [mm]	STD [mm]
4-00-0	+1.78	4.32	+1.79	4.80	+43.82	59.31
4-01-0	+1.82	4.33	+1.79	4.81	+14.78	12.54
4-02-0	+1.84	4.66	+0.81	4.90	+13.34	8.48
4-03-0	+2.11	4.73	+0.61	4.92	+12.88	9.69
4-04-0	+3.59	4.11	+0.05	3.54	+12.84	9.73
4-05-0	-0.11	5.68	-0.22	5.54	+2.59	4.75
5-00-0	-0.16	8.09	+1.01	8.31	+10.92	9.87
5-01-0	-2.31	7.30	+4.62	7.51	+5.92	6.00
5-02-0	+1.20	3.87	+3.64	4.21	+5.88	6.03
5-02-2	+2.91	8.91	+1.91	7.55	+6.64	8.42
5-03-0	+2.29	3.58	+1.63	3.65	+8.93	5.46
5-04-0	+2.34	3.51	+1.55	3.79	+8.96	5.42
5-05-0	+0.40	2.67	+1.32	3.31	+5.58	8.47

Table I.4: *Statistics of Dynamic Frame's orientation x-, y-, z-components time series.*

Run	S_{21}		C_{21}		S_{22}	
	Mean [mm]	STD [mm]	Mean [mm]	STD [mm]	Mean [mm]	STD [mm]
4-04-0	+11.51	0.88	-1.85	0.75	-5765.04	0.43
5-02-0	+11.47	0.69	-1.53	0.61	-5764.76	0.54
5-02-2	+11.43	0.73	-1.53	0.63	-5764.77	0.56
5-03-0	+11.42	2.51	-2.43	2.72	-5764.88	1.44

Table I.5: *Statistics of C_{20} time series.*

Run	Mean [E-04]	STD [E-04]
4-02-0	-4.841648752	0.000003072
4-03-0	-4.841648672	0.000002545
4-04-0	-4.841648665	0.000002549
5-02-0	-4.841648349	0.000002420
5-02-2	-4.841648646	0.000002129
5-03-0	-4.841651546	0.000002287

I.2 Orbit Comparisons

Table I.6: *Parameters of global Helmert Transformations between GPS orbits (Integrated ('Run') vs IGS final).*

Run	T_x [mm]	T_y [mm]	T_z [mm]	$S-1.0$ [ppb]	R_x [mas]	R_y [mas]	R_z [mas]
	Mean						
5-02-0	-0.85	+4.54	+11.61	-0.226	+0.056	-0.008	+0.052
5-02-1	-1.65	+1.26	+11.76	-0.228	+0.052	-0.009	+0.042
	STD						
5-02-0	4.79	5.43	7.60	0.073	0.054	0.070	0.047
5-02-1	4.27	5.20	9.56	0.074	0.060	0.084	0.065
	RMS						
5-02-0	4.86	7.07	13.87	0.238	0.078	0.070	0.070
5-02-1	4.57	5.34	15.15	0.239	0.079	0.084	0.077

Table I.7: *Correlation coefficients between time series of dynamic frame origin parameters and translational parameters of global Helmert transformations between GPS orbits (Integrated (5-02-0) vs IGS final).*

	T_x	T_y	T_z
C_{11}	+0.760	+0.016	-0.031
S_{11}	-0.032	+0.816	-0.021
C_{10}	-0.033	-0.070	+0.370

Table I.8: *Correlation coefficients between time series of dynamic frame orientation parameters and rotational parameters of global Helmert transformations between GPS orbits (Integrated (5-02-0) vs IGS final).*

	R_x	R_y	R_z
S_{21}	+0.074	+0.051	-0.001
C_{21}	-0.027	-0.104	-0.050
S_{22}	-0.072	+0.068	-0.040

Table I.9: *RMS of time series of translational parameters (T_x, T_y, T_z) of global Helmert transformations between GPS orbits (Integrated (5-02-0) vs IGS final).*

Application of C_{11}, S_{11}, C_{10} to T_x, T_y, T_z	T_x [mm]	T_y [mm]	T_z [mm]
- not applied	4.86	7.07	13.87
- applied	3.81	3.41	9.71

Table I.10: *RMS of time series of position differences between GRACE orbits (Integrated (5-02-0) vs JPL GNV1b).*

	Radial [mm]	Transversal [mm]	Normal [mm]
GRACE-A	63.0	25.2	29.6
GRACE-B	59.6	22.2	23.9

I.3 Observational Residuals

Table I.11: *Statistics of SLR residuals; cutoff limit for outlier removal: 20.0 cm.*

Run	GRACE-A	GRACE-B	PRN05	PRN06
	Number of observations			
	[/]	[/]	[/]	[/]
4-04-0	22626	20790	3101	2664
4-04-1	-	-	3095	2571
4-04-2	27751	25731	-	-
5-02-0	20698	19151	2591	2316
5-02-1	-	-	2615	2293
5-02-2	25723	23879	-	-
	Global RMS			
	[cm]	[cm]	[cm]	[cm]
4-04-0	3.60	3.86	5.54	5.52
4-04-1	-	-	6.02	5.83
4-04-2	4.41	4.77	-	-
5-02-0	3.71	3.34	7.94	7.42
5-02-1	-	-	7.92	7.31
5-02-2	3.98	3.72	-	-

Bibliography

[Alt 02a] Altamimi Z, Sillard P, Boucher C (2002) ITRF2000: A new release of the International Terrestrial Reference System for earth science applications, J Geophys Res, 107, No. B10, 2214, doi:10.1029/2001JB000561

[Alt 02b] Altamimi Z (2002) Discussion on How to Express a Regional GPS Solution in the ITRF, Report on the Symposium of the IAG Subcommission for Europe (EUREF), Dubrovnik, 2002

[Alt 02c] Altamimi Z, Boucher C, Sillard P (2002) New trends for the realization of the international terrestrial reference system, Adv Space Res 30(2):175-184

[Alt 11] Altamimi Z, Collilieux X, Metivier L (2011) ITRF2008: an improved solution of the international terrestrial reference frame, J Geod, Vol. 85, No. 8, Pages 457-473

[Beu 98] Beutler G, Rothacher M, Springer T, Kouba J, Neilan RE (1998) The International GPS Service (IGS): An Interdisciplinary Service in Support of Earth Sciences, 32nd COSPAR Scientific Assembly, Nagoya, Japan, July 12 to 19, 1998

[Beu 05] Beutler G (2005) Methods of Celestial Mechanics, Springer, Berlin, Heidelberg 2005, ISSN 0941-7834

[Bia 06] Biancale R, Bode A (2006) Mean Annual and Seasonal Atmospheric Tide Models Based on 3-hourly and 6-hourly ECMWF Surface Pressure Data, GFZ Potsdam, Scientific Technical Report STR06/01

[Ble 89] Blewitt G (1989) Carrier Phase Ambiguity Resolution for the Global Positioning System Applied to Geodetic Baselines up to 2000 km, J Geophys Res, 94(B8), 10,187-10,203, doi:10.1029/JB094iB08p10187

[Ble 06a] Blewitt G (2003) Self-consistency in reference frames, geocenter definition, and surface loading of the solid Earth, J Geophys Res, 108(B2), 2103, doi:10.1029/2002JB002082

[Boe 06a] Boehm J, Niell A, Tregoning P, Schuh H (2006) Global mapping function (GMF): a new empirical mapping function based on numerical weather model data, Geophys Res Lett 33:L07304, doi:10.1029/2005GL025546

[Boe 06b] Boehm J, Werl B, Schuh H (2006) Troposphere mapping functions for GPS and very long baseline interferometry from European Centre for Medium-Range Weather Forecasts operational analysis data, J Geophys Res, 111, B02406, doi:10.1029/2005JB003629

[Cas 02] Case K, Kruizinga G, Wu S (2002) GRACE Level 1B Data Product User Handbook, JPL Publication D-22027

[CHAMP 12] Challenging Minisatellite Payload (2012) Internet Site, `http://www-app2.gfz-potsdam.de/pb1/op/champ/`

[Che 05] Cheng MK, Tapley BD (2005) Correction to "Variations in the Earth's oblateness during the past 28 years", J Geophys Res, 110, B03406, doi:10.1029/2005JB003700

[Che 10] Cheng MK, Tapley BD, Ries JC (2010) Geocenter Variations from Analysis of SLR data, IAG Commission 1 Symposium 2010, Reference Frames for Applications in Geosciences (REFAG2010), Marne-La-Vallee, France, 4-8 October 2010

[Che 11] Cheng MK, Ries JC, Tapley BD (2011) Variations of the Earth's Figure Axis from Satellite Laser Ranging and GRACE, J Geophys Res, 116, B01409, doi:10.1029/2010JB000850

[Col 11] Collilieux X, Metivier L, Altamimi Z, van Dam T, Ray J (2011) Quality Assessment of GPS Reprocessed Terrestrial Reference Frame, J Geod (2011) 15:219-231, doi:10.1007/s10291-010-0184-6

[Dah 12] Dahle Ch, Flechtner F, Gruber C, König D, König R, Michalak G, Neumayer KH (2012) GFZ GRACE Level-2 Processing Standards Document for Level-2 Product Release 0005, (Scientific Technical Report - Data , 12/02), Potsdam, 20 p., doi:10.2312/GFZ.b103-12020

[Dav 84] Davis J, Herring T (1984) New atmospheric mapping function, Center of Astrophysics, Cambridge, Mass., Manuscript July 1984

[Deg 93] Degnan JJ (1993) Millimeter accuracy satellite laser ranging: a review, Contributions of Space Geodesy to Geodynamics: Technology, Geodynamics Series, D.E. Smith and D.L. Turcotte (Eds.), AGU Geodynamics Series, 25, pp. 133-162, 1993

[Don 97] Dong D, Dickey JO, Chao Y, Cheng MK (1997) Geocenter variations caused by atmosphere, ocean and surface ground water, Geophysical Research Letters, 24, 1867-1870

[Don 03] Dong D, Yunck T, Heflin M (2003) Origin of the International Terrestrial Reference Frame, J Geophys Res, 108, No. B4, 2200, doi:10.1029/2002JB002035

[Dor 96] Dormand JR (1996) Numerical Methods for Differential Equations, A Computational Approach, CRC Press, Boca Raton

[Dow 09] Dow JM, Neilan, RE, Rizos, C (2009) The International GNSS Service in a changing landscape of Global Navigation Satellite Systems, J Geod (2009) 83:191-198, doi:10.1007/s00190-008-0300-3

[Dun 03] Dunn C, et al. (2003) Instrument of GRACE: GPS Augments Gravity Measurements, GPS World, 14(2), 16-28

[Fer 77] Ferrari AJ (1977) Lunar Gravity: A Harmonic Analysis, J Geophys Res, Vol. 82, No. 20

[Fle 07] Flechtner F (2007) AOD1B Product Cescription Document for Product Releases 01 to 04, GRACE 327-750 (GR-GFZ-AOD-0001)

[Fle 10a] Flechtner F, Dahle Ch, Neumayer KH, König R, Förste Ch (2010) The Release 04 CHAMP and GRACE EIGEN Gravity Model, In: Flechtner F et al. (eds.) System Earth via Geodetic-Geophysical Space Techniques, pp. 41-58, Springer Heidelberg Dordrecht London New York, ISSN 2190-1635

[Fle 10b] Flechtner F (2010) Improved GRACE Level-1 and Level-2 Products and Their Validation by Ocean Bottom Pressure, In: Flechtner F et al. (eds.) System Earth via Geodetic-Geophysical Space Techniques, pp. 95-104, Springer Heidelberg Dordrecht London New York, ISSN 2190-1635

[Fli 92] Fliegel HF, Gallini TE (1992) Global Positioning System Radiation Force Model for Geodetic Applications, J Geophys Res, Vol. 97, No. B1, pp. 559-568

[Fli 96] Fliegel HF, Gallini TE (1996) Solar Foce Modeling of Block IIR Global Positioning Satellites, J Spacecraft Rockets, Vol. 33, No. 6, November-December 1996

[För 07] Förste Ch, Schmidt R, Stubenvoll R, Flechtner F, Meyer U, König R, Neumayer H, Biancale R, Lemoine JM, Bruinsma S, Loyer S, Barthelmes F, Esselborn S (2007) The GeoForschungsZentrum Potsdam/Groupe de Recherche de Geodesie Spatiale satellite-only and combined gravity field models: EIGEN-GL04S1 and EIGEN-GL04C, J Geod, Vol. 82, No. 6, pp. 331-346

[För 11] Förste Ch, Bruinsma S, Shako R, Marty JC, Flechtner F, Abrikosov O, Dahle Ch, Lemoine JM, Neumayer H, Biancale R, Barthelmes F, König R, Balmino G (2011) EIGEN-6 - A new combined global gravity field model including GOCE data from the collaboration of GFZ-Potsdam and GRGS-Toulouse, Geophys Res Abstr, Vol. 13, EGU2011-3242-2, 2011, EGU General Assembly 2011

[Fri 10] Fritsche M, Dietrich R, Rülke, Rothacher M, Steigenberger P (2010) Low-degree earth deformation from reprocessed GPS observations, GPS Solut 14:165-175, doi:10.1007/s10291-009-0130-7

[Fro 06] Frommknecht B, Fackler U, Flury J (2006) Integrated Sensor Analysis GRACE, In: Observation of the Earth System from Space, pp. 99-113, Springer Berlin Heidelberg New York, ISBN 3-540-29520-8

[Fro 10] Frommknecht B, Schlicht A (2010) The GRACE Gravity Sensor System, In: Flechtner F et al. (eds.) System Earth via Geodetic-Geophysical Space Techniques, pp. 105-118, Springer Heidelberg Dordrecht London New York, ISSN 2190-1635

[Ge 08] Ge M, Gendt G, Rothacher M, Shi C, Liu J (2008) J Geod, Vol. 82, No. 7, pp. 389-399, doi:10.1007/s00190-007-0187-4

[GGOS 12] GGOS - Global Geodetic Observing System (2012) Internet site, http://www.ggos.org/

[GRACE 12a] Gravity Recovery and Climate Experiment (2012a) Internet Site at CSR, http://www.csr.utexas.edu/grace/

[GRACE 12b] Gravity Recovery and Climate Experiment (2012b) Internet Site at GFZ, http://www.gfz-potsdam.de/portal/gfz/Struktur/Departments/Department+1/sec12/projects/grace

[Heck 95] Heck B (1995) Rechenverfahren und Auswertemodelle der Landesvermessung, Wichmann Heidelberg, 1995, ISBN 3-87907-269-8

[Her 93] Herring TA, Pearlman MR (1993) Future Developments and Synergism of Space Geodetic Measurement Techniques, In: Smith DE, Turcotte DL (eds) Contributions of Space Geodesy to Geodynamics: Crustal Dynamics, AGU Geodynamics Series, V.25, pp. 21-26

[Hei 67] Heiskanen WA, Moritz H (1967) Physical Geodesy, W.H. Freeman and Company, San Francisco and London

[Him 93] Himwich WE, Watkins MM, Ma C, MacMillan DS, Clark TA, Eanes RJ, Ryan JW, Schutz BE, Tapley BD (1993) The Consistency of the Scale of the Terrestrial Reference Frames Estimated from SLR and VLBI Data, In: Smith DE, Turcotte DL (eds) Contributions of Space Geodesy to Geodynamics: Crustal Dynamics, AGU Geodynamics Series, V.24, pp. 113-120

[Hof 01] Hofmann-Wellenhof B, Lichtenegger H, Collins J (2001) Global Positioning System - Theory and Practice, Fifth, revised edition, Springer Wien New York, 2001, ISBN 3-211-83534-2

[IAG 12] IAG - International Association of Geodesy (2012) Internet site, http://www.iag-aig.org/

[IGG 12a] IGG - Institute of Geodesy and Geophysics of TU Vienna (2012a) VMF1 Coefficients, http://www.ggosatm.hg.tuwien.ac.at/DELAY/GRID

[IGG 12b] IGG - Institute of Geodesy and Geophysics of TU Vienna (2012b) Global Mapping Function Source Code, http://www.ggosatm.hg.tuwien.ac.at/SOURCE/gmf.f

[IGS 12a] IGS - International GNSS Service (2012a) Internet Site, http://igscb.jpl.nasa.gov/

[IGS 12b] IGS - International GNSS Service (2012b) IGS08 Terrestrial Reference System Coordinates File, ftp://igscb.jpl.nasa.gov/igscb/station/coord/IGS08.snx

[IGS 12c] IGS - International GNSS Service (2012c) IGS08 GPS Phase Centre Variation File, ftp://igscb.jpl.nasa.gov/pub/station/general/igs08.atx

[IGS 12d] IGS - International GNSS Service (2012f) IONEX files, ftp://cddis.gsfc.nasa.gov/gps/products/ionex/2004/180/

[IGS 12e] IGS - International GNSS Service (2012d) Products Quality Overview, http://igscb.jpl.nasa.gov/components/prods.html

[IGS 12f] IGS - International GNSS Service (2012e) Site Guidelines, http://igscb.jpl.nasa.gov/network/guidelines/guidelines.html

[IGS 12g] IGS - International GNSS Service (2012g) Site Logs, ftp://igscb.jpl.nasa.gov/igscb/station/log

[ILRS 12a] ILRS - International Laser Ranging Service (2012a) Internet site, http://ilrs.gsfc.nasa.gov/

[ILRS 12b] ILRS - International Laser Ranging Service (2012b) Station Qualifications, http://ilrs.gsfc.nasa.gov/stations/site_procedures/station_qualification.html

[JPL 12a] JPL - Jet Propulsion Laboratory (2012a) Planetary and Lunar Ephemeris DE405, ftp://ssd.jpl.nasa.gov/pub/eph/planets/ascii/de405/header.405

[JPL 12b] JPL - Jet Propulsion Laboratory (2012b) Planetary and Lunar Ephemeris DE421, ftp://ssd.jpl.nasa.gov/pub/eph/planets/ascii/de421/header.421

[Kim 00] Kim J (2000) Simulation Study of A Low-Low Satellite-to-Satellite Tracking Mission, PhD thesis, The University of Texas at Austin, May 2000

[Koch 99] Koch KR (1999) Parameter Estimation and Hypothesis Testing in Linear Models, Springer, Berlin, Heidelberg 1999, ISBN 3-540-65257-4

[KoD 12] König D, König R (2012) Possibilities and Limits for Estimating a Dynamic and a Geometric Reference Frame Origin by the Integrated Approach Applied to the CHAMP-GRACE-GPS Constellation, In: Sneeuw N et al. (eds.) Proceedings VII Hotine-Marussi Symposium 2009, pp. 313-318, Springer Heidelberg, Dordrecht, London, New York, 2012, doi:10.1007/978-3-642-22078-4

[KoR 06] König R, Michalak G, Neumayer KH, Zhu SY (2006) Remarks on CHAMP Orbit Products, In: Observation of the Earth System from Space, pp. 17-26, Springer Berlin Heidelberg New York, ISBN 3-540-29520-8

[Kou 03] Kouba J (2003) A guide to using International GPS Service (IGS) products, ftp://igscb.jpl.nasa.gov/igscb/resource/pubs/GuidetoUsingIGSProducts.pdf

[Lya 04] Lyard F, Lefevre F, Letellier T, Francis O (2006) Modelling the global ocean tides: modern insights from FES2004, Ocean Dynamics (2006) 56: 394-415, Springer

[McC 04] McCarthy DD, Petit G (eds.) (2004) IERS Conventions (2003), Verlag des Bundesamts für Kartographie und Geodäsie, Frankfurt am Main

[Men 04] Mendes VB, Pavlis EC (2004) High-accuracy zenith delay prediction at optical wavelengths, Geophys Res Lett, Vol. 31, L14602, 2004, doi:10.1029/2004GL020308

[Neu 98] Neubert R, Grunwaldt L, Neubert J (1998) The Retro-Reflector for the CHAMP Satellite: Final Design and Realization, Proceedings 11th International Workshop on Laser Ranging, Deggendorf, Germany, September 21-25, p. 260, 1998

[Nie 96] Niell AE (1996) Global Mapping Functions for the Atmosphere Delay at Radio Wavelengths, J. Geophys. Res., 101, 3227-3246

[Pea 02] Pearlman MR, Degnan JJ, Bosworth JM (2002) The International Laser Ranging Service, Advances in Space Research, Vol. 30, No. 2, pp. 135-143

[Pet 10] Petit G, Luzum B (eds.) (2010) IERS Conventions 2010, IERS Technical Note 36; Frankfurt am Main: Verlag des Bundesamts für Kartographie und Geodäsie, 179 pp., ISBN 3-89888-989-6, 2010

[Plag 05] Plag HP (2005) The GGOS as the backbone for global observing and local monitoring: a user driven perspective, J Geodyn, 40, 479-486, doi:10.1016/j.jog.2005.06.012

[Rei 99] Reigber Ch, Schwintzer P, Lühr H (1999) The CHAMP geopotential mission, Boll Geof Teor Appl 40, 285-289

[Rie 11] Rietbroek R, Fritsche M, Brunnabend SE, Daras I, Kusche J, Schroeter J, Flechtner F, Dietrich R (2011) Global surface mass from a new combination of GRACE, modelled OBP and reprocessed GPS data, J Geodyn, In Press, Accepted Manuscript, Available online 23 February 2011, doi:10.1016/j.jog.2011.02.003

[Saa 73] Saastamoinen J (1973) Contributions to the theory of atmospheric refraction, Bull. Géod. 107 (1): 13-34

[Sav 12] Savcenko R, Bosch W (2012) EOT11a - empirical ocean tide model from multi-mission satellite altimetry, Report No. 89, Deutsches Geodaetisches Forschungsinstitut, Muenchen 2012

[Scha 98] Schaer S, Gurtner W, Feltens J (1998) IONEX: The IONosphere Map EXchange Format Version 1, ftp://igscb.jpl.nasa.gov/pub/data/format/ionex1.pdf

[Schm 07] Schmid R, Steigenberger P, Gendt G, Ge M, Rothacher M (2007) Generation of a consistent absolute phase center correction model for GPS receiver and satellite antennas, J Geod 81(12): 781-798, doi:10.1007/s00190-007-0148-y

[Schw 00] Schwintzer P, Kang Z, Perosanz F (2000) Accelerometry Aboard CHAMP, In: Rummel R, Drewes H, Bosch W, Hornik H (eds) IAG section II symposium, Munich 1998 Oct 5-9, Springer, pp. 197-200

[See 03] Seeber G (2003) Satellite Geodesy: foundations, methods, and applications, de Gruyter, Berlin, New York

[Sil 01] Sillard P, Boucher C (2001) A review of algebraic constraints in terrestrial reference frame datum definition, J Geod (2001) 75:63-73, doi:10.1007/s001900100166

[Sno 09] Snopek K, König D, König R (2009) Orbit Predictions for CHAMP and GRACE, In: Flechtner F et al. (eds.) System Earth via Geodetic-Geophysical Space Techniques, pp. 59-66, Springer, Heidelberg Dordrecht London New York, ISSN 2190-1635

[Tap 89] Tapley BD (1989) Fundamentals of orbit determination, In: Sanso F, Rummel R (eds) Theory of Satellite Geodesy and Gravity Field Determination, Springer Lecture Notes in Earth Sciences, 25, Springer, Berlin, Heidelberg, New York, pp. 235-260

[Tap 04] Tapley BD, Bettadpur S, Watkins M, Reigber C (2004) The gravity recovery and climate experiment: Mission overview and early results, Geophys Res Lett 31, L09607-1-4

[Teu 98] Teunissen PJG, Kleusberg A (1998) GPS for Geodesy, Springer, Berlin, Heidelberg, New York

[Tor 01] Torge W (2001) Geodesy, Third completely revised and extended edition, de Gruyter, Berlin, New York, 2001, ISBN 3-11-017072-8

[Tou 98] Touboul P, Willemenot E, Foulon B, Josselin V (1998) Accelerometers for CHAMP, GRACE, and GOCE space missions: synergy and evolution, Boll. Geof. Teor. Appl. 40, 321-327

[We 91] Wessel P, Smith WHF (1991) Free software helps map and display data, EOS trans. AGU, 72, 441, 1991

[Wu 06] Wu S, Kruizinga G, Bertiger W (2006) Algorithm Theoretical Basis Document for GRACE Level-1B Data Processing V1.2, GRACE 327-741 (JPL Publication D-27672)

[Wu 12] Wu X, Ray J, van Dam T (2012) Geocenter motion and its geodetic and geophysical implications, Journal of Geodynamics 58 (2012) 44-61

[Zhu 04] Zhu S, Reigber Ch, König R (2004) Integrated Adjustment of CHAMP, GRACE and GPS Data, J Geod, Vol. 78, No. 1-2, pp. 103-108, doi:10.1007/s00190-004-0379-0